Table 3.3.1 Deviation of Scaled Mean Radial Velocity at Re/Ro = 0.58 (near Exit Section)

% r/Ro	Re,i = 13700	Re,i = 7840	Re,i = 1960
0.036	-6.42	13.4	-6.94
0.109	-6.64	8.70	-2.06
0.182	3.82	-6.91	3.09
0.255	15.6	-5.45	-10.1
0.327	12.1	5.55	-17.7
0.400	-3.10	15.0	-11.9
0.473	9.76	13.2	-23.0
0.545	4.62	5.22	-9.83
0.618	11.3	-12.2	0.89
0.691	-4.82	-5.09	9.91
0.764	-1.60	-9.54	11.1
0.836	5.68	-20.1	14.4

CHAPTER 4

TURBULENCE INTENSITY

4.1 Introduction

The motion with irregular velocity fluctuations is considered as turbulent [36]. Turbulent fluid motion is an irregular condition of flow in which the various quantities show a random variation with time and space coordinates, so that statistically distinct average values can be discerned [37]. Turbulent flows, therefore, are studied both experimentally and theoretically as a statistical phenomenon.

It is generally assumed that a turbulent flow consists of a mean flow and a fluctuation about the mean value, that is

$$V_r'(t) = V_r(t) - \overline{V}_r$$
$$V_\theta'(t) = V_\theta(t) - \overline{V}_\theta$$
$$V_z'(t) = V_z(t) - \overline{V}_z \qquad (4\text{-}1)$$

The mean velocity components of the flow, $\overline{V}_r$, $\overline{V}_\theta$ and $\overline{V}_z$, may be taken either with respect to time at a fixed point (temporal mean) or with respect to one of the coordinates at a given instant of time (spatial mean). In this study, the mean velocity components are taken with respect to time at a fixed point. The fluctuating velocity components, V_r', V_θ' and V_z', are defined as the difference between the total velocity components at any instant, V_r, V_θ and V_z, and the mean velocity components.

One of the important characteristics used to describe a turbulent flow is the intensity. Since Dryden and Kuethe [38] in 1930, the violence or the intensity of turbulence fluctuations has usually been defined as the ratio of the root-mean-square velocity to the average velocity, that is

Turbulence Intensity = $\sqrt{V'^2} / \overline{V}$

where

$\sqrt{V'^2}$ = root-mean-square velocity

$\overline{V}$ = time average, spatial average or ensemble average velocity

When the fluctuating velocities and the mean velocities are obtained, such as from measurements, the turbulence intensity of the flow can be determined. In this thesis, a model of turbulence intensity and mathematical approximation are presented based on the experimental results.

4.2 Tangential Component of Turbulence Intensity at Main Section

4.2.1 Model

From the observations of the experimental results shown in Figures 4.2.1.1 to 4.2.1.3, the distribution of the tangential component of the turbulence intensity along the radial direction of a vortex chamber from the centre to the wall is found as follows. The tangential component of the turbulence intensity tends to its maximum value at the centre of the vortex chamber, drops rapidly from the maximum value to the minimum value, then increases slowly along the radial direction after passing its minimum value point. At some place near the wall of the vortex chamber, an apparent change of the slope of the distribution curve takes place. It is clear that the turbulence intensity is a function of the location.

Comparing the profiles of the tangential component of the turbulence intensity with those of the tangential velocity obtained under the same conditions, an important characteristic is observed: the minimum value of the tangential component of the turbulence intensity always corresponds to

the maximum value of the tangential velocity. In other words, they appear at the same location inside the vortex chamber as shown in Figure 4.2.1.4.

Based on this important finding and the observed features of the tangential component of the turbulence intensity, a model of the tangential component of the turbulence intensity is proposed. The distribution of the tangential component of the turbulence intensity may be divided into three regions: the central core region, the outer region and the boundary layer region along a radial direction as shown in Figure 4.2.1.5.

The central core region is defined from the centre of the vortex chamber to the place corresponding to the tangential component of the minimum turbulence intensity (the highest tangential velocity). The flow pattern in this region is generally considered as a forced vortex motion.

The outer region is defined to be between and bounded by the central core region and the boundary layer region. The flow pattern in this region is generally considered as a free vortex motion.

The boundary layer region begins approximately at normalized radius $r/R_o = 0.9$, and ends at the wall of the vortex chamber: $r/R_o = 1.0$. In the boundary layer region, viscous effects are significant.

Based on their particular characteristics, individual mathematical approximation is adopted for each region.

4.2.2 Mathematical Approach in Central Core Region

In the central core region, the tangential component of the turbulence intensity decreases from the maximum value to a minimum value along the radial direction.

The contraction ratio affects both the magnitude of the tangential component of the turbulence intensity and the range of this region. With a

smaller contraction ratio, its magnitude will be smaller and the range will be narrow. The range based on the normalized radius always follows and is always smaller than the numerical value of the contraction ratio. This behaviour could be explained by the influence of the open exit hole where the central core region faces. The open exit directly affect the flow field.

The inlet Reynolds number affects the magnitude of the tangential component of the turbulence intensity, but does not affect the range.

It is found that a mathematical expression containing an exponential function will be the best approximation to reflect these phenomena and influence factors. That is, the distribution of the tangential component of the turbulence intensity in the central core region can be formulated as:

$$I_{tc} = B \cdot \exp[-D\,(\overline{R})^{0.4}] \tag{4-2}$$

In this equation, coefficients B and D are constants. All experimental data points of the tangential component of the turbulence intensity under the same condition should be represented by this equation. Thus, B and D can be determined by substituting any two pairs of experimental data under the same testing conditions into the following equations:

$$B = I_{t1} \cdot \exp[D \cdot (\overline{R})_1^{0.4}] \tag{4-3}$$

$$D = \frac{\ln(I_{t1}/I_{t2})}{(\overline{R})_2^{0.4} - (\overline{R})_1^{0.4}} \tag{4-4}$$

where I_{t1} and $(\overline{R})_1$ are data from measurement point 1. I_{t2} and $(\overline{R})_2$ are data from measurement point 2.

If the experimental condition is changed, coefficients B and D will change their numerical values correspondingly. But, B and D will have new constant values for the whole central core region as long as the conditions (R_e/R_o , $R_{e,i}$, etc.) are maintained to be the same within the whole region. It is

further found that B and D are functions of the contraction ratio and the inlet Reynolds number. They can be formulated by exponential functions as follows:

$$B = B_1 \cdot \exp[B_2(\frac{R_e}{R_o})] \tag{4-5}$$

$$D = D_1 \cdot \exp[D_2(\frac{R_e}{R_o})] \tag{4-6}$$

B_1, B_2, D_1 and D_2 appear to be constants. They are not affected by the change of contraction ratio, but, they are affected by the change of the inlet Reynolds number. They are the functions of the inlet Reynolds number. Scattering all numerical values of B and D obtained from variety of contraction ratios, but at each inlet Reynolds number yields curves of B versus R_e/R_o and D versus R_e/R_o. A sample is shown in Figure 4.2.2.1. Using curve fitting technique, the coefficients of equations (4-5) and (4-6), B_1, B_2, D_1 and D_2, can be determined. The numerical values of B_1, B_2, D_1 and D_2 for each inlet Reynolds number and all contraction ratios are listed in Table 4.2.1.

A sample of the distribution curves of the tangential component of the turbulence intensity for the central core region based on equation (4-2) is shown in Figure 4.2.2.2.

4.2.3 Mathematical Approach in Outer Region

In the outer region, the tangential component of the turbulence intensity increases continuously from the minimum value along the radial direction.

It is found that the contraction ratio has very little influence on the tangential component of the turbulence intensity. At any given location, the measurement shows that the tangential component of the turbulence

intensity under different contraction ratios is around a certain corresponding value. Therefore, the effect of contraction ratios in the outer region is not considered to be included as an independent factor or coefficient.

The inlet Reynolds number affects the values of the tangential component of the turbulence intensity. A simpler mathematical expression of the tangential component of the turbulence intensity for the outer region is proposed as follows:

$$I_{to} = A_o \cdot \exp(-C_o \cdot \overline{R}) \qquad (4\text{-}7)$$

A_o and C_o are functions of the inlet Reynolds number, but are constants for a given inlet Reynolds number. A_o and C_o can be determined according to the following steps:

(1) To a given inlet Reynolds number, average experimental data of the tangential component of the turbulence intensity obtained at a given radius but with a variety of contraction ratios to result in a unique datum of the tangential component of the turbulence intensity corresponding to that given radius;

(2) Plot all obtained average data along the radial direction to form a curve of mean value of the tangential component of the turbulence intensity versus radius corresponding to a given inlet Reynolds number;

(3) Use curve fitting technique based on the exponential function to determine A_o and C_o.

(4) Repeat above steps for each inlet Reynolds number.

The numerical values of A_o and C_o corresponding to each inlet Reynolds numbers are listed in Table 4.2.1. A sample of the distribution curve of the tangential component of the turbulence intensity for the outer region, using equation (4-7), is shown in Figure 4.2.3.1.

4.2.4 Mathematical Approach in Boundary Layer Region

No existing theory, presently, could be applied directly to the boundary layer of confined vortex flows. However, the free-vortex model may be assumed to be extended to the boundary layer including the wall of the vortex chamber. The experimental findings show that the similar behaviour of the tangential component of the turbulence intensity as presented in the outer region can be observed in the boundary layer region. The tangential component of the turbulence intensity increases continuously except with a higher gradient.

The contraction ratio has very little influence to the tangential component of the turbulence intensity. At any given location, the measurement shows that the tangential component of the turbulence intensity under different contraction ratios are around a certain value.

The inlet Reynolds number affects the values of the tangential component of the turbulence intensity. Thus, a similar expression based on the exponential function used for the outer region can be applied to describe the distribution of the tangential component of the turbulence intensity in the boundary layer region as follows:

$$I_{tb} = A_b \cdot \exp(-C_b \cdot \overline{R}) \qquad (4\text{-}8)$$

The method of determining A_b and C_b is the same as that used to determine A_o and C_o in the outer region, which is detailed in the previous section. The numerical values of A_b and C_b are listed in Table 4.2.1. A sample of the distribution curve of the tangential component of the turbulence intensity for the boundary layer region is shown in Figure 4.2.4.1.

The tangential velocity at the wall of the vortex chamber is zero. Therefore, the tangential component of the turbulence intensity is equal to zero at the wall. Equation (4-8) is not suitable for the case at the wall. That is, equation (4-8) can not be applied to the location where radius "r "is equal to the inside radius of the vortex chamber "R_o".

Combining all findings and the empirical equations for the central core region, the outer region and the boundary layer region, three groups of curves representing overall distributions of the tangential component of the turbulence intensity of vortex chamber flows, corresponding to three different inlet Reynolds numbers, are obtained as shown in Figures 4.2.4.2, 4.2.4.3 and 4.2.4.4 respectively.

4.3 Tangential Component of Turbulence Intensity near Exit Section

4.3.1 General

Based on the experimental results shown in Figures 4.3.1.1 to 4.3.1.3, the three-region model of the tangential component of the turbulence intensity proposed for the main section of the vortex chamber is found still suitable for the modelling of the tangential component of the turbulence intensity near the exit section inside the vortex chamber.

However, the range of each divided region, that is, the location of borders for each region, is different from the main section to near the exit section although they are under the same testing conditions as well as that the maximum tangential velocities appear at almost the same location at both sections. The border line between the central core region and the outer region is set based on the minimum value location of the tangential component of the turbulence intensity. At the main section, it is the location corresponding

to the maximum tangential velocity. However, near the exit section inside the vortex chamber, it is not the location corresponding to the maximum tangential velocity.

Near the exit section, the numerical value of the normalized radius r/R_o corresponding to the minimum value of the tangential component of the turbulence intensity is always slightly larger than that of the contraction ratio R_e/R_o. However, at the main section it is always smaller than that of the contraction ratio. This characteristic can be explained by that the actual range of the closed space of the exit plate is from the radius of exit hole, R_e, to the radius of the wall of the vortex chamber, R_o. What the central core region faces, in fact, is the open space of the exit hole. Because of the strong influence of the open space of the exit hole, the central core region of the tangential component of the turbulence intensity near the exit section inside the vortex chamber is bigger than that at the main section of the vortex chamber.

4.3.2 Analysis

The distribution curves of the tangential component of the turbulence intensity near the exit section inside the vortex chamber for the central core region are provided based on the experimental data and curve fitting technique.

The distributions of the tangential component of the turbulence intensity in the outer region and the boundary layer region near the exit section are found to be similar to those at the main section. Therefore, the form of the equation obtained for the purpose of estimating the tangential component of the turbulence intensity in the outer region and that in the boundary layer region at the main section are still suitable for estimating the tangential component of the turbulence intensity in the outer region and that

in the boundary layer region near the exit section. Similar equations with different constant coefficients can be used as shown in the following:

$$I_{to/b} = A_{o/b} \cdot \exp(-C_{o/b} \cdot \overline{R}) \tag{4-9}$$

$$I_{tb/b} = A_{b/b} \cdot \exp(-C_{b/b} \cdot \overline{R}) \tag{4-10}$$

The numerical values of constants $A_{o/b}$, $C_{o/b}$, $A_{b/b}$ and $C_{b/b}$ can be determined following the same procedure as mentioned in the section 4.2.3. Similarly, the contraction ratio has very little influence to the tangential component of the turbulence intensity, and inlet Reynolds number has apparent effect. As a consequence, $A_{o/b}$, $C_{o/b}$, $A_{b/b}$ and $C_{b/b}$ will be constants to all contraction ratios and vary with the inlet Reynolds number. The numerical values of $A_{o/b}$, $C_{o/b}$, $A_{b/b}$ and $C_{b/b}$ are obtained and listed in Table 4.2.1. Samples of the distribution curves for the outer region and the boundary layer region are shown in Figure 4.3.2.1 and 4.3.2.2.

The overall distribution curves of the tangential component of the turbulence intensity near the exit section inside the vortex chamber, based on the empirical equations and the experimental data, are obtained and shown in Figures 4.3.2.3, 4.3.2.4 and 4.3.2.5 for application.

4.4 Radial Component of Turbulence Intensity

4.4.1 Main Section

It is observed that at the main section the location of the radial component of the minimum turbulence intensity does not concord to the location of the maximum radial velocity.

It is found that the distribution of the radial component of the turbulence intensity varies at different axial locations inside the vortex chamber. The magnitude of the radial component of the turbulence intensity

at the main section is higher than that of the tangential component of the turbulence intensity. The minimum level of the radial component of the turbulence intensity are about 10 times of that of the tangential component of the turbulence intensity as shown in Figures 4.4.1.1 and 4.4.1.2. It may be due to the relatively small mean value of the radial velocity. It is difficult to model and to formulate the radial component of the turbulence intensity at the main section of the vortex chamber, neither in the distribution nor in the magnitude.

4.4.2 Near Exit Section

The distributions of the radial component of the turbulence intensity near the exit section inside the vortex chamber are obtained experimentally as shown in Figures 4.4.2.1 to 4.4.2.3.

It is found from the analysis of experimental results that, for any given contraction ratio, the radial component of the turbulence intensity near the exit section at different inlet Reynolds numbers can be approximated by a unique curve as shown in Figures 4.4.2.4 to 4.4.2.9 respectively. It means that, near the exit section inside the vortex chamber, the contraction ratio has apparent influence on the radial component of the turbulence intensity, but, the inlet Reynolds number has little effect.

It is also found from the analysis of experimental results that the radial component of the turbulence intensity tends to its maximum value at the centre of the vortex chamber. The minimum value of the radial component of the turbulence intensity, at any given contraction ratio, always appears at the place where the numerical value of the normalized radius is slightly greater than that of the contraction ratio. This is also observed for the tangential component of the turbulence intensity near the exit section. The

location where the minimum value of the radial component of the turbulence intensity appears is always at the location where the maximum radial velocity exists as shown in Figure 4.4.2.10. The ranges of the magnitude of the radial component of the turbulence intensity from the maximum value to the minimum value are similar for all different contraction ratios.

Based on these observations, a model similar to that presented for the tangential component of the turbulence intensity may be proposed for the radial component of the turbulence intensity. This model could consist of three regions: the central core region, the outer region and the boundary layer region along a radial direction from the centre of the vortex chamber to its wall.

The central core region is defined from the centre of the vortex chamber to the place where the minimum value of the radial component of the turbulence intensity (the maximum radial velocity) appears. In this region, the value of the radial component of the turbulence intensity decreases rapidly and continuously from the centre of the vortex chamber to the border of the outer region.

The outer region is defined to be between and bounded by the central core region and the boundary layer region. In this region, the value of the radial component of the turbulence intensity increases slowly and continuously along the radial direction from the minimum value location.

The boundary layer region begins approximately at the normalized radius $\overline{R} = 0.9$, and ends at the wall of the vortex chamber: $\overline{R} = 1.0$. To the boundary layer region near the exit section, which actually refers to the flow existing at the circular corner of the vortex chamber, measurement of the radial component of the turbulence intensity met some technical difficulties.

The experiments are performed at the location near the exit plate. Therefore, what the central core region faces, in fact, is the open space of the exit hole. The flow near the exit section inside the vortex chamber exists only in the outer region and the boundary layer region. The measurements show that the boundary layer region which consists of circular corner between the exit plate and the wall of the vortex chamber seems to be a dead zone for the flow in the radial direction.

As a mathematical approach, the distribution of the radial component of the turbulence intensity can be approximated by exponential functions. Since the distribution of the radial component of the turbulence intensity are quite different for different contraction ratios, no unique expression or empirical formula is available for this purpose.

4.5 Minimum Turbulence Intensity

It is found from experimental studies that the location of the minimum turbulence intensity (both tangential and radial components) is a function of the contraction ratio. However. it is not a function of the inlet Reynolds number as shown in Figures 4.5.1, 4.5.2, 4.4.2.4 to 4.4.2.9. In Figure 4.5.1, the minimum values of the tangential component of the turbulence intensity corresponding to different inlet Reynolds numbers appear at the same location, $r/R_o \approx 0.25$, which means the inlet Reynolds number does not affect the location of the tangential component of the minimum turbulence intensity. Similarly, the same conclusion can be drawn from Figures 4.5.2, 4.4.2.4 to 4.4.2.9. Since the swirl number β is a function of the contraction ratio, it can be concluded that the location of the minimum turbulence intensity depends on the swirl number.

The forced-vortex flow in the central part of the vortex chamber can be considered as a solid motion like a core bounded by a cylindrical surface. The radius of that cylindrical surface is defined as the vortex core critical radius where the maximum mean tangential velocity appears. The location of the maximum mean tangential velocity at the main section is always corresponding to that of the tangential component of the minimum turbulence intensity. Since the inlet Reynolds number does not affect the location of the tangential component of the turbulence intensity, it does not affect the location of the maximum mean tangential velocity either. In other words, the inlet Reynolds number does not affect the vortex core critical radius. Therefore, the critical radius of the vortex core depends on the swirl number.

Near the exit section, the location of the tangential component of the minimum turbulence intensity does not correspond to that of the maximum mean tangential velocity This is an important difference existing between near the exit section and the main section. Furthermore, at the main section, the numerical value of the location (radius) for the tangential component of the minimum turbulence intensity is always less than that of the contraction ratio. However, near the exit section, the numerical value of the location for the tangential component of the minimum turbulence intensity is always greater than that of the contraction ratio.

Near the exit section, the location of the radial component of the minimum turbulence intensity does not correspond to that of the maximum mean tangential velocity. Instead, it corresponds to the location of the maximum mean radial velocity.

These characteristics are mainly due to the effects of the open hole at the exit, the boundary layer flow along the exit plate surface and etc.

Based on the experimental results, correlations between the location of the minimum turbulence intensity and the contraction ratios can be approximated by linear functions. Plots of the correlations are shown in Figure 4.5.3. The linear correlations are as follows:

For the tangential component of the minimum turbulence intensity at the main section,

$$\frac{R_c}{R_o} = -0.1954 + 1.180\left(\frac{R_e}{R_o}\right) \tag{4-11}$$

For the tangential component of the minimum turbulence intensity near the exit section,

$$\frac{R_{min}}{R_o} = 0.1064 + \frac{R_e}{R_o} \tag{4-12}$$

For the radial component of the minimum turbulence intensity near the exit section,

$$\frac{R_{min}}{R_o} = 0.1311 + 0.8420\left(\frac{R_e}{R_o}\right) \tag{4-13}$$

At the main section, the magnitude of the tangential component of the minimum turbulence intensity is not only a function of the contraction ratio but also a function of the inlet Reynolds number. In general, the smaller the contraction ratio, the lower the minimum magnitude; the higher the inlet Reynolds number the lower the minimum magnitude. The correlation between the magnitude and the location can be approximated as follows:

$$I_{t,min} = a + b\left(\frac{R_c}{R_o}\right) \tag{4-14}$$

The numerical values of constants "a" and "b" are listed in Table 4.5.1.

Near the exit section, it is found that the smaller the contraction ratio, the lower the magnitude of the tangential component of the minimum

turbulence intensity. The effect of the inlet Reynolds number to the minimum value of the magnitude is smaller near the exit section than that at the main section. The correlation of the magnitude versus the location can be expressed as follows:

$$I_{t,min,b} = c + d\left(\frac{R_{min}}{R_o}\right) \tag{4-15}$$

The numerical values of constants "c" and "d" are listed in Table 4.5.1.

The magnitude of the radial component of the minimum turbulence intensity near the exit section is affected by the contraction ratio, not by the inlet Reynolds number. It is found that, at around the contraction ratio of 0.40, the radial component of the minimum turbulence intensity reaches its maximum magnitude. Two formulas are conducted to indicate the minimum value of the radial component of the minimum turbulence intensity for small contraction ratios and large contraction ratios respectively:

For $R_e/R_o < 0.5$,

$$I_{r,min} = 0.08844 + 0.8086\left(\frac{R_{min}}{R_o}\right) \tag{4-16}$$

For $R_e/R_o \geq 0.5$,

$$I_{r,min} = 0.6702 - 0.7418\left(\frac{R_{min}}{R_o}\right) + 0.5416\left(\frac{R_{min}}{R_o}\right)^2 \tag{4-17}$$

4.6 SUMMARY

It can be concluded that the turbulence intensity always tends to its maximum value at the centre of the vortex chamber. The influence factors to the turbulence intensity are summarized in Table 4.6.1. The influence factors to the characteristics of the minimum turbulence intensity, location and magnitude, are included in Table 4.6.2.

For the tangential compc ient of the turbulence intensity, the overall empirical distribution curves are presented in Figures 4.2.4.2 to 4.2.4.4 for the main section and in Figures 4.3.2.3 to 4.3.2.5 for near the exit section.

The differences between the experimental data corresponding to different locations and their average values within the main section are shown in Figure 4.6.1. The satisfactory results of the quantity analysis are shown in Table 4.6.3. The deviations between the prediction using the empirical equations and the experimental data at the main section are listed in Table 4.6.4. At small contraction ratios ($R_e/R_o < 0.5$), over 80 % of points are within a deviation of 10 %.

Near the exit section, the accuracy of prediction by the empirical equations for the outer region and the boundary layer region is within 10 %. The deviations between the prediction and the experimental data are shown in Tables 4.6.5 and 4.6.6. 70 % of points are within 5 %.

The above analysis shows that the proposed empirical equations can well predict the tangential component of the turbulence intensity inside the vortex chamber. Therefore, they are within acceptable limits of confidence.

For the radial component of the turbulence intensity, the distribution curves based on the average measurement values are presented in the section 4.4.2. Tables 4.6.7 and 4.6.8 show the deviations of the radial component of the turbulence intensity near the exit section inside the vortex chamber under small contraction ratios and large contraction ratios respectively. The deviations here refer to the differences between each individual raw measurement datum and the average value. They are satisfactory in general.

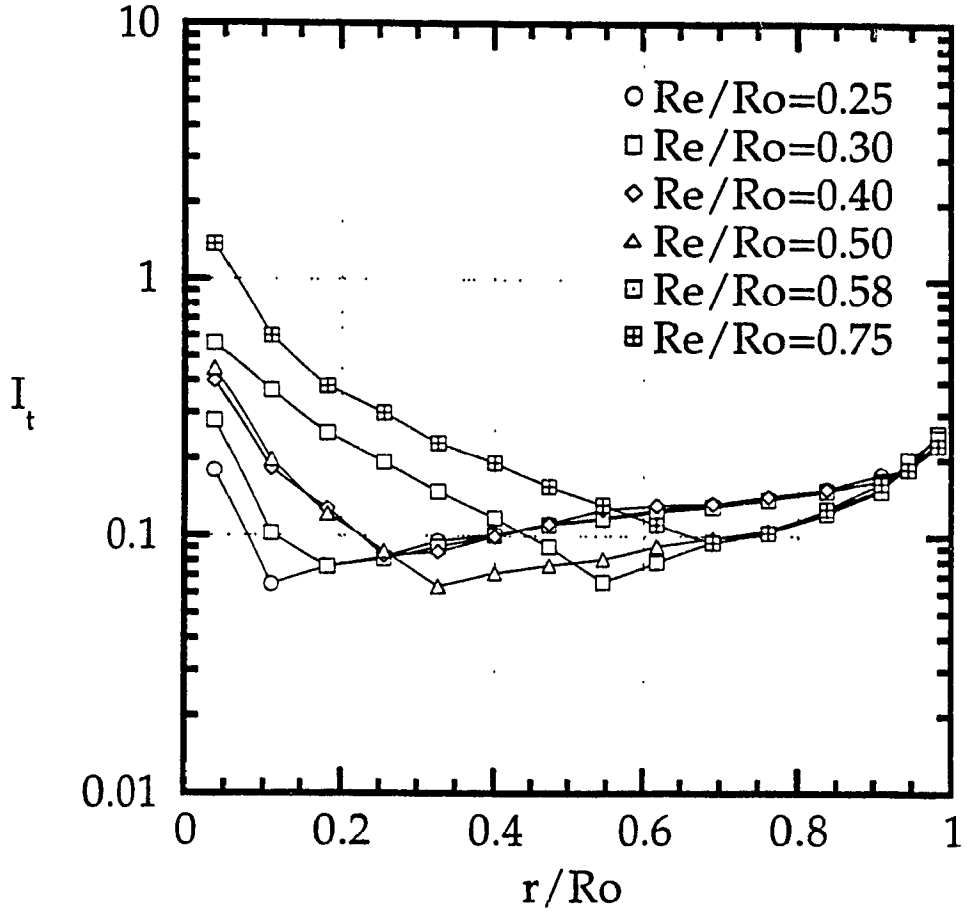

Figure 4.2.1.1 Experimental Tangential Component of Turbulence Intensity at Main Section (Re,i = 1960)

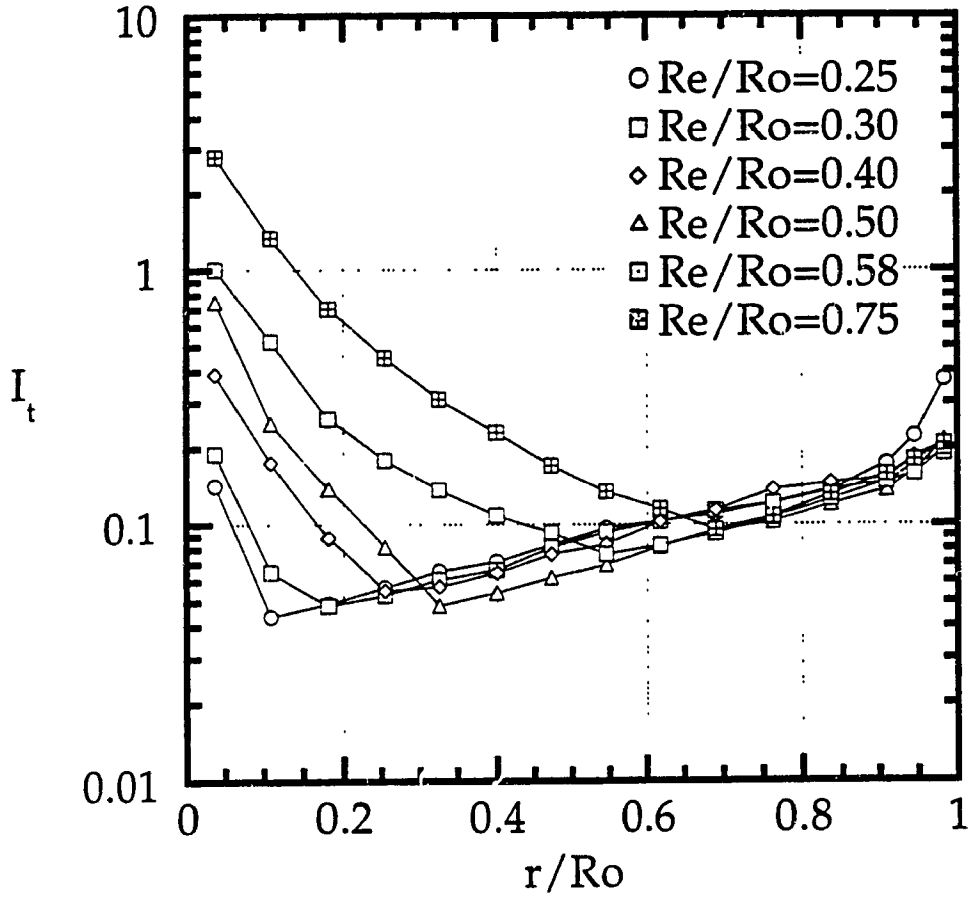

Figure 4.2.1.2 Experimental Tangential Component of Turbulence Intensity at Main Section (Re,i = 7840)

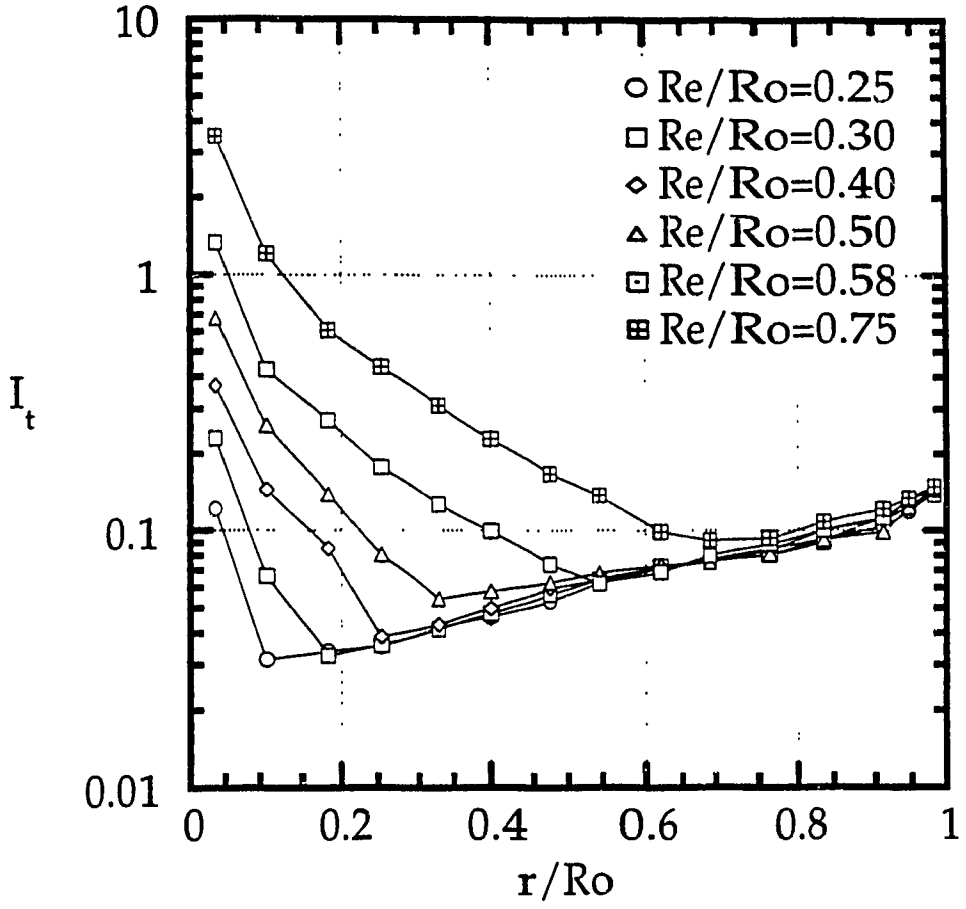

Figure 4.2.1.3 Experimental Tangential Component of Turbulence Intensity at Main Section (Re,i = 13700)

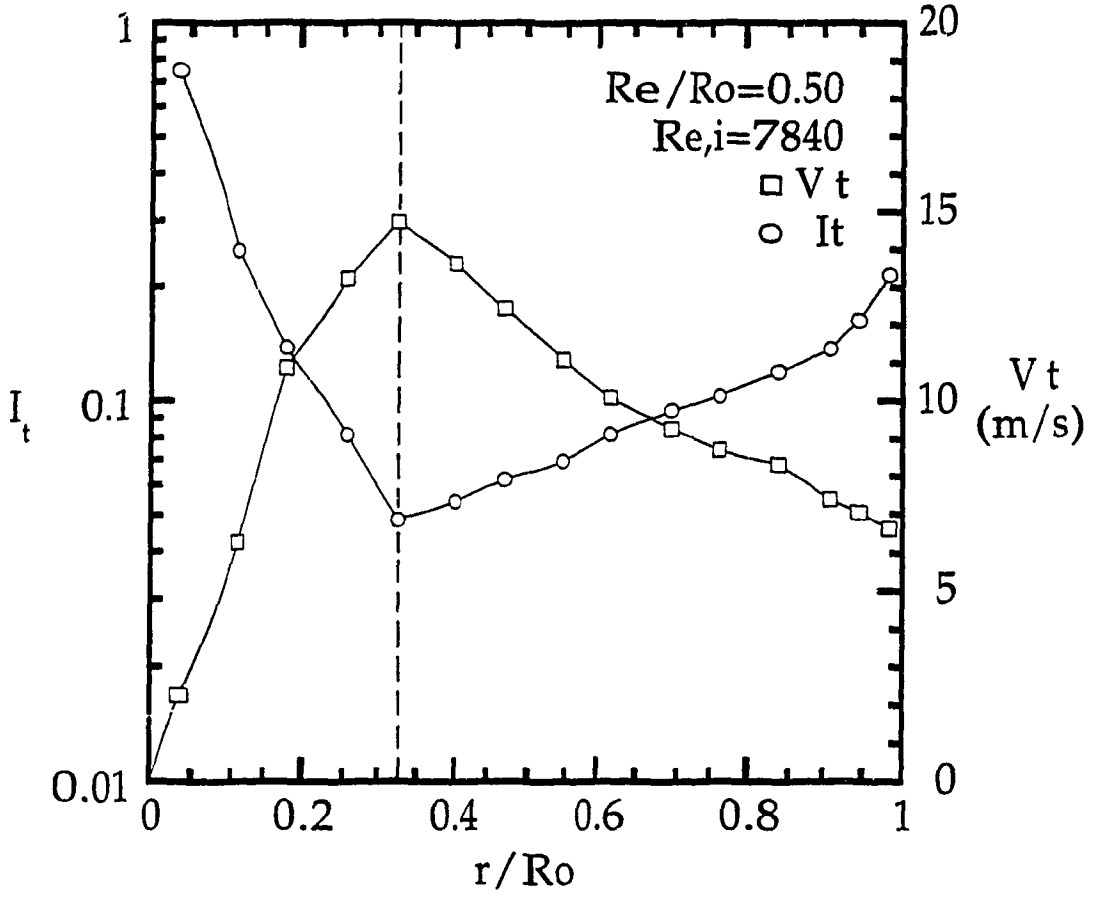

Figure 4.2.1.4 Tangential Component of Turbulence Intensity versus Mean Tangential Velocity at Main Section (exp.)

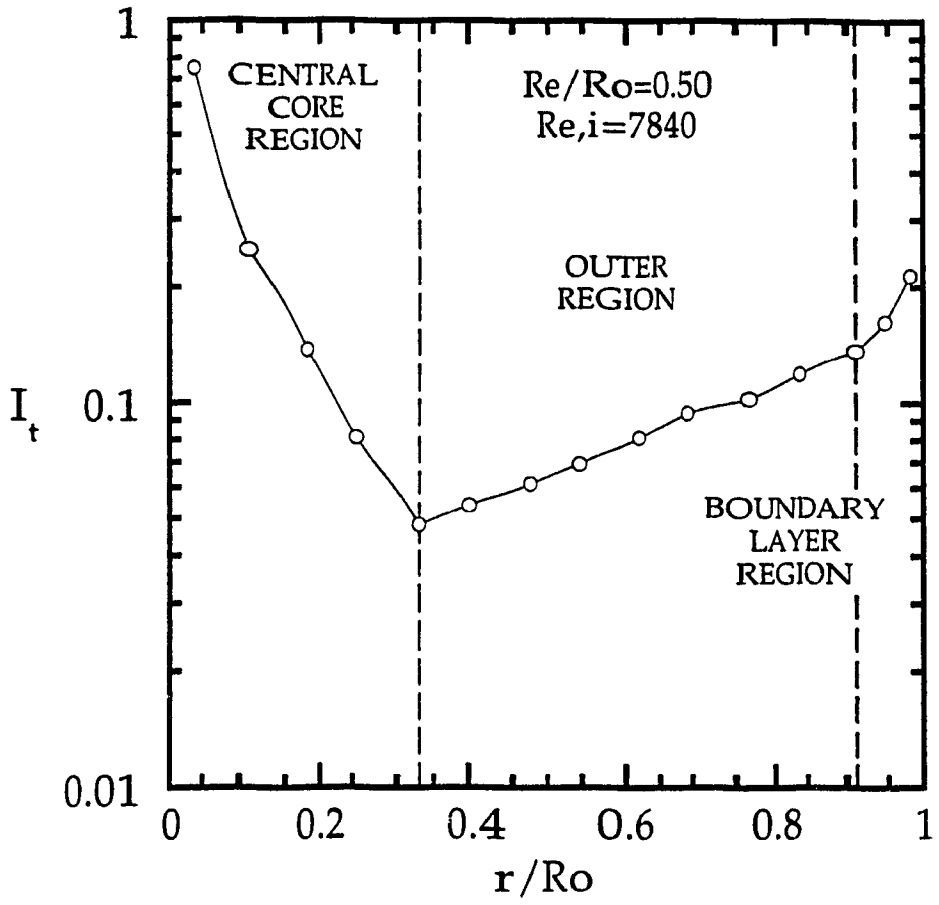

Figure 4.2.1.5 Three-Region Model of Tangential Component of Turbulence Intensity at Main Section

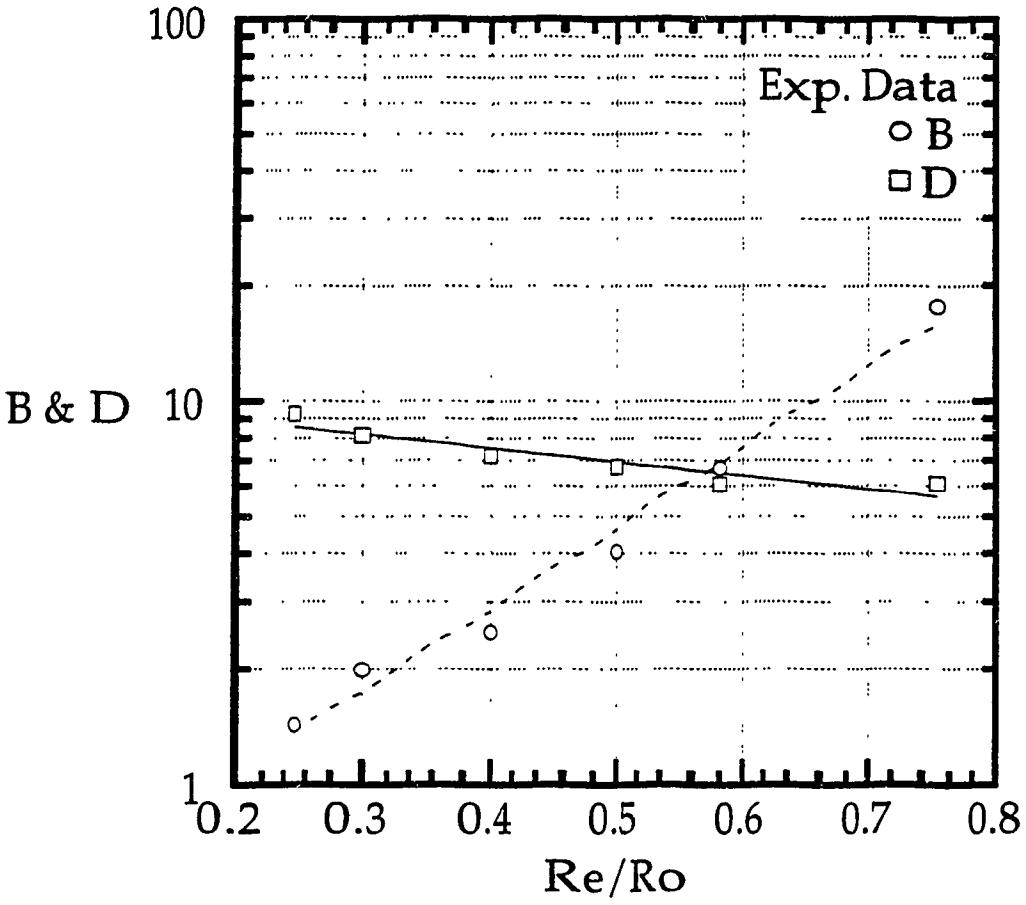

Figure 4.2.2.1 Correlations of B & D versus Re/Ro (Re,i = 13700, lines - eqs.4-5 & 4-6)

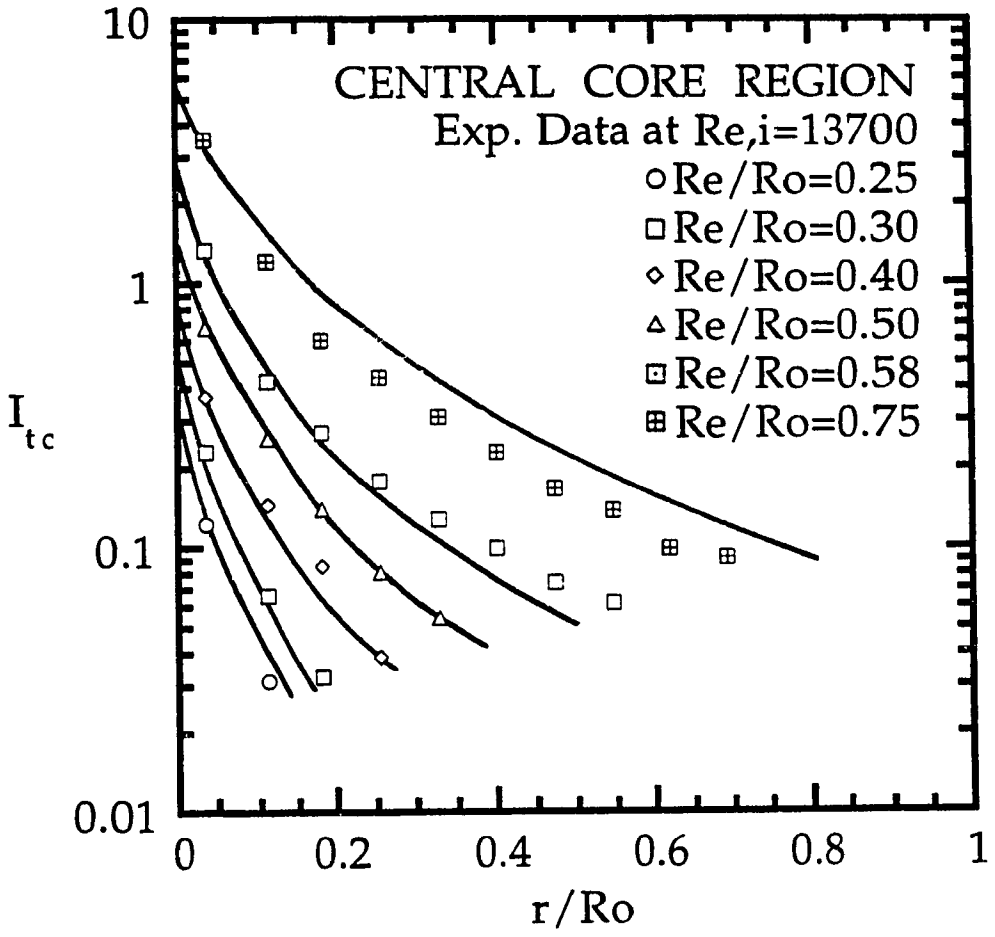

Figure 4.2.2.2 Tangential Component of Turbulence Intensity for Central Core Region at Main Section (lines - eq.4-2)

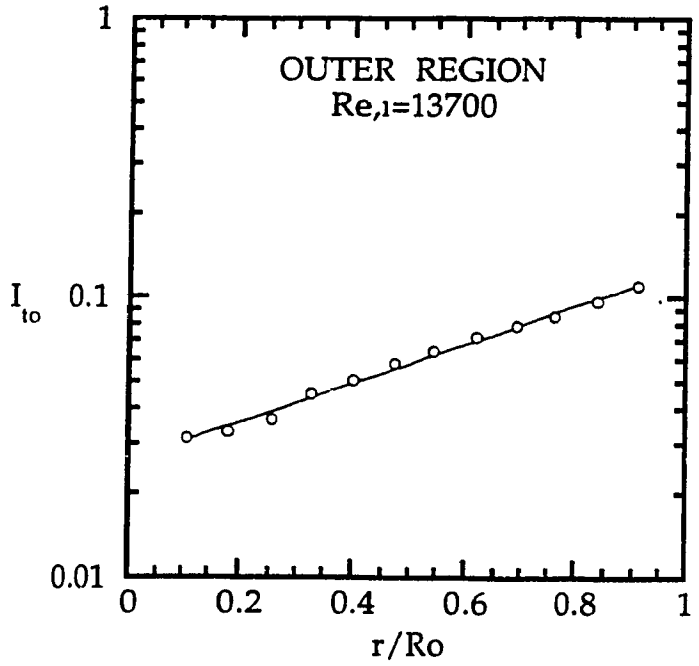

Figure 4.2.3.1 Tangential Component of Turbulence Intensity for Outer Region at Main Section (line - eq.4-7)

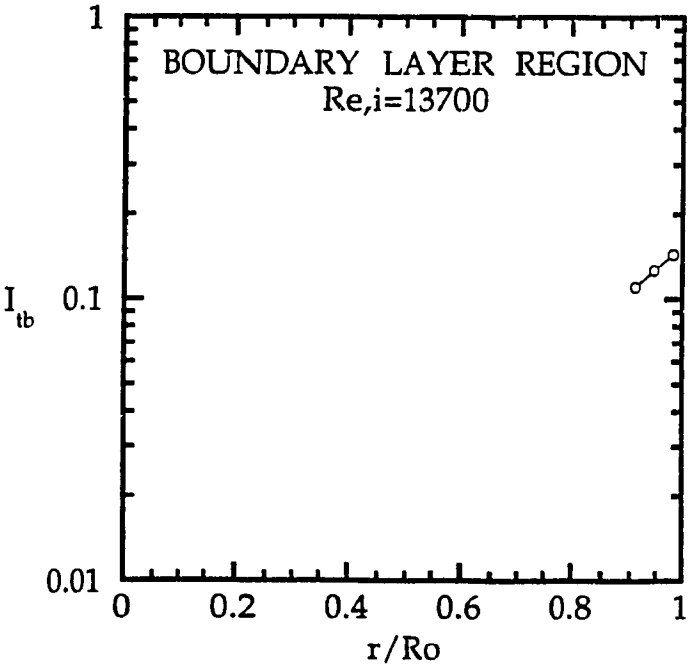

Figure 4.2.4.1 Tangential Component of Turbulence Intensity for Boundary Layer Region at Main Section (line - eq.4-8)

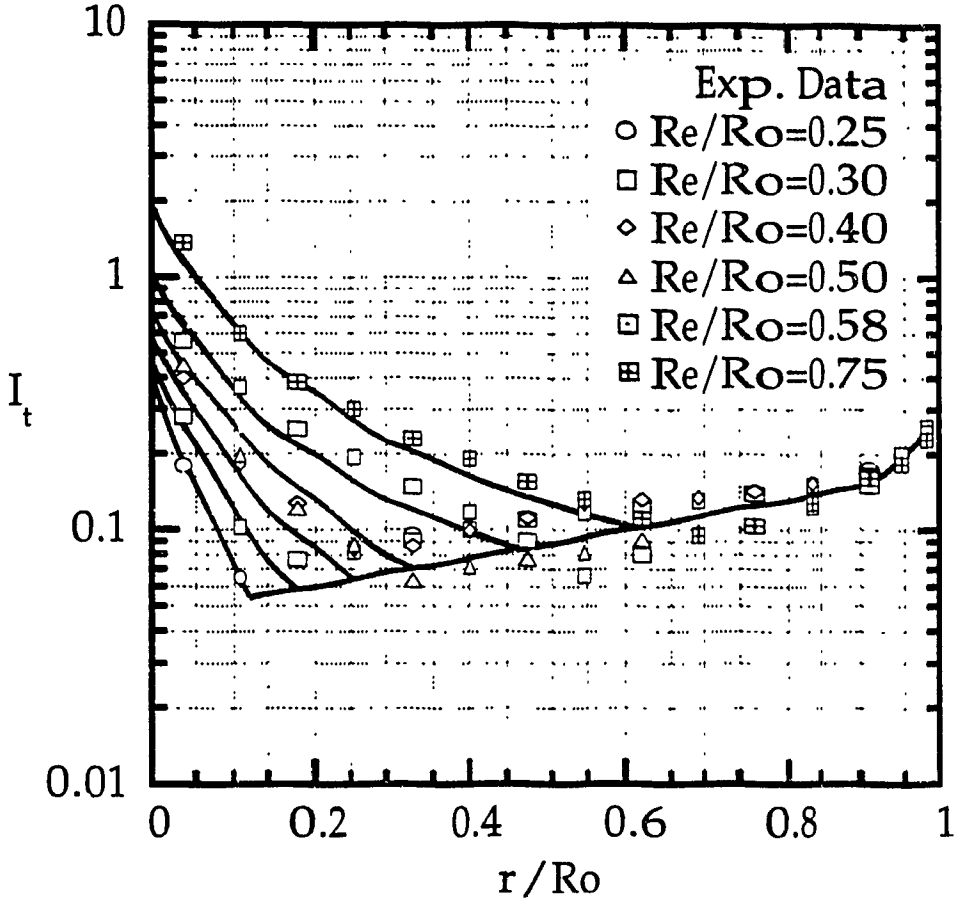

Figure 4.2.4.2 Tangential Component of Turbulence Intensity at Main Section (Re,i = 1960, lines - empirical eqs.)

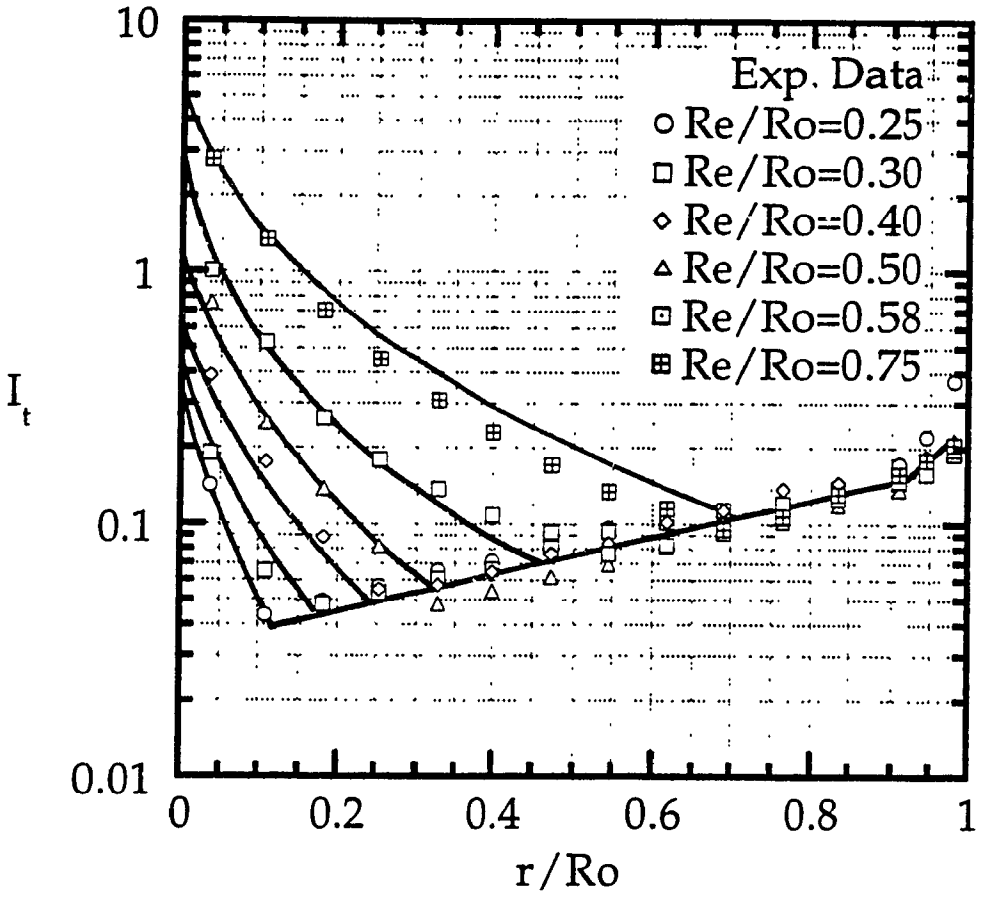

Figure 4.2.4.3 Tangential Component of Turbulence Intensity at Main Section (Re,i = 7840, lines - empirical eqs.)

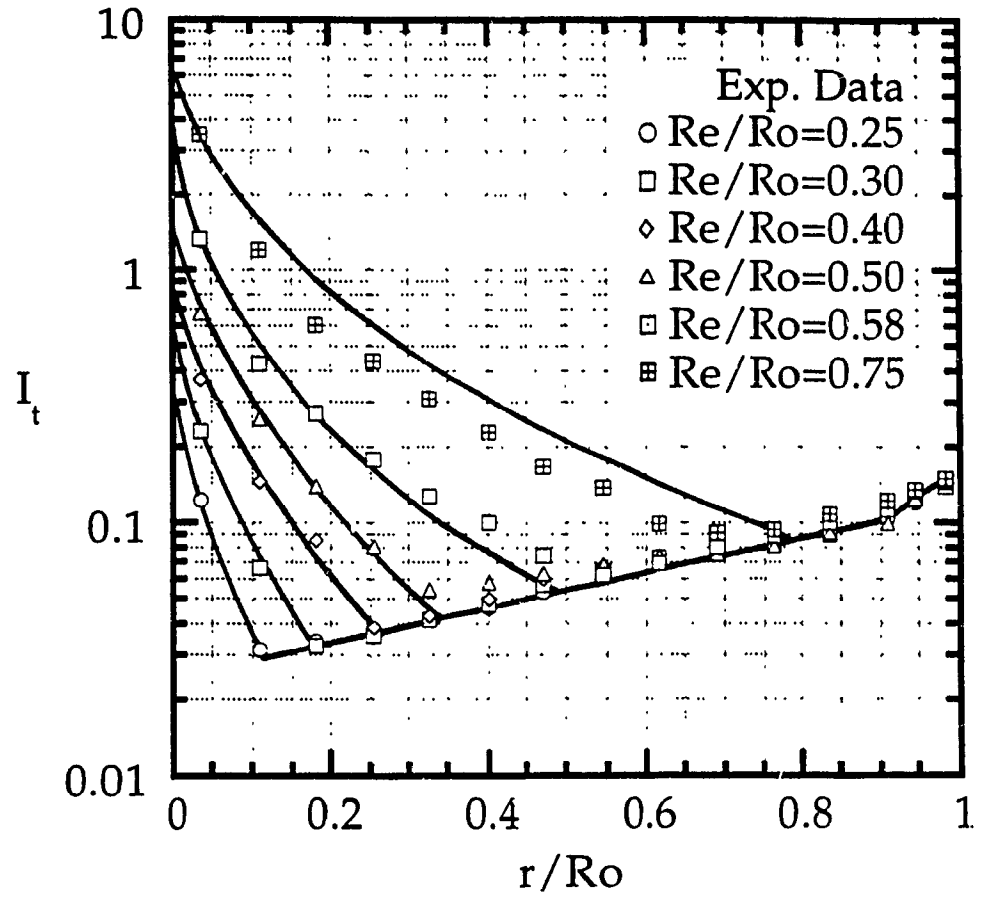

Figure 4.2.4.4 Tangential Component of Turbulence Intensity at Main Section (Re,i = 13700, lines - empirical eqs.)

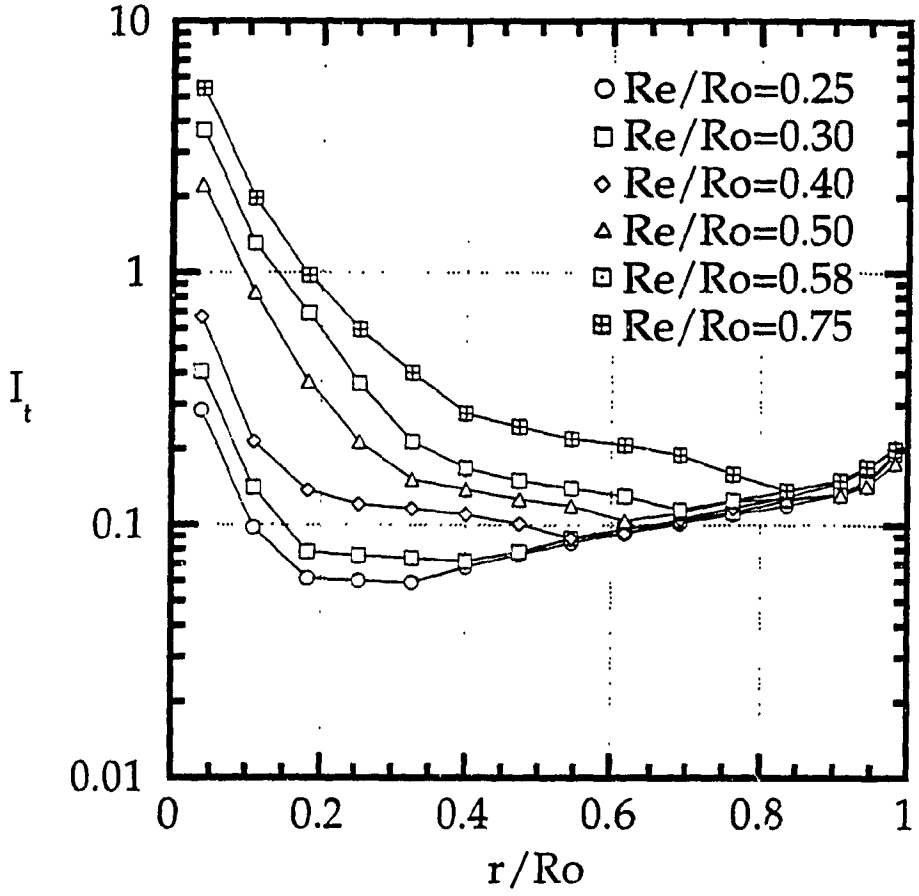

Figure 4.3.1.1 Experimental Tangential Component of Turbulence Intensity near Exit Section (Re,i = 1960)

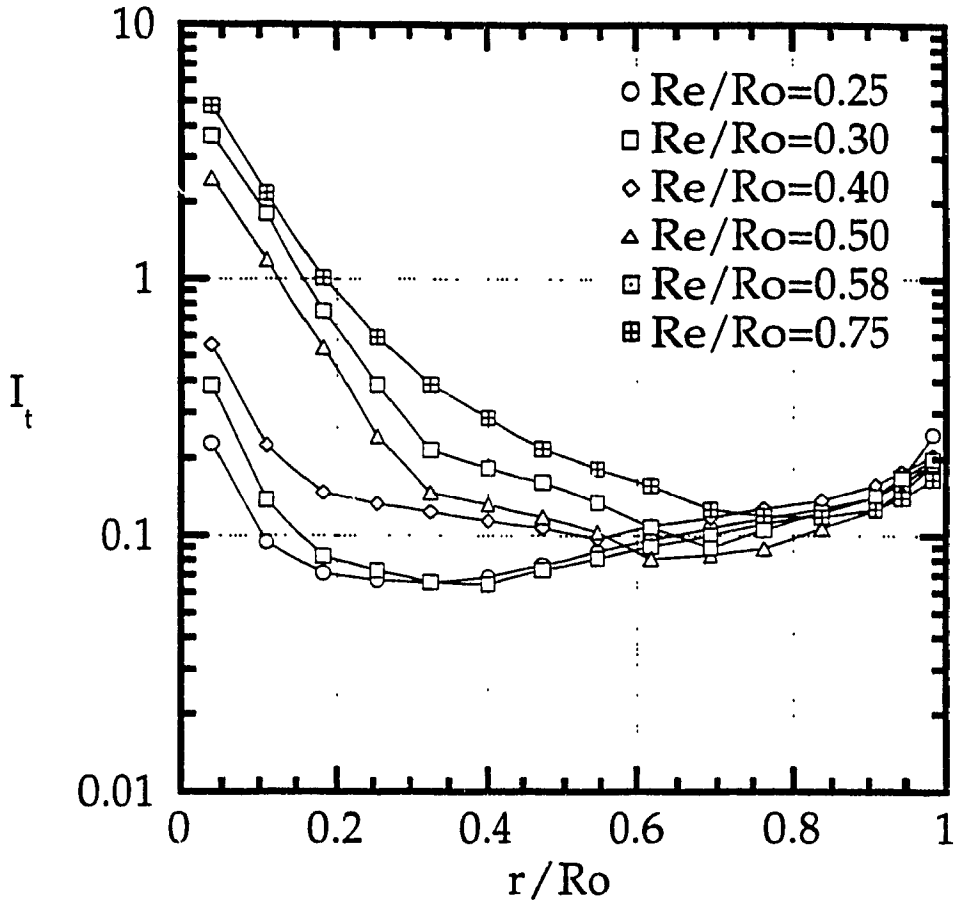

Figure 4.3.1.2 Experimental Tangential Component of Turbulence Intensity near Exit Section (Re,i = 7840)

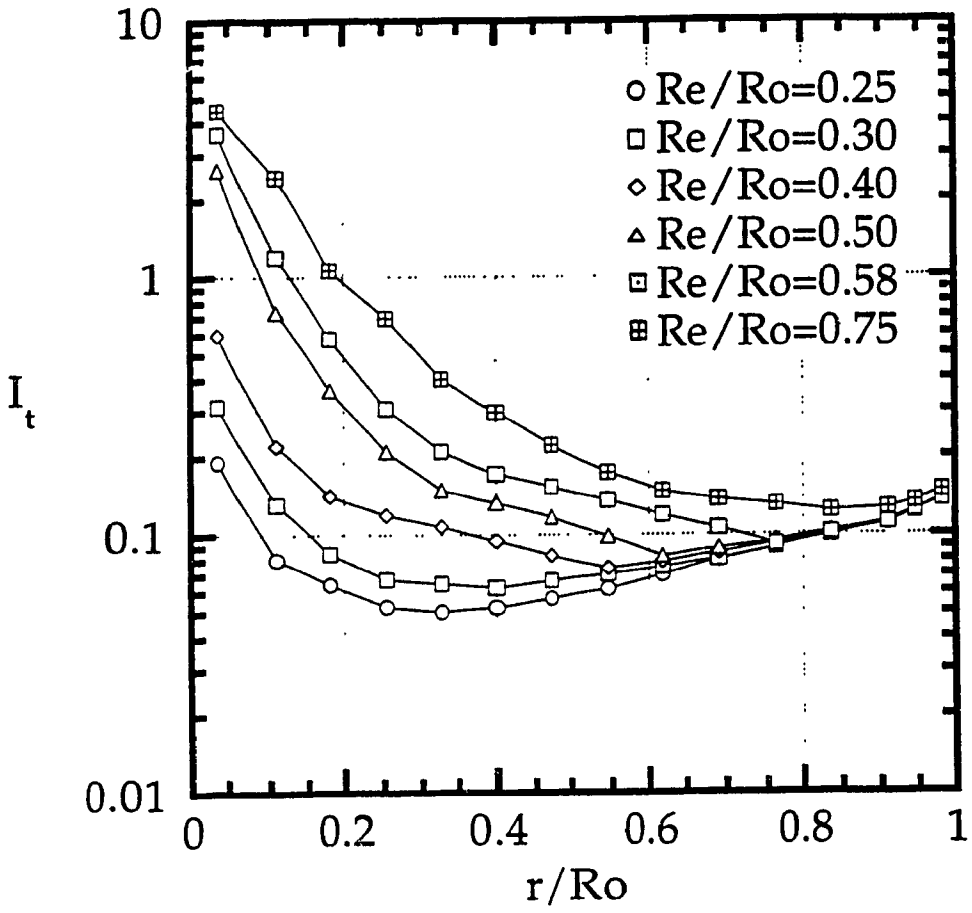

Figure 4.3.1.3 Experimental Tangential Component of Turbulence Intensity near Exit Section (Re,i = 13700)

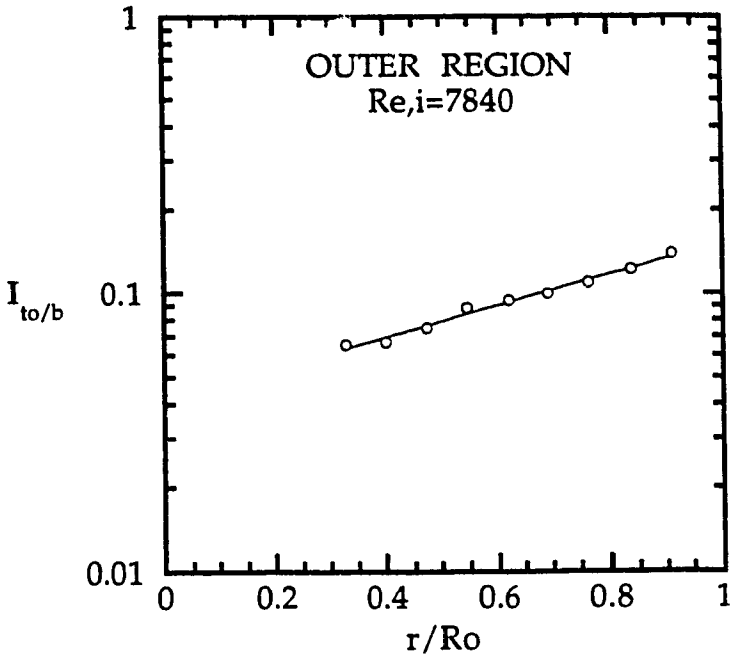

Figure 4.3.2.1 Tangential Component of Turbulence Intensity for Outer Region near Exit Section (line - eq.4-9)

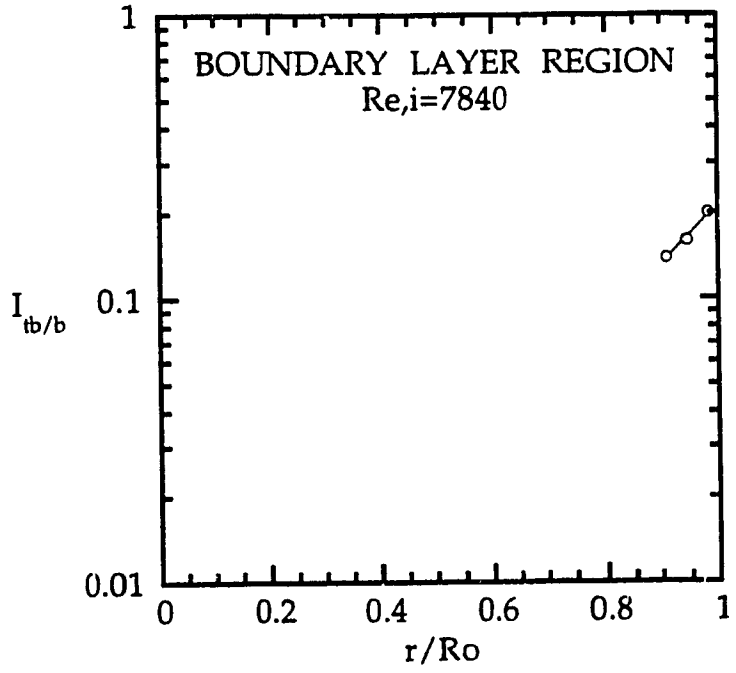

Figure 4.3.2.2 Tangential Component of Turbulence Intensity for Boundary Layer Region near Exit Section (line - eq.4-10)

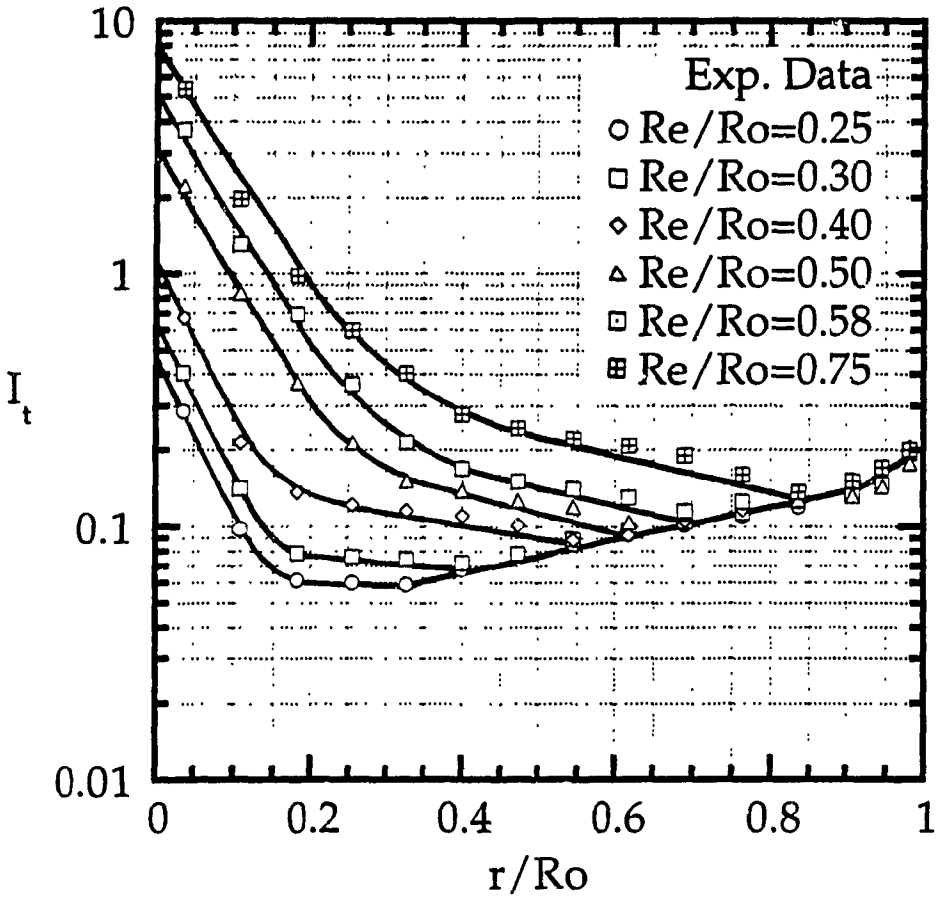

Figure 4.3.2.3 Tangential Component of Turbulence Intensity near Exit Section (Re,i = 1960, lines - empirical eqs.)

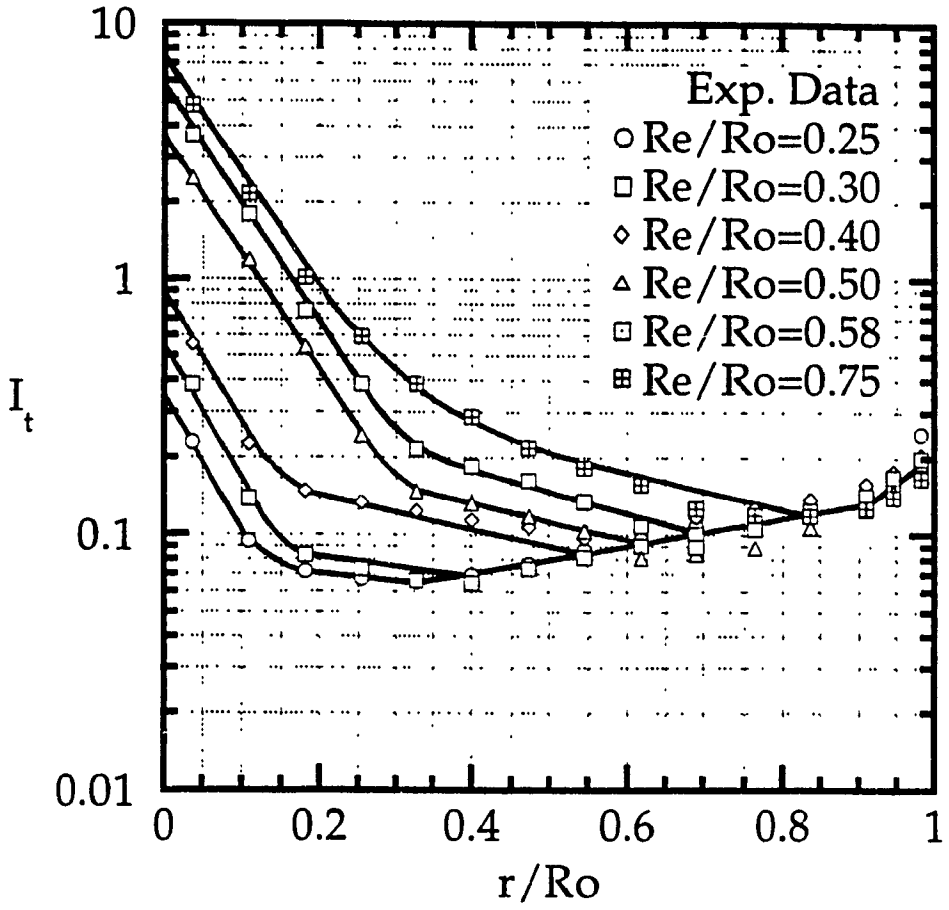

Figure 4.3.2.4 Tangential Component of Turbulence Intensity near Exit Section (Re,i = 7840, lines - empirical eqs.)

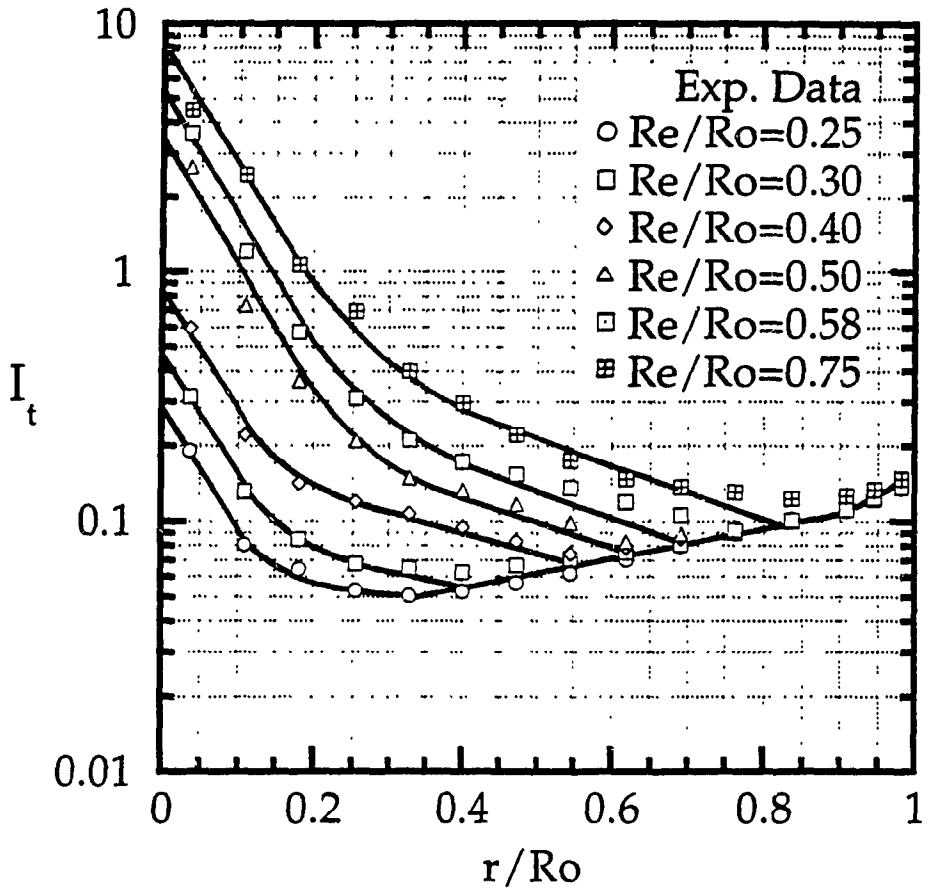

Figure 4.3.2.5 Tangential Component of Turbulence Intensity near Exit Section (Re,i=13700, lines - empirical eqs.)

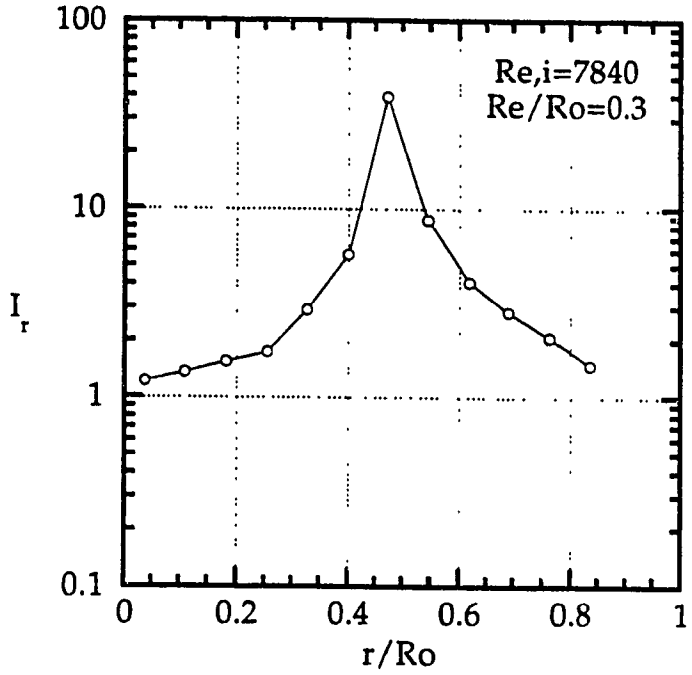

Figure 4.4.1.1 Experimental Radial Component of Turbulence Intensity at Main Section (69% Vortex Chamber Length)

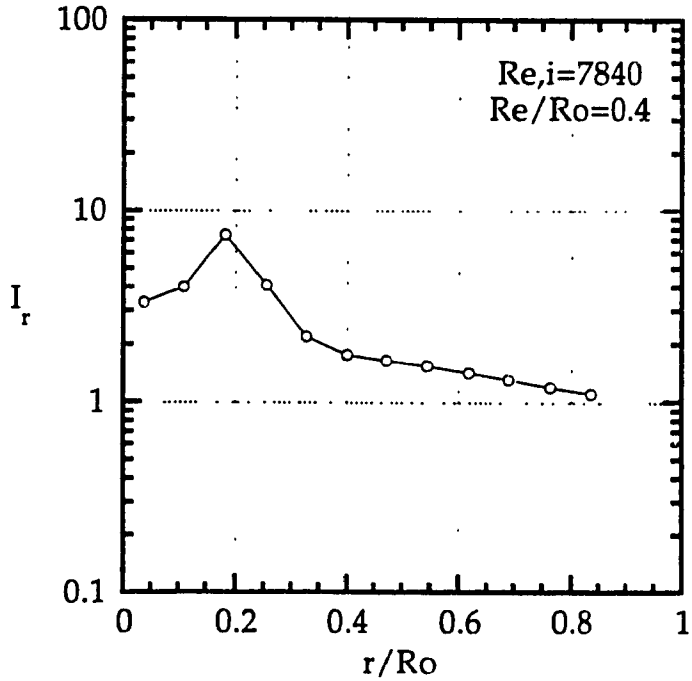

Figure 4.4.1.2 Experimental Radial Component of Turbulence Intensity at Main Section (50% Vortex Chamber Length)

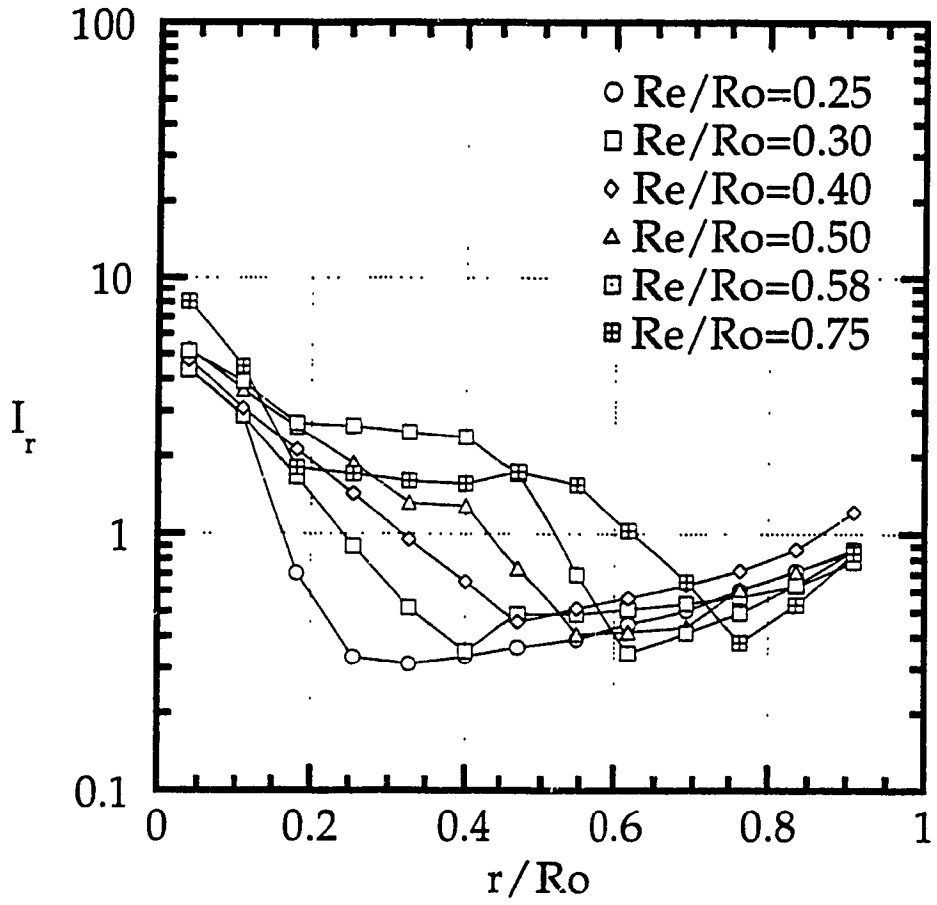

Figure 4.4.2.1 Experimental Radial Component of Turbulence Intensity near Exit Section (Re,i = 1960)

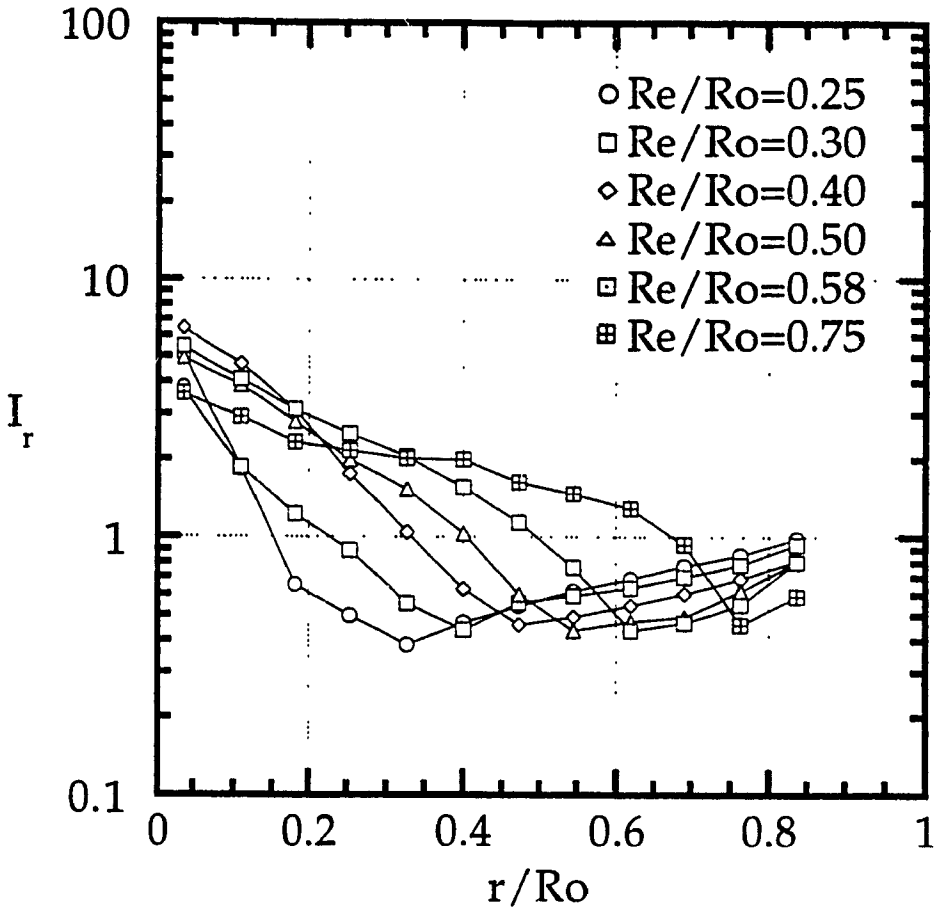

Figure 4.4.2.2 Experimental Radial Component of Turbulence Intensity near Exit Section (Re,i = 7840)

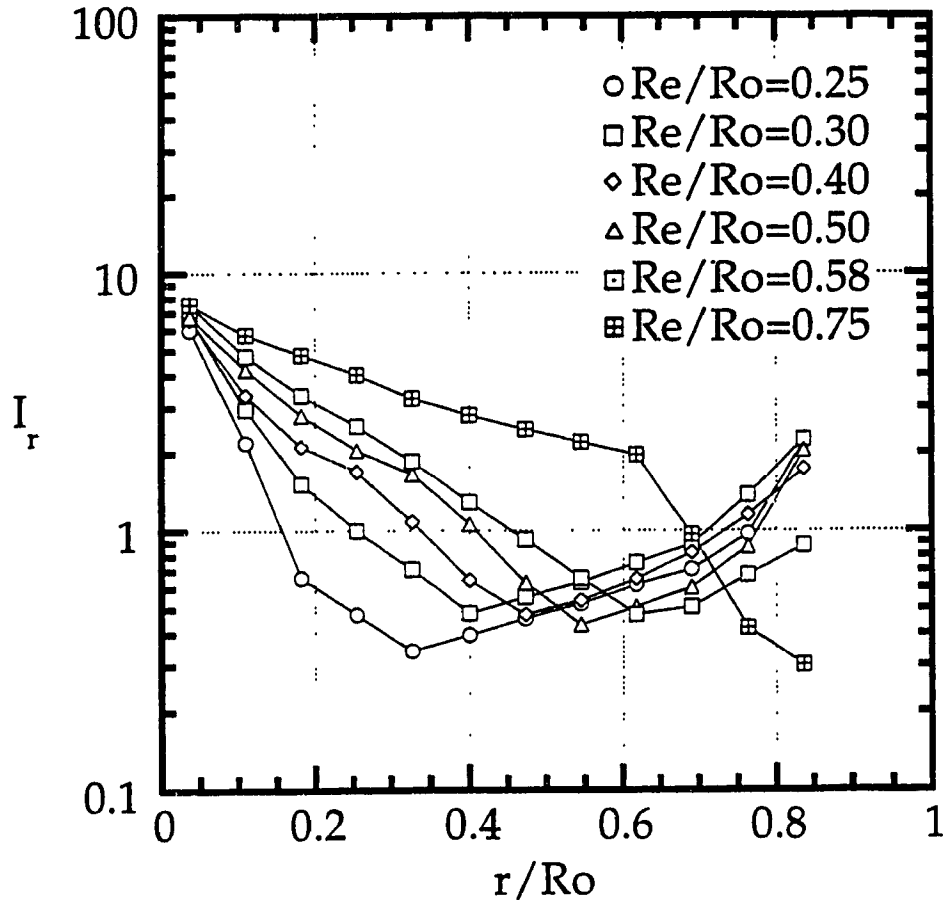

Figure 4.4.2.3 Experimental Radial Component of Turbulence Intensity near Exit Section (Re,i = 13700)

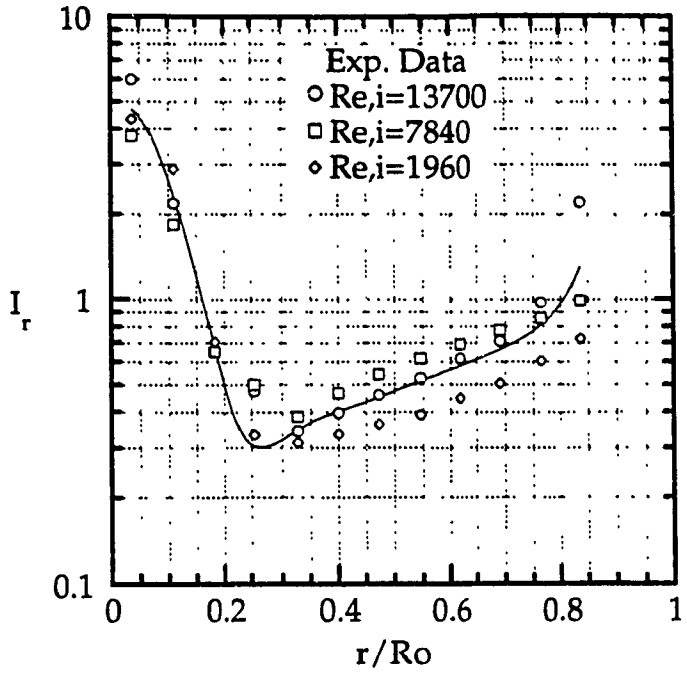

Figure 4.4.2.4 Radial Component of Turbulence Intensity near Exit Section (Re/Ro=0.25, line - average value)

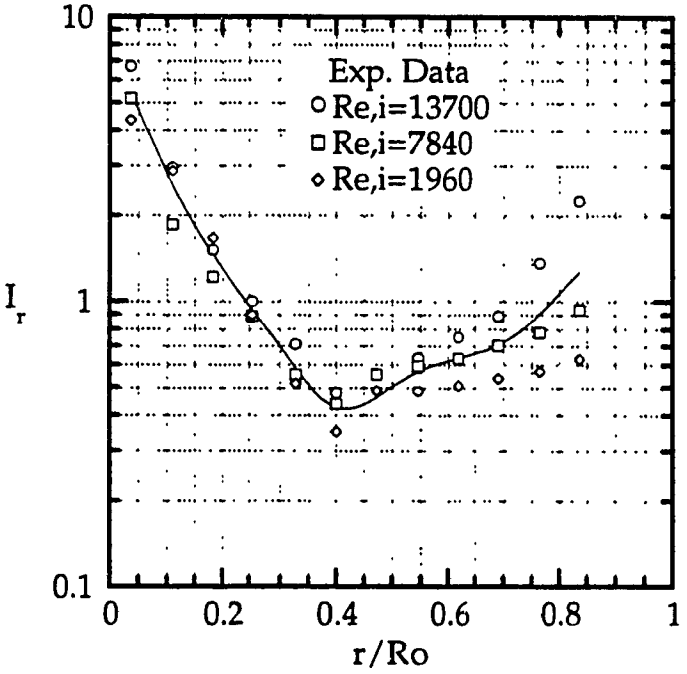

Figure 4.4.2.5 Radial Component of Turbulence Intensity near Exit Section (Re/Ro=0.30, line - average value)

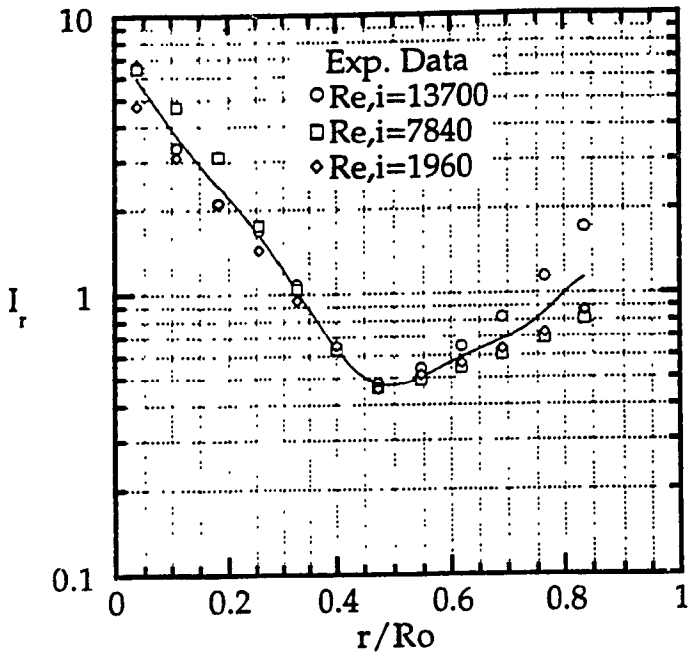

Figure 4.4.2.6 Radial Component of Turbulence Intensity near Exit Section (Re/Ro=0.40, line - average value)

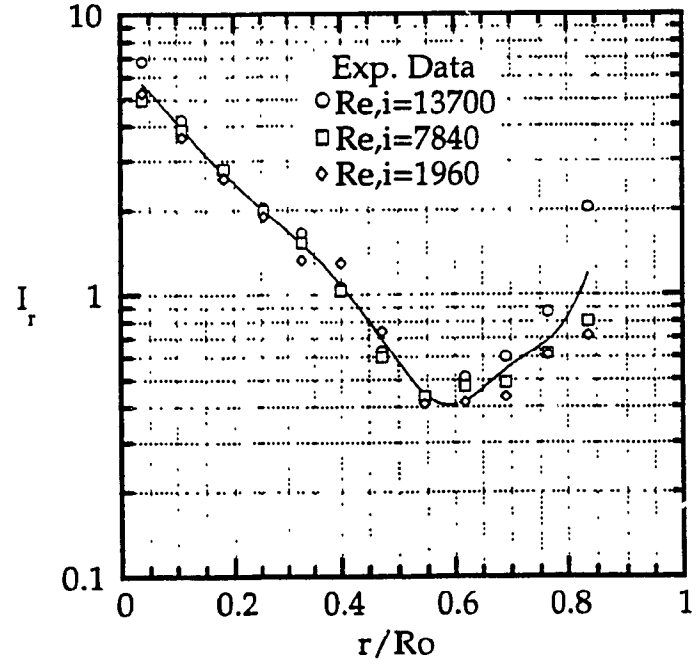

Figure 4.4.2.7 Radial Component of Turbulence Intensity near Exit Section (Re/Ro=0.50, line - average value)

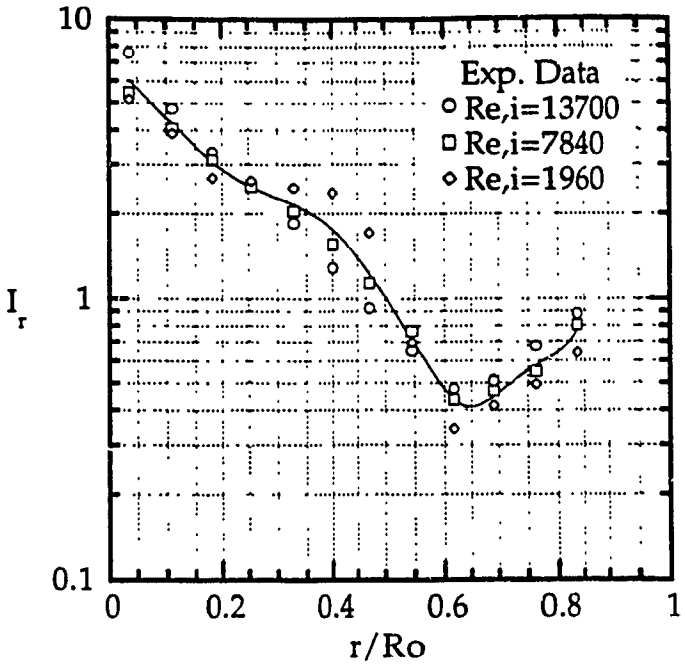

Figure 4.4.2.8 Radial Component of Turbulence Intensity near Exit Section (Re/Ro=0.58, line - average value)

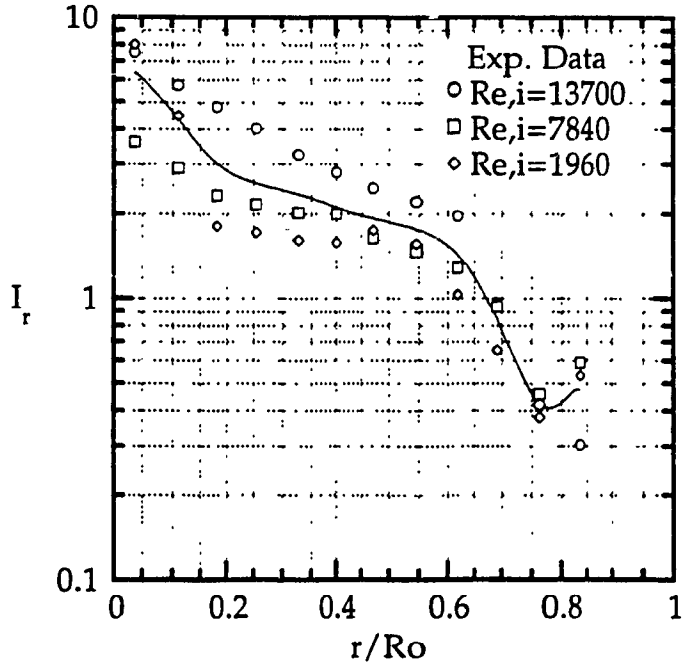

Figure 4.4.2.9 Radial Component of Turbulence Intensity at near Exit Section (Re/Ro=0.75, line - average value)

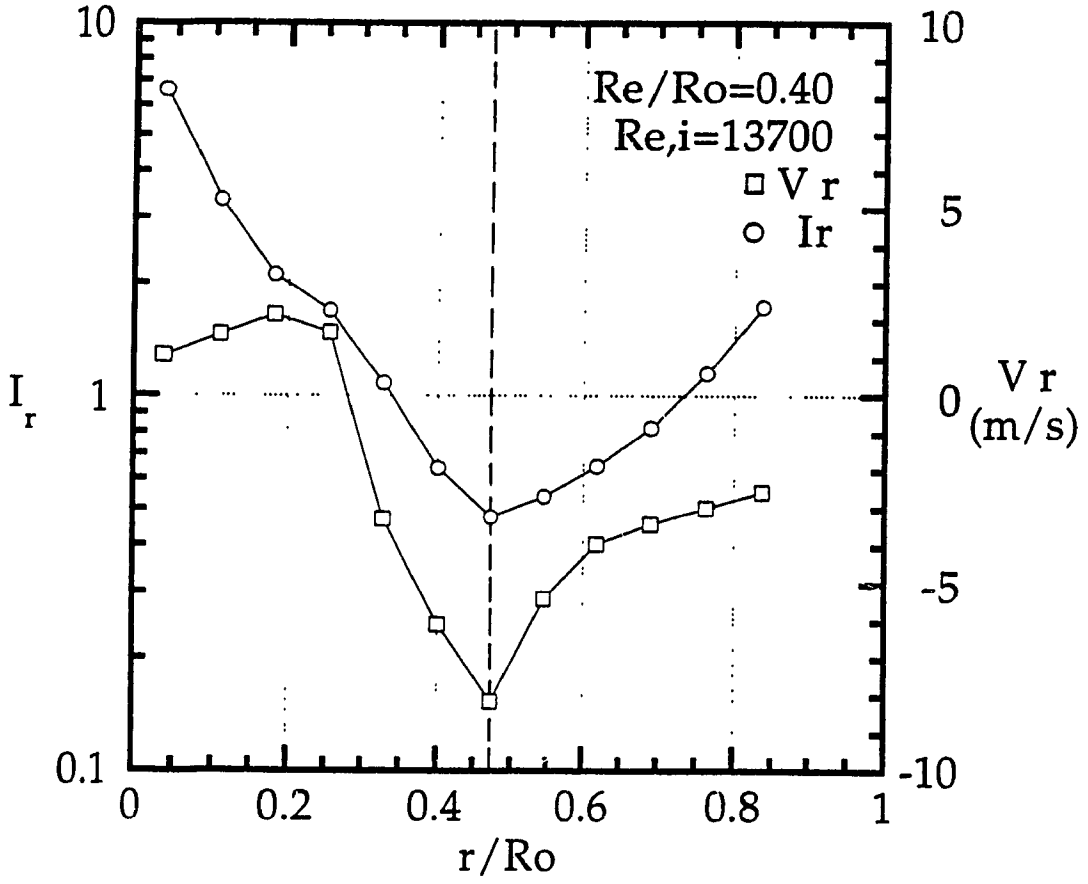

Figure 4.4.2.10 Radial Component of Turbulence Intensity versus Mean Radial Velocity near Exit Section (exp.)

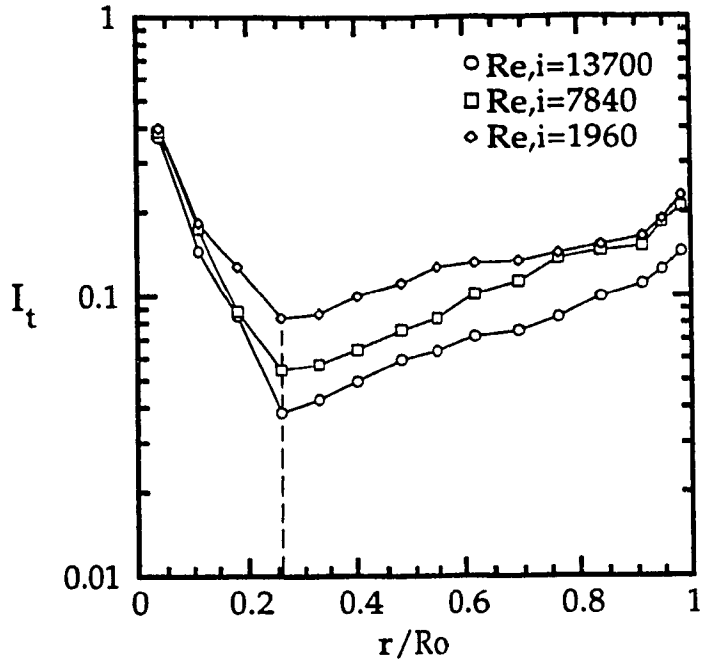

Figure 4.5.1 Experimental Tangential Component of Turbulence Intensity at Main Section (Re/Ro = 0.4)

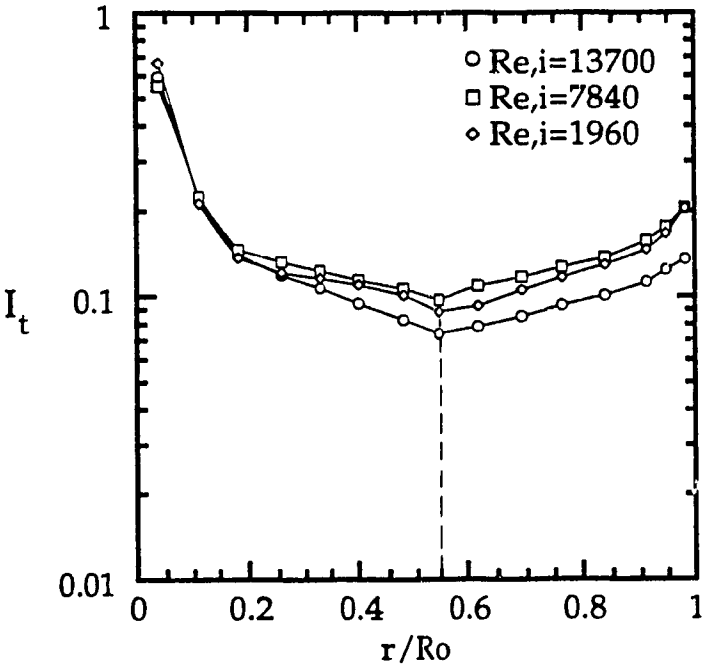

Figure 4.5.2 Experimental Tangential Component of Turbulence Intensity near Exit Section (Re/Ro = 0.4)

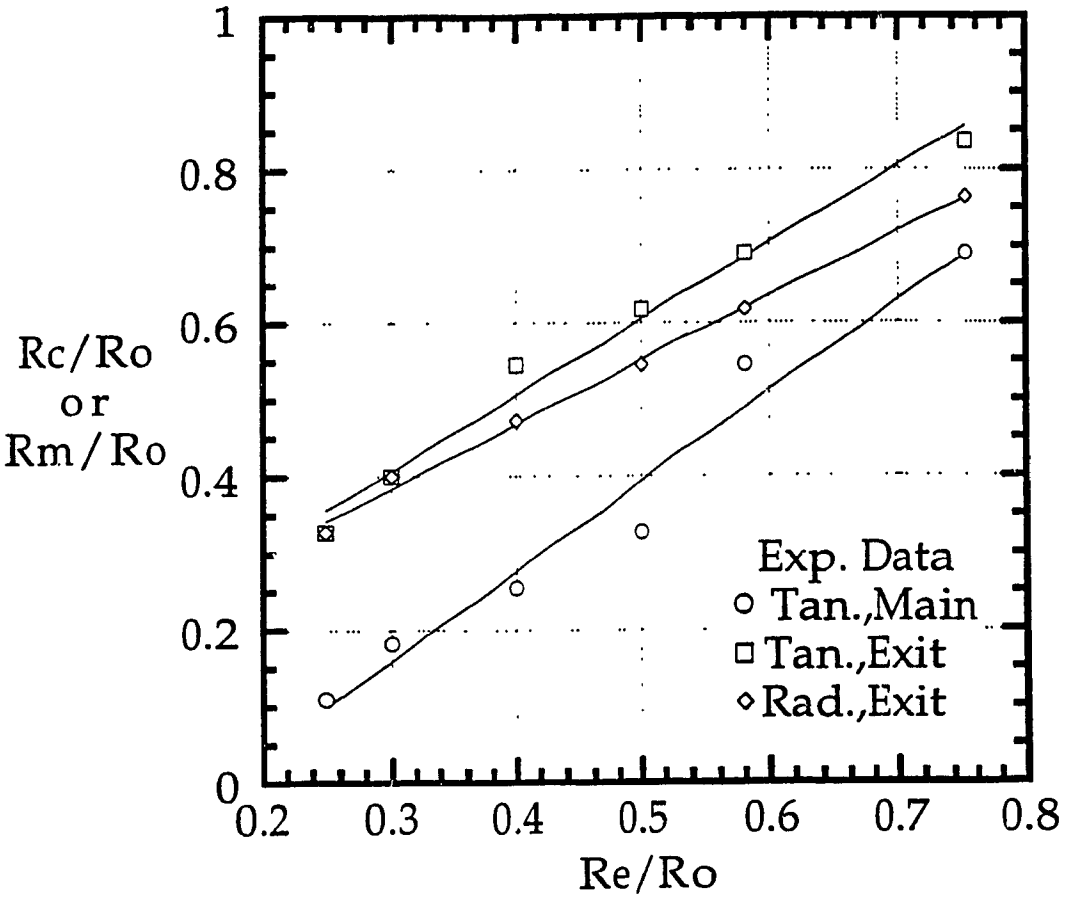

Figure 4.5.3 Location of Minimum Turbulence Intensity (lines - eqs.4-11, 4-12, 4-13)

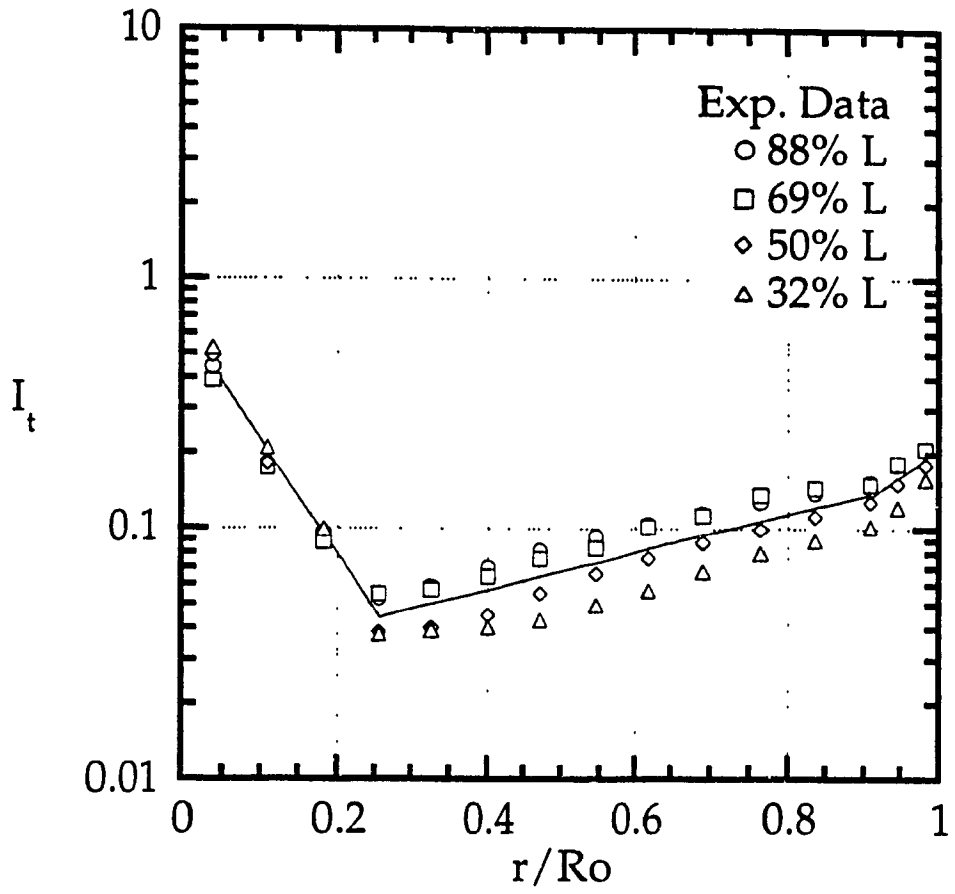

Figure 4.6.1 Tangential Component of Turbulence Intensity at Main Section (Re/Ro=0.40, Re,i=7840, L=Vortex Chamber Length)

Table 4.2.1 Numerical Values of B_1, B_2, D_1, D_2, A_o, C_o, A_b, C_b, $A_{o/b}$, $C_{o/b}$, $A_{b/b}$ and $C_{b/b}$

$R_{e,i}$	1960	7840	13700	Remarks
B_1	0.659	0.334	0.403	Main Section
B_2	1.92	4.88	4.89	
D_1	7.75	9.01	10.5	
D_2	-0.942	-0.671	-0.828	
A_o	0.0619	0.0362	0.0260	Main Section
C_o	-0.970	-1.54	-1.60	
A_b	0.00124	0.000773	0.00394	
C_b	-5.34	-5.79	-3.67	
$A_{o/b}$	0.0386	0.0413	0.0324	Exit Section
$C_{o/b}$	-1.46	-1.31	-1.38	
$A_{b/b}$	0.00233	0.00148	0.00970	
$C_{b/b}$	-4.49	-4.99	-2.71	

Table 4.5.1 Numerical Values of a, b, c and d

$R_{e,i}$		1960	7840	13700	Remarks
R_e/R_o	a	0.0513	0.0349	0.0253	Main Section
< 0.5	b	0.131	0.0773	0.0495	
R_e/R_o	a	0.0193			
≥ 0.5	b	0.102			
R_e/R_o	c	0.0175	0.00985	0.0179	Exit Section
< 0.5	d	0.131	0.156	0.105	
R_e/R_o	c	0.0122	-0.0287	-0.0359	
≥ 0.5	d	0.149	0.175	0.189	

Table 4.6.1 Influence Factors on Turbulence Intensity

Turbu. Intensity		Influence Parameters			Empiric.
Section	Region	$R_{e,i}$	R_e/R_o	β	Equation
Tangent., Main	Core	Yes	Yes	Yes	4-2
	Outer	Yes	No	No	4-7
	B. L.	Yes	No	No	4-8
Tangent., near Exit	Core	Yes	Yes	Yes	
	Outer	Yes	No	No	4-9
	B. L.	Yes	No	No	4-10
Radial, near Exit	Core	No	Yes	Yes	
	Outer	No	Yes	Yes	

Tangent. = Tangential
B.L. = Boundary Layer

Table 4.6.2 Influence Factors on Minimum Turbulence Intensity

Min. Turbulence Intensity		Influence Parameters			Empiric. Equation
		$R_{e,i}$	R_e/R_0	β	
Tangent., Main	Location	No	Yes	Yes	4-11
	Magn.	No	Yes	Yes	4-14
Tangent., near Exit	Location	No	Yes	Yes	4-12
	Magn.	No	Yes	Yes	4-15
Radial, near Exit	Location	No	Yes	Yes	4-13
	Magn.	No	Yes	Yes	4-16, 4-17

Magn. = Magnitude

Table 4.6.3 Deviation of Tangential Component of Turbulence Intensity at Different Locations within Main Section (Re/Ro = 0.40, Re,i = 7840)

%	L/L_{total}	L/L_{total}	L/L_{total}	L/L_{total}
r/R_o	= 88 %	= 69 %	= 50 %	= 32 %
0.036	-4.12	-15.5	5.94	13.7
0.109	-3.07	-6.55	-2.87	12.5
0.182	0.04	-7.29	2.87	4.38
0.255	14.4	19.2	-15.9	-17.7
0.327	20.6	16.9	-17.8	-19.6
0.400	27.3	17.3	-18.0	-26.6
0.473	27.6	18.8	-13.6	-32.8
0.545	27.4	14.2	-9.38	-32.2
0.618	23.0	20.2	-10.2	-33.0
0.691	19.6	17.7	-8.01	-29.4
0.764	15.2	23.0	-10.2	-28.1
0.836	14.3	19.7	-8.13	-25.9
0.909	15.4	12.7	-4.43	-23.7
0.945	13.3	15.2	-4.79	-23.7
0.982	10.3	10.5	-4.64	-16.1

Table 4.6.4 Deviation of Tangential Component of Turbulence Intensity at $Re,i = 7840$ (Main Section)

%	R_e/R_o	R_e/R_o	R_e/R_o	R_e/R_o	R_e/R_o	R_e/R_o
r/R_o	= 0.25	= 0.30	= 0.40	= 0.50	= 0.58	= 0.75
0.036	4.99	7.35	-3.29	-8.03	10.6	9.52
0.109	-1.97	6.40	-21.4	7.30	-12.9	2.20
0.182	-2.56	-0.85	-18.7	6.74	-1.35	17.6
0.255	-5.45	0.90	-2.42	12.7	-7.86	22.9
0.327	-8.61	-1.22	4.81	24.0	-17.0	28.2
0.400	-6.17	1.22	3.67	23.6	-24.2	29.1
0.473	-9.68	-7.28	-1.50	21.5	-34.1	34.0
0.545	-12.8	-10.4	0.31	20.8	10.1	34.4
0.618	-8.92	-8.13	-8.17	15.0	13.9	26.0
0.691	-4.60	-6.95	-7.31	11.1	13.8	10.3
0.764	-2.49	-2.67	-14.1	14.3	11.1	9.48
0.836	-3.43	-4.52	-9.74	10.1	4.82	0.31
0.909	-15.1	0.64	-2.90	7.47	-0.23	-6.54
0.945	-16.8	7.69	0.54	13.9	17.0	3.06
0.982	-38.4	20.0	8.84	6.35	15.1	10.6

Table 4.6.5 Deviation of Tangential Component of Turbulence Intensity for Outer Region at Re,i = 1960 (near Exit Section)

%	R_e/R_o	R_e/R_o	R_e/R_o	R_e/R_o	R_e/R_o	R_e/R_o
r/R_o	= 0.25	= 0.30	= 0.40	= 0.50	= 0.58	= 0.75
0.327	0.00					
0.400	-2.66	2.66				
0.473	-1.07	1.07				
0.545	-2.61	1.47	1.14			
0.618	-3.73	-0.10	-3.85	7.67		
0.691	-5.73	-3.09	-2.11	4.27	6.67	
0.764	-6.43	-4.45	-0.96	5.50	6.36	
0.836	-7.21	-2.67	0.13	-1.50	5.54	5.71
0.909	-5.93	-5.83	4.19	-6.25	6.66	7.14

Table 4.6.6 Deviation of Tangential Component of Turbulence Intensity for Boundary Layer Region at Re,i = 13700 (near Exit Section)

%	R_e/R_o	R_e/R_o	R_e/R_o	R_e/R_o	R_e/R_o	R_e/R_o
r/R_o	= 0.25	= 0.30	= 0.40	= 0.50	= 0.58	= 0.75
0.909	-3.13	-2.28	-1.09	-1.96	-2.37	10.8
0.945	-1.35	-2.26	-0.51	-1.62	-0.99	6.75
0.982	-1.51	-0.59	-2.02	-0.80	-1.49	6.43

Table 4.6.7 Deviation of Radial Component of Turbulence Intensity at $Re/\bar{R}o = 0.25$ (near Exit Section)

% r/R_o	$R_{e,i}$ = 13700	$R_{e,i}$ = 7840	$R_{e,i}$ = 1960
0.036	27.3	-19.6	-7.69
0.109	-5.31	-20.1	25.4
0.182	-1.95	-3.01	4.96
0.255	9.11	14.4	-23.5
0.327	-1.14	10.9	-9.78
0.400	-0.66	16.8	-16.1
0.473	1.19	19.3	-20.5
C 545	2.83	20.8	-23.6
0.618	5.56	18.1	-23.6
0.691	7.04	16.9	-23.9
0.764	20.0	5.32	-25.3
0.836	68.9	-24.4	-44.6

Table 4.6.8 Deviation of Radial Component of Turbulence Intensity at Re/Ro = 0.50 (near Exit Section)

% r/R_o	$R_{e,i}$ = 13700	$R_{e,i}$ = 7840	$R_{e,i}$ = 1960
0.036	19.7	-12.5	-7.18
0.109	7.43	-0.80	-6.63
0.182	2.49	2.56	-5.05
0.255	3.37	0.96	-4.33
0.327	10.0	1.85	-11.9
0.400	-5.95	-8.28	14.2
0.473	-4.20	-8.46	12.7
0.545	1.76	2.29	-4.05
0.618	9.34	1.51	-10.8
0.691	18.5	-3.97	-14.5
0.764	24.0	-11.5	-12.5
0.836	72.1	-32.5	-39.6

CHAPTER 5

KINETIC ENERGY

5.1 General

The simplest statistical properties of a turbulent flow are the mean squares and second-order mean products of the velocity fluctuation components at a fixed point. The mean squares of fluctuating velocity components in the radial, tangential and axial directions can be regarded as twice the kinetic energy of the fluctuating motion in each direction. The half of the sum of the mean squares of the three velocity fluctuation components is generally regarded as the total turbulence kinetic energy due to the fluctuating motion, which is independent of the coordinate axes as a scalar.

The equations of motion for turbulent flows are

radial direction

$$\rho(\overline{V}_r\frac{\partial\overline{V}_r}{\partial r} + \frac{1}{r}\overline{V}_\theta\frac{\partial\overline{V}_r}{\partial\theta} + \overline{V}_z\frac{\partial\overline{V}_r}{\partial z} - \frac{\overline{V}_\theta^2}{r})$$
$$= -\frac{\partial\overline{p}}{\partial r} + \mu(\nabla^2\overline{V}_r - \frac{\overline{V}_r}{r^2} - \frac{2}{r^2}\frac{\partial\overline{V}_\theta}{\partial\theta}) -$$
$$- \rho[\frac{\partial}{\partial r}(\overline{V_r'^2}) + \frac{1}{r}\frac{\partial}{\partial\theta}(\overline{V_r'V_\theta'}) + \frac{\partial}{\partial z}(\overline{V_r'V_z'}) + \frac{1}{r}(\overline{V_r'^2} - \overline{V_\theta'^2})] \qquad (5\text{-}1)$$

tangential direction

$$\rho(\overline{V}_r\frac{\partial\overline{V}_\theta}{\partial r} + \frac{1}{r}\overline{V}_\theta\frac{\partial\overline{V}_\theta}{\partial\theta} + \overline{V}_z\frac{\partial\overline{V}_\theta}{\partial z} + \frac{\overline{V}_r\overline{V}_\theta}{r})$$
$$= -\frac{1}{r}\frac{\partial\overline{p}}{\partial\theta} + \mu(\nabla^2\overline{V}_\theta - \frac{\overline{V}_\theta}{r^2} + \frac{2}{r^2}\frac{\partial\overline{V}_r}{\partial\theta}) -$$
$$- \rho[\frac{\partial}{\partial r}(\overline{V_r'V_\theta'}) + \frac{1}{r}\frac{\partial}{\partial\theta}(\overline{V_\theta'^2}) + \frac{\partial}{\partial z}(\overline{V_\theta'V_z'}) + \frac{2}{r}(\overline{V_r'V_\theta'})] \qquad (5\text{-}2)$$

axial direction

$$\rho(\overline{V}_r\frac{\partial\overline{V}_z}{\partial r} + \frac{1}{r}\overline{V}_\theta\frac{\partial\overline{V}_z}{\partial\theta} + \overline{V}_z\frac{\partial\overline{V}_z}{\partial z})$$
$$= -\frac{\partial\overline{p}}{\partial z} + \mu\nabla^2\overline{V}_z - \rho[\frac{\partial}{\partial r}(\overline{V_r'V_z'}) + \frac{1}{r}\frac{\partial}{\partial\theta}(\overline{V_\theta'V_z'}) + \frac{\partial}{\partial z}(\overline{V_z'^2}) + \frac{1}{r}(\overline{V_r'V_z'})] \quad (5\text{-}3)$$

The term on the left-hand side of equations represents the inertia force (D'Alembert's principle). The terms on the right-hand side of equations represent the pressure gradient, the viscous stresses in terms of the mean velocity gradient, and the Reynolds stresses or the apparent stresses due to the exchange of momentum in the turbulent mixing process.

Based on these equations, analyses of the kinetic energy and the Reynolds shear stresses are performed. The concerning derivation is detailed in the Appendix A.

5.2 Equations of Kinetic Energy for Mean Motion

5.2.1 Equation for Radial Direction

For an axisymmetric flow with negligible axial gradient, the equation of the kinetic energy in the radial direction due to the mean motion is derived as follows:

$$\overline{V}_r\frac{\partial}{\partial r}(\frac{1}{2}\overline{V}_r^2) - \overline{V}_r(\frac{\overline{V}_\theta^2}{r})$$
$$= -\frac{\overline{V}_r}{\rho}\frac{\partial\overline{p}}{\partial r} + \nu\overline{V}_r[(\frac{\partial^2\overline{V}_r}{\partial r^2} + \frac{1}{r}\frac{\partial\overline{V}_r}{\partial r}) - \frac{\overline{V}_r}{r^2}] - \overline{V}_r[\frac{\partial}{\partial r}(\overline{V_r'^2}) + \frac{1}{r}(\overline{V_r'^2} - \overline{V_\theta'^2})] \quad (5\text{-}4)$$

or

$$\frac{1}{2}\overline{V}_r^2 = \int \{-\frac{1}{\rho}\frac{\partial\overline{p}}{\partial r} + \nu(\frac{\partial^2\overline{V}_r}{\partial r^2} + \frac{1}{r}\frac{\partial\overline{V}_r}{\partial r} - \frac{\overline{V}_r}{r^2}) -$$
$$-[\frac{\partial}{\partial r}(\overline{V_r'^2}) + \frac{1}{r}(\overline{V_r'^2} - \overline{V_\theta'^2})] + \frac{\overline{V}_\theta^2}{r}\}\,dr \quad (5\text{-}5)$$

The terms on the right-hand side of equation (5-5) represent the contribution of the pressure gradient, the contribution of the viscous part in terms of the mean radial velocity gradient and the mean radial velocity, the contribution of the Reynolds normal stresses $\overline{V_r'^2}$ and $\overline{V_\theta'^2}$, and the contribution of the inertia part to the kinetic energy. However, there is no apparent effect of the Reynolds shear stresses and the normal stress $\overline{V_z'^2}$ on the kinetic energy.

The fourth term is equivalent to the normal acceleration of the rotating particles, which is balanced with the centrifugal force required by a circular motion. The first term is the pressure gradient along the radial direction, which is equivalent to a centrifugal force acting in the opposite direction. The first term and the fourth term are almost equal in the magnitude, but are in the opposite directions. Therefore, equation (5-5) can be simplified as follows:

$$\frac{1}{2}\overline{V}_r^2 = \int \{\nu(\frac{\partial^2\overline{V}_r}{\partial r^2} + \frac{1}{r}\frac{\partial\overline{V}_r}{\partial r} - \frac{\overline{V}_r}{r^2}) - [\frac{\partial}{\partial r}(\overline{V_r'^2}) + \frac{1}{r}(\overline{V_r'^2} - \overline{V_\theta'^2})]\}\, dr \qquad (5\text{-}6)$$

The major contribution to the kinetic energy is shown to be the viscousness and the normal stresses. In the case of a non-viscous flow, the viscous effects can be neglected. Thus, equation (5-6) can be further simplified as follows:

$$\frac{1}{2}\overline{V}_r^2 = -\int [\frac{\partial}{\partial r}(\overline{V_r'^2}) + \frac{1}{r}(\overline{V_r'^2} - \overline{V_\theta'^2})]\, dr \qquad (5\text{-}7)$$

It is shown that only the Reynolds normal stresses in the radial and tangential directions contribute to the kinetic energy in the radial direction due to the mean motion.

5.2.2 Equation for Tangential Direction

For an axisymmetric flow with negligible axial gradient, the equation of the kinetic energy in the tangential direction due to the mean motion is derived as follows:

$$\overline{V}_r\frac{\partial}{\partial r}(\frac{1}{2}\overline{V}_\theta^2) + \overline{V}_r(\frac{\overline{V}_\theta^2}{r})$$
$$= \nu\overline{V}_\theta(\frac{\partial^2\overline{V}_\theta}{\partial r^2} + \frac{1}{r}\frac{\partial\overline{V}_\theta}{\partial r} - \frac{\overline{V}_\theta}{r^2}) - \overline{V}_\theta[\frac{\partial}{\partial r}(\overline{V_r'V_\theta'}) + \frac{2}{r}\overline{V_r'V_\theta'}] \qquad (5\text{-}8)$$

or

$$\frac{1}{2}\overline{V}_\theta^2 = \int \{\nu\frac{\overline{V}_\theta}{\overline{V}_r}(\frac{\partial^2\overline{V}_\theta}{\partial r^2} + \frac{1}{r}\frac{\partial\overline{V}_\theta}{\partial r} - \frac{\overline{V}_\theta}{r^2}) - \frac{\overline{V}_\theta}{\overline{V}_r}[\frac{\partial}{\partial r}(\overline{V_r'V_\theta'}) + \frac{2}{r}\overline{V_r'V_\theta'}] - \frac{\overline{V}_\theta^2}{r}\}\,dr \qquad (5\text{-}9)$$

The terms on the right-hand side of equation (5-9) represent the contribution of the viscous part in terms of the mean tangential velocity gradient and the mean tangential velocity, the contribution of the Reynolds shear stress $\overline{V_r'V_\theta'}$, and the contribution of the inertia part to the kinetic energy. There is no apparent effect of the Reynolds normal stresses and the Reynolds shear stresses, except $\overline{V_r'V_\theta'}$, on the kinetic energy, and no apparent effect of the pressure gradient on the kinetic energy either.

In the case of simple vortex flows, $\overline{V}_\theta = c/r$ and $\overline{V}_\theta = mr$, the first term will be zero. Equation (5-9) becomes

$$\frac{1}{2}\overline{V}_\theta^2 = -\int \{\frac{\overline{V}_\theta}{\overline{V}_r}[\frac{\partial}{\partial r}(\overline{V_r'V_\theta'}) + \frac{2}{r}\overline{V_r'V_\theta'}] - \frac{\overline{V}_\theta^2}{r}\}\,dr \qquad (5\text{-}10)$$

The major contributors to the kinetic energy in the tangential direction due to the mean motion are the Reynolds radial-tangential shear stress and the inertia force.

5.2.3 Equation for Axial Direction

Similarly, for an axisymmetric flow with negligible axial gradient, the equation of the kinetic energy in the axial direction due to the mean motion is derived as follows:

$$\overline{V}_r \frac{\partial}{\partial r}\left(\frac{1}{2}\overline{V}_z^2\right) = \nu\overline{V}_z\left(\frac{\partial^2\overline{V}_z}{\partial r^2} + \frac{1}{r}\frac{\partial\overline{V}_z}{\partial r}\right) - \overline{V}_z\left[\frac{\partial}{\partial r}\left(\overline{V_r'V_z'}\right) + \frac{1}{r}\overline{V_r'V_z'}\right] \tag{5-11}$$

or

$$\frac{1}{2}\overline{V}_z^2 = \int \left\{\nu\frac{\overline{V}_z}{\overline{V}_r}\left(\frac{\partial^2\overline{V}_z}{\partial r^2} + \frac{1}{r}\frac{\partial\overline{V}_z}{\partial r}\right) - \frac{\overline{V}_z}{\overline{V}_r}\left[\frac{\partial}{\partial r}\left(\overline{V_r'V_z'}\right) + \frac{1}{r}\overline{V_r'V_z'}\right]\right\} dr \tag{5-12}$$

The terms on the right-hand side of equation (5-12) represent the contribution of the viscous part, in terms of the mean axial velocity gradient, and the contribution of the Reynolds shear stress $\overline{V_r'V_z'}$ to the kinetic energy. There is no apparent effect of the Reynolds normal stresses and the Reynolds shear stresses, except $\overline{V_r'V_z'}$, on the kinetic energy, and no apparent effect of either the pressure gradient or the inertia part on the kinetic energy. The viscousness and the radial-axial shear stress make the major contribution to the kinetic energy in the axial direction due to the mean motion.

For a non-viscous flow or in the case where the viscous effect is much smaller than the effect due to the shear stress, equation (5-12) can be further simplified, that is,

$$\frac{1}{2}\overline{V}_z^2 = -\int \frac{\overline{V}_z}{\overline{V}_r}\left[\frac{\partial}{\partial r}\left(\overline{V_r'V_z'}\right) + \frac{1}{r}\overline{V_r'V_z'}\right] dr \tag{5-13}$$

It is shown that the Reynolds radial-axial shear stress is the major contributor to the kinetic energy in the axial direction due to the mean motion.

5.3 Equations of Total Kinetic Energy

For an axisymmetric flow with negligible axial gradient, the equations of total kinetic energy for turbulent flows are derived as follows:

radial direction

$$\frac{1}{2}\overline{V}_r^2 + \frac{1}{2}\overline{V_r'^2} = \int \{-\frac{1}{\rho}\frac{\partial p}{\partial r} + \frac{\nu}{\overline{V}_r}(\overline{V}_r\overline{\nabla^2 V_r} + \overline{V_r'\nabla^2 V_r'} - \frac{2}{r^2}\overline{V}_r^2 - \frac{2}{r^2}\overline{V_r'^2}) - \frac{1}{\overline{V}_r}[\frac{1}{2}\overline{V_r'\frac{\partial}{\partial r}(V_r'^2)} - \frac{1}{r}\overline{V_r'V_\theta'^2}] + \frac{1}{r}(\overline{V}_\theta^2 + \overline{V_\theta'^2})\}\, dr \tag{5-14}$$

tangential direction

$$\frac{1}{2}\overline{V}_\theta^2 + \frac{1}{2}\overline{V_\theta'^2} = \int \{\frac{\nu}{\overline{V}_r}(\overline{V}_\theta\overline{\nabla^2 V_\theta} + \overline{V_\theta'\nabla^2 V_\theta'} - \frac{\overline{V}_\theta^2}{r^2} - \frac{\overline{V_\theta'^2}}{r^2}) - \frac{1}{\overline{V}_r}[\frac{1}{2}\overline{V_r'\frac{\partial}{\partial r}(V_\theta'^2)} + \frac{1}{r}\overline{V_r'V_\theta'^2}] - \frac{1}{r}(\overline{V}_\theta^2 + \overline{V_\theta'^2})\}\, dr \tag{5-15}$$

axial direction

$$\frac{1}{2}\overline{V}_z^2 + \frac{1}{2}\overline{V_z'^2} = \int [\frac{\nu}{\overline{V}_r}(\overline{V}_z\overline{\nabla^2 V_z} + \overline{V_z'\nabla^2 V_z'}) - \frac{1}{2\overline{V}_r}\overline{V_r'\frac{\partial}{\partial r}(V_z'^2)}]\, dr \tag{5-16}$$

The terms on the left-hand side of above equations represent the mean motion part and the fluctuating motion part of the total kinetic energy. Only in the radial direction, there is an effect of the pressure gradient on the total kinetic energy. The viscousness contributes to the total kinetic energy in all directions. The total kinetic energy is destroied, generated or transported by viscous stress fluctuations. The third-order products of turbulent fluctuations represent the transportation of the total kinetic energy. The inertia effect on the total kinetic energy by the mean and fluctuating velocities appears only in the radial and tangential directions. The equation of the total kinetic energy

in the radial direction contain all effects from the pressure gradient, the viscous stress, the turbulent fluctuation and the inertia force. The equation of the total kinetic energy in the axial direction has the simplest form among them, only containing the effects from the viscous stress and the inertia force.

5.4 Equations of Kinetic Energy for Fluctuating Motion

For an axisymmetric flow with negligible axial gradient, the equations of kinetic energy due to fluctuating motion are derived as:

radial direction

$$\frac{\partial}{\partial r}(\frac{1}{2}\overline{V_r'^2}) - \frac{2}{r}(\frac{1}{2}\overline{V_r'^2}) - \frac{2}{\overline{V}_r}\frac{\nu}{r^2}(\frac{1}{2}\overline{V_r'^2})$$
$$= -\frac{\nu}{\overline{V}_r}(\overline{V_r'\frac{\partial^2 V_r'}{\partial r^2}} + \frac{1}{r}\overline{V_r'\frac{\partial V_r'}{\partial r}}) + \frac{1}{\overline{V}_r}[\frac{1}{2}\overline{V_r'\frac{\partial}{\partial r}(V_r'^2)} - \frac{1}{r}\overline{V_r'V_\theta'^2}] \qquad (5\text{-}17)$$

tangential direction

$$\frac{\partial}{\partial r}(\frac{1}{2}\overline{V_\theta'^2}) + \frac{2}{r}(\frac{1}{2}\overline{V_\theta'^2}) + \frac{2}{\overline{V}_r}\frac{\nu}{r^2}(\frac{1}{2}\overline{V_\theta'^2})$$
$$= \frac{\nu}{\overline{V}_r}(\overline{V_\theta'\frac{\partial^2 V_\theta'}{\partial r^2}} + \frac{1}{r}\overline{V_\theta'\frac{\partial V_\theta'}{\partial r}}) + \frac{\overline{V}_\theta}{\overline{V}_r}[\frac{\partial}{\partial r}(\overline{V_r'V_\theta'}) + \frac{2}{r}(\overline{V_r'V_\theta'})] -$$
$$- \frac{1}{\overline{V}_r}[\frac{1}{2}\overline{V_r'\frac{\partial}{\partial r}(V_\theta'^2)} + \frac{1}{r}\overline{V_r'V_\theta'^2}] \qquad (5\text{-}18)$$

axial direction

$$\frac{\partial}{\partial r}(\frac{1}{2}\overline{V_z'^2}) = \frac{\nu}{\overline{V}_r}(\overline{V_z'\frac{\partial^2 V_z'}{\partial r^2}} + \frac{1}{r}\overline{V_z'\frac{\partial V_z'}{\partial r}}) + \frac{\overline{V}_z}{\overline{V}_r}[\frac{\partial}{\partial r}(\overline{V_r'V_z'}) + \frac{1}{r}(\overline{V_r'V_z'})]$$
$$+ \frac{1}{2\overline{V}_r}\overline{V_r'\frac{\partial}{\partial r}(V_z'^2)} \qquad (5\text{-}19)$$

The terms on the right-hand side of above equations express the influences from the viscous effects, the shear stresses and the fluctuating velocities to the kinetic energy. In the radial direction, the effect of the shear stress is not observed.

From the above analysis, the contributions made by all components to the turbulence kinetic energy are clear. However, using analytical methods or numerical methods to solve these equations further to determine the turbulence kinetic energy is still very difficult. Therefore, determination through experiments is the major method to obtain the turbulence kinetic energy quantitatively.

5.5 Turbulence Kinetic Energy

5.5.1 Tangential Component of Turbulence Kinetic Energy at Main Section

At the main section of the vortex chamber, it is observed from the experimental results presented in Figures 5.5.1.1 to 5.5.1.7 that the magnitude of the tangential component of the turbulence kinetic energy tends to its maximum value at the centre of the vortex chamber. It decreases along the radial direction from the centre towards the side wall of the vortex chamber. It drops to its minimum value inside the outer region, then starts to increase its value along the radial direction gradually. In the boundary layer region, a higher rate of increasing the tangential component of the turbulence kinetic energy is observed.

The contraction ratio affects the regime of the flow. In the cases with a small contraction ratio ($R_e/R_o < 0.5$), viscous effect is dominant. However, in the cases with a large contraction ratio ($R_e/R_o \geq 0.5$), viscous effect to the flow is less important. These effects influence the behaviour of the tangential component of the turbulence kinetic energy.

It is found that the influence from the inlet Reynolds number to the tangential component of the turbulence kinetic energy can be eliminated by scaling. The effects of the contraction ratio are considered in the scaling formulas.

For the contraction ratios less than 0.50, a scaling formula

$$K_{t,s} = R_{e,i} \cdot \frac{K_t}{K_{in}} \tag{5-20}$$

where

$$K_t = \frac{1}{2}\overline{V_\theta'^2} \tag{5-21}$$

$$K_{in} = \frac{1}{2}\overline{V}_{in}^2 \tag{5-22}$$

is found to form a unique curve of the scaled tangential component of the turbulence kinetic energy at the main section of the vortex chamber for different inlet Reynolds numbers. The plots are illustrated in Figures 5.5.1.8 to 5.5.1.10.

For the contraction ratios between 0.50 and 0.75, another scaling formula

$$K_{t,s} = R_{e,i}^{0.6} \cdot \frac{K_t}{K_{in}} \tag{5-23}$$

is found for the same purpose. The concerning plots are shown in Figures 5.5.1.11 to 5.5.1.13.

For the cases with a contraction ratio less than 0.5, the contraction ratio seems to have very little influence to the location of the minimum value of the scaled tangential component of the turbulence kinetic energy at the main section of the vortex chamber. The locations of the minimum values of the scaled tangential component of the turbulence kinetic energy at the main section under different contraction ratios less than 0.5 appear at around a normalized radius of 0.6. Furthermore, the minimum values corresponding to all contraction ratios less than 0.5 are almost the same and equal to about 100 based on equation (5-20). It means that, in the cases of viscous domination, the location and the magnitude of the minimum value of the

scaled tangential component of the turbulence kinetic energy is independent of the contraction ratio, and independent of the swirl number which is a function of the contraction ratio.

For contraction ratios less than 0.5, the smaller the value of the contraction ratio, the higher the maximum value of the scaled tangential component of the turbulence kinetic energy can be reached at the centre. At the outer region and the boundary layer region, the levels of the scaled tangential component of the turbulence kinetic energy are compatible. The approximate magnitude ranges of the scaled tangential component of the turbulence kinetic energy are between 100 to 1000 based on equation (5-20) as shown in Figure 5.5.1.14.

For the cases where the contraction ratio is greater than 0.5, non viscous domination, not only the inlet Reynolds number but also the contraction ratio affect the location (radius) and the magnitude of the minimum value of the scaled tangential component of the turbulence kinetic energy at the main section of the vortex chamber. With the increase of the contraction ratio, the minimum value of the scaled tangential component of the turbulence kinetic energy appears at the place with larger numerical value of the radius. The magnitude ranges of the scaled tangential component of the turbulence kinetic energy are within 1.5 to 9.0 based on equation (5-23) as shown in Figure 5.5.1.15.

It is found that the numerical value of the normalized radius where the minimum value of the scaled tangential component of the turbulence kinetic energy appears is always close, but slightly smaller than that of the contraction ratio.

5.5.2 Tangential Component of Turbulence Kinetic Energy near Exit Section

Near the exit section inside the vortex chamber, it is found from the analysis of the experimental results that the magnitude of the tangential component of the turbulence kinetic energy reaches its maximum value at the central core region as shown in Figures 5.5.2.1 to 5.5.2.6. For the contraction ratios less than 0.5, it tends to its maximum value at the centre of the vortex chamber. However, for the contraction ratios greater than 0.5, it reaches its maximum value within the central core region, at around a normalized radius of 0.1. It reaches its minimum value at the border between the outer region and the boundary layer region. In the boundary layer region, the magnitude of the tangential component of the turbulence kinetic energy starts to increase again along the radial direction.

Near the exit section inside the vortex chamber, for any contraction ratio except 1.0, which refers to an open exit condition and in which there is no physical exit surface, a scaling formula

$$K_{t,s} = R_{e,i}^{0.3} \frac{K_t}{K_{in}} \qquad (5\text{-}24)$$

is found to eliminate the influence of the inlet Reynolds number to form a unique curve. The plots of the scaled tangential component of the turbulence kinetic energy near the exit section inside the vortex chamber are illustrated in Figures 5.5.2.7 to 5.5.2.12.

It can be found from these curves that the magnitude ranges of the scaled tangential component of the turbulence kinetic energy near the exit section are approximately identical for all contraction ratios, and are from about 0.15 to 6.0 based on equation (5-24).

5.5.3 Radial Component of Turbulence Kinetic Energy at Main Section

It is found that the radial component of the turbulence kinetic energy at the main section will tend to its maximum value at the centre of the vortex chamber. Along the radial direction from the centre to the side wall of the vortex chamber, it will decrease and drop to its minimum value in the outer region, then start to increase its value as shown in Figures 5.5.3.1 and 5.5.3.2.

It is found that the radial component of the turbulence kinetic energy at the main section is affected by many factors such as location, contraction ratio and so on. It seems that the flow will have a higher level of the radial component of the turbulence kinetic energy when it approaches the exit, which corresponds to a higher percentage of the vortex chamber length.

It is found that the numerical value of the normalized radius referring to the minimum value of the radial component of the turbulence kinetic energy is approximately equal to that of the contraction ratio. In other words, the radial component of the turbulence kinetic energy at the main section will reach its minimum value at the place where the value of the normalized radius equals to that of the contraction ratio of the vortex chamber.

5.5.4 Radial Component of Turbulence Kinetic Energy near Exit Section

The overall performances of the radial component of the turbulence kinetic energy near the exit section inside the vortex chamber are shown in Figures 5.5.4.1 to 5.5.4.6.

It is found from the experimental results that the radial component of the turbulence kinetic energy near the exit section inside the vortex chamber is influenced by both the contraction ratio and the inlet Reynolds number. The behaviour of the radial component of the turbulence kinetic energy near the exit section is so sophisticated that there is no simple way which can be

used to describe it. No simple formula can be found to collapse the curves of the radial component of the turbulence kinetic energy (different inlet Reynolds numbers with a given contraction ratio) into one, although it is possible for the tangential component of the turbulence kinetic energy.

The difference between the radial component of the turbulence kinetic energy under the small contraction ratio and that under the large contraction ratio is obvious. For the contraction ratio less than 0.5, the radial component of the turbulence kinetic energy tends to its maximum value at the centre of the vortex chamber. Then, it decreases along the radial direction from the centre towards the wall. Only in the cases of high inlet Reynolds number (13700), will its magnitude increase again when approaching the boundary layer region. In general, the magnitude level of the radial component of the turbulence kinetic energy at small contraction ratio is lower than that at large contraction ratio. However, the magnitude ranges for the small contraction ratios are approximately identical.

For the contraction ratio greater than 0.5, the radial component of the turbulence kinetic energy will not reach its maximum value at the centre of the vortex chamber. The location of the maximum value of the radial component of the turbulence kinetic energy will change if the contraction ratio changes. The maximum value location (radius) will increase with the increase of the contraction ratio.

In the cases where the contraction ratio is greater than 0.5, the magnitude of the radial component of the turbulence kinetic energy will reduce gradually as a response to the increasing contraction ratio.

5.5.5.Total Turbulence Kinetic Energy

The total turbulence kinetic energy is the total contribution of turbulence kinetic energy in all directions. That is, the contribution of fluctuating velocities in the radial, tangential and axial directions. The total turbulence kinetic energy (T.T.K.E.) is the half of the sum of the mean squares of fluctuating velocities in all directions, that is,

$$\text{T.T.K.E.} = \frac{1}{2}(\overline{V_r'^2} + \overline{V_\theta'^2} + \overline{V_z'^2}) \tag{5-25}$$

If the levels of fluctuating velocities in the radial, tangential and axial directions are equal or compatible, the total turbulence kinetic energy can be estimated by the fluctuating velocities in any two directions, such as

$$\text{T.T.K.E.} \approx \frac{3}{4}(\overline{V_r'^2} + \overline{V_\theta'^2}) \tag{5-26}$$

It is a general approximation used by many investigators such as Stieglmeier et al [39] and Liou et al [40].

Plots of the total turbulence kinetic energy at the main section of the vortex chamber are illustrated in Figures 5.5.5.1 and 5.5.5.2. At the main section, the turbulence kinetic energy due to the fluctuating tangential velocity is investigated in detail. However, less information is provided about the turbulence kinetic energy due to the fluctuating radial velocity. Therefore, to the certain combinations of the contraction ratios and the inlet Reynolds numbers, the total turbulence kinetic energy at the main section could not be provided except through rough estimation which considers three times of the tangential component of the turbulence kinetic energy to be the total turbulence kinetic energy. This is based on the assumption that the levels of fluctuating velocities in all directions are equal or compatible.

Near the exit section inside the vortex chamber, not only the tangential component of the turbulence kinetic energy but also the radial component of the turbulence kinetic energy are investigated in detail. The total turbulence kinetic energy is obtained based on the tangential component of the turbulence kinetic energy and the radial component of the turbulence kinetic energy, using equation (5-26). The results are illustrated in Figures 5.5.5.3 to 5.5.5.8.

It is clear that the total turbulence kinetic energy near the exit section inside the vortex chamber is influenced by both the contraction ratio and the inlet Reynolds number. Any influence factor which affects either the tangential component or the radial component of the turbulence kinetic energy will affect the total turbulence kinetic energy.

Near the exit section inside the vortex chamber, apparent difference can be observed between the distributions of the total turbulence kinetic energy at the small contraction ratios and the large contraction ratios. Among either the small contraction ratios or the large contraction ratios, similar behaviour of the total turbulence kinetic energy can be observed. In general, near the exit section, the magnitude level of the total turbulence kinetic energy at small contraction ratio is lower than that at large contraction ratios. This is due to the influence of the radial component of the turbulence kinetic energy as well as the tangential component of the turbulence kinetic energy. The same conclusion can be drawn as those from the analyses of the radial component of the turbulence kinetic energy and the tangential component of the turbulence kinetic energy near the exit section. To the flows with the same inlet Reynolds number but with different contraction ratios less than 0.5, the magnitude ranges of total turbulence kinetic energy are approximately the same. It means that, in the cases of viscous domination, the total

turbulence kinetic energy depends on the inlet Reynolds number more than on the contraction ratio.

For the large contraction ratio, the maximum value of the total turbulence kinetic energy will not appear at the centre of the vortex chamber. The maximum value location will move far away from the centre with the increase of the contraction ratio. After the total turbulence kinetic energy passes its maximum value point, it will decrease along the radial direction to its minimum value.

At large contraction ratios, the magnitude level of the total turbulence kinetic energy is usually higher than that at small contraction ratios. However, for the large contraction ratios, as the contraction ratio increases from 0.5 to 0.75, the magnitude of the total turbulence kinetic energy will decrease as shown in Figure 5.5.5.6 to 5.5.5.8.

5.6 SUMMARY

The influence factors on the magnitude of the turbulence kinetic energy are listed in Table 5.6.1. The locations corresponding to the maximum and the minimum turbulence kinetic energy are summarized in Table 5.6.2.

The comparison of the tangential component of the turbulence kinetic energy with a variety of the contraction ratios using empirical scaling formulas are shown in Figures 5.5.1.14, 5.5.1.15 and 5.6.1. The analyses listed in Tables 5.6.3 and 5.6.4 show that over 73 % of points are within the deviation of 10 % when the formulas are applied.

The experimental results show that, near the exit section, the magnitude level of the radial component of the turbulence kinetic energy at a lower inlet Reynolds number is lower than that at a higher inlet Reynolds

number. The behaviour at the small contraction ratios is different from that at the large contraction ratio as shown in Figures 5.6.2 and 5.6.3.

The total turbulence kinetic energy possesses all the characteristics of both the tangential component and the radial component of the turbulence kinetic energy. It is not only affected by the contraction ratio but also the inlet Reynolds number. Figures 5.6.4 and 5.6.5 show these characteristics. The concerning deviations between the curve fittings and the experimental data are listed in Tables 5.6.5 and 5.6.6. 95 % of the points are within 10 %. Among them 80 % of the points are within 5 %.

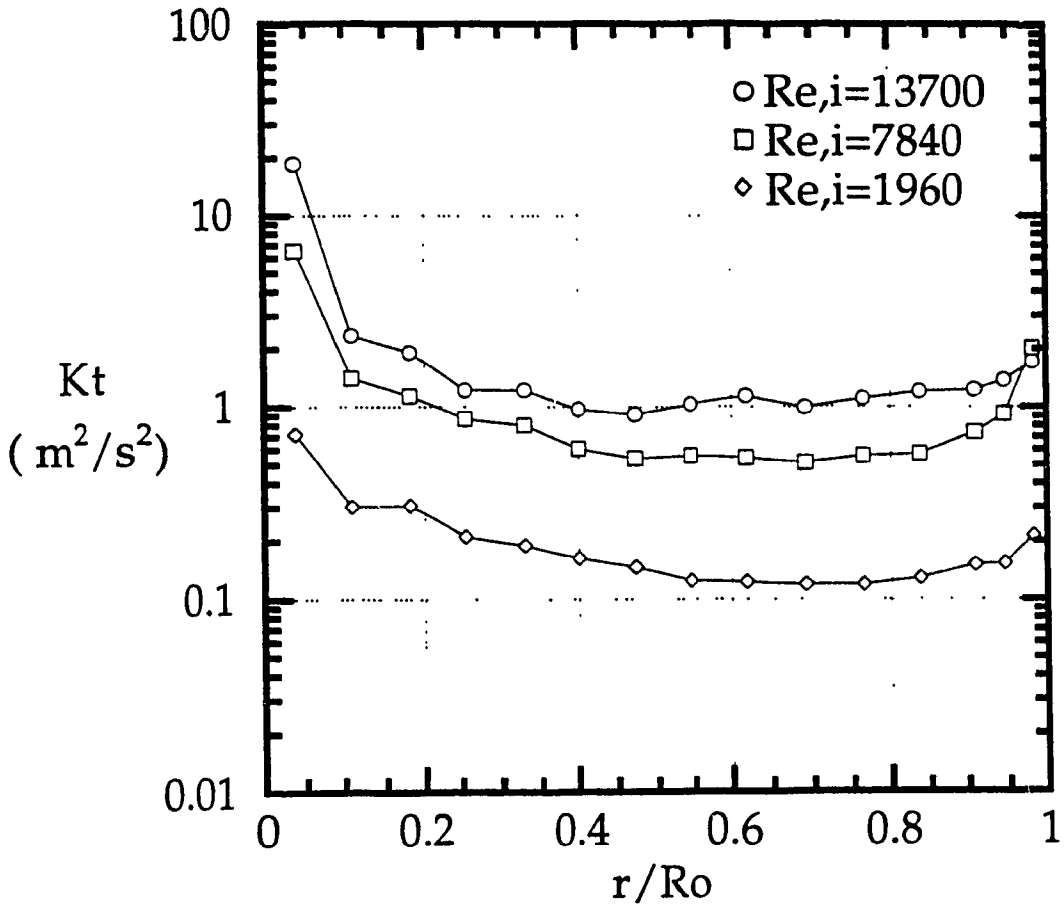

Figure 5.5.1.1 Experimental Tangential Component of Turbulence Kinetic Energy at Main Section (Re/Ro = 0.25)

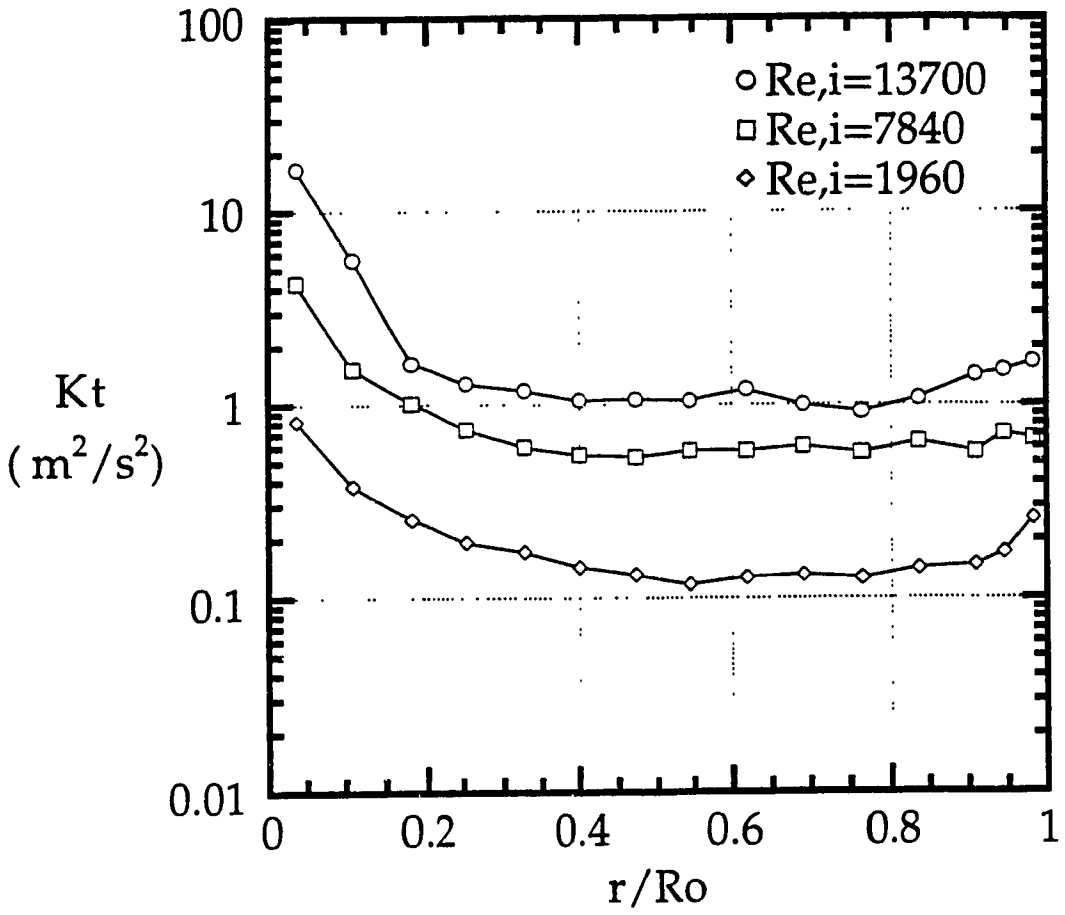

Figure 5.5.1.2 Experimental Tangential Component of Turbulence Kinetic Energy at Main Section (Re/Ro = 0.30)

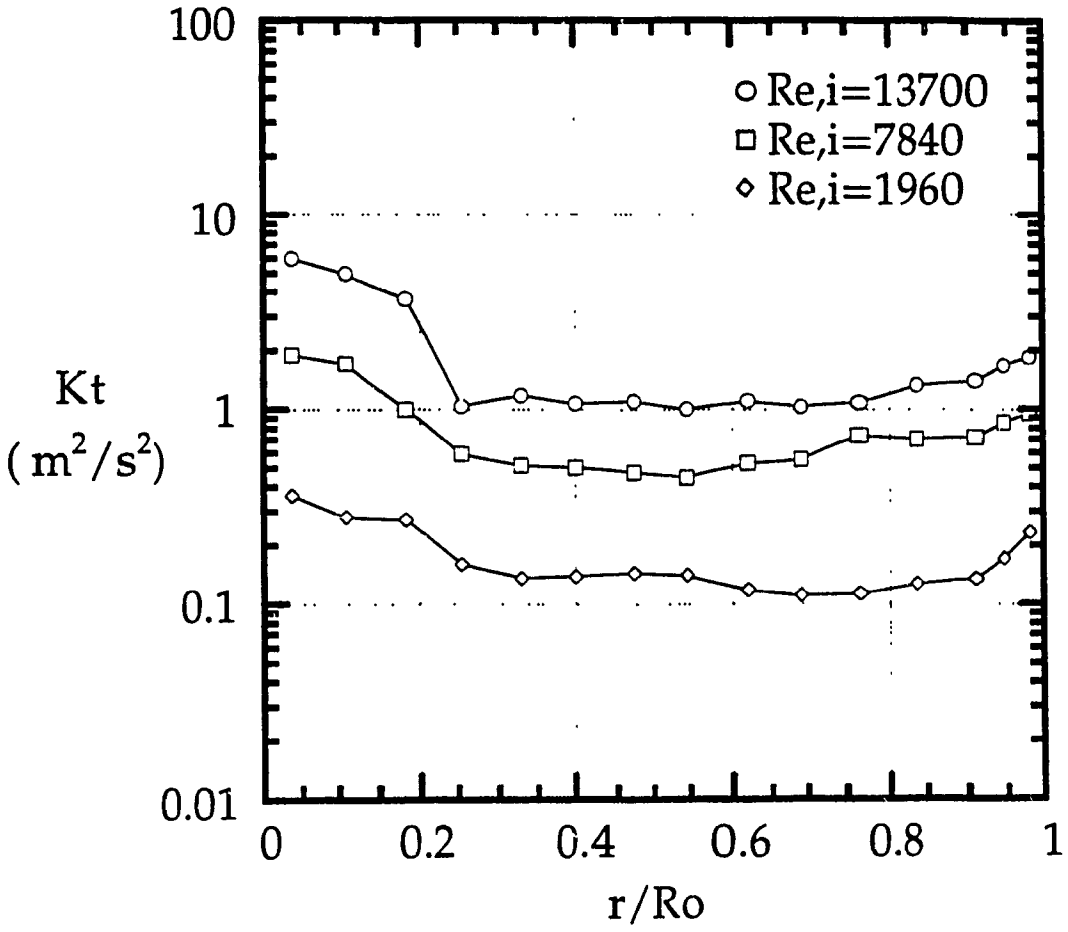

Figure 5.5.1.3 Experimental Tangential Component of Turbulence Kinetic Energy at Main Section (Re/Ro = 0.40)

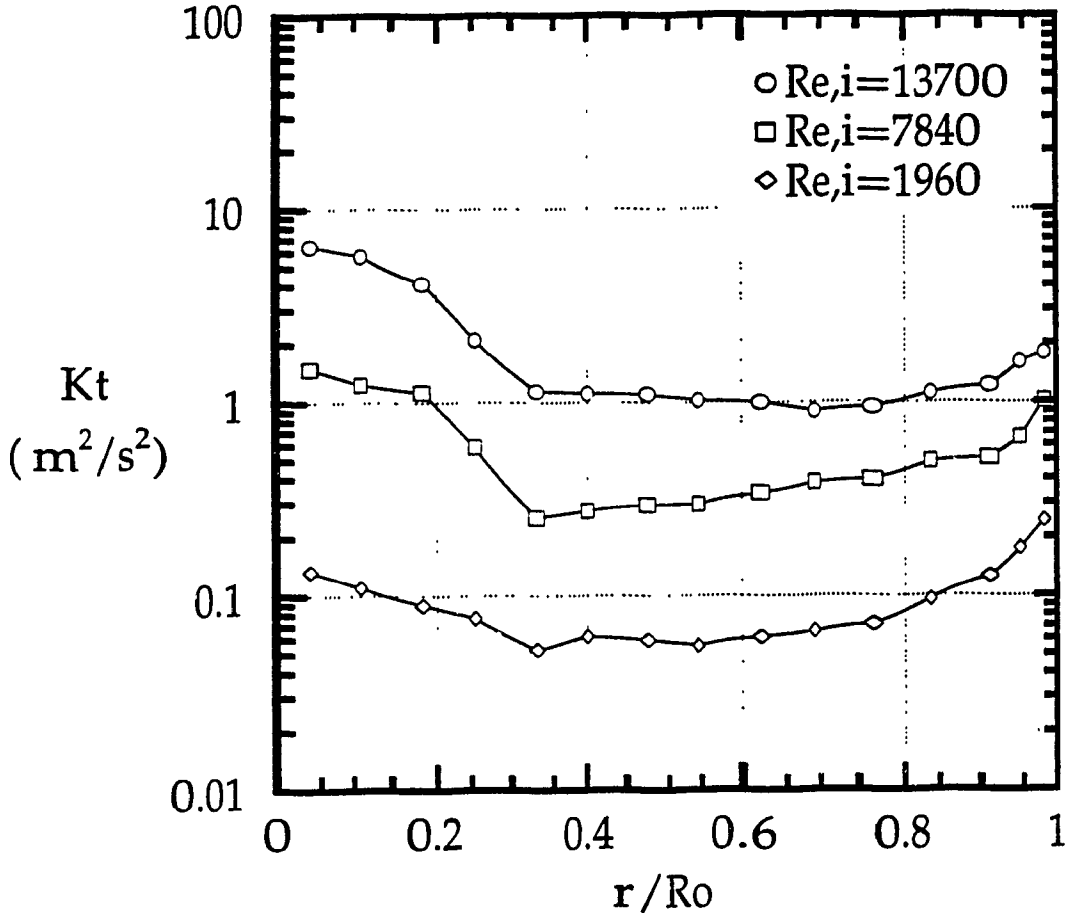

Figure 5.5.1.4 Experimental Tangential Component of Turbulence Kinetic Energy at Main Section (Re/Ro = 0.50)

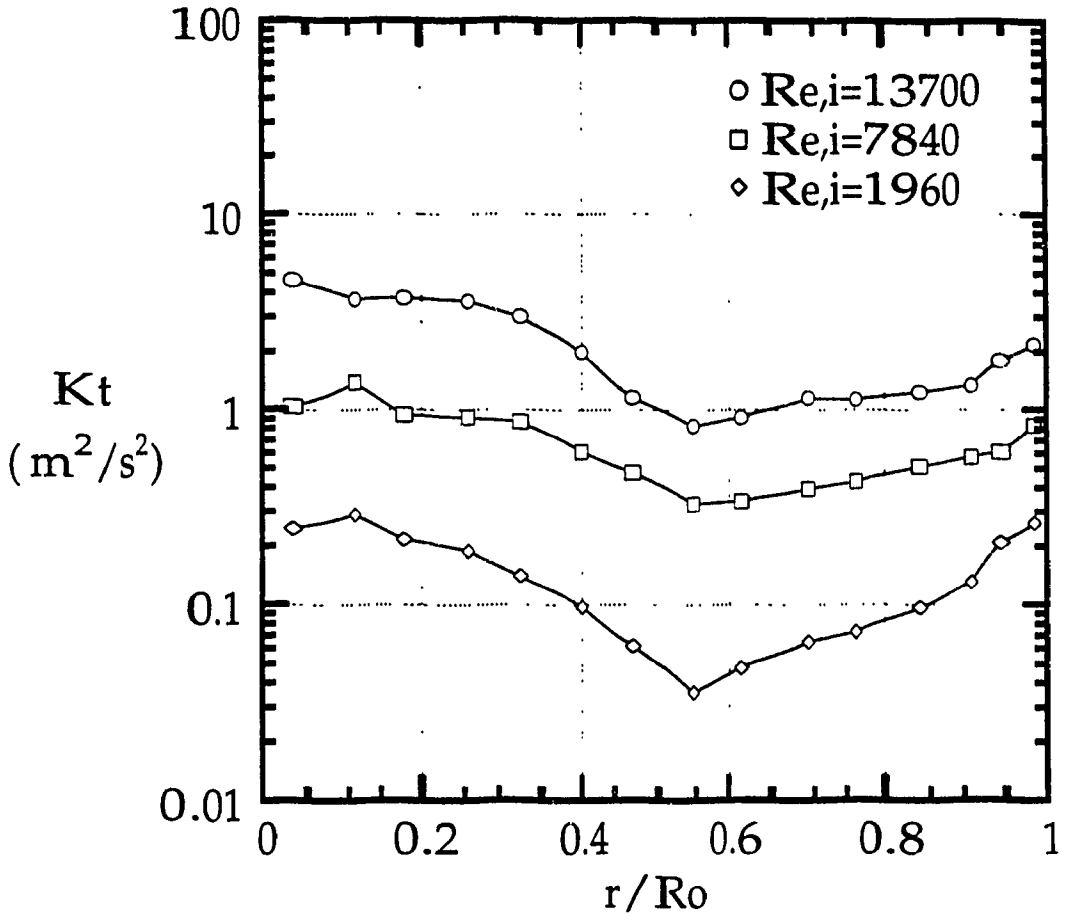

Figure 5.5.1.5 Experimental Tangential Component of Turbulence Kinetic Energy at Main Section (Re/Ro = 0.58)

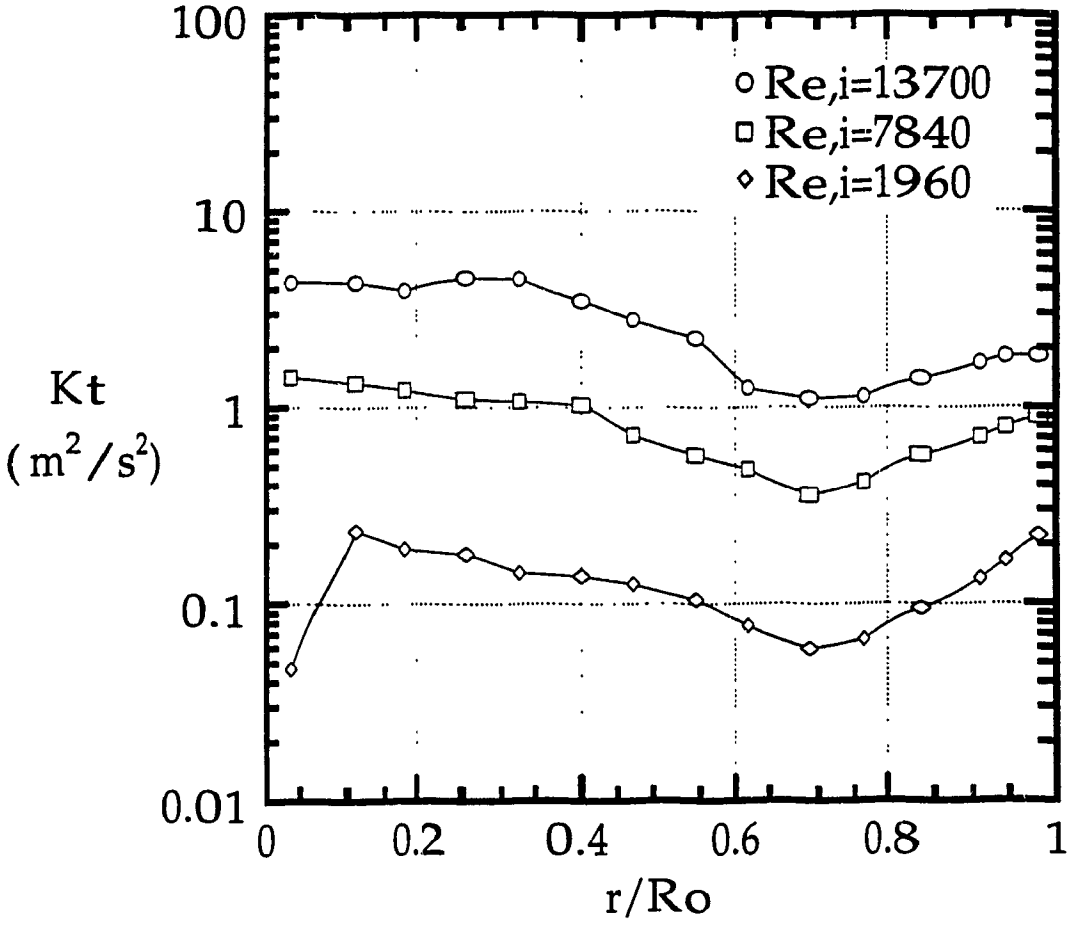

Figure 5.5.1.6 Experimental Tangential Component of Turbulence Kinetic Energy at Main Section (Re/Ro = 0.75)

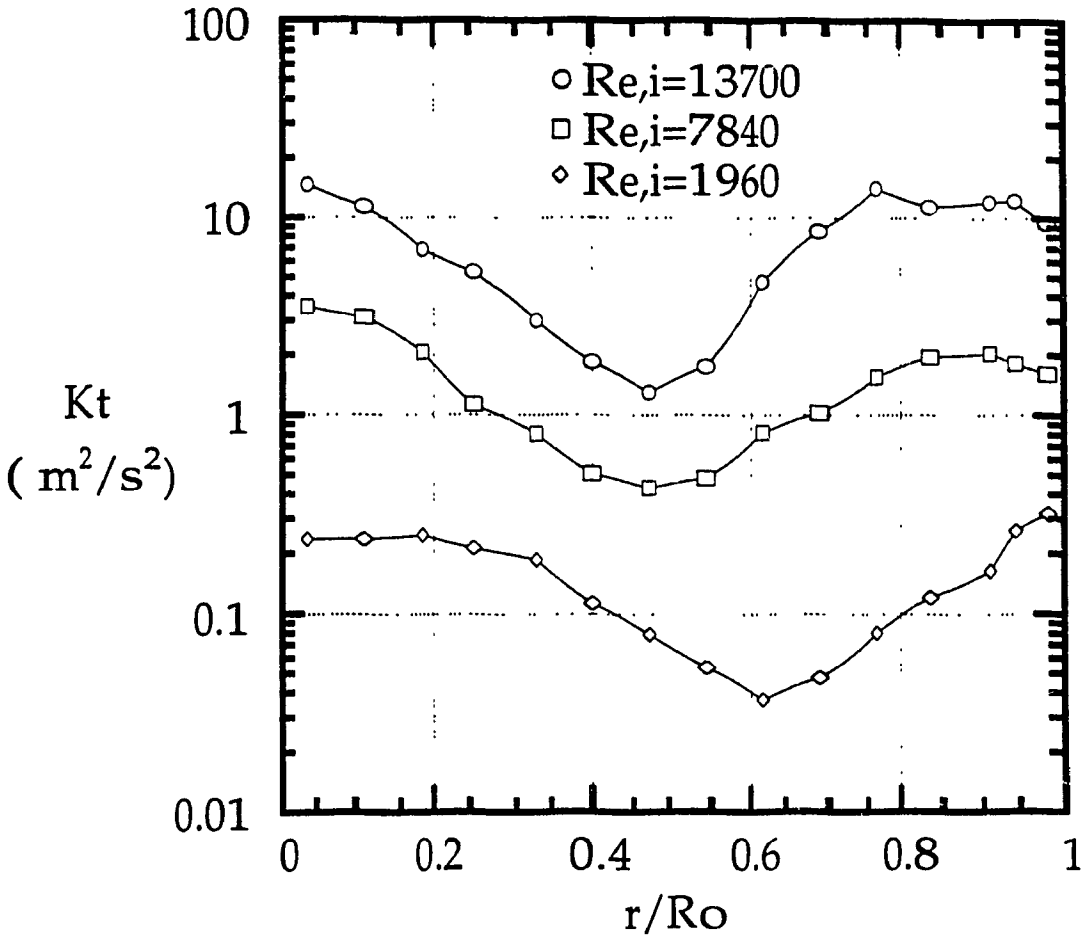

Figure 5.5.1.7 Experimental Tangential Component of Turbulence Kinetic Energy at Main Section (Re/Ro = 1.0)

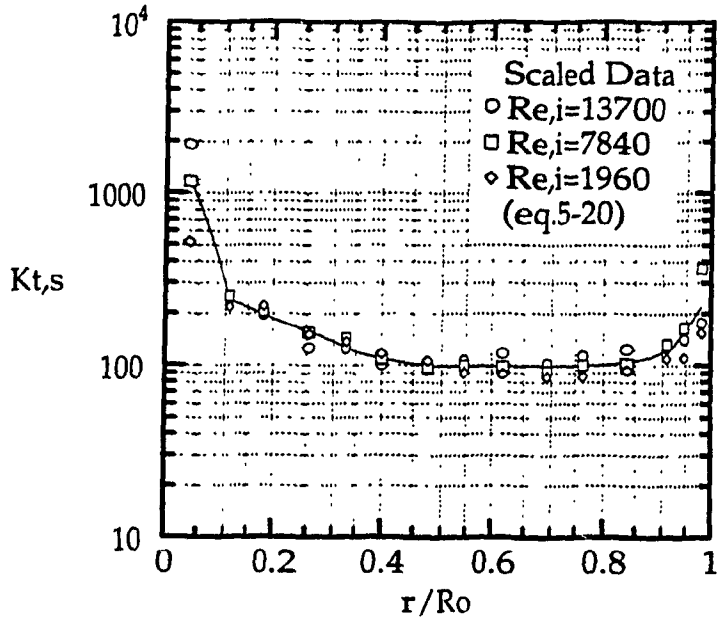

Figure 5.5.1.8 Scaled Tangential Component of Turbulence Kinetic Energy at Main Section at Re/Ro = 0.25 (line - average value)

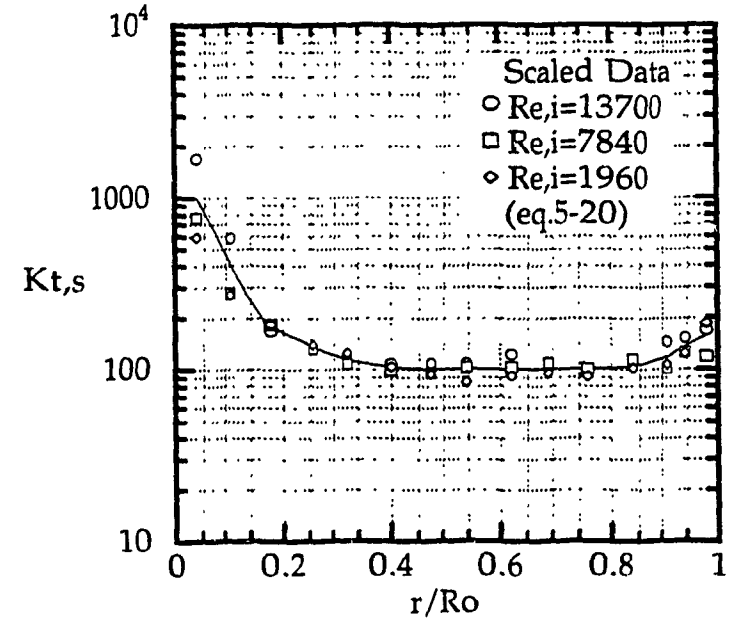

Figure 5.5.1.9 Scaled Tangential Component of Turbulence Kinetic Energy at Main Section at Re/Ro = 0.30 (line - average value)

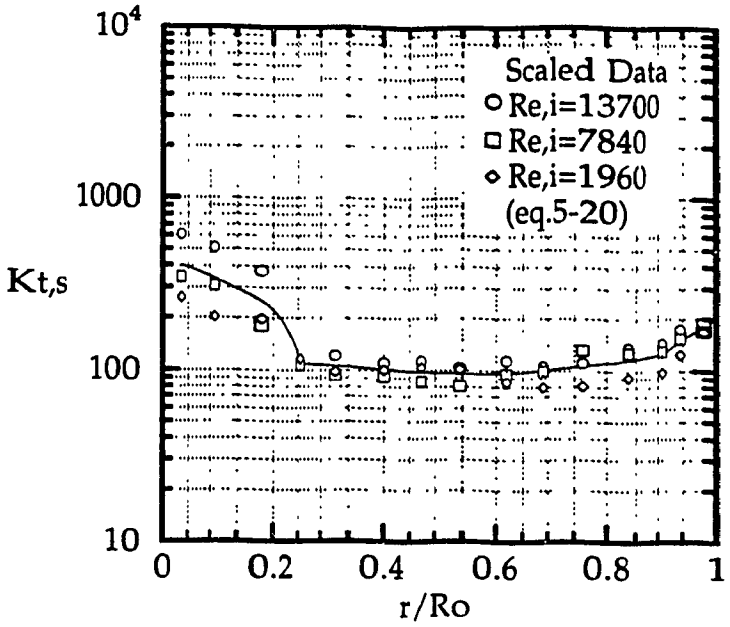

Figure 5.5.1.10 Scaled Tangential Component of Turbulence Kinetic Energy at Main Section at Re/Ro = 0.40 (line - average value)

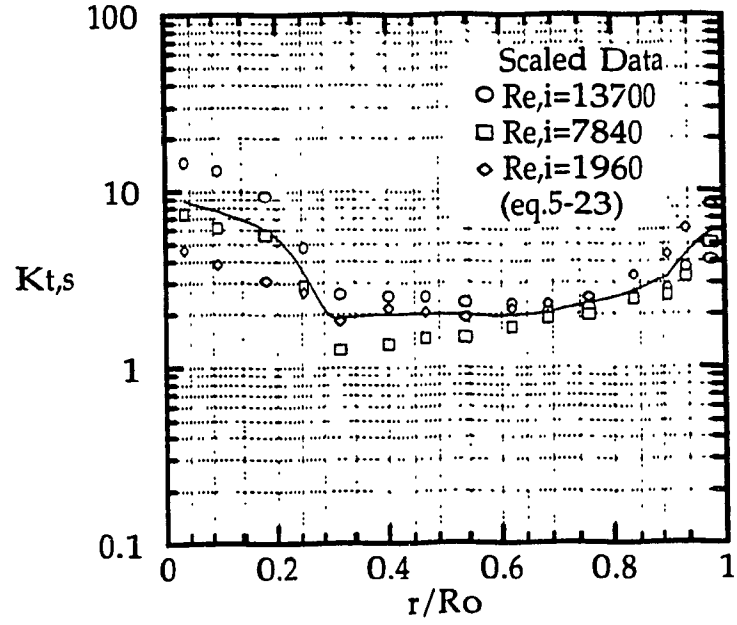

Figure 5.5.1.11 Scaled Tangential Component of Turbulence Kinetic Energy at Main Section at Re/Ro = 0.50 (line - average value)

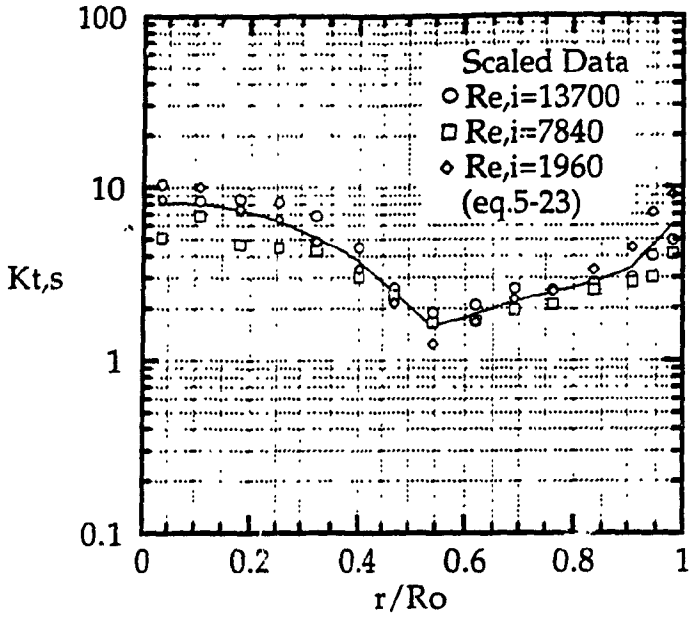

Figure 5.5.1.12 Scaled Tangential Component of Turbulence Kinetic Energy at Main Section at Re/Ro = 0.58 (line - average value)

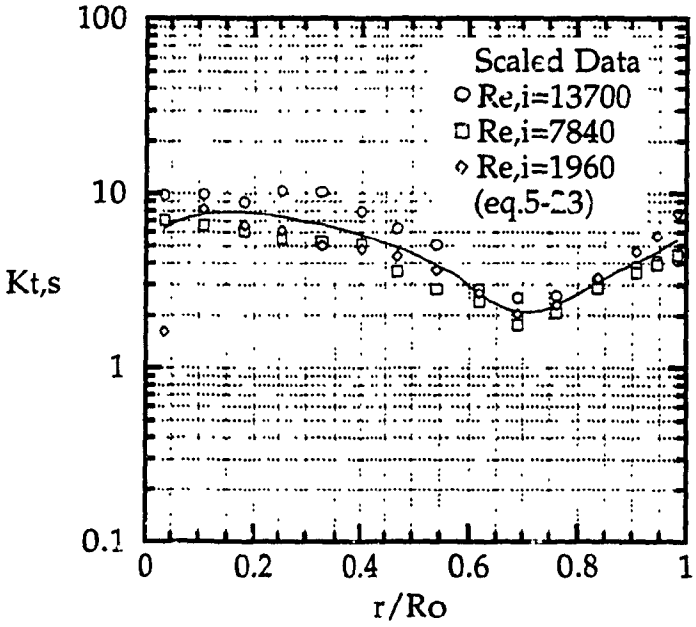

Figure 5.5.1.13 Scaled Tangential Component of Turbulence Kinetic Energy at Main Section at Re/Ro = 0.75 (line - average value)

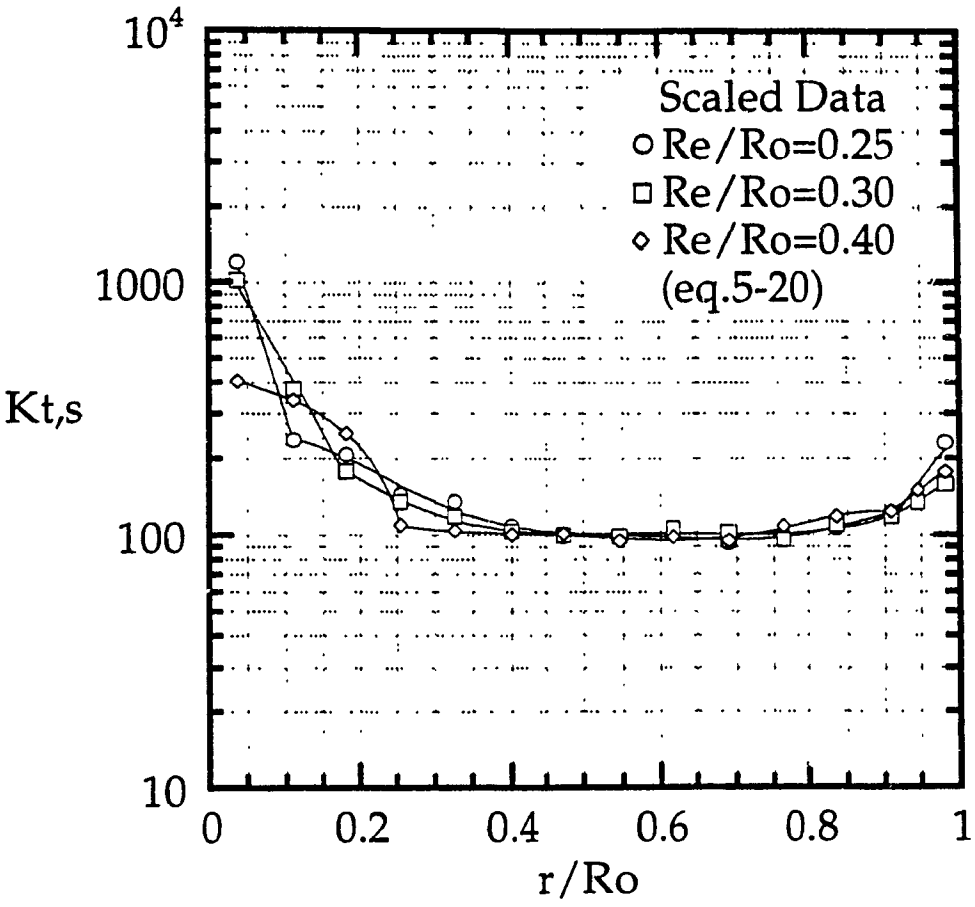

Figure 5.5.1.14 Scaled Tangential Component of Turbulence Kinetic Energy at Main Section (Re/Ro < 0.50)

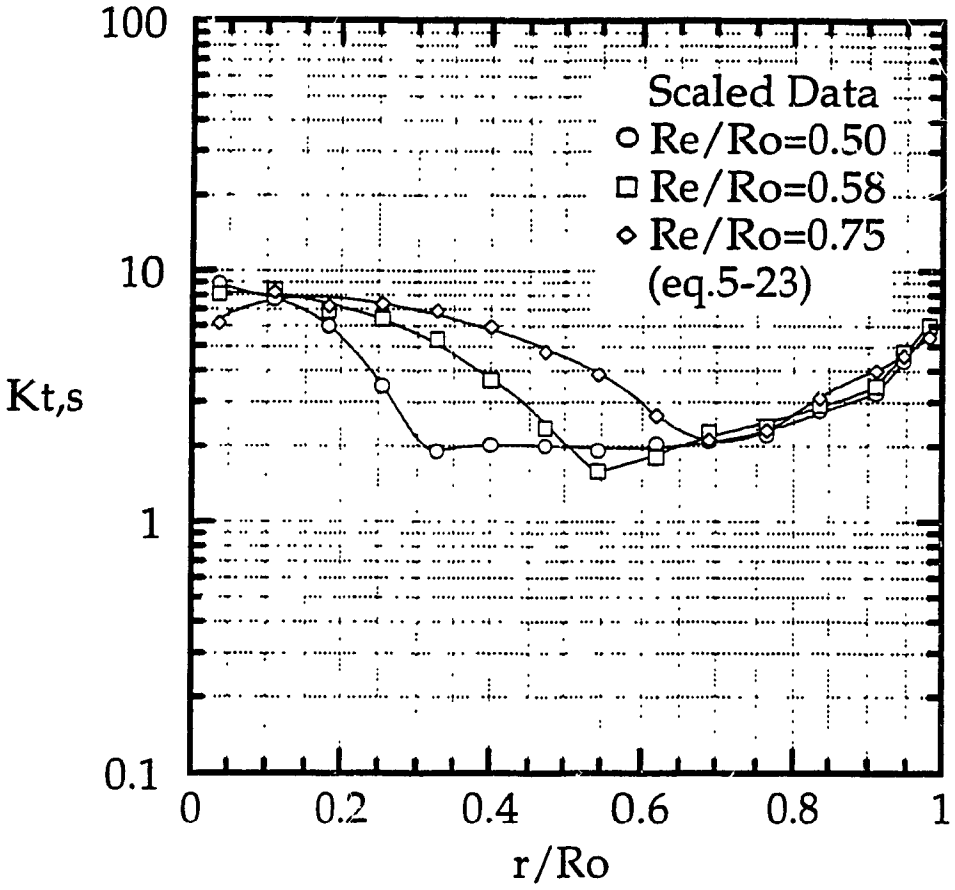

Figure 5.5.1.15 Scaled Tangential Component of Turbulence Kinetic Energy at Main Section (Re/Ro ≥ 0.50)

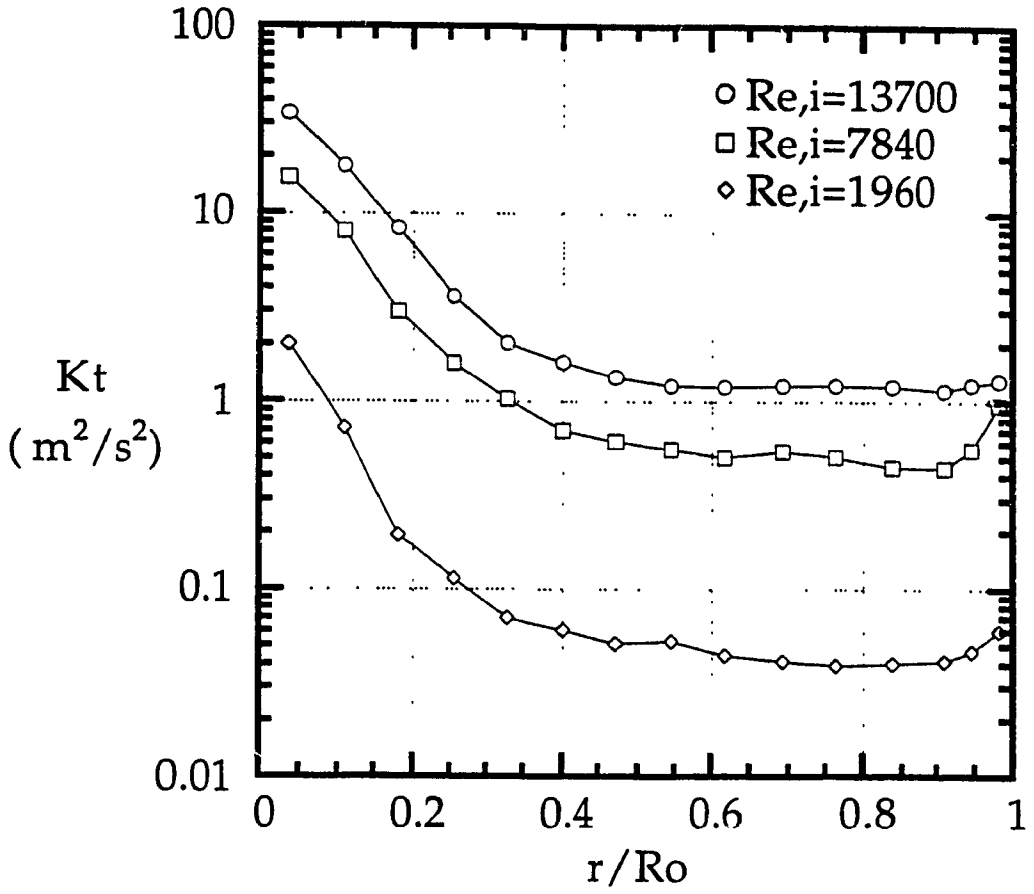

Figure 5.5.2.1 Experimental Tangential Component of Turbulence Kinetic Energy near Exit Section (Re/Ro = 0.25)

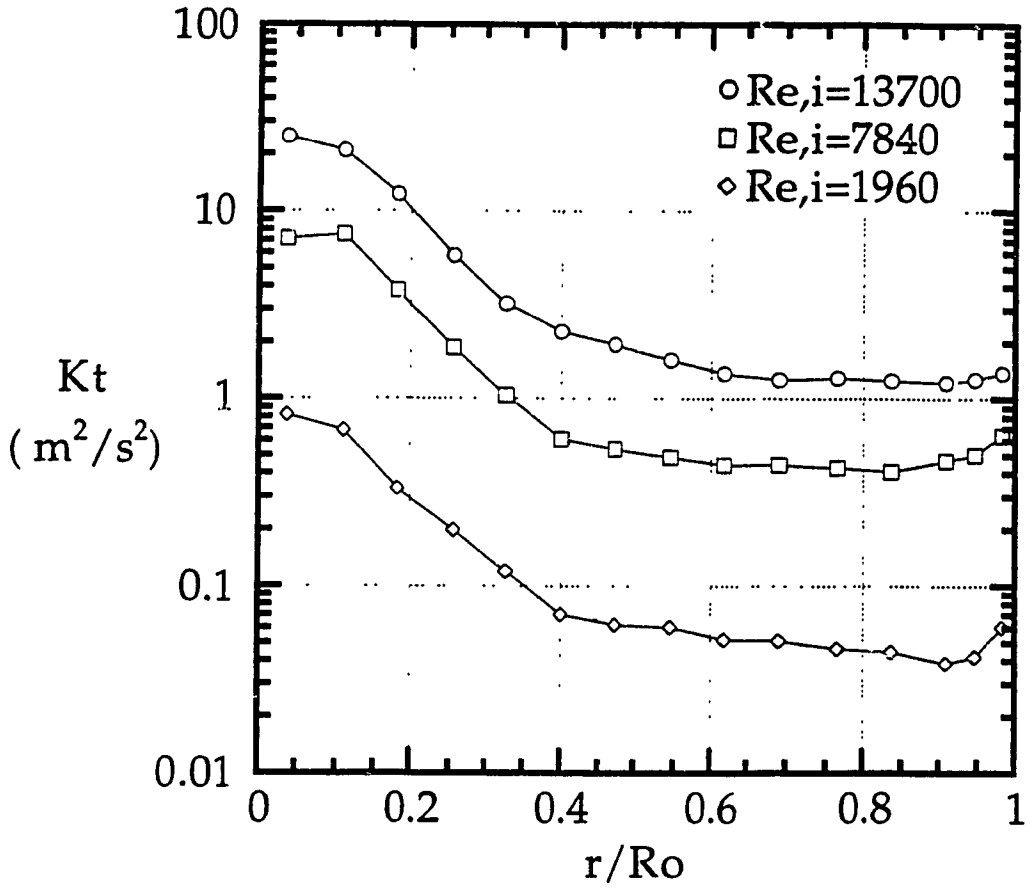

Figure 5.5.2.2 Experimental Tangential Component of Turbulence Kinetic Energy near Exit Section (Re/Ro = 0.30)

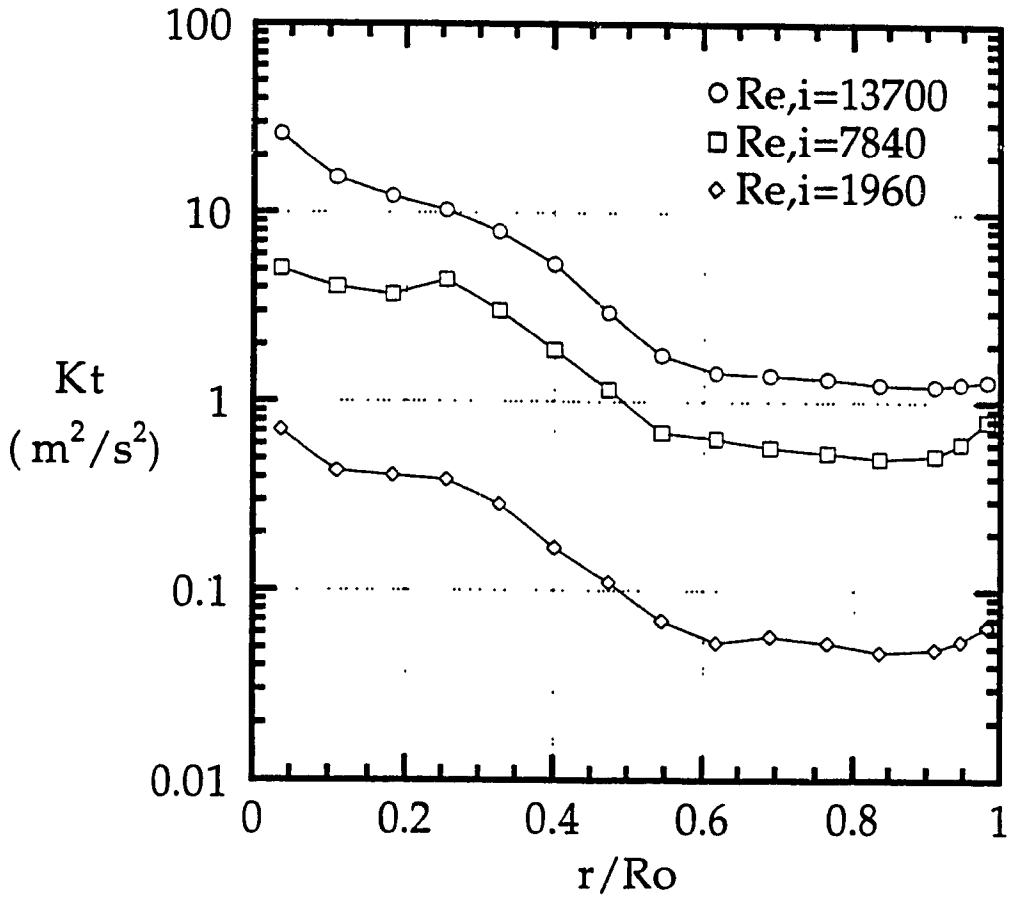

Figure 5.5.2.3 Experimental Tangential Component of Turbulence Kinetic Energy near Exit Section (Re/Ro = 0.40)

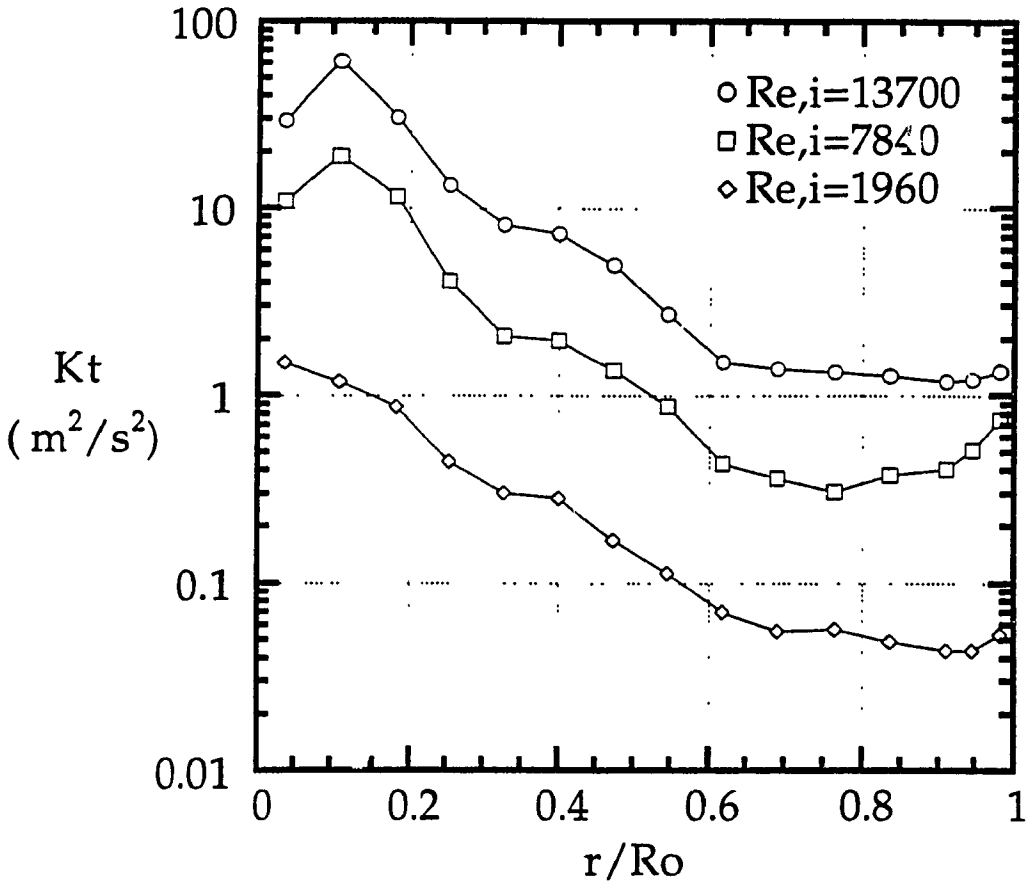

Figure 5.5.2.4 Experimental Tangential Component of Turbulence Kinetic Energy near Exit Section (Re/Ro = 0.50)

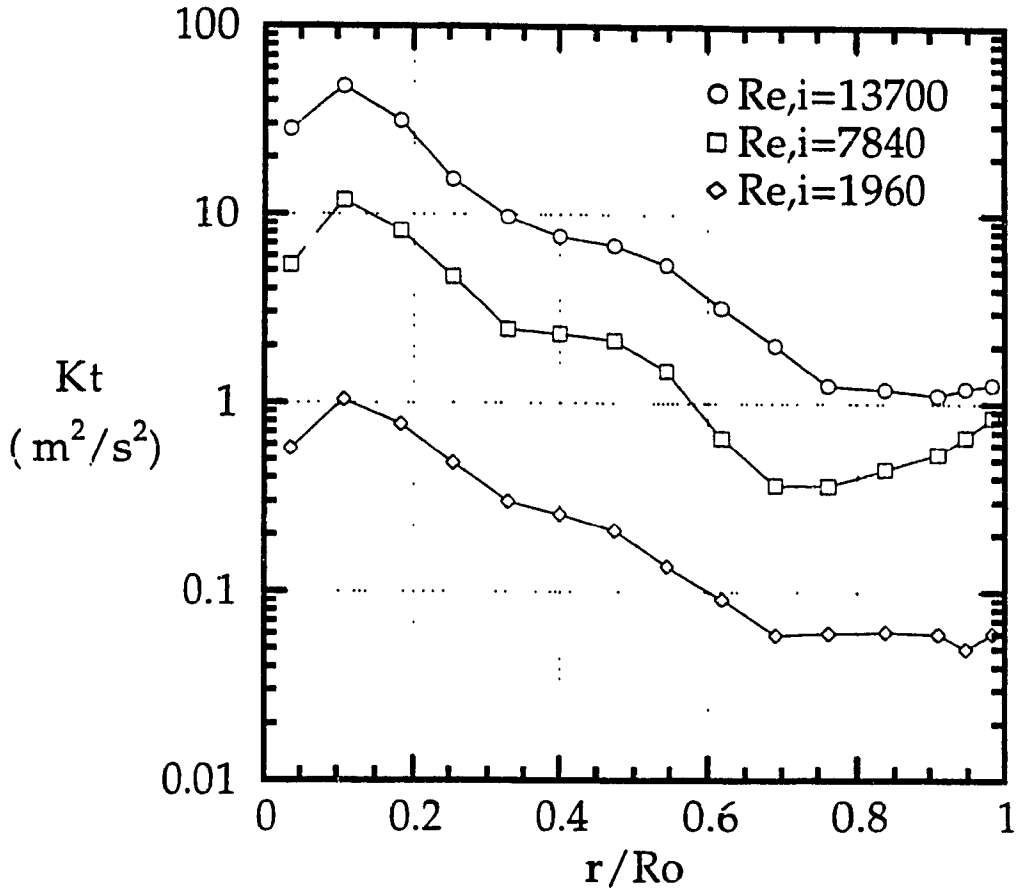

Figure 5.5.2.5 Experimental Tangential Component of Turbulence Kinetic Energy near Exit Section (Re/Ro = 0.58)

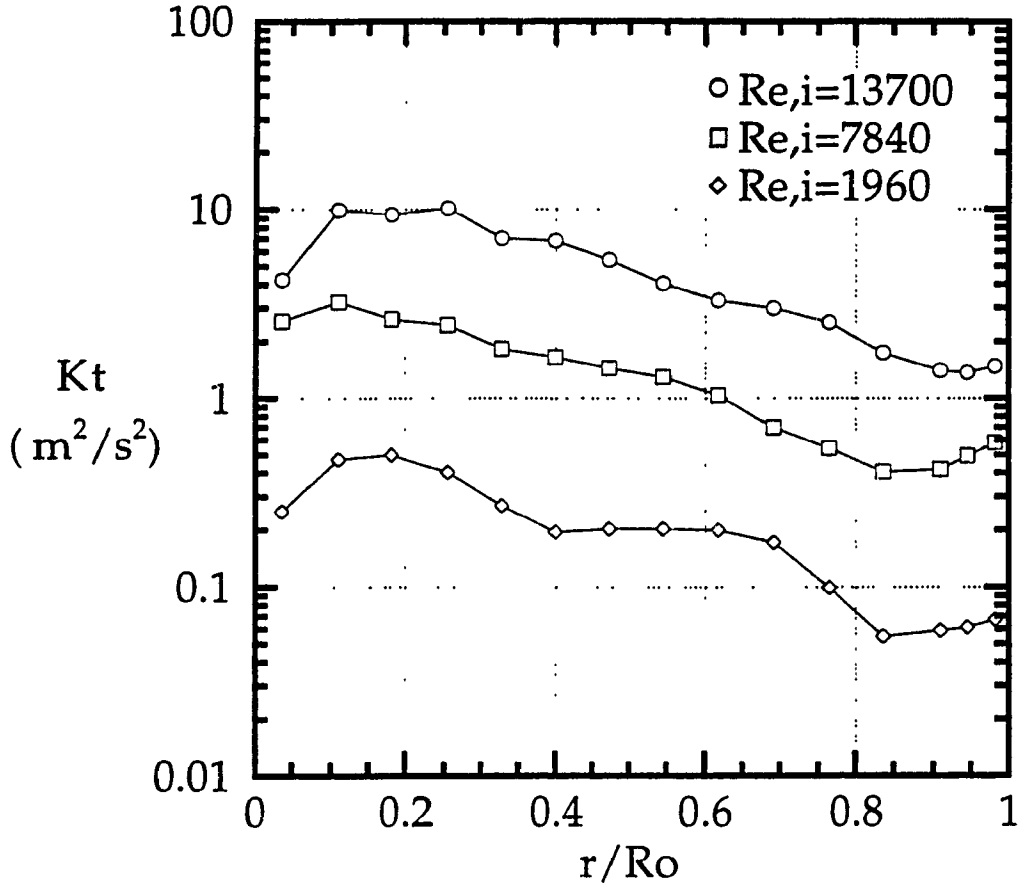

Figure 5.5.2.6 Experimental Tangential Component of Turbulence Kinetic Energy near Exit Section (Re/Ro = 0.75)

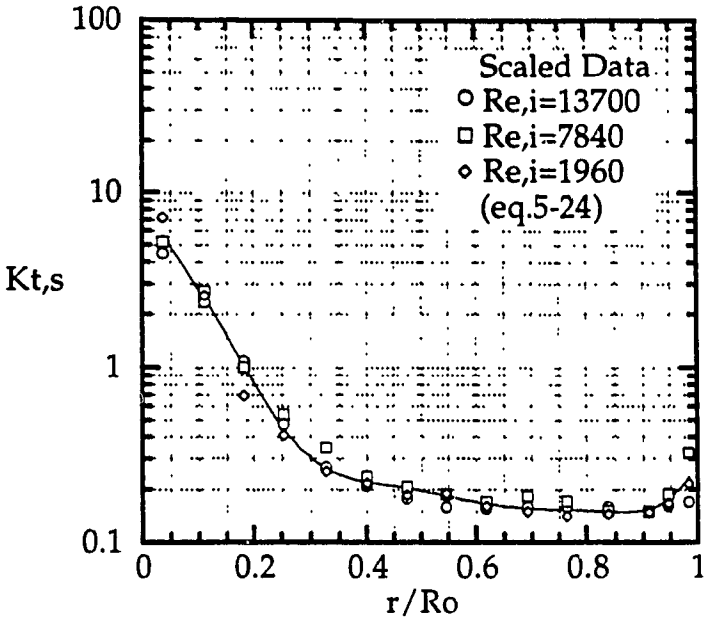

Figure 5.5.2.7 Scaled Tangential Component of Turbulence Kinetic Energy near Exit Section at Re/Ro = 0.25 (line - average value)

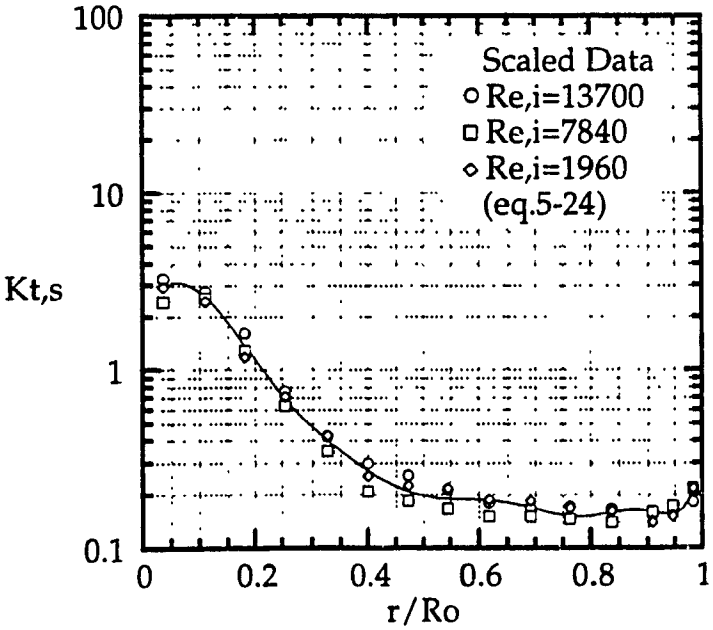

Figure 5.5.2.8 Scaled Tangential Component of Turbulence Kinetic Energy near Exit Section at Re/Ro = 0.30 (line - average value)

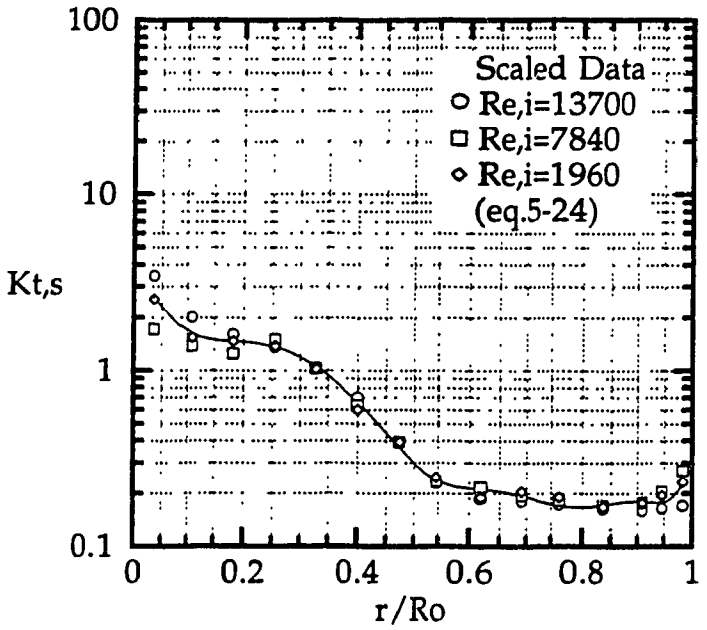

Figure 5.5.2.9 Scaled Tangential Component of Turbulence Kinetic Energy near Exit Section at Re/Ro = 0.40 (line - average value)

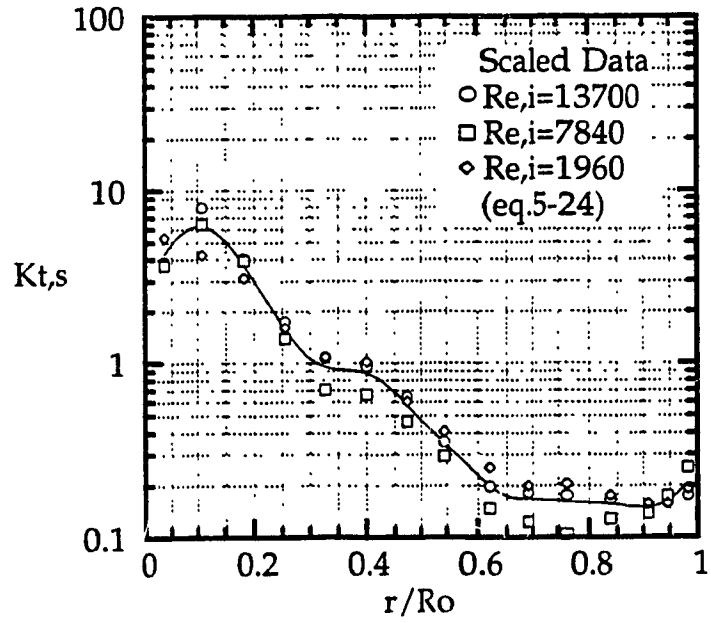

Figure 5.5.2.10 Scaled Tangential Component of Turbulence Kinetic Energy near Exit Section at Re/Ro = 0.50 (line - average value)

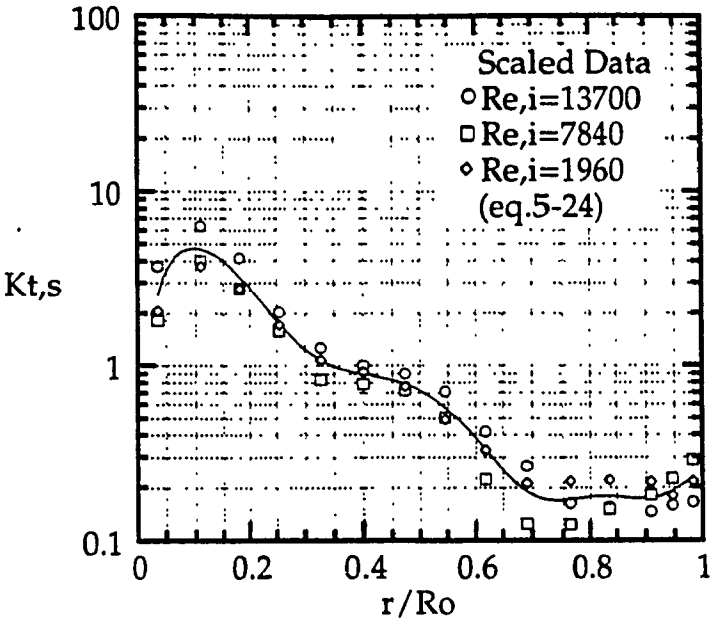

Figure 5.5.2.11 Scaled Tangential Component of Turbulence Kinetic Energy near Exit Section at Re/Ro = 0.58 (line - average value)

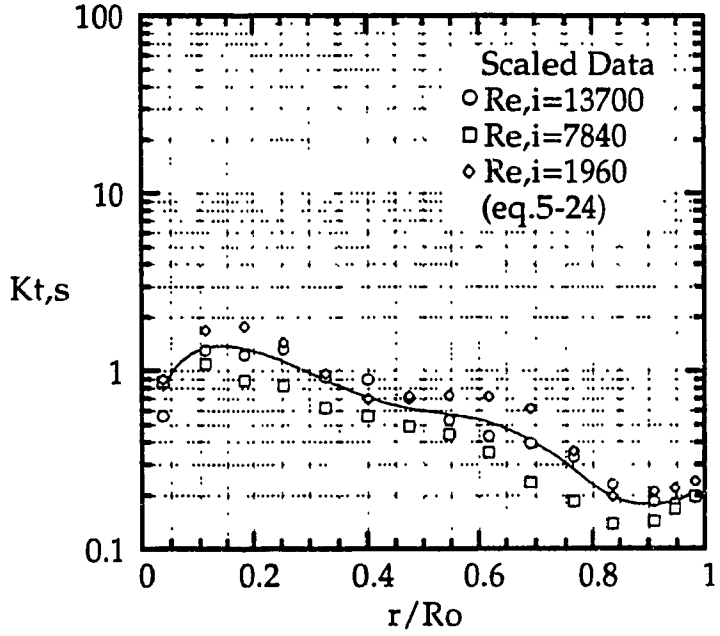

Figure 5.5.2.12 Scaled Tangential Component of Turbulence Kinetic Energy near Exit Section at Re/Ro = 0.75 (line - average value)

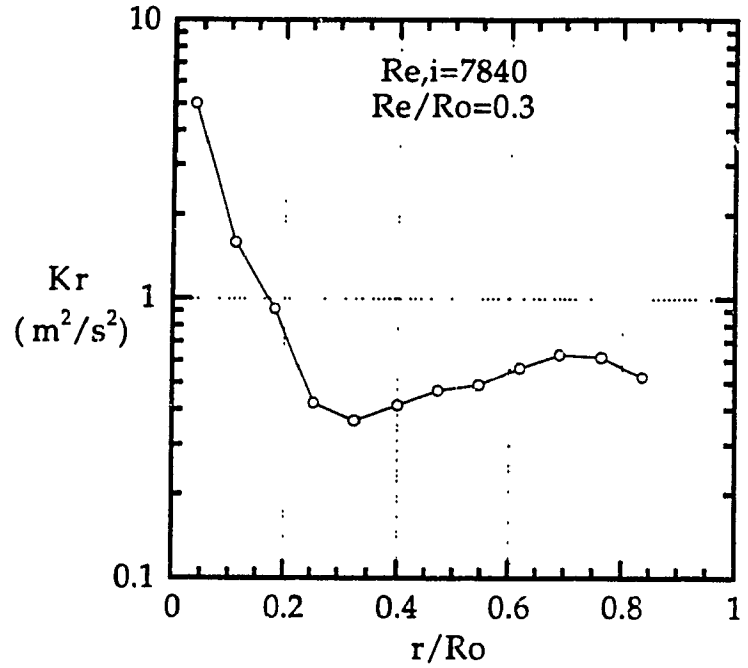

Figure 5.5.3.1 Experimental Radial Component of Turbulence Kinetic Energy at Main Section (69% Vortex Chamber Length)

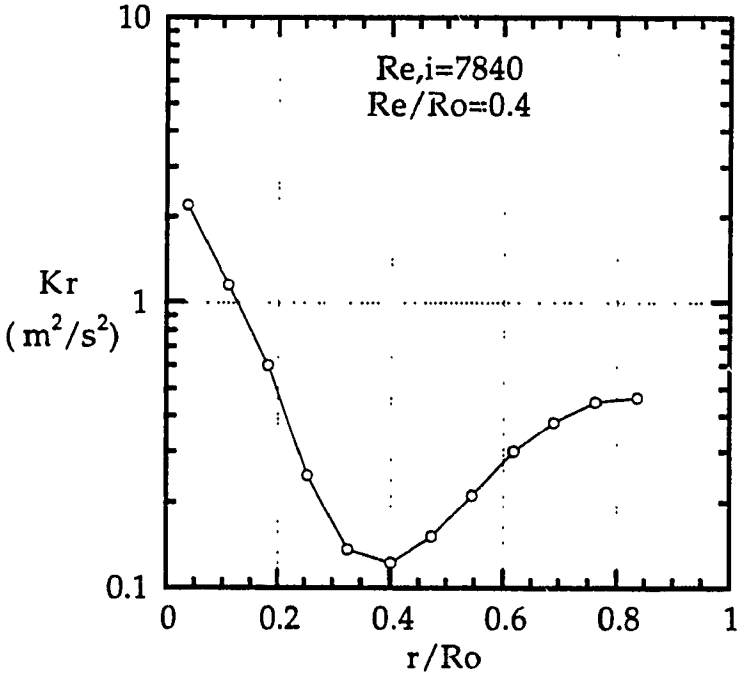

Figure 5.5.3.2 Experimental Radial Component of Turbulence Kinetic Energy at Main Section (50% Vortex Chamber Length)

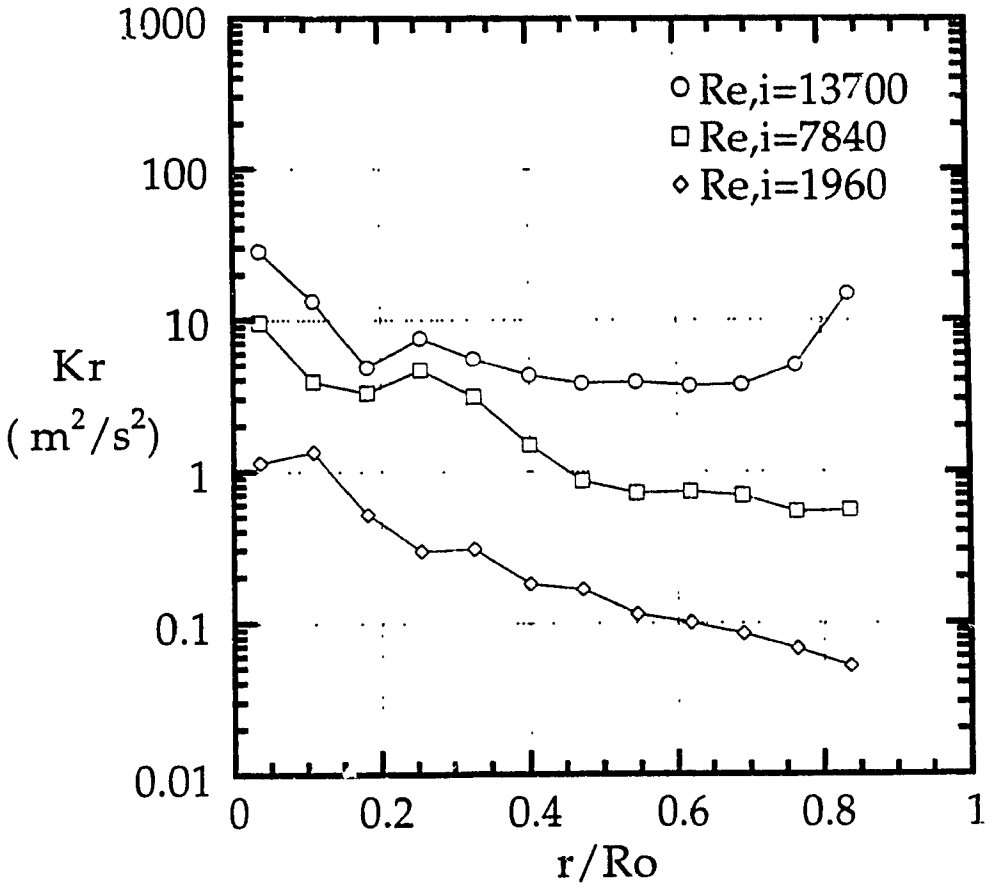

Figure 5.5.4.1 Experimental Radial Component of Turbulence Kinetic Energy near Exit Section (Re/Ro = 0.25)

National Library of Canada

Acquisitions and Bibliographic Services Branch

395 Wellington Street
Ottawa, Ontario
K1A 0N4

Bibliothèque nationale du Canada

Direction des acquisitions et des services bibliographiques

395, rue Wellington
Ottawa (Ontario)
K1A 0N4

Your file Votre référence

Our file Notre référence

NOTICE

The quality of this microform is heavily dependent upon the quality of the original thesis submitted for microfilming. Every effort has been made to ensure the highest quality of reproduction possible.

If pages are missing, contact the university which granted the degree.

Some pages may have indistinct print especially if the original pages were typed with a poor typewriter ribbon or if the university sent us an inferior photocopy.

AVIS

La qualité de cette microforme dépend grandement de la qualité de la thèse soumise au microfilmage. Nous avons tout fait pour assurer une qualité supérieure de reproduction.

S'il manque des pages, veuillez communiquer avec l'université qui a conféré le grade.

La qualité d'impression de certaines pages peut laisser à désirer, surtout si les pages originales ont été dactylographiées à l'aide d'un ruban usé ou si l'université nous a fait parvenir une photocopie de qualité inférieure.

Canada

Experimental and Theoretical Studies on Confined Vortex Flow Structures

Li Yan

A Thesis

in

The Department

of

Mechanical Engineering

Presented in Partial Fulfilment of the Requirements
for the Degree of Doctor of Philosophy at
Concordia University
Montreal, Quebec, Canada

August 1995

ISBN 0-612-05077-7

Canada

CONCORDIA UNIVERSITY
SCHOOL OF GRADUATE STUDIES

This is to certify that the thesis prepared

By: **LI YAN**

Entitled: ***Experimental and Theoretical Studies on Confined Vortex Flow Structures***

and submitted in partial fulfillment of the requirements for the degree of

DOCTOR OF PHILOSOPHY (Mechanical Engineering)

complies with the regulations of the University and meets the accepted standards with respect to originality and quality.

Signed by the final examining committee:

Otto Schwelb — Chair
Dr. O. Schwelb

Ashwani K. Gupta — External Examiner
Dr. A.K. Gupta

F. Haghighat — External-to-Program
Dr. F. Haghighat

V. Latinovic — Examiner
Dr. V.N. Latinovic

R. A. Neemeh — Examiner
Dr. R. Neemeh

J. Svoboda — Examiner
Dr. J.V. Svoboda

S. Lin — Thesis Co-Supervisor
Dr. S. Lin

G.H. Vatistas — Thesis Co-Supervisor
Dr. G.H. Vatistas

Approved by _____
Chair of Department or Graduate Programme Director

October 6 19 95

_____
Dean of Faculty

ABSTRACT

Experimental and Theoretical Studies on
Confined Vortex Flow Structures

Li Yan, Ph.D.
Concordia University, 1995

The structure of confined air vortex flow including turbulence effects has been studied experimentally and theoretically.

A measurement technique using Laser Doppler Velocimetry (LDV) was developed to investigate the characteristics of confined air vortex flows: the turbulence intensity, the turbulence kinetic energy, the Reynolds stresses, the mean and fluctuating velocities, etc. Special types of testing devices were designed and built to extend the one-component LDV to three-dimensional measurements. The air vortex flow was produced in a cylindrical chamber using various contraction ratios and inlet Reynolds numbers.

A physical model for the turbulence intensity in the tangential direction for a confined air vortex flow is proposed based on experimental observations. The model divides the turbulence intensity distribution along the radius of the vortex chamber into three regions based on individual characteristic features. A mathematical approach is utilized to obtain expressions for turbulence intensity and to predict the turbulence intensity within the vortex chamber under different conditions.

Equations concerning the kinetic energies due to the mean motion, the fluctuating motion and the two combined have been derived. Experimental results reveal the behaviour of turbulence kinetic energy in the confined vortex flow. The contribution of each parameter to the kinetic energy as well as the overall performances of the kinetic energy is analyzed.

Furthermore, the distribution profiles for both the Reynolds shear stresses and the Reynolds normal stresses in confined air vortex flows are presented. The former is obtained by solving the energy differential equations analytically, and the latter is obtained from the air vortex chamber flow experiments.

Meanwhile, the mean velocities and fluctuating velocities are investigated experimentally. A new profile for the tangential velocity distribution is proposed. An integration is formulated to determine the vortex core size. A computer program is developed for calculation of numerical values of the vortex core size corresponding to different configurations.

ACKNOWLEDGMENTS

The author is sincerely grateful to his supervisors, Drs. G. H. Vatistas and S. Lin, for their guidance and encouragement throughout the effort which has resulted in this thesis. Without their suggestions, ideas, and insight into problems, the work could not have been successfully concluded. The author greatly appreciates the concern and kindness which they extend not only to the author but also to author's family.

The author is also sincerely grateful to Dr. R. A. Neemeh for his supervision at the beginning stage and his advice throughout the years.

The author wishes to thank his wife, Dong Pei-Fang, family and friends for their understanding, encouragement and support throughout his university years.

Finally, the author would like to acknowledge the Fellowship, Scholarships and support from Concordia University, FCAR, and NSERC.

TABLE OF CONTENTS

LIST OF FIGURES

LIST OF TABLES

NOMENCLATURE

A	area
A_b, $A_{b/b}$	constants
A_i	inlet area of vortex chamber
A_o	outlet area of vortex chamber
A_o, $A_{o/b}$	constants
a, a_n	constants ($n = 0, 1, 2, ...$)
B, B_1, B_2	constants
b, b_n	constants ($n = 0, 1, 2, ...$)
C_b, $C_{b/b}$	constants
C_o, $C_{o/b}$	constants
c, c_n	constants ($n = 0, 1, 2, ...$)
D, D_1, D_2	constants
D_{in}	inlet diameter of vortex chamber
D_o	diameter of vortex chamber
d, d_n, e_n	constants ($n = 0, 1, 2, ...$)
F	function
F_r, F_θ, F_z	body forces in radial, tangential and axial direction, respectively
f_a - f_e	functions
G, g	functions
$I_{r,min}$	radial component of minimum turbulence intensity
I_t	tangential component of turbulence intensity
$I_{t.min}$	tangential component of minimum turbulence intensity at main section of vortex chamber
$I_{t,min,b}$	tangential component of minimum turbulence intensity near exit section inside vortex chamber

I_{tb}, $I_{tb/b}$	tangential components of turbulence intensity in boundary layer region at main section and near exit section inside vortex chamber, respectively
I_{tc}	tangential component of turbulence intensity in central core region at main section of vortex chamber
I_{to}, $I_{to/b}$	tangential components of turbulence intensity in outer region at main section and near exit section inside vortex chamber, respectively
K	turbulence kinetic energy $K = \frac{1}{2}\overline{(V')^2}$
K_t	tangential component of turbulence kinetic energy $K_t = \frac{1}{2}\overline{(V'_\theta)^2}$
K_{in}	kinetic energy at inlet of vortex chamber $K_{in} = \frac{1}{2}(\overline{V}_{in})^2$
$K_{t,s}$, $K_{z,s}$	scaled turbulence kinetic energy in tangential and axial directions, respectively
L	length of vortex chamber
m, n	constants
$\vec{n}$	unit vector
p	pressure
p_i	pressure at inlet
p_o	pressure at outlet
$\Delta\tilde{p}$	dimensionless pressure difference
Q	flow rate
$\bar{R}$	normalized radius, ratio of radius r to R_o
R_c	radius of vortex core
R_e	radius of exit of vortex chamber

R_o	radius of vortex chamber
R_e/R_o	contraction ratio
R_{min}	radius corresponding to minimum value
$R_{e,i}$	Reynolds number at inlet of vortex chamber $R_{e,i} = \overline{V}_{in} \cdot D_{in}/\nu$
$R_{e,o}$	Reynolds number inside vortex chamber $R_{e,o} = \overline{V}_{in} \cdot D_o/\nu$
r	radius
$\tilde{r}$	ratio of radius r to R_e
$\hat{r}$	ratio of radius r to R_c
r, θ, z	radial, tangential and axial coordinates, respectively
T.T.K.E.	total turbulence kinetic energy
t	time
V	time average, spatial average or ensemble average velocity
V'	fluctuating velocity
V_i	velocity component at inlet
V_o	velocity component at outlet
V'_R, V'_T, V'_Z	scaled fluctuating velocity components in radial, tangential and axial directions, respectively
$\overline{V}_R, \overline{V}_T, \overline{V}_Z$	scaled mean velocity components in radial, tangential and axial directions, respectively
V_r, V_θ, V_z	velocity components in radial, tangential and axial directions, respectively
V'_r, V'_θ, V'_z	fluctuating velocity components in radial, tangential and axial directions, respectively
$\overline{V}_r, \overline{V}_\theta, \overline{V}_z$	mean velocity components in radial, tangential and axial directions, respectively

V_{ro}, V_{to}, V_{zo}	velocity components at outlet in radial, tangential and axial directions, respectively
$\overline{V}_{in}$	mean velocity at inlet of vortex chamber
$V_{r,s}$	scaled mean radial velocity $V_{r,s} = R_{e,i}^{0.25}(\overline{V}_r/\overline{V}_{in})$
V_t	tangential velocity inside vortex chamber
V_{tin}	tangential velocity at inlet of vortex chamber
$\overline{V}_t$	normalized tangential velocity $\overline{V}_t = V_t/V_{tin}$
$\overline{V}_{t,s}$	dimensionless mean tangential velocity $\overline{V}_{t,s} = (V_t/\overline{V}_{in})/(R_c/R_o)$
X, Y, Z	Cartesin coordinates
X_n	function
β	swirl number $\beta = (A_i/A_o)^2/[\lambda^{4-2n}(\cos\varphi)^2]$
ζ	ratio of radius R_c to R_o
λ	ratio of radius R_e to R_o
μ	dynamic viscosity
ν	kinematic viscosity
ξ	ratio of radius R_c to R_e
ρ	density
σ_{rr}, $\sigma_{\theta\theta}$, σ_{zz}	normal stress components
$\sigma_{r\theta}$, $\sigma_{\theta z}$, σ_{zr}	shear stress components
$\bar{\tau}_{\theta\theta}$	scaled normal stress component (equations 6-28, 6-29, 6-30)
Φ_t, Φ_z	viscous effects in tangential and axial directions, respectively
φ	angle at inlet of vortex chamber

CHAPTER 1

INTRODUCTION

1.1 Previous Work on Vortex Flows

Vortex flow is so common that its existence everywhere seems not to be realized. Although the vortex flow could be explained as "a volume of matter the particles of which rotate rapidly around an axis" [1], "any flow possessing vorticity" [2], and so on, phenomena and applications of the vortex flow are far beyond these explanations. Historical images of vortex flow and fine arts of vortex flow are discovered in Asia tracing back to the ancient time, such as the stone carving of vortex in the Summer Palace in Beijing. Hurricanes, typhoons and tornados which create, never to be forgotten, disasters are an important aspect of the vortex flows. Spirals on shells of nautilus, dust devils and fire whirls are observed from nature, although not everybody paies attention to them.

Focusing on the vortex flow phenomena in engineering, many applications can be illustrated such as vortex separators, vortex combustors, vortex pumps, vortex tubes and so on. With the development of science and technology, physical and chemical properties of particles, dusts and fumes have become more and more clear. Separating harmful particles from flows becomes necessary and urgent in order to protect human beings, animals and the environment from pollution. New types of separators using the vortex principle are highly demanded from industries. Although studies of vortex flows have been carried out by many investigators since last century, previous experience and techniques are found to be far beyond the ability to handle this new situation. Therefore, grasping the fundamental mechanisms and

behaviour of turbulent flow in vortex chambers is becoming an important task for scientists and engineers.

To confined vortex flow which refers to the vortex flow contained within solid boundaries, the Thomson-Rankine vortex model [3] which was composed of free vortex and forced vortex was proposed a hundred years ago. Later, Burgers [4] derived an exact solution of the Navier-Stokes equations for three-dimensional vortex flow. Based on more than four hundred publications, "A Review of Confined Vortex Flows" was presented by Lewellen [5] in 1971, which gave an extensive and almost complete account of knowledge to the confined vortex flow up to that date. Mathematical approach from the integral equations of motion by Wormley [6] resulted in "An Analytical Model for the Incompressible Flow in Short Vortex Chamber". Numerical solution of Wormley's model, considering eddy viscosity, was obtained by Kwok et al [7]. Experimental investigations on the cold aerodynamic structure of gas flow in a vertical chamber were performed by Baluev and Troyankin [8]. The effects of design parameters on the aerodynamics of their experimental model were further studied by themselves [9]. Meanwhile, important work on turbulent flow structure of such flows were carried out by Ustimenko and Buchman [10]. In their experimental investigation, a hot-wire probe was immersed into the flow. Bank and Ganvin [11] indicated confined vortex flow characteristics based on their measurements in such a flow. Theoretical and experimental studies of confined vortex flows by Reydon and Gauvin [12] also showed some common behaviour and characteristics. Engineering applications promoted researches in the vortex flows. Energy separation in vortex tubes which were usually used to create low temperature for refrigeration was investigated [13]. Double vortex combustion chamber was optimized [14] not only to be able to burn

low calorific value solid particles but also to be able to burn them efficiently. Studies and applications of confined vortex flows in nuclear rockets [15], particle separators [16] and so on [17] are so well known that they are not repeated here.

Last decade, new findings on the velocity distribution on the exit plane of a rotating chamber, pressure drop across the chamber as well as vortex core size were reported by Shakespeare and Levy [18]. Theoretical and experimental studies on vortex chamber flows by Vatistas et al [19] showed that dimensionless quantities of vortex core size, static pressure drop across the chamber and radial static pressure distribution were functions of the chamber geometry only. The dimensionless radius of reverse flow was dependent solely on the chamber geometrical parameters [20]. Further research indicated that a non-dimensional pressure drop across the chamber could be determined by a single dimensionless number [21], and that a derived similarity relationship for the pressure drop had been found applicable to both stationary and rotating vortex chambers [22]. It was found that Oseen's equation for an unconfined vortex was adequate to approximate a confined vortex, and a similarity relationship for a radial profile of tangential velocity was obtained [23]. Using a new empirical formula for the tangential velocity, a simple vortex model was proposed [24].

As mentioned above, through the efforts of many researchers, theories of laminar flow in a variety of cases, including confined vortex flows, are quite developed. Analytical models of confined vortex flows as well as analytical or numerical solutions of these have been completed and modified since last century. However, when turbulent flow is involved, the existing theories are still rather deficient for many cases. Osborne Reynolds introduced the time-averaging concept and rewrote continuity and momentum

equations in terms of mean or time-averaged turbulent variables in 1895. But, close form analytical solutions of these equations could not be obtained, because in addition to dealing with four variables (pressure and velocities in three-dimension) the four continuity and momentum equations contained additional six unknown variables which are usually called Reynolds stresses. Therefore, several semi-empirical theories used as alternatives to turbulent flows have been developed and found to be useful in engineering practice.

The k-ε turbulence model (also called two-equation model, turbulent kinetic energy k and dissipation rate ε) was proposed to attempt different problems by specifying several constants in the equations and computing turbulent flow using numerical methods [25]. However, investigation results by Nejad et al [26] showed that the k-ε turbulence model is inadequate for representing the complex turbulent structure of confined swirling flows. Therefore, experimental approach is still a most suitable method for studying the turbulent flow structure.

It has been found that the major challenge for the experimental approach is providing the method to be used in highly turbulent condition. Eaton and Johnston [27] pointed out that highly turbulent flow with frequent velocity reversals limited the reliability of the measurements made with hot-wire anemometers. The accuracy of conventional measuring instruments, such as hot-wire anemometers and pitot probes, was questionable in swirling flows [26]. These measurements suffered from directional ambiguity and flow disturbance. In addition, there was some doubt about the ability of these instruments to cope adequately with high levels of turbulent fluctuations. No one would argue that immersing a probe into the flow will distort the flow field.

Since recently, as a result of technological development, the Laser Doppler Anemometry (or called Laser Doppler Velocimetry) has become a powerful tool for flow measurements. Escudier et al [28] utilized LDA for flow measurement in 1980. Granger [29] performed experiments using LDV in a vertical vortex chamber with water. However, this thesis seems to be the first report of applying LDV technique directly to the measurements of air vortex chamber flows.

1.2 The Study and New Findings

Regardless of how much importance is brought about the fundamental research of mechanisms, behaviours and structures of turbulent flows in vortex chambers, its importance can not be over-emphasized. All applications that employ the vortex principle are based on fundamental research. Everything from the force analysis to the design criteria is closely related to the mean flow motion as well as the fluctuating flow motion. The drag force, pressure, separation efficiency, etc. are always functions of flow characteristics such as velocities, turbulence intensities and so on. Accurate and detailed information about the flow characteristics is always required. However, only the LDV technique, in principle, can provide the required top quality image because it is a non intrusive extensive measurement, which will not interfere with or disturb the flow fields as other conventional methods did. Furthermore, the LDV has a very good response to the flow with a high level of turbulent fluctuations where conventional methods are either inaccurate or inapplicable [26], [27]. This is why this study is more advanced and the obtained results are more accurate and reliable.

In this study, the structure of confined air vortex flow with a high level of turbulence (up to turbulence intensity of 8) has been investigated

experimentally and theoretically because many unknowns exist in the turbulent flow and most applications of confined vortex flows, from the engineering point of view, fall in the category of turbulent flow.

A LDV measurement technique was developed to study the air flow structure in vortex chambers. Flow measurements were taken in all directions near the exit section and at the main section inside the vortex chamber. Abundant data from experiments were analyzed, resulting in a solid background for modelling.

As a fundamental step, the mean velocity and the fluctuating velocity of air vortex flows are investigated. The study is extensively extended to the flow field near the exit section (2.5 mm to the exit plane) inside the vortex chamber, which is very difficult for conventional approaches. A new model, including the formulation of mean tangential velocity profile and the determination of vortex core radii, is proposed. Based on the study of the mean and fluctuating velocities in the confined air vortex flows, the analyses of the turbulence intensity, the kinetic energy and the Reynolds stresses are completed.

A physical model of turbulence intensity for confined air vortex flows is presented. The model indicates that the turbulence intensity distribution along the radius of the vortex chamber can be divided into three regions: the central core region, the outer region and the boundary layer region. A mathematical approach which is based on experimental data and uses both the least square method and the interpolating method is carried out to determine the turbulence intensity quantitatively, which results in empirical equations for each region and under different inlet Reynolds numbers and contraction ratios. A complete indication of the tangential component of the turbulence intensities inside the vortex chamber, from near the exit section to

the main section, as well as the radial component of the turbulence intensity near the exit section inside the vortex chamber is provided in this study.

The kinetic energy of vortex flows is studied theoretically and experimentally. Derived equations concerning the kinetic energies due to the mean motion, the fluctuating motion and the two combined provide important information about the regime of kinetic energies in the vortex flows and the contributions of each component to the kinetic energy. Experimental results show the behaviour of turbulence kinetic energy in the air vortex flow and establish the background for a mathematic approach. Empirical expressions for the turbulence kinetic energy are proposed. They consider the effects of the flow rate and the contraction ratio.

Furthermore, the Reynolds equations applied to confined vortex flows as well as the equations concerning the Reynolds stresses in confined vortex flows are derived. By solving the differential equations derived from the kinetic energy analysis, analytical results of the Reynolds shear stresses are obtained. Using a computer program developed for this calculation, numerical results of the Reynolds shear stresses are given. Meanwhile, measurement results of the Reynolds normal stresses are analyzed to form mathematic expressions.

Since most new results and conclusions are based on the experimental investigation and analysis using dimensionless or normalized units, they have broad meanings and applications. The information obtained through this research promotes further better understanding of the structure of confined air vortex flows.

CHAPTER 2

EXPERIMENTS

2.1 General

A technique using Laser Doppler Anemometry (Dantec) has been developed to measure air confined vortex flows. The LDA had not been applied to such flow fields before, and the LDA supplier did not have any experience in such air flow measurement. Fortunately, through a lot of efforts, these technical difficulties have been overcome. The goal of investigating turbulent flow structure in confined vortex flows has been achieved successfully.

The experiments were performed at different sections inside the vortex chamber, from 32.4 % to 99.4 % of the vortex chamber length starting at the inlet side end of the vortex chamber. Different inlet air flow rates, ranging from $0.0047m^3/s$ (10cfm) to $0.033m^3/s$ (70cfm), corresponding to the inlet Reynolds numbers from 1960 to 13700, were applied in the experiments. At each set air flow rate, the contraction ratio R_e/R_o was varied from 0.25 to 1.0.

During the experiments velocities of micron particles following the flow are measured by the LDA. Hence, mean velocity, fluctuating velocity, root-mean-square velocity, turbulence intensity, and other correlations are obtained. The collected data are stored for further processing.

The experimental system and apparatus, measurement techniques and developments, experimental variables and combinations will be described in the following sections. The obtained results will be highlighted and discussed later.

2.2 Experimental System and Apparatus

2.2.1 System

The experimental system, consisting of two major parts: air vortex generation and flow measurement, has been designed and built in the Fluid Mechanics Laboratory at Concordia University. The system is schematically illustrated in Figure 2.2.1.1.

Compressed air is supplied to the inlets of the vortex generator. A control valve is mounted on the air supply line in order to set the desired volumetric flow rate. A rotameter is used to measure the volumetric flow rate. When the air flow passes through the vortex generator to the vortex chamber, a swirl is imparted to the field. That is, the vortex flow is generated inside the vortex chamber. The vortex chamber has a cylindrical shape with constant circular cross-section area, and has an exit plate on which there is a central exit hole. Finally, the air flow passes through the central exit hole to the atmosphere.

A Laser Doppler Anemometer is used for the flow measurements. When two laser beams are made to interfere by a front lens, a small measurement region is created. When flow particles move through this region, light signals are generated and are converted into electric signals. A computer system, then, processes the electric signals and provides the results.

In order to determine the air flow structure at different space positions, a traversing device is designed to move the vortex chamber. By the device any required measurement location can be reached.

2.2.2 Vortex Chamber and Vortex Generator

The structure of the vortex chamber and the vortex generator is shown in Figure 2.2.2.1. The vortex chamber which is made of plexiglas for the

purpose of laser beams penetrating as well as visualization is mounted on the vortex generator. Its geometrical parameters can be adjusted easily by replacing different plexiglas components. The vortex chamber used for the current experiments has an inside diameter of 13.97 cm (5.5 in.) and a total length of 43.18 cm (17 in., $16^{15}/_{16}$ in. for the chamber plus thickness of seal pads). On the top of the vortex chamber, there is an exit plate which has a hole in the centre. The exit area of the vortex chamber depends on the size of the hole. By replacing the exit plates with a different size of the hole, the exit area of the vortex chamber can be adjusted. For the experiments reported here, the diameter of the exit hole varies from 3.49 cm (1.375 in.) to 13.97 cm (5.5 in.).

The vortex generator has four perpendicular air inlets where the compressed air is induced. Inside the vortex generator, there is a vortex generation block as shown in the top part of Figure 2.2.2.2. When the air flow passes through the block, it is guided to enter the vortex chamber in the tangential direction so that swirl is formed inside the vortex chamber. The block used for the present experiments has 16 ports with the inlet diameter D_{in} of 1.27 cm (0.5 in.) and the inlet angle φ of 30^{o} to the coordinate, which are shown in the bottom part of Figure 2.2.2.2.

2.2.3 Laser Doppler Anemometry

The Laser Doppler Anemometer is an ideal instrument for flow measurement in the complex flow fields, such as swirling flows with high levels of turbulent fluctuations, since it is nonintrusive, calibration free, and can provide good spatial and temporal resolution.

The principle that the LDA works on is the Doppler shift. The major components of the LDA are illustrated in Figure 2.2.1.1. By stimulated

emission of radiation, the laser beam generator produces intense coherent light with a very small bandwidth. When the light passes through the beamsplitter and the bragg cell, two laser beams split from the same original illumination source are formed by the beamsplitter, and a fixed optical frequency shift between the two laser beams is introduced in the bragg cell based on the principle of the Doppler effect. Then, the two beams pass through the front lens, and are made to interfere. This produces "fringes" and creates a small measurement region. When particles immersed in the fluid move through this region, in other words, cross the fringe pattern, they scatter light which is modulated at the Doppler frequency. A Doppler shift of the frequency of the light is caused. The spacing between the fringes provides the relation between the moving particle velocity and the Doppler frequency. If a particle crosses two laser beams simultaneously, two Doppler shifts are created. The combination of these two Doppler shifts produces a "beat frequency" at the difference between the frequencies of the two original signals. This "beat frequency" is the Doppler frequency. It is equal to the dot product of the particle velocity with the difference between the scattered and the incident wave vectors. In the LDA, the scattered light signals are picked up by the PM optics (photomultiplier) where the light signals are converted into electric signals.

A one-component Argon-ion Laser Doppler Anemometer (Dantec) is used for all flow measurements. It has a wavelength of 514.4 nm (green) and operates at 300 mW. Two parallel laser beams, each having a Gaussian beam diameter of 0.82 mm, are separated by 60 mm. They are focused by a front lens with a focal length of 310 mm. The interference of the two laser beams produces 93 fringes with each fringe spacing of 2.67 μm. The probe measurement volume which is created by the interference is ellipsoidal in

shape. The approximate dimensions of the probe measurement volume are major axes of 2.57 mm and minor axes of 0.25 mm. Two bragg cells are used to provide a net optical frequency shift of 40 MHz. The burst detector bandwidth is set from 0.003 MHz to 0.500 MHz, corresponding to the velocity bandwidth from 0.12 MHz to 36.0 MHz. It allows for the measurements to be made for both reverse flow and forward flow. That is, corresponding to a maximum range of particle velocity from - 16.0 m/s to 80.1 m/s. The data acquisition, storage, processing and presentation are done by a Flow Velocity Analyzer (Dantec 58N20 FVA Signal Processor) and a IBM-AT compatible computer with the FLOware Version 3.0 (Dantec).

2.3 Measurement Techniques

2.3.1 Scatter System Setting

The LDA was set in a backward scatter system originally by the supplier for the flow measurements. It was found that the backward scatter system provided lower data rate and higher level of noise. The PM optics in the backward scatter system picked up too much background noise. When performing measurements in the boundary layer flow near the vortex chamber wall, the noise caused by the reflected beam from the vortex chamber wall (made of plexiglas) was so strong that the PM tube was trapped in overload. Therefore, the forward scatter system was finally adopted to perform the measurement. The forward scatter system could provide data rate up to 100 kHz. The forward scatter system also provided higher ratio of signal to noise.

To further improve the LDA performance, particularly in the aspect of noise reduction, the influence of the view angle of the PM optics was studied. Weighing both noise level and signal intensity yielded an optimum angle of

15° between the central line of the PM optics and the LDA measurement surface. Under such an arrangement, direct illumination from the transmitting beams could be avoided. The noise due to the strong beam reflection from the plexiglas wall was reduced significantly and the whole range velocity measurement, from the boundary layer flow region to the main flow region, could be performed.

2.3.2 Seeding and Seeding Method

As mentioned before, the particle velocity can be detected only if particles immersed in the fluid move through the LDA measurement region. For the liquid flow measurement, such as water, the amount of micro-particles in the liquid is sufficient. The size of these micro-particles is big enough to scatter laser beams. Therefore, the LDA works well in liquid flow without adding any seed.

In the pure air flow, because the density of the air is lower than that of the liquid, not many micro-particles are contained in the fluid and the size of these micro-particles is too small to scatter laser beams. The LDA does not work if seeding is not added. Therefore, special seeding particles have to be introduced to make the LDA work. Several kinds of seeds can be used to seed the flow. Considering safety, cost, and easy handling, petroleum distillate whose major composition is Aliphatic HydroCarbon, $(CH_2)N$, has been selected as the seeding for the experiments. By a fog machine, the petroleum distillate is evaporated to form fog. Then, inducing the fog into the air flow, the progress of the flow can be sensed by the LDA. Fog Fluid #8207 from ROSCO Laboratories Inc. is also used in the experiments. Fog Fluid #8207 is better for the protection of the environment, but, it seems to produce lower density of fog than the petroleum distillate. However, it is acceptable. In fact,

what the LDA senses is the movement of the seeding particles. Therefore, it is required to form a homogeneous air flow with seeding particles to make the flow measurement sufficiently accurate.

Several procedures were tried to introduce the seeding particles to the air flow and to mix them with air uniformly. A convergent-divergent nozzle was designed such that the seeding particles could be sucked by vacuum. This method did not work at high flow rate because of the higher pressure level of the compressed air source. A centrifugal blower was used to force the seeding particles into the air flow. However, condensation of the petroleum distillate on the blower was a problem. Eventually, the seeding particles generated directly by the fog machine were introduced at the centre of the vortex generator, where the vortex flow created a small low pressure region.

2.3.3 Three Dimensional Measurement

An electric traversing system was supplied with the LDA. It moves the front lens in one direction only as shown in Figure 2.2.1.1. In order to extend the one-component LDA to the radial, tangential, and axial component measurement, a mechanical traversing device with position indicators was designed as shown in Figure 2.3.3.1. The vortex chamber and vortex generator are mounted on the mechanical traversing device by a metal frame. The frame makes it possible to set the vortex chamber and vortex generator in either vertical orientation or horizontal orientation as shown in Figures 2.2.1.1 and 2.3.3.2 respectively. The frame is moved by a worm gearing system. Thus, the vortex generator and the vortex chamber can be moved in X, Y, Z direction and be set at any measurement position. The positioning accuracy of the mechanical device is estimated to be 0.25 mm (0.01 in.) in all directions. During the experiments, the electric traversing system is used only to set

measurement region at a reference point such as the centre of the vortex chamber. The setting of measurement points of the whole measurement range is carried out by using the mechanical traversing device to move the vortex chamber manually.

To measure the radial component, the vortex chamber is set in the vertical orientation and at a required location of measurement section, which is determined by a required distance in the axial direction of the vortex chamber (Z direction) to a reference point. Two laser beams are focused on the centre of the vortex chamber as shown in Figure 2.3.3.3. Then, moving the vortex chamber along the X axis to each measurement point, the radial component profile is obtained. The dotted circles in Figure 2.3.3.3 refer to moving the vortex chamber and measuring the radial component at other arbitrary locations after setting.

To measure the tangential component, the vortex chamber is also set in the vertical orientation and at a required location of the measurement section, which is the same as for measuring the radial component. However, two laser beams are focused on the central line of the vortex chamber in the Y direction as shown in Figure 2.3.3.4. Then, moving the vortex chamber along the Y axis to each measurement point (or adjusting the LDA focusing point along the Y axis), the tangential component profile is obtained. The dotted circles in Figure 2.3.3.4 refer to moving the vortex chamber and measuring the tangential component at other arbitrary locations after setting.

To measure the axial component, the vortex chamber is rotated 90° from the position of measuring the radial component or the tangential component to the horizontal orientation as shown in Figure 2.3.3.2. The horizontal central line of the vortex chamber is set to be on the measurement surface formed by the two laser beams. The location of measurement section

is set to be based on the required distance in the Z direction as shown in Figure 2.3.3.5. Then, moving the vortex chamber in the Y direction, the axial component profile is obtained. The dotted rectangular in Figure 2.3.3.5 refer to moving the vortex chamber and measuring the axial component at other arbitrary location after setting.

By this arrangement, the measurement of the radial and axial components can be performed for the same point, and the same applies for the measurement of the tangential and axial components. However, it is impossible to perform the measurement of the radial and tangential components for the same point. Therefore, the three dimensional component measurement is based on the assumptions that the tested vortex chamber has a perfect cylindrical shape and that the air flow is symmetric to the axial central line and homogeneous. The combination of the radial, tangential and axial components results in space vectors.

2.3.4 Sampling and Aberration Correction

In the experiments sampling is controlled based on the combination of realization and time, either that individual realizations are accumulated up to 4000 for each component at each measurement point, or that the sampling time reaches 30 seconds to insure that all low frequency phenomena are included in the sample.

When the laser beam penetrates the plexiglas wall of the vortex chamber, beam refraction takes place because the medium of plexiglas is different from that of air. Optical aberrations on the probe volume will occur if the refractions of two laser beams are not identical. In the measurements of tangential component and axial component, two laser beams are always bent in the same degree because, ideally, the wall structures which the laser beams

pass through are symmetric. The observed optical aberration in the measurements of the tangential component and the axial component is so small (~ 0.25 mm) that it can be neglected. Compensations for the optical aberration in the measurements of the tangential component and the axial component were not considered in the reported experiments. However, in the measurements of radial component, two laser beams will interfere at points which are not on the central line of the vortex chamber. Optical aberrations do occur because the two laser beams are bent in different angles as the beams penetrate the plexiglas wall with different curvature as shown in Figure 2.3.4.1. In that figure, as an example, the dotted circles refer to a new location of the vortex chamber in which the measurement point is not on the central line of the vortex chamber. Apparent optical aberration takes place in the Y direction. The optical aberration is smaller in the X direction if compared with that in the Y direction. Therefore, methods to eliminate errors due to the curved optical interface should be adopted.

Using two cylindrical plano-convex lenses placed symmetrically on opposite sides of the vortex chamber to reduce aberration effects is a method proposed by Durrett et al [30]. The method used currently in the radial component measurement is to trace the optical aberration and to set a series of modified new location indication for each measurement point. A correcting curve for the measurement location is made in the following way. First, the spatial intervals between two measurement points in the X direction are set to be even. Then, the vortex chamber is moved to each measurement point in the X direction. Meanwhile, the location of the laser beam interference point in the Y direction is traced by the mechanical traversing device. The optical aberration in the Y direction can be detected by resetting the laser beam interference point to be on the diameter line of the

vortex chamber. The indicator on the mechanical traversing device shows the moving distance in the Y direction, which corresponds to the deviation caused by beam refractions. By dotting the modified locations of all measurement points on a Cartesian coordinate, a smooth correcting curve is obtained. Required corrections for optical aberrations at any other measurement points can be determined from the plot or the equation by curve fitting technique, which are presented in Figure 2.3.4.2. By this method, the optical aberration effects can be reduced to a minimum level over the whole measurement range, and induced errors are within an allowable range.

2.4 Experimental Variables

Particle velocity measurements were made at different sections inside the vortex chamber under three different inlet air flow rates: 0.0047 m^3/s (10 cfm), 0.019 m^3/s (40 cfm) and 0.033 m^3/s (70 cfm) respectively, which are corresponding to three inlet Reynolds numbers: 1960, 7840 and 13700 defined as:

$$R_{e,i} = \frac{\overline{V}_{in} \cdot D_{in}}{\nu} \qquad (2\text{-}1)$$

where

$\overline{V}_{in}$ = mean inlet velocity

D_{in} = inlet diameter

ν = kinematic viscousity

The contraction ratio which is defined as the ratio of the radius of the exit hole, R_e, to the radius of the vortex chamber, R_o, was varied from R_e/R_o = 0.25, 0.30, 0.40, 0.50, 0.58, 0.75 to 1.0 which corresponds to a fully open exit state.

The measurement surface is perpendicular to the Z-axis. The distances between the measurement surface to the exit plate in the axial direction are different. To the section near the exit inside the vortex chamber, the measurement surface is set to have a distance of 2.5 mm (0.1 in.) to the exit plate surface, corresponding to 0.6% of the vortex chamber length. To the main section which is assumed within 30% to 90% of the vortex chamber length, the measurement surface is set to have a distance of 298.5 mm (11.75 in.) to the inlet side end of the vortex chamber, corresponding to 69.1% of the vortex chamber length. Besides, at the contraction ratio of 0.40, the measurements of tangential components are performed at three other locations: 381 mm (15 in.) to the bottom, corresponding to 88.2% of the vortex chamber length; 215.9 mm (8.5 in.) to the bottom, corresponding to 50% of the vortex chamber length; 139.7 mm (5.5 in.) to the bottom, corresponding to 32.4% of the vortex chamber length. It is designed to cover the assumed main section from 30% to 90% of the vortex chamber length. The measurement of the radial component is performed at an extra location: 215.9 mm (8.5 in.) to the bottom, corresponding to 50% of the vortex chamber length.

In each experiment, measurements are performed along a diameter direction of the measurement surface, from one side wall of the vortex chamber to the centre, then, from the centre to another side wall. That is, the entire diameter of the vortex chamber. The purpose of this measurement arrangement is to insure the accuracy of the experiments. A symmetric profile should be obtained to verify whether the measurement points are on the diameter of the vortex chamber and whether the origin of measurement system coordinate is identical with the geometric centre of the vortex chamber. In fact, for the purposes of analysis, calculation and presentation, acquiring data along the radius is sufficient. The spatial interval between two

measuring points is set to be 5 mm (0.2 in.) for most of points. Since the flow will not slip on the wall, the beginning and ending measurement points are set to have a distance of 2.5 mm (0.1 in.) to the wall, and a spatial interval of 2.5 mm (0.1 in.) is set for the next two measurement points as these measurements are considered in the boundary layer region or near the boundary layer region. For the presently tested vortex chamber with a diameter of 140 mm (5.5 in.), there are 30 measurement points in each diameter direction.

2.5 Experimental Accuracy

2.5.1 Experimental Errors

Although there is no outside calibration required for the LDA measurement, there are many factors contributing to the experimental errors.

Sampling is one of the major factors, which will directly influence the accuracy of the measurements. A detailed discussion of the accuracy of the measurements will be in the next section.

Seeding is also a major influence factor. The LDA measurement is based on the detection of the motion of the seeding particles. Ideally, the seeding particles will exist in and follow the air flow homogeneously. However, it seems to be impossible to avoid the minor variation of the fog concentration. When the air flow containing seeding particles enters the vortex chamber, the centrifugal force due to swirling flow inside the vortex chamber has a tendency to separate the seeding particles and to destroy the homogeneous flow, but, the concentration (or density) of seeding particles in the flow is still satisfactory to the requirement of the LDA. The measurement shows that the experimental errors due to possible non-homogeneous seeding is so small that it could be neglected.

The accuracy of the measurement location could be one of the sources of errors. The mechanical traversing device has an estimated positioning accuracy of 0.25 mm (0.01 in.). Although the location of measurement points were set at certain fixed numerical values, it is impossible, in fact, to repeatedly set the measurement point at exactly the same location. In other words, minor spatial location deviation can not be eliminated in repeated moving and setting measurement points.

When the laser beam penetrates the plexiglas wall of the vortex chamber, beam refraction must occur as the beam passes through different mediums: air-plexiglas-air. The beam refraction will affect the accuracy of setting measurement location. Furthermore, the uniform thickness of the wall could not be perfect; The cylindrical shape of the vortex chamber could not be perfect; The centralization of the LDA and the vortex chamber could not be perfect, etc. These small influence factors eventually may result in some experimental errors. During the experiments, definitely, a lot of effort had been made to eliminate or reduce these errors to the minimum level.

2.5.2 Measurement Accuracy

The accuracy of measurements is directly related with the sampling: the number of realizations to be taken to obtain a good mean value and standard deviation; the time interval of the sampling to be set to insure that all low frequency phenomena are included. Of course, the more the realizations, the better the accuracy. The longer the time interval of the sampling, the better the accuracy. However, taking unlimited realizations is unrealistic, which is limited by the computer memories. Unlimited sampling time will meet the same problem as unlimited realizations meet. Based on the work of Donohue et al [31] and Yanta and Smith [32] certain accuracy can

be obtained by taking a reasonable number of realizations which can be determined as follows.

The confidence limits for estimating the population mean μ has the following correlation

$$\mu \leq X \pm \frac{Z_c \cdot \sigma}{\sqrt{N}} \qquad (2\text{-}2)$$

where

μ = population mean

X = sample mean

σ = population standard deviation

N = number of data points

Z_c = coefficient determined by the Gaussian function

It has been derived that the number of required realizations is equal to $Z_c/(\text{error})^2$, which is independent of the flow conditions [29]. For a 95 % confidence level, a minimum of about 800 realizations is needed. In general, more than 1000 realizations for each measurement point will give a good accuracy. For instance, in the work of Gouldin et al, "Velocity Field Characteristics of a Swirling Flow Combustor". [33], 1000 realizations for isothermal flow and 500 realizations for combusting flow were adopted. 2000 samples were acquired in Singler's work [34]. In the "Experimental Study of Compressible Turbulent Mixing Layers" [35] 2000 samples were taken at each measurement location.

In this study, 4000 realizations were taken for each measurement point, which corresponded to an approximate 97 % confidence level. It insured that the sample deviation did not differ by more than 3 % from the true population standard deviation.

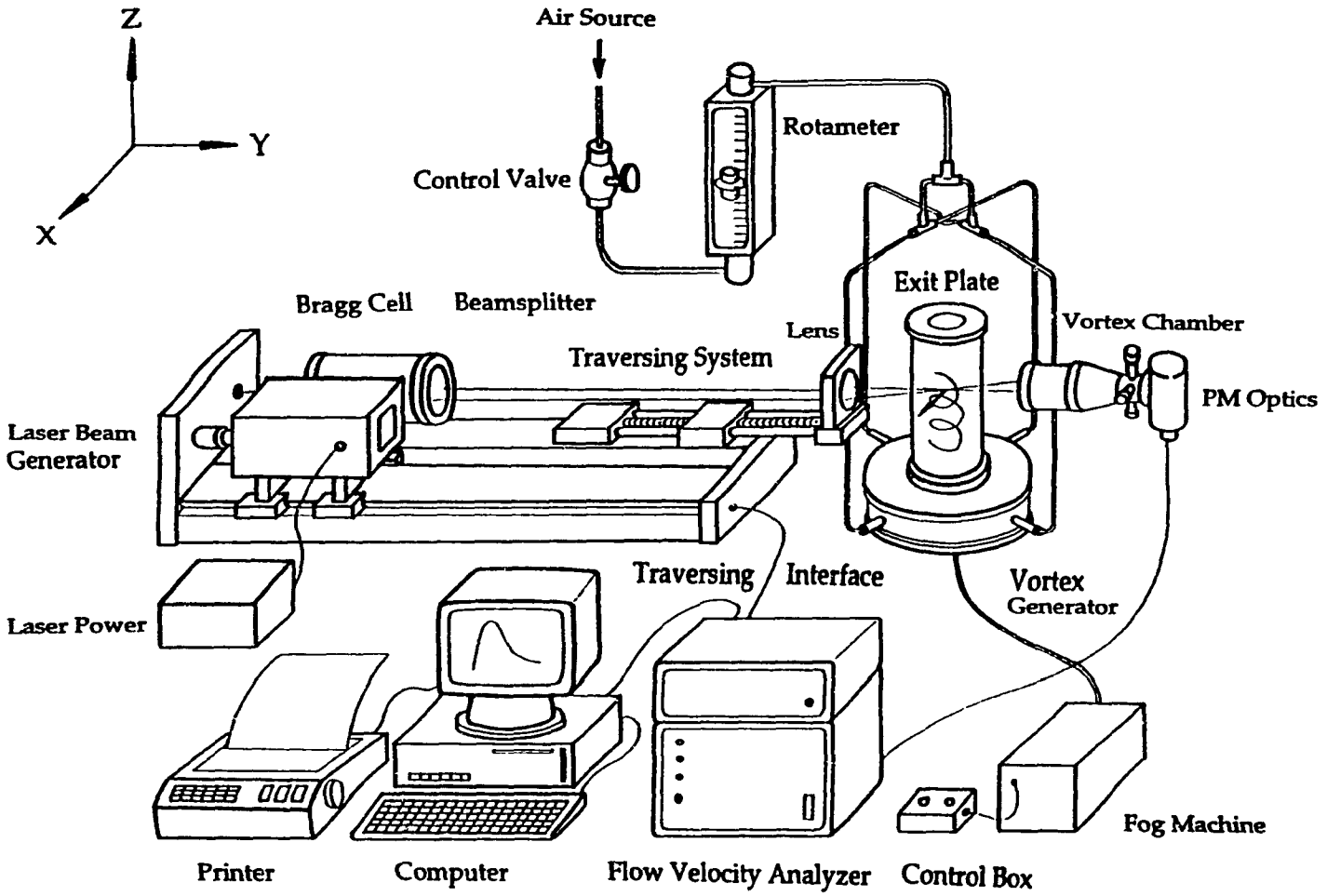

Figure 2.2.1.1 Experimental System (Vertical Orientation)

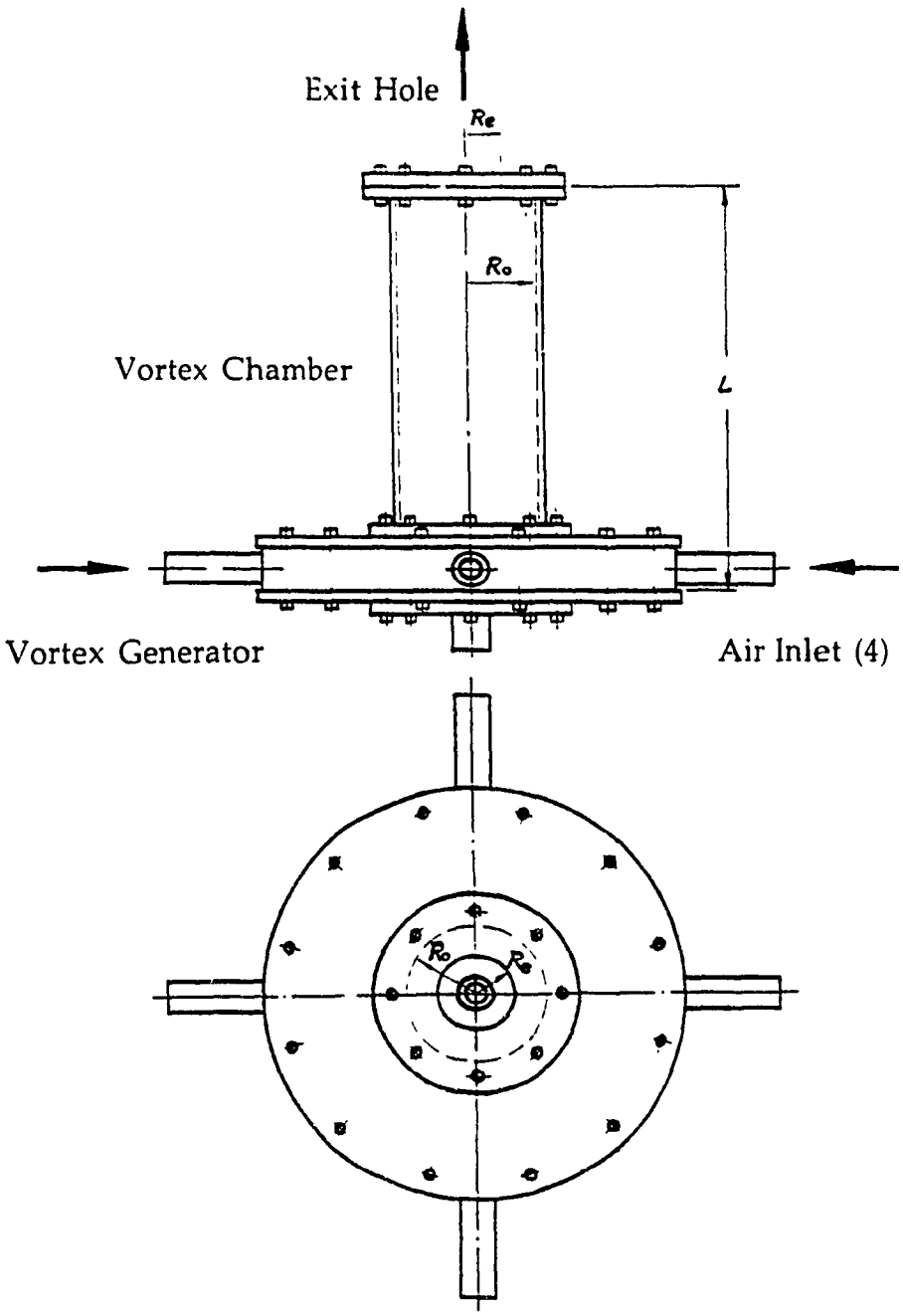

Figure 2.2.2.1 Vortex Chamber and Vortex Generator

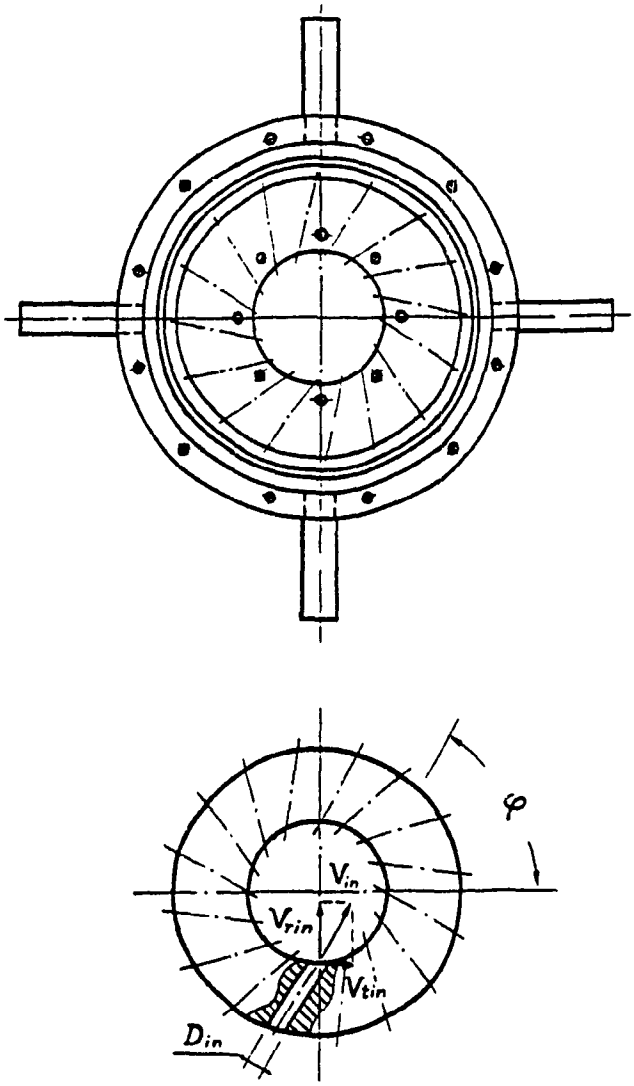

Figure 2.2.2.2 Vortex Generation Block

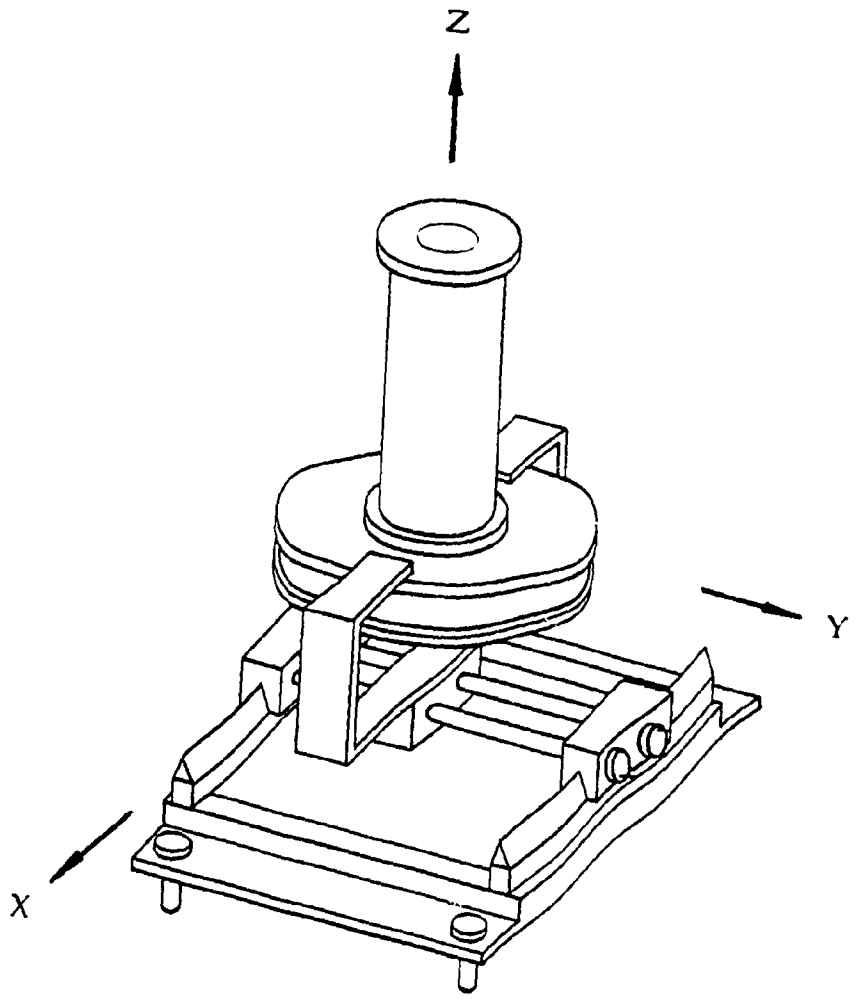

Figure 2.3.3.1 Mechanical Traversing Device

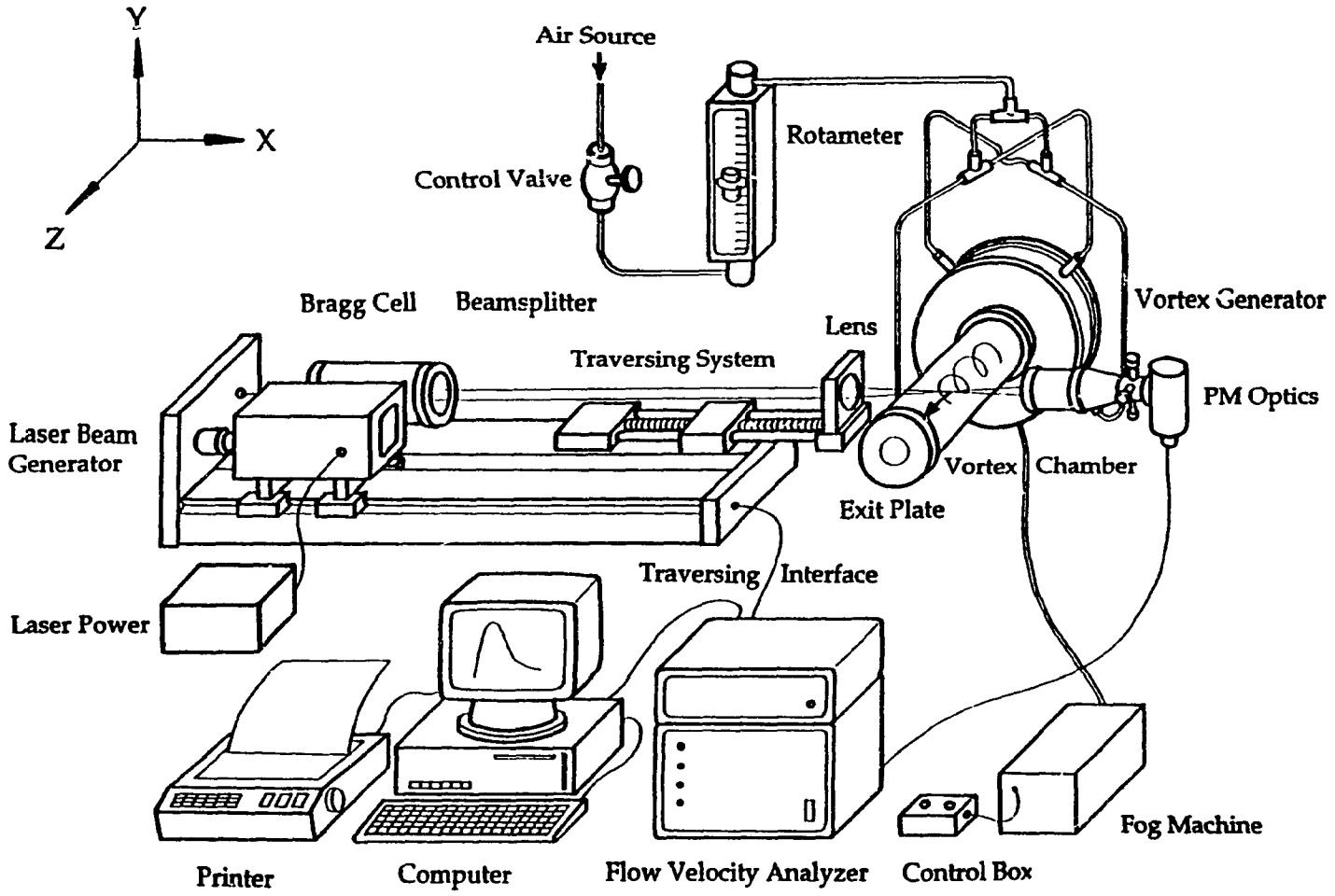

Figure 2.3.3.2 Experimental System (Horizontal Orientation)

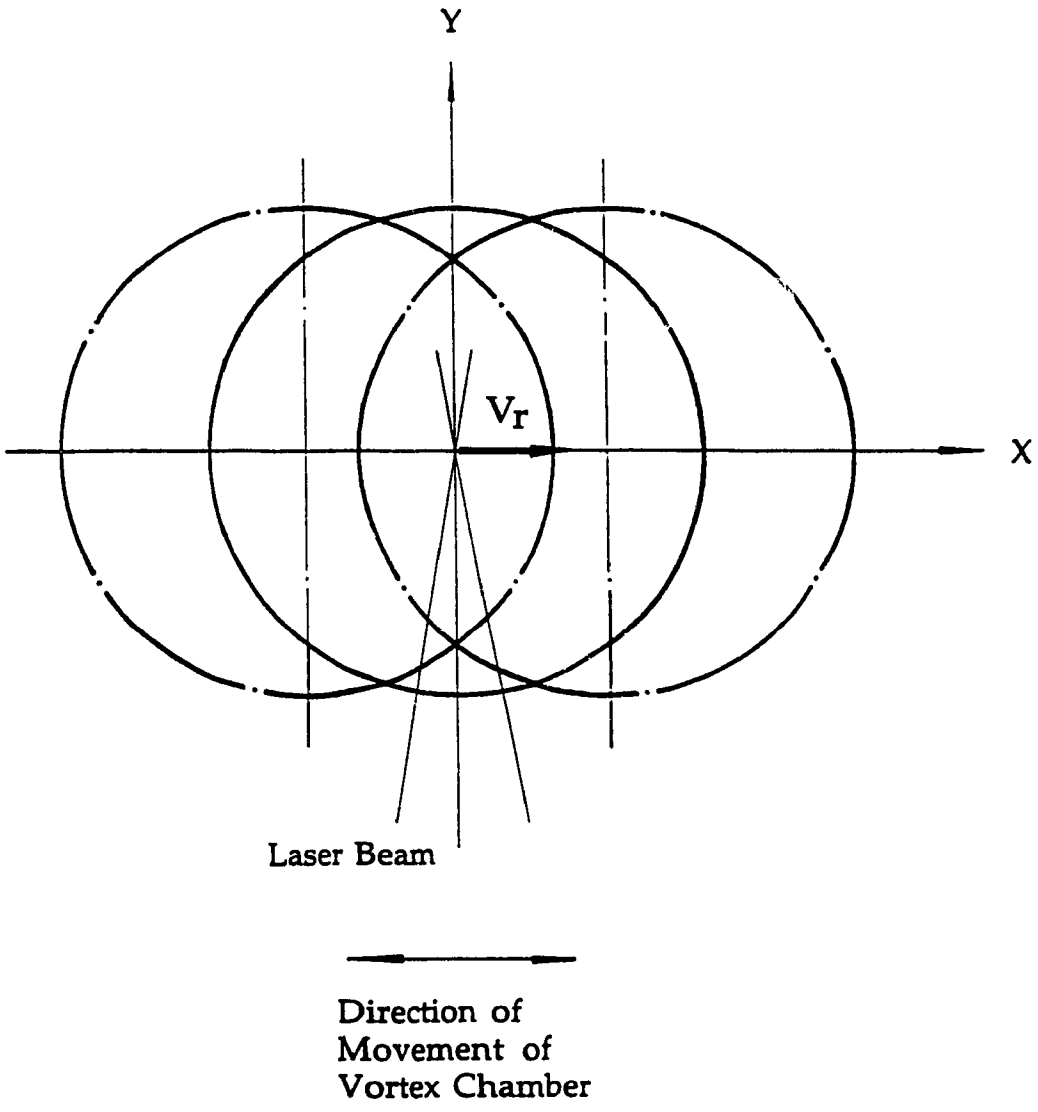

Figure 2.3.3.3 Radial Component Measurement

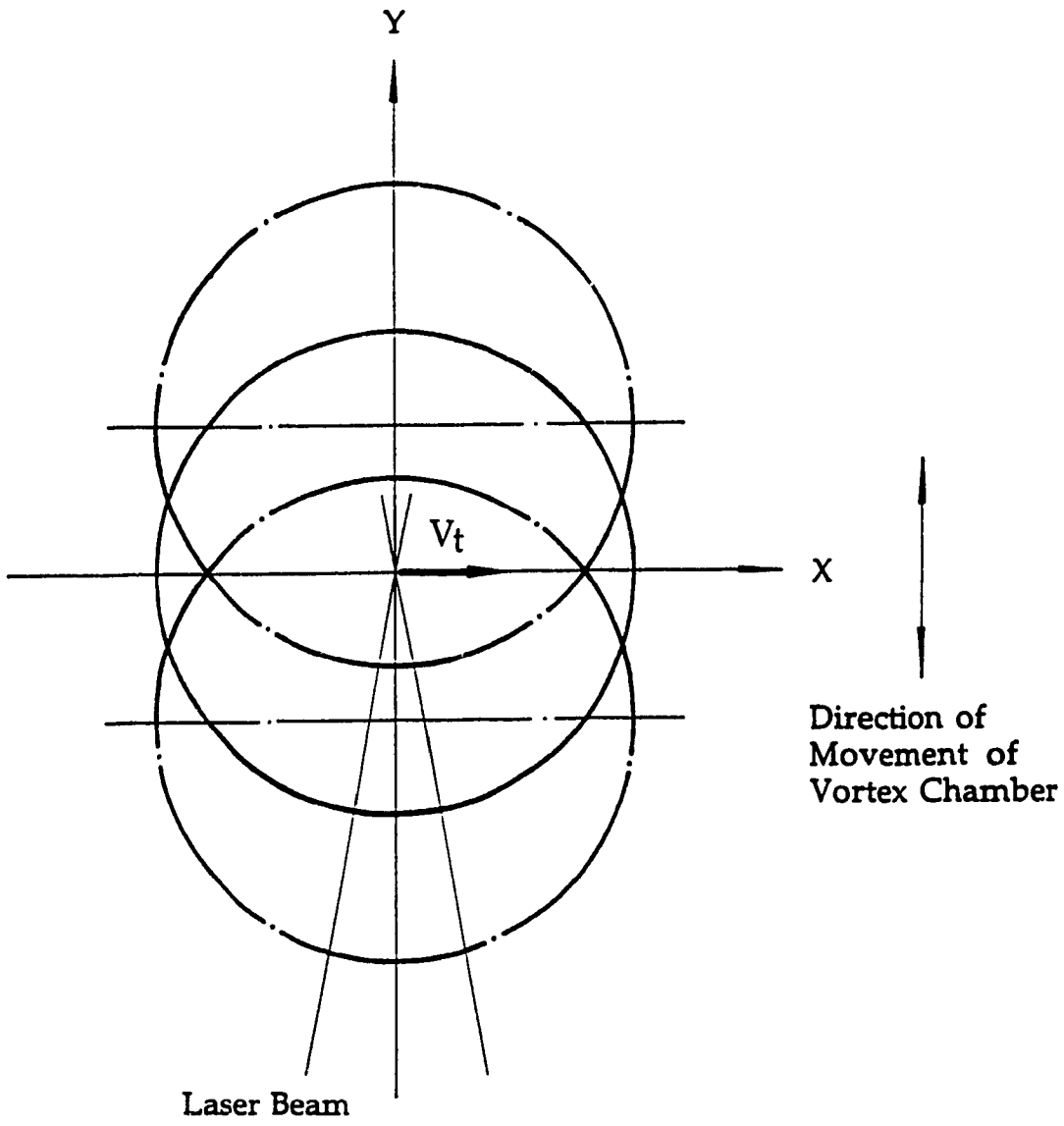

Figure 2.3.3.4 Tangential Component Measurement

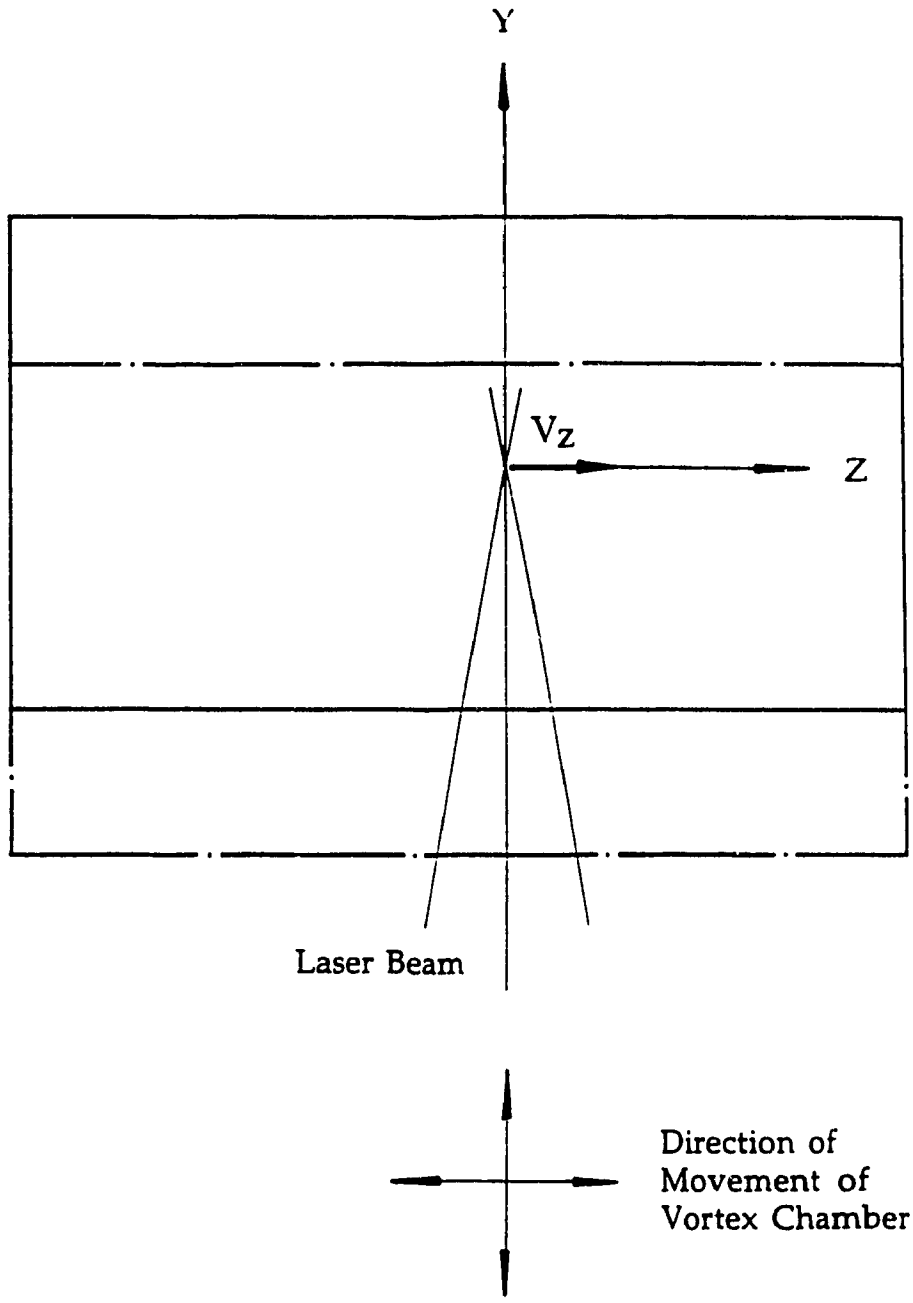

Figure 2.3.3.5 Axial Component Measurement

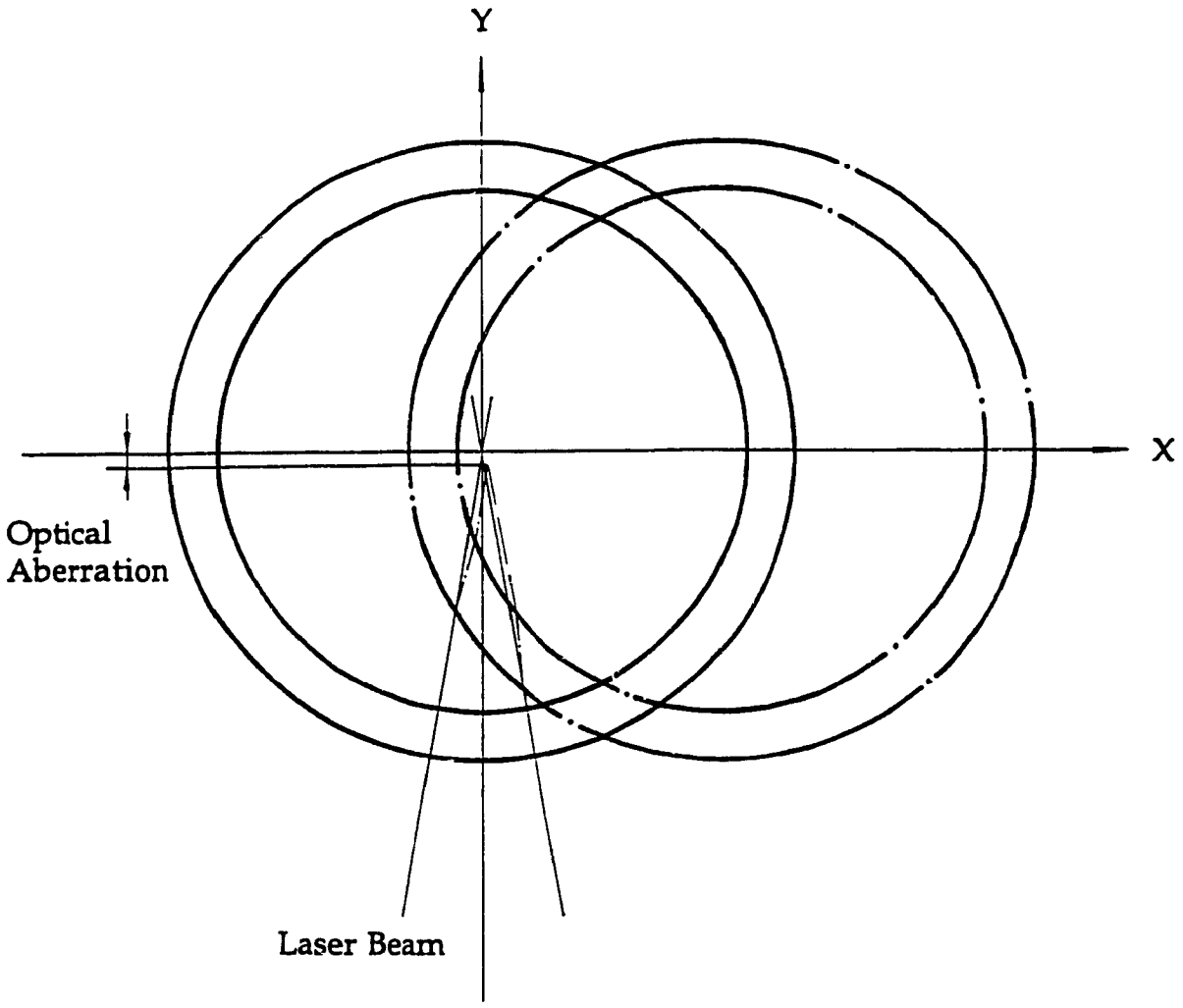

Figure 2.3.4.1 Optical Aberration

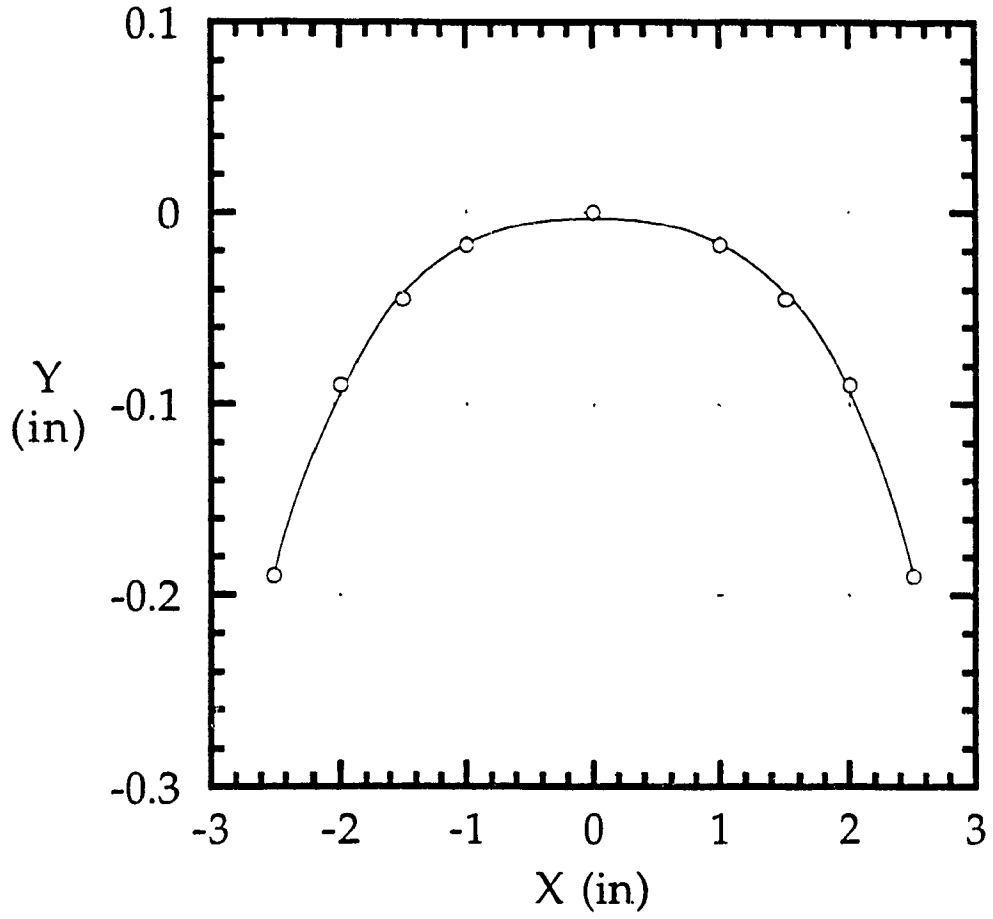

Figure 2.3.4.2 Location Correction for Radial Component Measurement

CHAPTER 3

MEAN FLOW

3.1 General

Many investigators have contributed to the modelling of the mean velocity in vortex flows, such as the Thomson-Rankine vortex model which idealized the mean tangential velocity of confined vortex flows as a combination of free-vortex motion and forced-vortex motion [3]. By presenting a new empirical formula for the mean tangential velocity, other velocity components were obtained from the equations of motion by Vatistas et al [24]. However, these models are based on the flow behaviour presented at the main section of the vortex chamber only.

In this work, extensive investigations of mean velocity inside the vortex chamber, from the main section to near the exit section, were performed experimentally, using the extensive nonintrusive LDA technique. A new model, including the formulation of velocity profiles and the determination of the vortex core radius, is proposed.

3.2 Mean Tangential Velocities

The recent study of the tangential velocity in confined air vortex flows is much wider and more accurate than those of previous investigations. Experimental results of mean tangential velocity at both the main section and near the exit section are obtained and presented in Figures 3.2.1 to 3.2.6.

The obtained results indicate that some mean tangential velocity models such as that proposed by Vatistas et al [24] could be extended into a wider range of applications.

One of the most important findings is that the inlet Reynolds number has no influence on the location of the maximum mean tangential velocity. It means that the location of the maximum mean tangential velocity depends on the swirl number. Since the defined swirl number β is a function of the contraction ratio R_e/R_o, the contraction ratio, instead of the swirl number, is used as an independent parameter in many analyses.

It is found that the numerical value of the normalized radius R referring to the maximum mean tangential velocity is always less than that of the contraction ratio R_e/R_o under which testing is done. This correlation is found not to be affected by the inlet Reynolds number.

The mean tangential velocities at the main section and near the exit section inside the vortex chamber have similar or almost exact velocity distributions under the same contraction ratio and the same inlet Reynolds number. The mean tangential velocity is zero at the centre of the vortex chamber. It increases its magnitude along the radial direction. In the cases of small contraction ratios, the mean tangential velocity increases very rapidly. Then, it reaches its maximum value and starts to reduce its value gradually along the radial direction until the wall of the vortex chamber. All velocity reduction curves with different contraction ratios will collapse to form a unique trace. Under the same experimental conditions, the difference between the mean tangential velocities at different locations within the main section is small, which is shown in Figure 3.2.7. The deviation is listed in Table 3.2.1. 89 % of points are within 10 % of the deviation. It indicates that one tangential velocity profile can be applied for the whole main section.

It is found that the mean tangential velocity can be normalized by the inlet tangential velocity to form identical distributions through the whole vortex chamber. The normalized mean tangential velocity V_t/V_{tin} at a lower

inlet tangential velocity is slightly higher than that at a higher inlet tangential velocity. Maps of average normalized tangential velocity are proposed as shown in Figures 3.2.8 and 3.2.9 for the main section and near the exit section inside the vortex chamber respectively. Sample deviations between individual tangential velocity to the average tangential velocity based on different inlet Reynolds numbers at the same section are listed in Tables 3.2.2 and 3.2.3 for the main section and near exit section respectively. 89 % points are within 10 % deviation.

For either the absolute value or the normalized value, the magnitude of the maximum mean tangential velocity near the exit section inside the vortex chamber is always slightly higher than that at the main section of the vortex chamber.

Since the forced-vortex flow in the centre of the vortex chamber can be considered as a core, which is defined as the space bounded by a cylindrical surface having the same radius with the point of the maximum mean tangential velocity [19], a distribution of dimensionless mean tangential velocity $\overline{V}_{t,s}$ versus scaled radius $\hat{r}$ can be formed as shown in Figure 3.2.10 with following dimensionless factors:

$$\overline{V}_{t,s} = \frac{V_t}{\overline{V}_{in}} \cdot \frac{R_c}{R_o} \qquad (3\text{-}1)$$

$$\hat{r} = r / R_c \qquad (3\text{-}2)$$

where

R_c = radius of vortex core

The experimental results further prove that this correlation can be extended for different sections, contraction ratios and inlet Reynolds numbers.

Based on the previous investigation carried out by Vatistas et al [23], a new approach for the determination of core size and the formulation of tangential velocity profile is developed.

A normalized tangential velocity profile is proposed as follows:

$$\overline{V}_t = \frac{V_t}{V_{tin}}$$

$$= \frac{1}{\overline{R}^n} \cdot \frac{1 - \exp(-a\overline{R}^2)}{1 - \exp(-a)} \tag{3-3}$$

where

$$\overline{R} = \frac{r}{R_o} \tag{3-4}$$

Differentiating the normalized tangential velocity yields

$$\frac{d\overline{V}_t}{d\overline{R}} = -\frac{n}{\overline{R}^{n+1}} \cdot \frac{1 - \exp(-a\overline{R}^2)}{1 - \exp(-a)} + \frac{1}{\overline{R}^n} \cdot \frac{2a\overline{R} \cdot \exp(-a\overline{R}^2)}{1 - \exp(-a)} \tag{3-5}$$

At the location where the radius equals to the core size, the tangential velocity reaches its maximum. Therefore,

$$\left(\frac{d\overline{V}_t}{d\overline{R}}\right)_{\overline{R}=\zeta} = 0 \tag{3-6}$$

where

$$\zeta = \frac{R_c}{R_o} \tag{3-7}$$

Substituting equations (3-5), (3-7) into (3-6) yields

$$(n + 2X_n)\exp(-X_n) - n = 0 \tag{3-8}$$

where

$$X_n = a\zeta^2 \tag{3-9}$$

When "n" is determined according to the experimental data, "X_n" can be obtained from equation (3-8). Further, if the core radius is known, the constant "a" can be determined, and the normalized tangential velocity can be expressed as follows:

$$\overline{V}_t = \frac{1}{\overline{R}^n} \frac{1 - \exp[-X_n(\overline{R}/\zeta)^2]}{1 - \exp(-X_n/\zeta^2)} \tag{3-10}$$

Let

$$\lambda = \frac{R_e}{R_o} \tag{3-11}$$

$$\xi = \frac{R_c}{R_e} \tag{3-12}$$

and

$$\tilde{r} = \frac{r}{R_e} \tag{3-13}$$

The tangential velocity can be expressed as follows:

$$V_t = \frac{V_{tin}}{\tilde{r}^n \lambda^n} \frac{1 - \exp[-X_n(\tilde{r}^2/\xi^2)]}{1 - \exp[-X_n/(\lambda^2\xi^2)]} \tag{3-14}$$

Considering the vortex chamber to be a control volume, applying the principle of momentum conservation yields

$$\int_{A_o} (\frac{1}{2}\rho V_o^2 + p_o)\, \vec{V}_o \cdot \vec{n}\, dA + \int_{A_i} (\frac{1}{2}\rho V_i^2 + p_i)\, \vec{V}_i \cdot \vec{n}\, dA = 0 \tag{3-15}$$

where

$$V_o^2 = V_{ro}^2 + V_{to}^2 + V_{zo}^2 \tag{3-16}$$

Since

$$V_{ro} \approx 0 \tag{3-17}$$

Equation (3-15) can be rewritten as:

$$\int_{A_o} (\tfrac{1}{2}\rho V_{to}^2)\,\vec{V}_o\cdot\vec{n}\,dA + \int_{A_o} (\tfrac{1}{2}\rho V_{zo}^2 + p_o)\,\vec{V}_o\cdot\vec{n}\,dA +$$
$$+ \int_{A_i} (\tfrac{1}{2}\rho V_i^2 + p_i)\,\vec{V}_i\cdot\vec{n}\,dA = 0 \qquad (3\text{-}18)$$

Since

$$V_{zo} = \text{constant} \qquad (3\text{-}19)$$

$$\tfrac{1}{2}\rho V_{zo}^2 + p_o = \text{constant} \qquad (3\text{-}20)$$

$$\tfrac{1}{2}\rho V_i^2 + p_i = \text{constant} \qquad (3\text{-}21)$$

(detailed in [20]) and

$$\int_{A_o} \vec{V}_o\cdot\vec{n}\,dA = \int_{A_i} \vec{V}_i\cdot\vec{n}\,dA = Q \qquad (3\text{-}22)$$

Equation (3-19) can be simplified as:

$$\int_{A_o} (\tfrac{1}{2}\rho V_{to}^2)\,\vec{V}_o\cdot\vec{n}\,dA + (\tfrac{1}{2}\rho V_{zo}^2 + p_o)\,Q - (\tfrac{1}{2}\rho V_i^2 + p_i)\,Q = 0 \qquad (3\text{-}23)$$

Since

$$\vec{V}_o\cdot\vec{n}\,dA = R_e^2\cdot V_{zo}\cdot 2\pi\tilde{r}\cdot d\tilde{r} \qquad (3\text{-}24)$$

Combining equations (3-14) and (3-24) yields

$$\int_{A_o} (\tfrac{1}{2}\rho V_{to}^2)\,\vec{V}_o\cdot\vec{n}\,dA =$$
$$= \int_{\xi}^{1} \frac{\rho}{2}\cdot\left[\frac{V_{tin}^2}{\tilde{r}^{2n}\lambda^{2n}}\cdot\left\{\frac{1 - \exp[-X_n(\tilde{r}^2/\xi^2)]}{1 - \exp[-X_n/(\lambda^2\xi^2)]}\right\}^2\right]_o \cdot R_e^2\cdot V_{zo}\cdot 2\pi\tilde{r}\cdot d\tilde{r}$$
$$= \frac{\rho V_{tin}^2 Q}{\lambda^{2n}(1 - \xi^2)}\cdot\int_{\xi}^{1} g(\tilde{r}, \xi)\,d\tilde{r} \qquad (3\text{-}25)$$

where

$$Q = V_{z\omega}\cdot\pi(R_e^2 - R_c^2) \tag{3-26}$$

$$g(\tilde{r}, \xi) = \tilde{r}^{1-2n}\left\{\frac{1 - \exp[-X_n(\tilde{r}^2/\xi^2)]}{1 - \exp[-X_n/(\lambda^2\xi^2)]}\right\}^2 \tag{3-27}$$

Substituting equation (3-25) into (3-23) yields

$$\frac{\rho V_{tin}^2 Q}{\lambda^{2n}(1 - \xi^2)}\cdot\int_\xi^1 g(\tilde{r}, \xi)\, d\tilde{r} + \left(\frac{1}{2}\rho V_{z\omega}^2 + p_\omega\right) Q - \left(\frac{1}{2}\rho V_i^2 + p_i\right) Q = 0 \tag{3-28}$$

Equation (3-28) can be rewritten as:

$$\frac{2(p_i - p_\omega)}{\rho\cdot V_i^2} + 1 = \left(\frac{V_{tin}}{V_i}\right)^2 \frac{2}{\lambda^{2n}(1 - \xi^2)}\cdot\int_\xi^1 g(\tilde{r}, \xi)\, d\tilde{r} + \left(\frac{V_{z\omega}}{V_i}\right)^2 \tag{3-29}$$

Since

$$\frac{V_{tin}}{V_i} = \cos\varphi \tag{3-30}$$

(see Figure 2.2.2.2, $V_i = V_{in}$) and

$$\frac{V_{z\omega}}{V_i} = \frac{Q}{\pi(R_e^2 - R_c^2)V_i} = \frac{A_i/A_\omega}{\lambda^2(1 - \xi^2)} \tag{3-31}$$

where

$$A_i = \frac{Q}{V_i} \tag{3-32}$$

$$A_\omega = \pi R_\omega^2 \tag{3-33}$$

Equation (3-29) can be simplified as:

$$\Delta\tilde{p} = \frac{2}{1-\xi^2}\int_{\xi}^{1} g(\tilde{r},\xi)\,d\tilde{r} + \frac{\beta}{(1-\xi^2)^2} \tag{3-34}$$

where

$\Delta\tilde{p}$ = dimensionless pressure difference [22]

$$\Delta\tilde{p} = \left[\frac{2(p_i - p_o)}{\rho \cdot V_i^2} + 1\right]\frac{\lambda^{2n}}{(\cos\varphi)^2} \tag{3-35}$$

β = swirl number

$$\beta = \frac{(A_i/A_o)^2}{\lambda^{4-2n}(\cos\varphi)^2} \tag{3-36}$$

For $\Delta\tilde{p}$ being a minimum,

$$\frac{d(\Delta\tilde{p})}{d\xi} = \frac{4\xi}{(1-\xi^2)^2}\int_{\xi}^{1} g(\tilde{r},\xi)\,d\tilde{r} + \frac{2}{1-\xi^2}\frac{d}{d\xi}\int_{\xi}^{1} g(\tilde{r},\xi)\,d\tilde{r} + \frac{4\beta\xi}{(1-\xi^2)^3} = 0 \tag{3-37}$$

or

$$2(1-\xi^2)\xi\int_{\xi}^{1} g(\tilde{r},\xi)\,d\tilde{r} + (1-\xi^2)^2\cdot\frac{d}{d\xi}\int_{\xi}^{1} g(\tilde{r},\xi)\,d\tilde{r} + 2\beta\xi = 0 \tag{3-38}$$

Using Leibniz's Theorem yields

$$\frac{d}{d\xi}\int_{\xi}^{1} g(\tilde{r},\xi)\,d\tilde{r} = \int_{\xi}^{1}\frac{\partial g(\tilde{r},\xi)}{\partial\xi}\,d\tilde{r} - g(\tilde{r}=\xi,\xi)\frac{d\xi}{d\xi} \tag{3-39}$$

Substituting equation (3-39) into (3-38) yields

$$2(1-\xi^2)\xi\int_{\xi}^{1} g(\tilde{r},\xi)\,d\tilde{r} + (1-\xi^2)^2\int_{\xi}^{1}\frac{\partial g(\tilde{r},\xi)}{\partial\xi}\,d\tilde{r} -$$

$$-(1-\xi^2)^2\cdot g(\tilde{r}=\xi,\xi)\frac{d\xi}{d\xi} + 2\beta\xi = 0 \tag{3-40}$$

Differentiating equation (3-27) yields

$$\frac{\partial g(\tilde{r}, \xi)}{\partial \xi} = \frac{4\tilde{r}^{1-2n} X_n \xi^{-3}\{1 - \exp[-X_n(\tilde{r}^2/\xi^2)]\}}{\{1 - \exp[-X_n/(\lambda^2\xi^2)]\}^2}\{ - \tilde{r}^2 \exp[-X_n(\tilde{r}^2/\xi^2)] +$$
$$+ \lambda^{-2}\exp[-X_n/(\lambda^2\xi^2)]\frac{1 - \exp[-X_n(\tilde{r}^2/\xi^2)]}{1 - \exp[-X_n/(\lambda^2\xi^2)]}\} \qquad (3\text{-}41)$$

and substituting $\tilde{r} = \xi$ into equation (3-27) yields

$$g(\tilde{r} = \xi, \xi)\frac{d\xi}{d\xi} = \xi^{1-2n}\left\{\frac{1 - \exp(-X_n)}{1 - \exp[-X_n/(\lambda^2\xi^2)]}\right\}^2 \qquad (3\text{-}42)$$

Substituting equations (3-27), (3-41), (3-42) into (3-40) yields

$$2(1 - \xi^2)\xi\int_{\xi}^{1} \tilde{r}^{1-2n}\left\{\frac{1 - \exp[-X_n(\tilde{r}^2/\xi^2)]}{1 - \exp[-X_n/(\lambda^2\xi^2)]}\right\}^2 d\tilde{r} +$$
$$+ (1 - \xi^2)^2\int_{\xi}^{1} \frac{4\tilde{r}^{1-2n} X_n \xi^{-3}\{1 - \exp[-X_n(\tilde{r}^2/\xi^2)]\}}{\{1 - \exp[-X_n/(\lambda^2\xi^2)]\}^2}\{ - \tilde{r}^2\exp[-X_n(\tilde{r}^2/\xi^2)] +$$
$$+ \lambda^{-2}\exp[-X_n/(\lambda^2\xi^2)]\frac{1 - \exp[-X_n(\tilde{r}^2/\xi^2)]}{1 - \exp[-X_n/(\lambda^2\xi^2)]}\} d\tilde{r} -$$
$$- (1 - \xi^2)^2 \cdot \xi^{1-2n}\left\{\frac{1 - \exp(-X_n)}{1 - \exp[-X_n/(\lambda^2\xi^2)]}\right\}^2 + \frac{2(A_i/A_o)^2\xi}{\lambda^{4-2n}(\cos\varphi)^2} = 0 \qquad (3\text{-}43)$$

The vortex core radius R_c can be determined through ξ which is obtained from the above equation (3-43). A computer program has been developed to solve this equation using numerical methods. The listings of the computer program as well as the typical input data and the output results are shown in the Appendix D. Empirical constant "n" of 0.8 and corresponding "X_n" of 1.6188 are used in the computation, which provides better match of the computation results to the experimental data. Table 3.2.4 shows the computational results of the vortex core radii corresponding to

each contraction ratio. Since the vortex core radius is always located at the point of the maximum mean tangential velocity, the inlet Reynolds number has no influence to the vortex core radii.

The proposed new normalized tangential velocity profile, equation (3-10), can be rewritten with determined "n" and "X_n" as follows:

$$\overline{V}_t = \frac{1}{\overline{R}^{0.8}} \cdot \frac{1 - \exp[-1.6188(\overline{R}/\zeta)^2]}{1 - \exp(-1.6188/\zeta^2)} \qquad (3\text{-}44)$$

Plots using this new profile are shown in Figure 3.2.11. It is seen that at small contraction ratios the predicted curves are well coincided with the experimental datum points. Relatively bigger deviations are observed for large contraction ratios. It is because the condition of the strong vortex does not exist under the large contraction ratio. By changing the numerical values of "n" and "X_n", it is possible to provide a normalized tangential velocity profile suitable for the large contraction ratio.

3.3 Mean Radial Velocities

Distributions of mean radial velocity at different locations within the main section obtained from the experiments are shown in Figures 3.3.1 and 3.3.2.

It is found that the magnitude of the mean radial velocity at the main section of the vortex chamber is very small if it is compared to the magnitude of the mean tangential velocity under the same testing condition. The maximum difference of the measured value of the mean radial velocity is less than 8 % of that of the mean tangential velocity. A comparison of the mean radial velocity with the mean tangential velocity at the same condition is shown in Figure 3.3.3. Therefore, at the main section of the vortex chamber,

the mean radial velocity can be considered as an unimportant item to be neglected, which is a reasonable assumption made by many investigators.

Near the exit section inside the vortex chamber, the effect of the mean radial velocity on the vortex flow is significant. The behaviour of the mean radial velocity there is illustrated in Figures 3.3.4 to 3.3.9. In the plots of mean radial velocity versus radius, the positive value of the mean radial velocity means that its direction is identical to that of the radial axis from the centre of the vortex chamber to the wall of the vortex chamber. The negative value of the mean radial velocity means that its direction is opposite to that of the radial axis. That is, the flow in the radial direction will be from the side wall of the vortex chamber towards the centre.

It is found from the experimental observation that the maximum mean radial velocity near the exit section, for any given contraction ratio, always appears at the place where the numerical value of the normalized radius is slightly greater than that of the contraction ratio. Then, from that maximum value point to the wall, the magnitude of the mean radial velocity decreases gradually with the increase of the numerical value of the normalized radius. Within that region, the radial velocity vector has the direction towards the centre of the vortex chamber, therefore, it is presented with a negative value. It indicates that there is some secondary flow in this region.

For each given contraction ratio, the trends of the mean radial velocity distributions near the exit section, corresponding to different inlet Reynolds numbers, are similar. Therefore, the mean radial velocity can be scaled as

$$V_{r,s} = R_{e,i}^{0.25} \cdot \frac{\overline{V}_r}{\overline{V}_{in}} \qquad (3\text{-}45)$$

where

$V_{r,s}$ = scaled mean radial velocity

Corresponding scaled distribution curves are shown in Figures 3.3.10 to 3.3.15. It has been seen that the mean radial velocity distributions under different contraction ratios are quite different. Simple analytical expressions which could be applied for all mean radial velocity distributions are extremely difficult to be conducted. Using numerical methods, the mean radial velocities at any location near the exit section with various conditions can be estimated. A map of the scaled mean radial velocity is formed as shown in Figure 3.3.16 for application. Table 3.3.1 shows a sample deviation between the experimental data and numerical approximation.

The fluctuating velocities were measured in the experiments. Based on those, analyses of the turbulence intensity, the kinetic energy and the Reynolds stresses can be carried out.

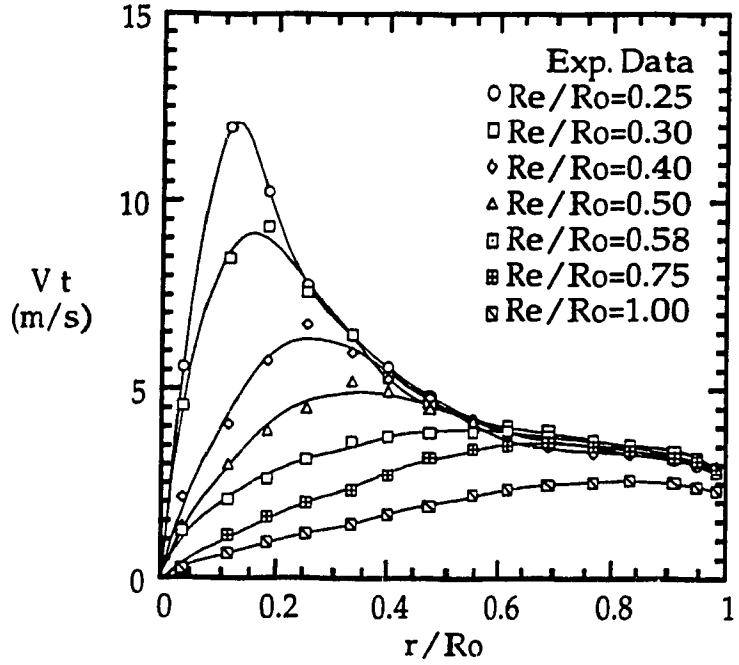

Figure 3.2.1 Mean Tangential Velocity at Main Section at Re,i = 1960 (lines - curve fitting)

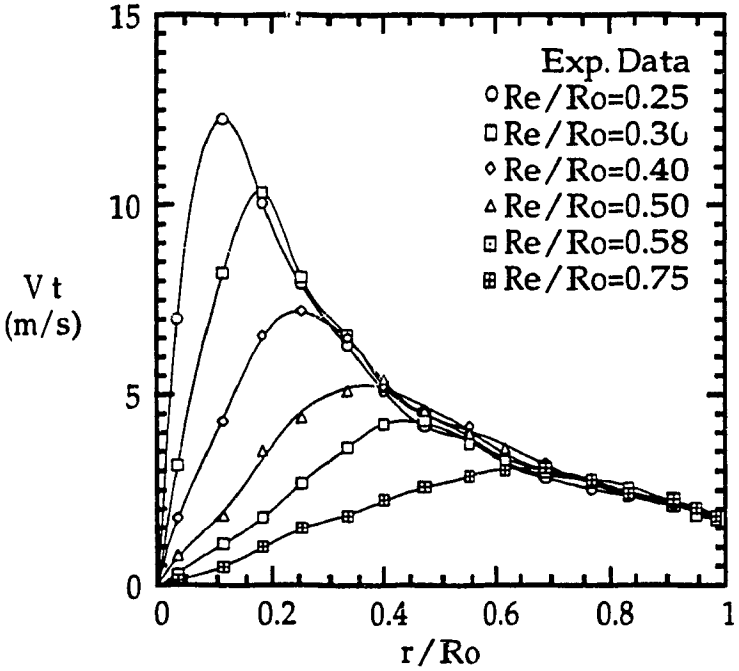

Figure 3.2.2 Mean Tangential Velocity near Exit Section at Re,i = 1960 (lines - curve fitting)

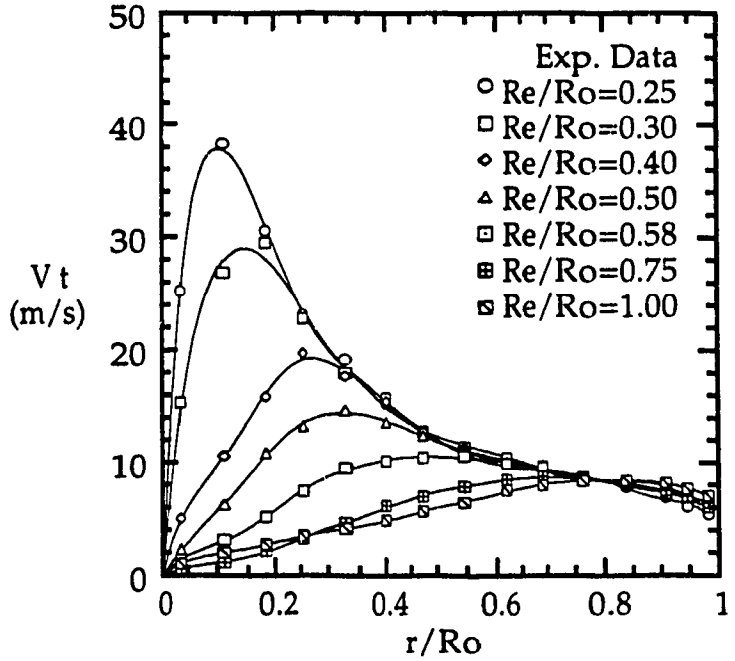

Figure 3.2.3 Mean Tangential Velocity at Main Section at Re,i = 7840 (lines - curve fitting)

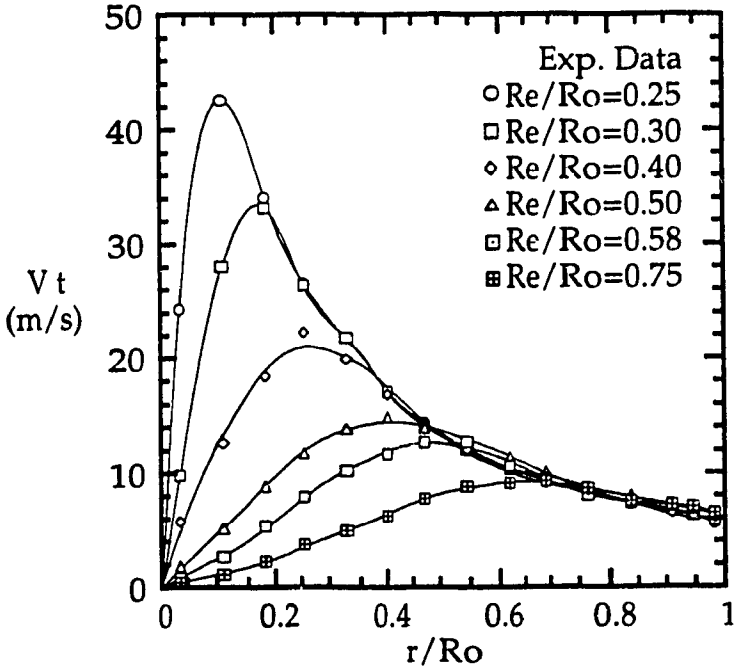

Figure 3.2.4 Mean Tangential Velocity near Exit Section at Re,i = 7840 (lines - curve fitting)

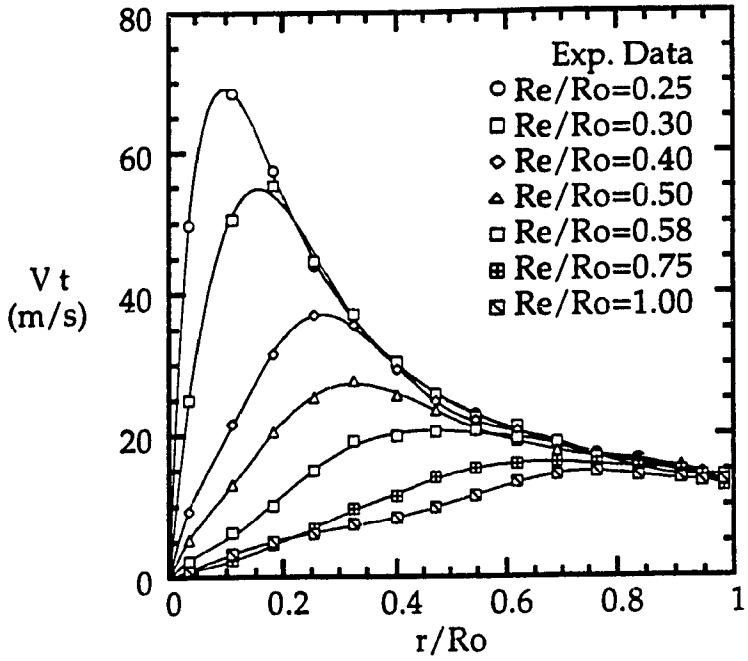

Figure 3.2.5 Mean Tangential Velocity at Main Section at Re,i = 13700 (lines - curve fitting)

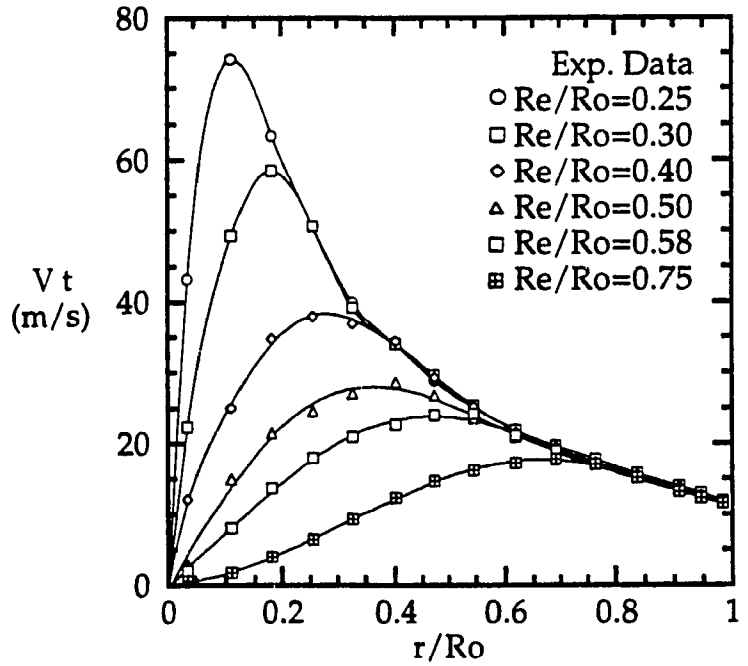

Figure 3.2.6 Mean Tangential Velocity near Exit Section at Re,i = 13700 (lines - curve fitting)

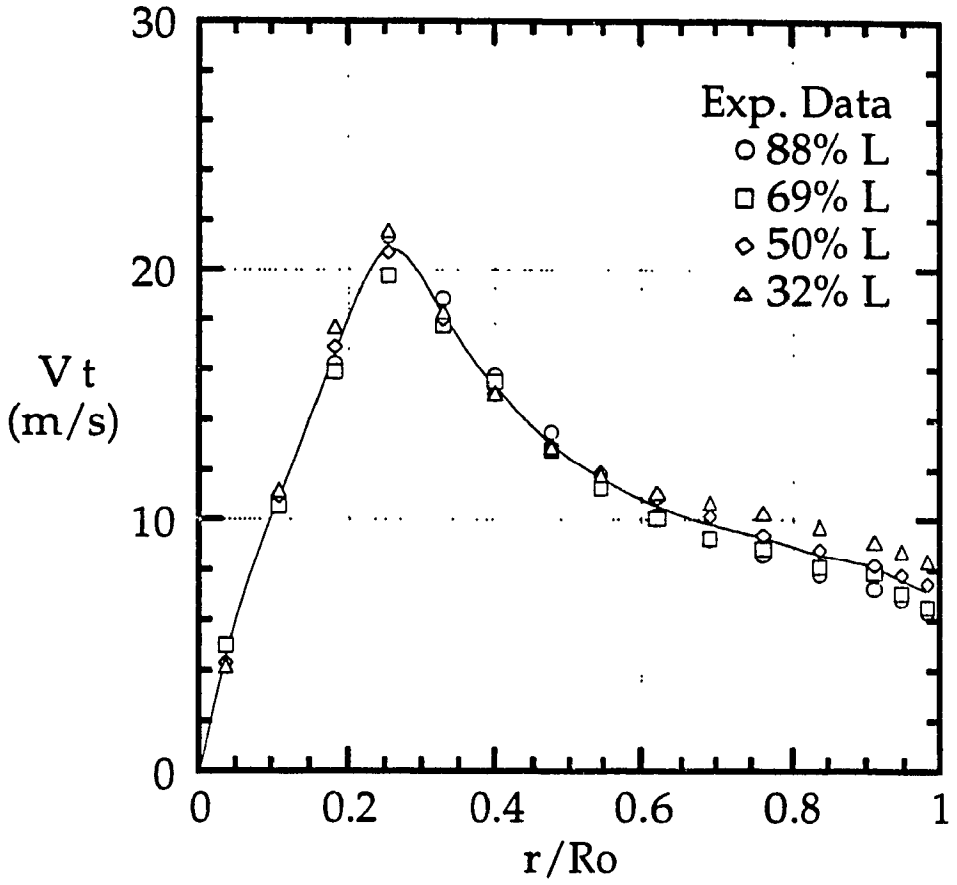

Figure 3.2.7 Mean Tangential Velocity at Main Section (Re/Ro = 0.40, Re,i = 13700, L = Vortex Chamber Length)

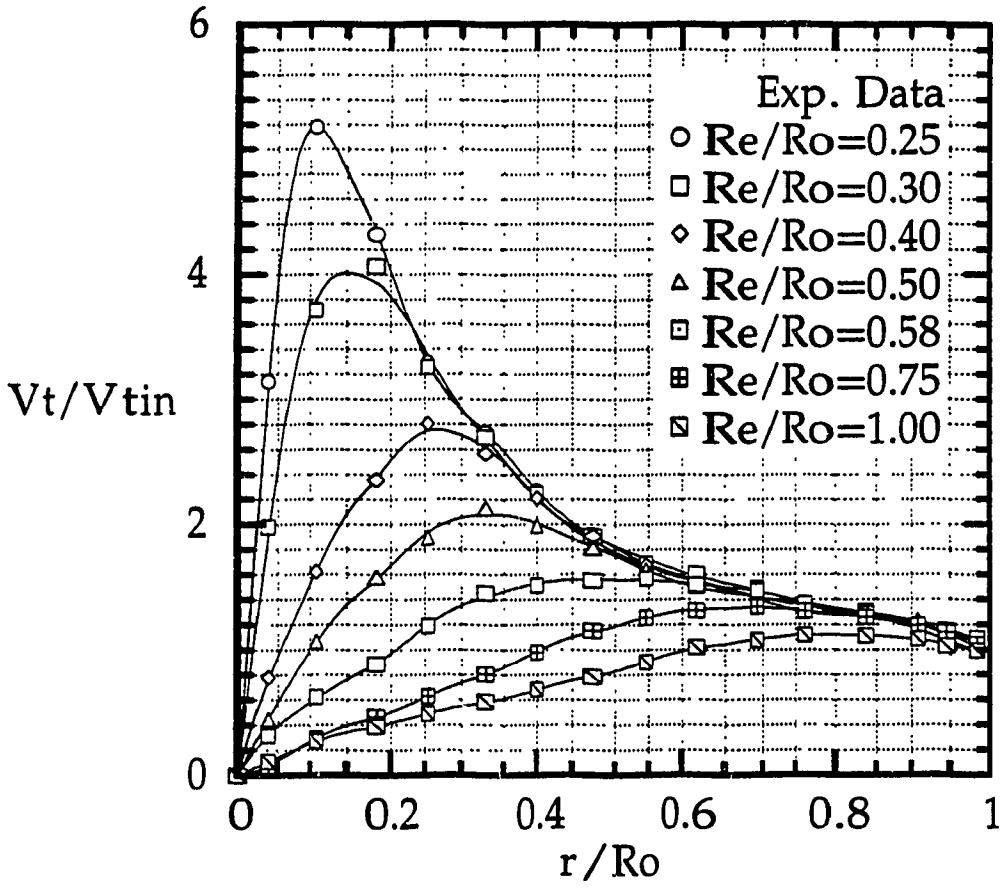

Figure 3.2.8 Normalized Mean Tangential Velocity at Main Section (lines - curve fitting)

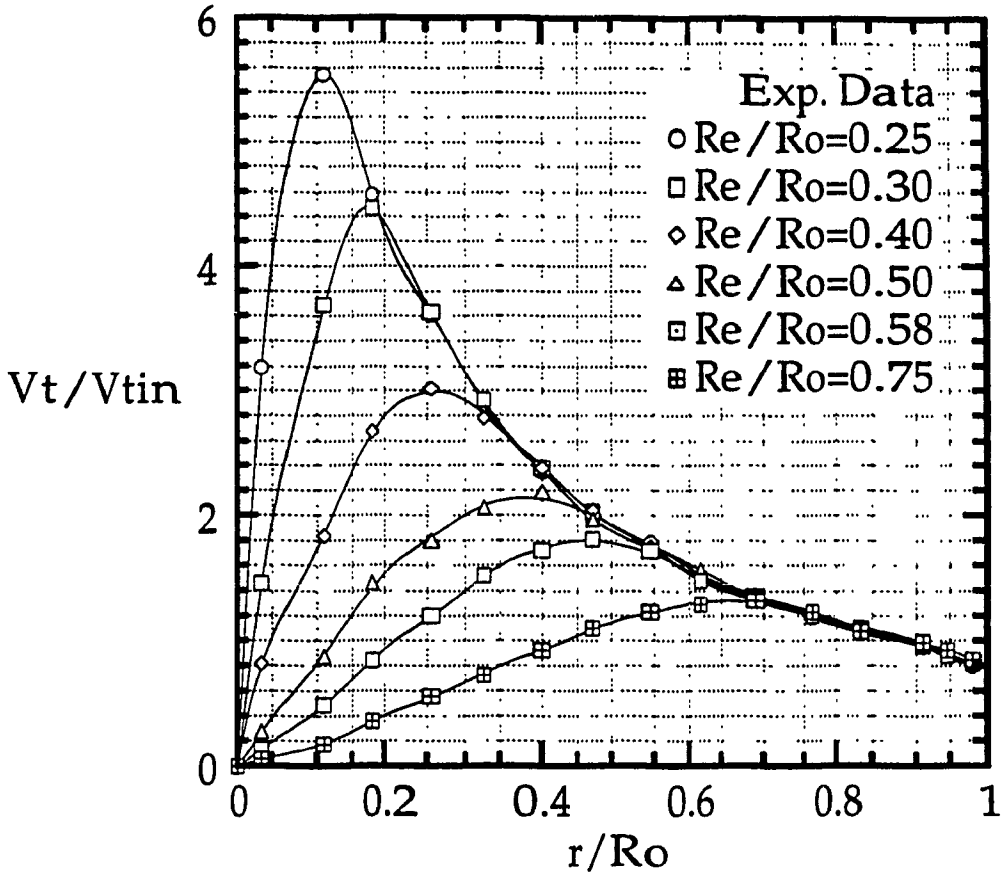

Figure 3.2.9 Normalized Mean Tangential Velocity near Exit Section (lines - curve fitting)

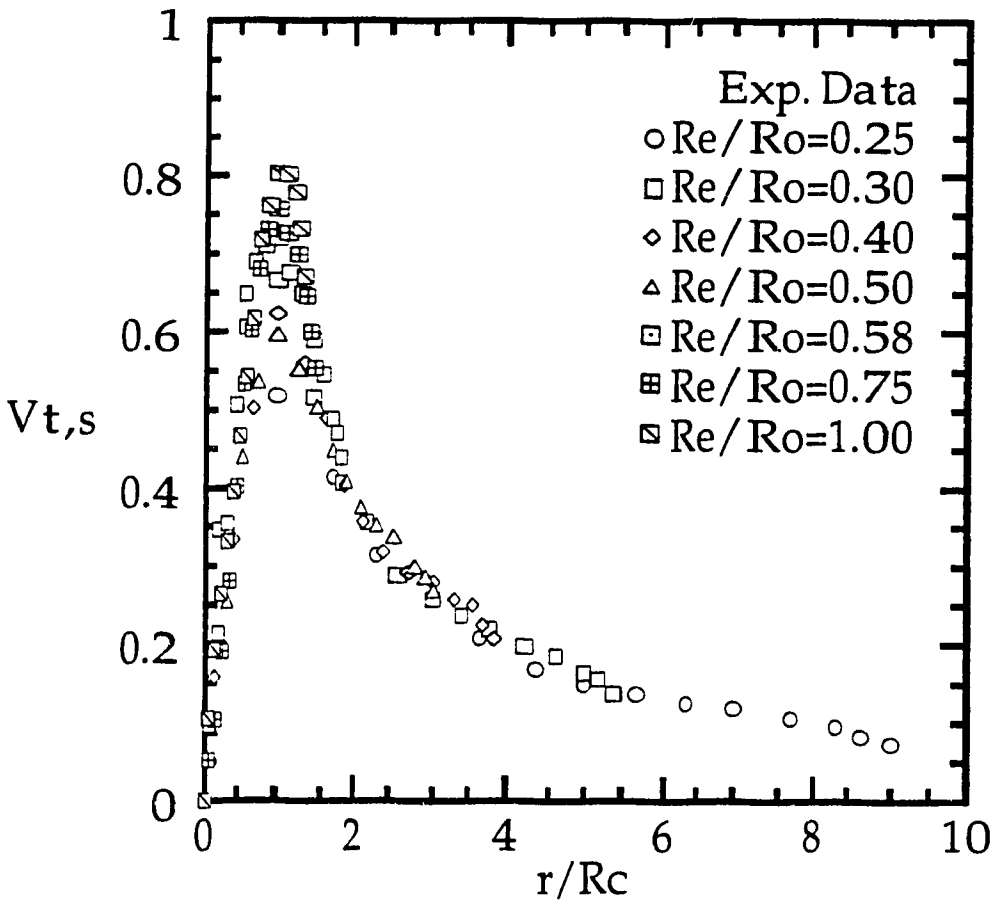

Figure 3.2.10 Dimensionless Mean Tangential Velocity at Re,i = 7840 (line - curve fitting)

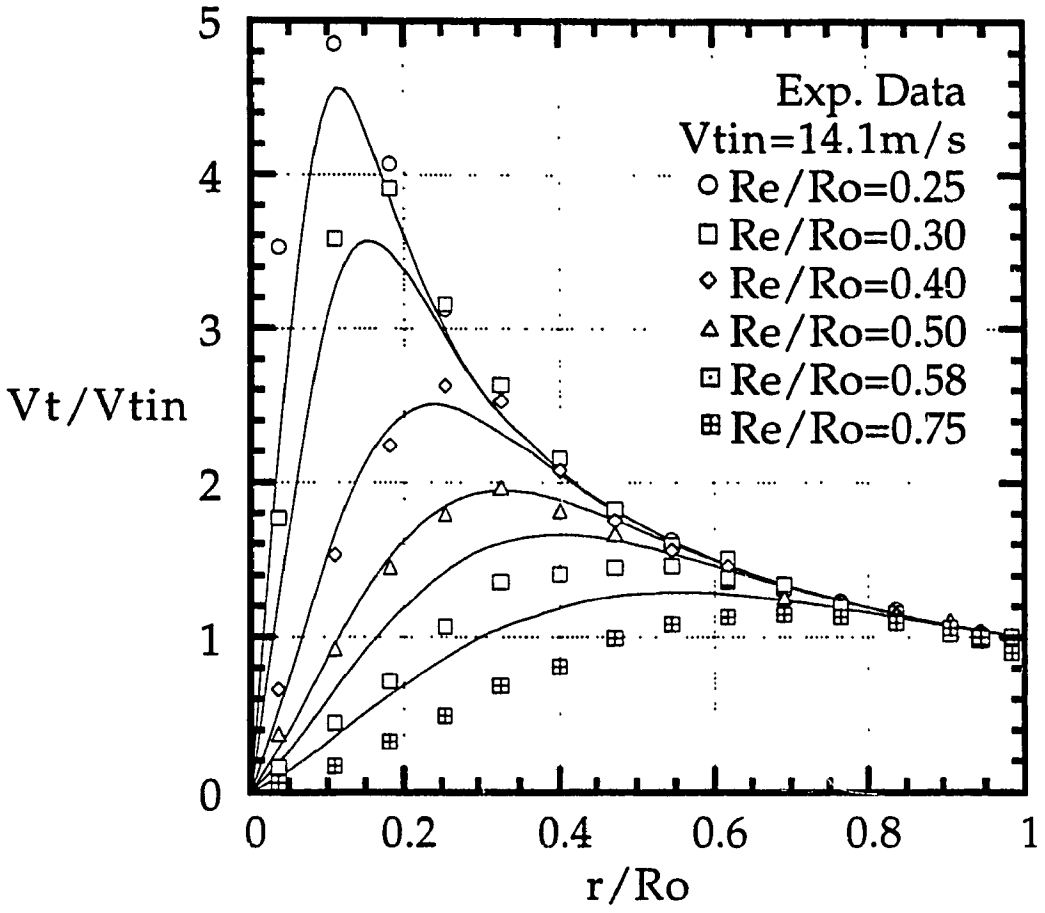

Figure 3.2.11 Simulation of Tangential Velocity Distributions (lines - eq.3-44)

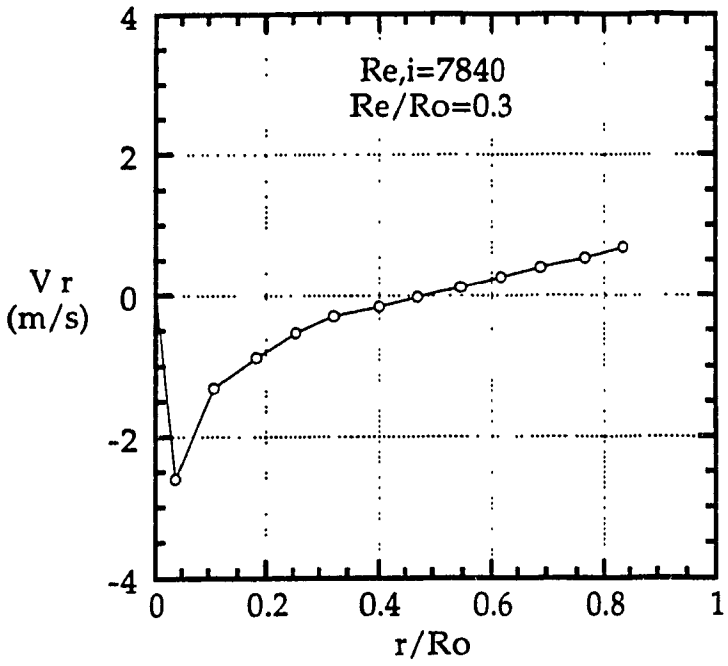

Figure 3.3.1 Experimental Mean Radial Velocity at Main Section (69% Vortex Chamber Length)

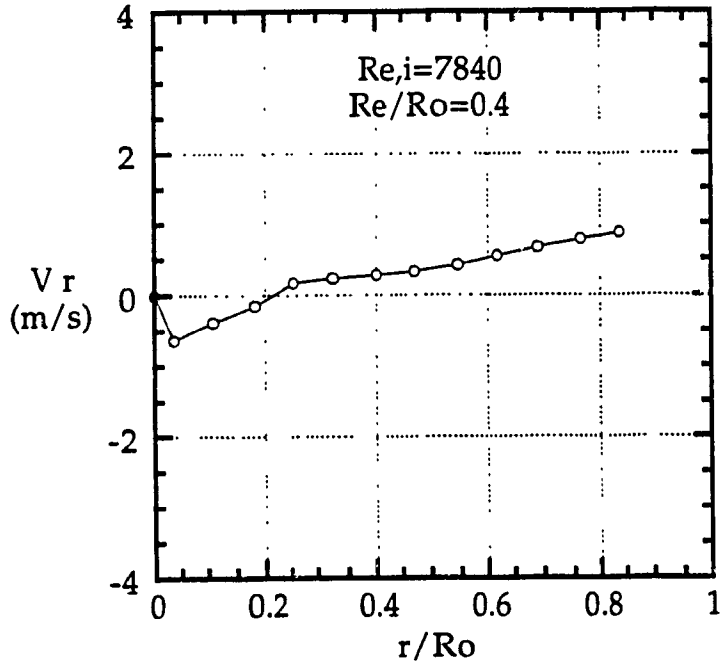

Figure 3.3.2 Experimental Mean Radial Velocity at Main Section (50% Vortex Chamber Length)

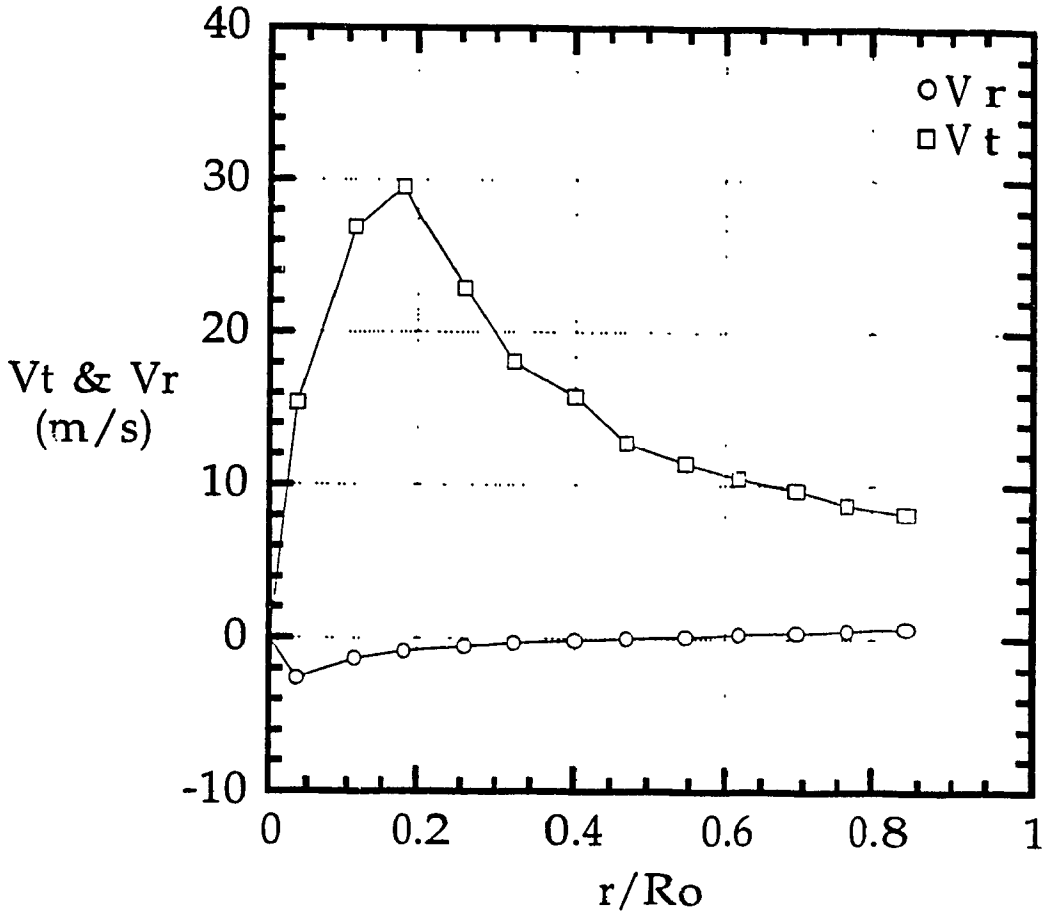

Figure 3.3.3 Comparison of Mean Radial Velocity with Mean Tangential Velocity at Main Section (Experment, Re,i=7840, Re/Ro=0.3)

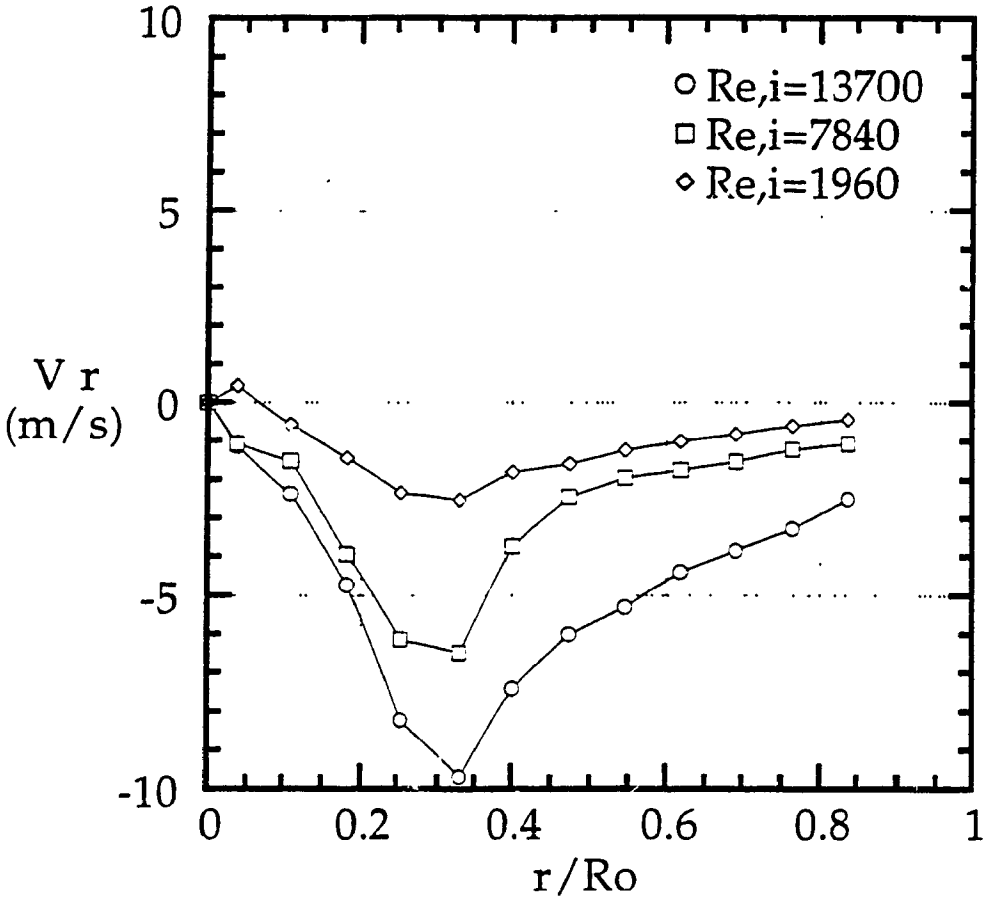

Figure 3.3.4 Experimental Mean Radial Velocity near Exit Section (Re/Ro = 0.25)

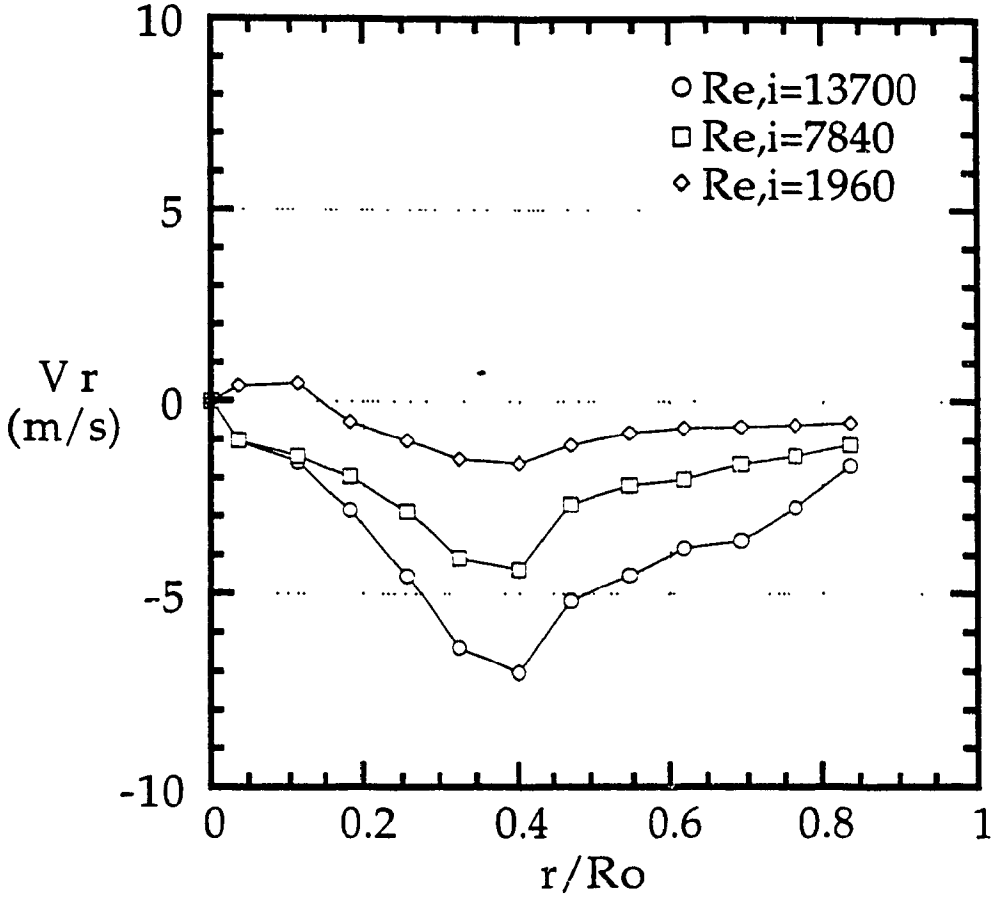

Figure 3.3.5 Experimental Mean Radial Velocity near Exit Section (Re/Ro = 0.30)

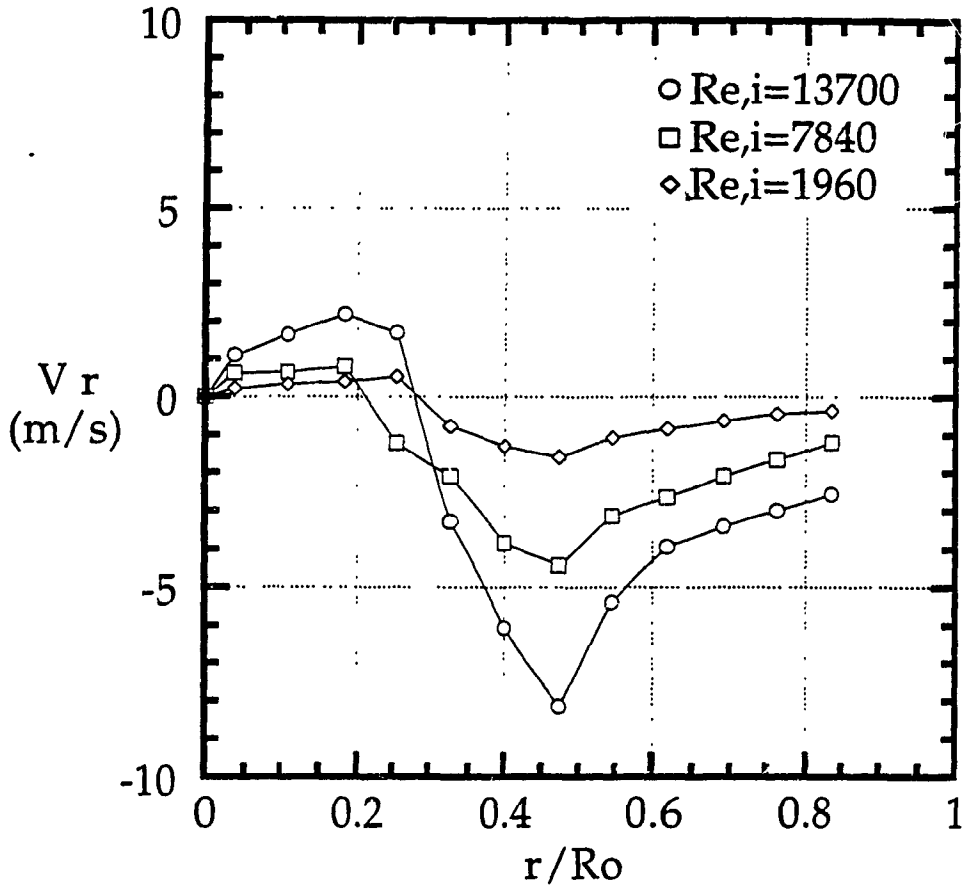

Figure 3.3.6 Experimental Mean Radial Velocity near Exit Section (Re/Ro = 0.40)

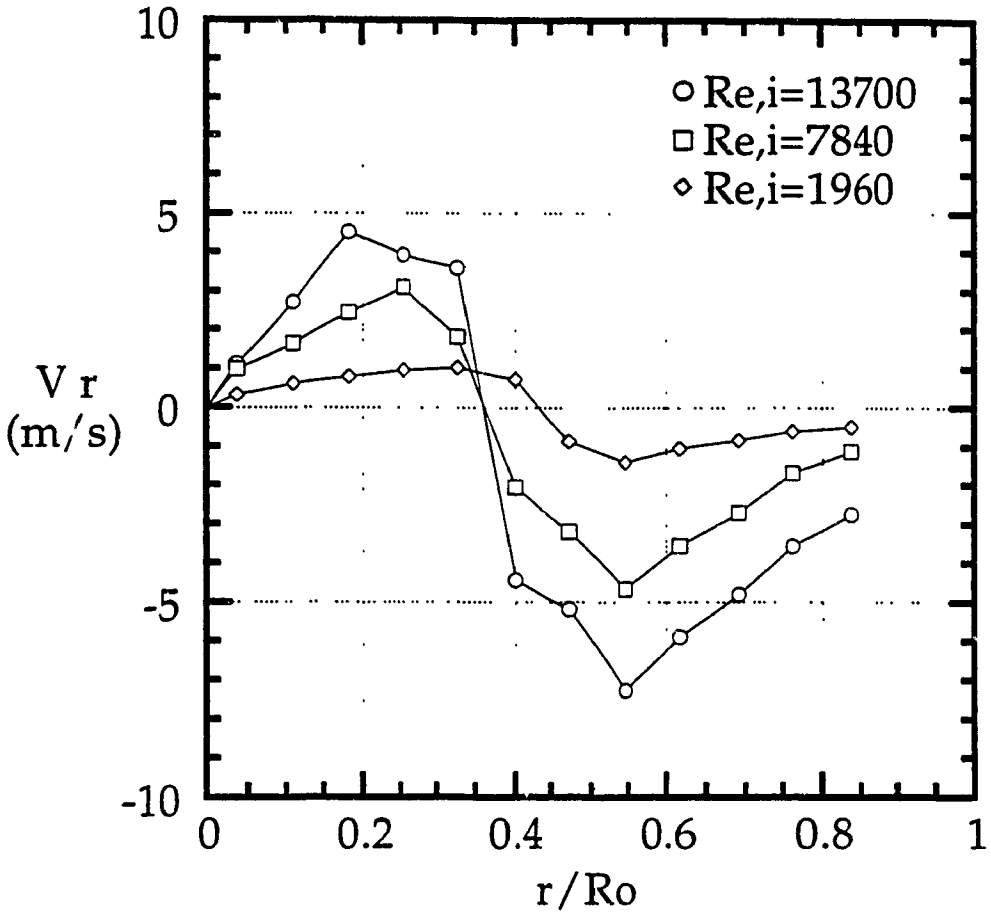

Figure 3.3.7 Experimental Mean Radial Velocity near Exit Section (Re/Ro = 0.50)

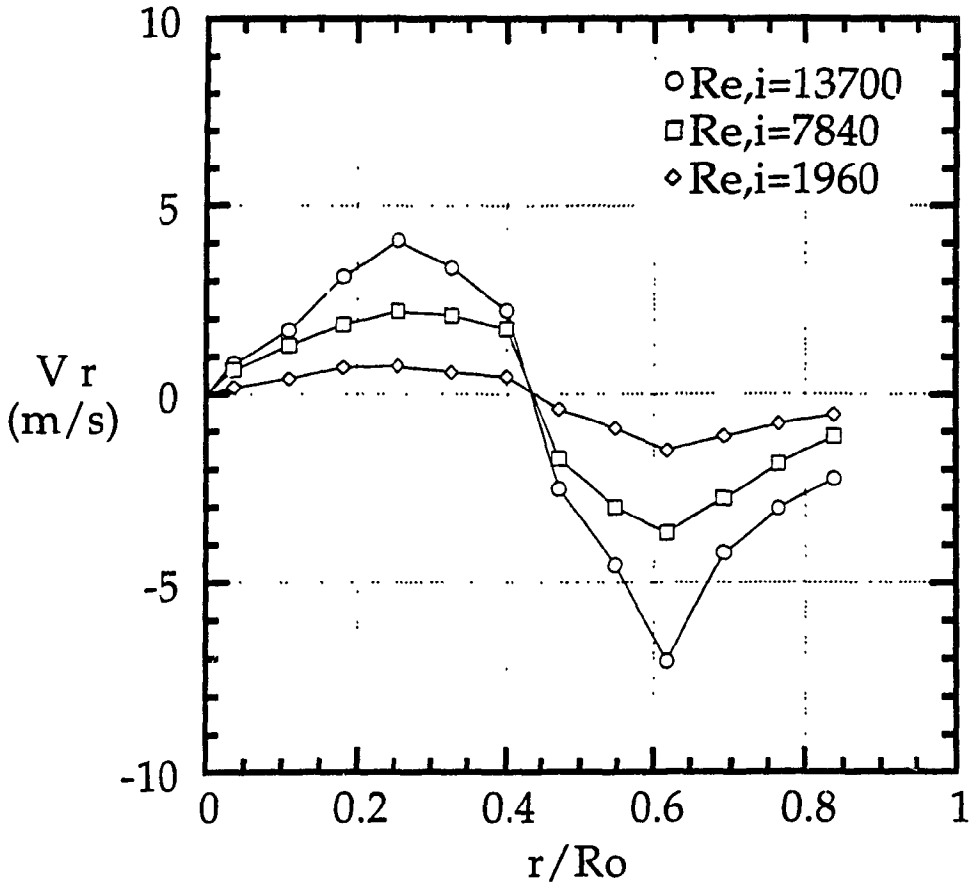

Figure 3.3.8 Experimental Mean Radial Velocity near Exit Section (Re/Ro = 0.58)

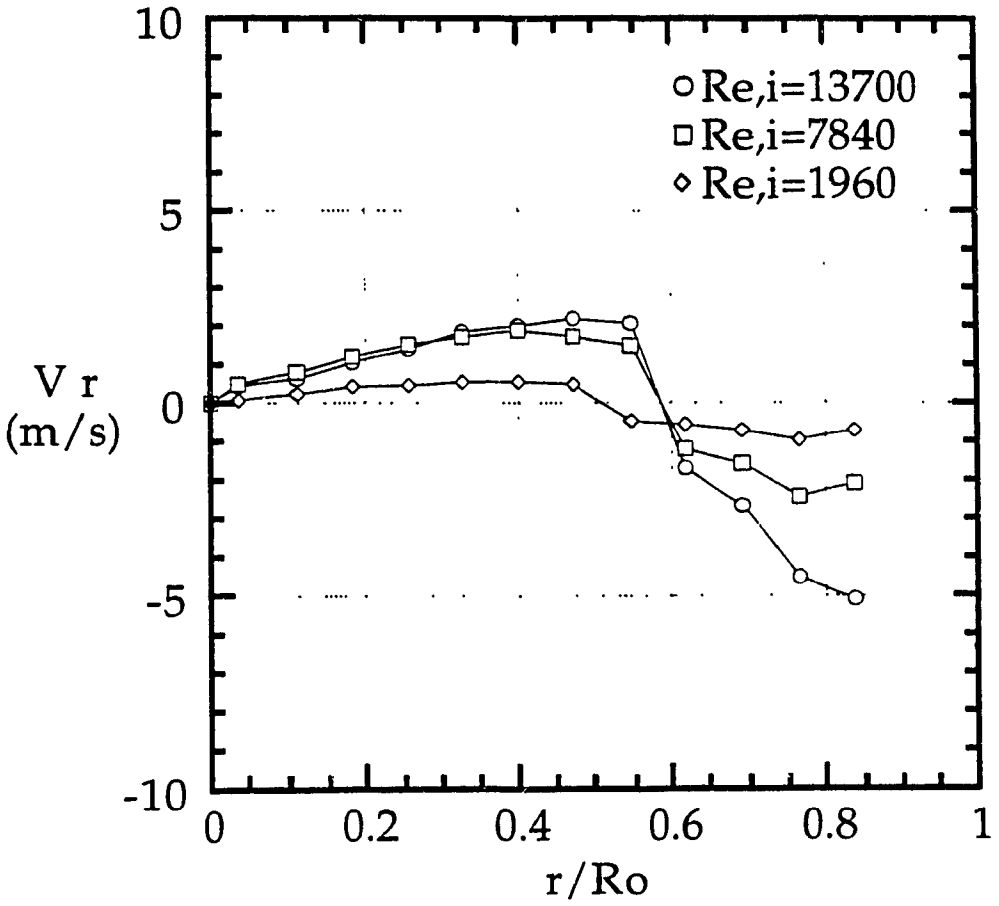

Figure 3.3.9 Experimental Mean Radial Velocity near Exit Section (Re/Ro = 0.75)

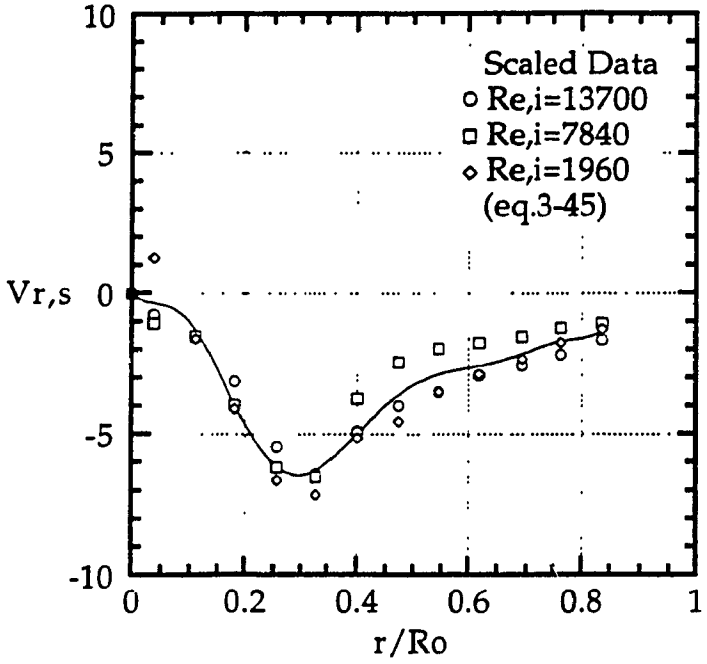

Figure 3.3.10 Scaled Mean Radial Velocity near Exit Section at Re/Ro = 0.25 (line - average value)

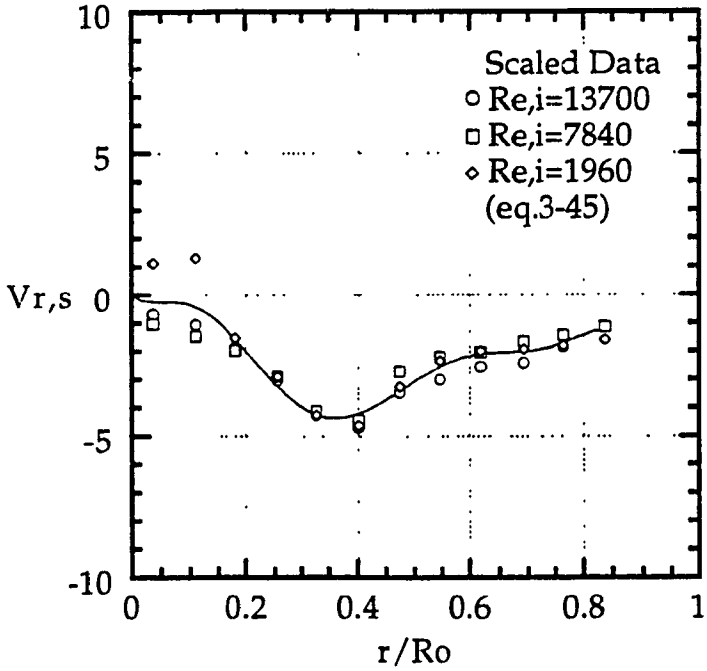

Figure 3.3.11 Scaled Mean Radial Velocity near Exit Section at Re/Ro = 0.30 (line - average value)

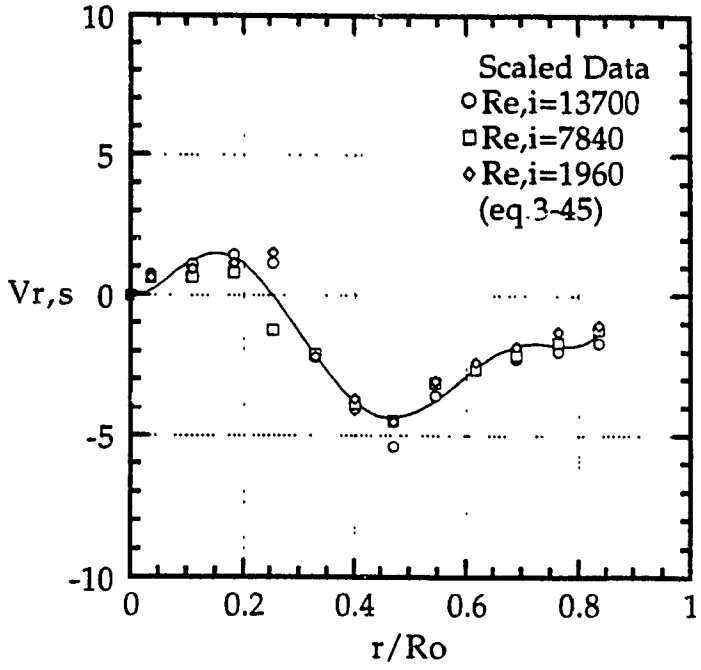

Figure 3.3.12 Scaled Mean Radial Velocity near Exit Section at Re/Ro = 0.40 (line - average value)

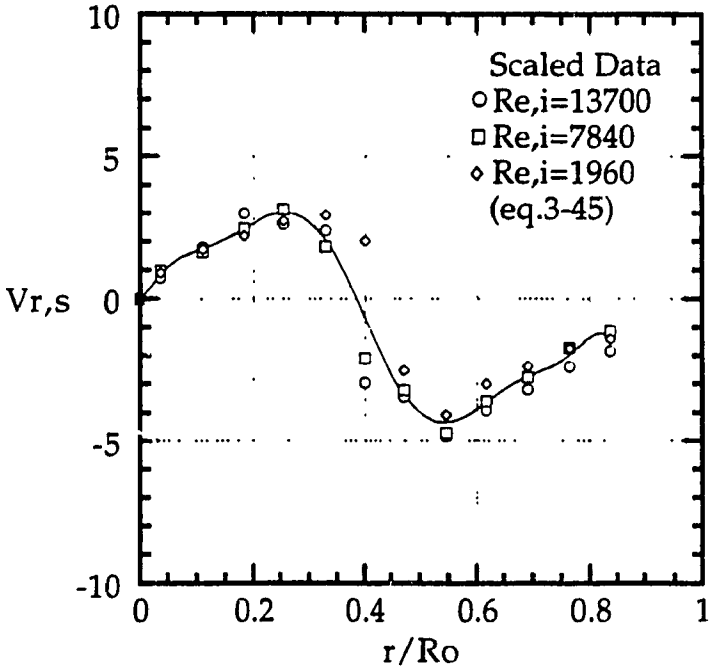

Figure 3.3.13 Scaled Mean Radial Velocity near Exit Section at Re/Ro = 0.50 (line - average value)

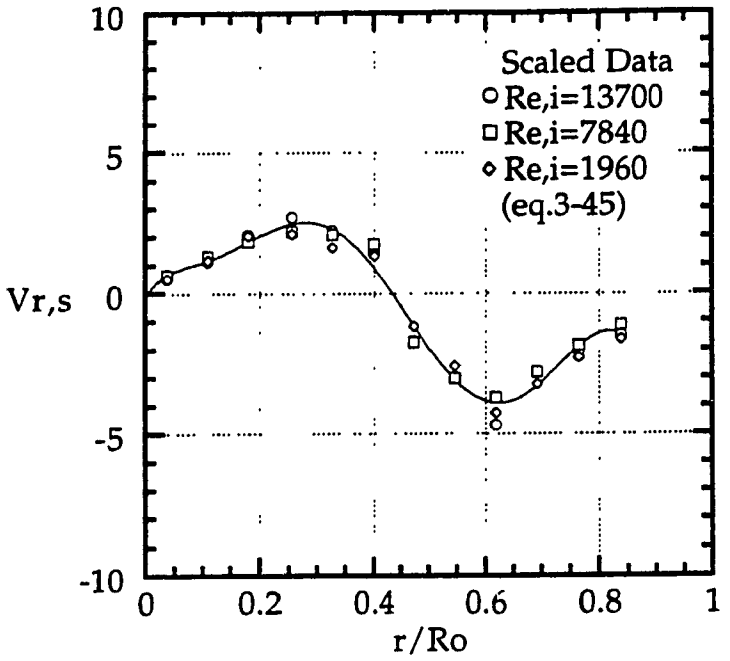

Figure 3.3.14 Scaled Mean Radial Velocity near Exit Section at Re/Ro = 0.58 (line - average value)

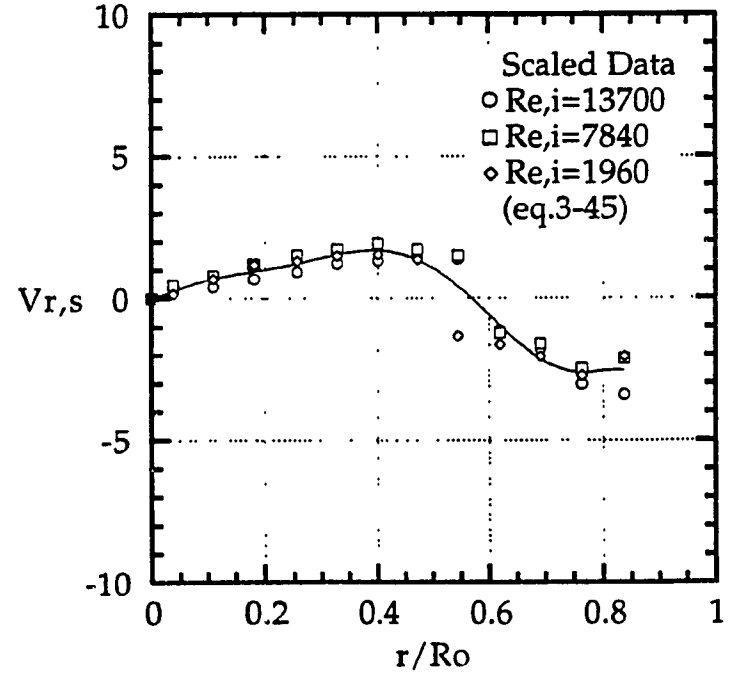

Figure 3.3.15 Scaled Mean Radial Velocity near Exit Section at Re/Ro = 0.75 (line - average value)

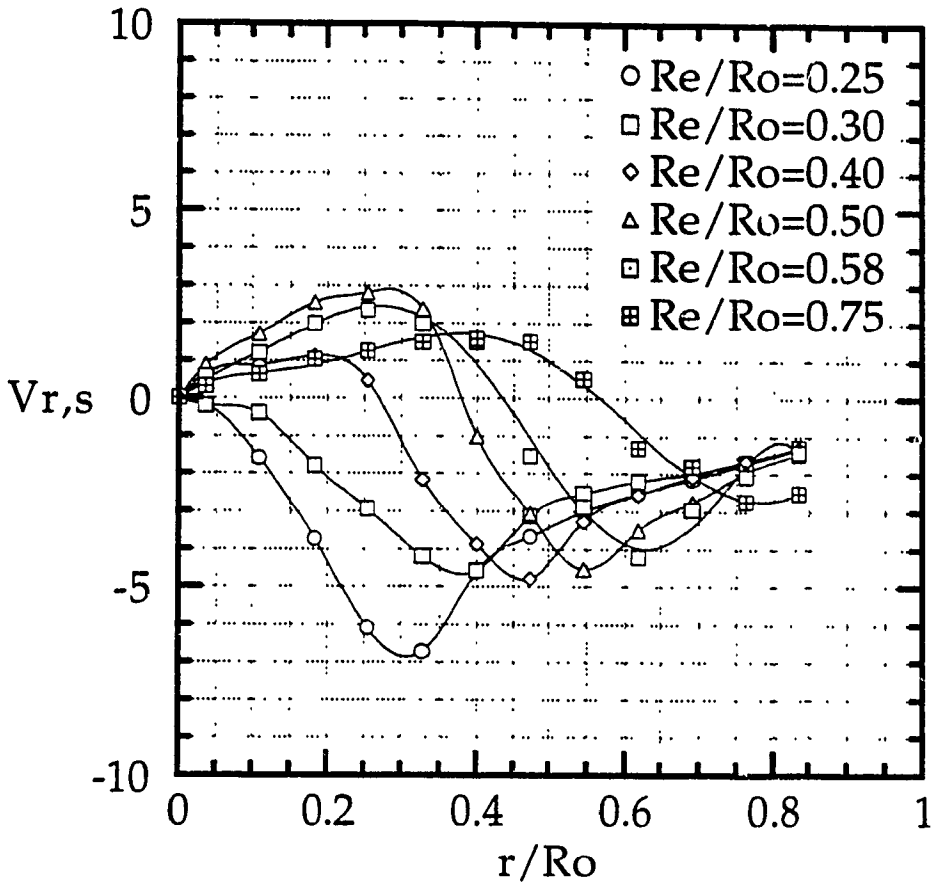

Figure 3.3.16 Scaled Mean Radial Velocities near Exit Section (lines - average value)

Table 3.2.1 Deviation of Mean Tangential Velocity at Different Locations within Main Section (Re/Ro = 0.40, Re,i = 7840)

% r/R_o	L/L_{total} = 88 %	L/L_{total} = 69 %	L/L_{total} = 50 %	L/L_{total} = 32 %
0.036	8.52	8.15	-6.94	-9.73
0.109	-1.60	-2.65	1.06	3.19
0.182	-2.71	-4.67	1.20	6.18
0.255	2.36	-5.15	-0.66	3.45
0.327	3.38	-2.65	-1.18	0.45
0.400	2.76	1.07	-1.99	-1.84
0.473	3.64	-1.94	-0.76	-0.95
0.545	0.78	-3.54	1.71	1.05
0.618	-3.57	-4.58	2.90	5.26
0.691	-6.35	-5.73	3.20	8.89
0.764	-7.12	-4.66	0.91	10.9
0.836	-9.11	-5.53	2.04	12.6
0.909	-10.7	-2.67	0.93	12.4
0.945	-10.5	-6.98	2.54	14.9
0.982	-11.8	-8.88	3.83	16.8

Table 3.2.2 Deviation of Tangential Velocity at Re,i = 13700 to Average Tangential Velocity (Main Section)

%	R_e/R_o	R_e/R_o	R_e/R_o	R_e/R_o	R_e/R_o	R_e/R_o	R_e/R_o
r/R_o	= 0.25	= 0.30	= 0.40	= 0.50	= 0.58	= 0.75	= 1.00
0.036	12.2	-10.6	-15.3	-16.2	-49.4	-27.1	-40.2
0.109	-6.28	-3.47	-5.66	-13.1	-27.8	-41.9	-11.9
0.182	-5.75	-3.70	-4.94	-8.06	-19.2	-29.9	-8.60
0.255	-5.07	-3.01	-6.37	-4.96	-10.2	-21.7	-9.94
0.327	-3.96	-2.41	-1.72	-7.61	-6.41	-15.1	-9.72
0.400	-5.96	-4.28	-5.88	-8.61	-6.95	-17.0	-12.6
0.473	-5.92	-4.15	-8.16	-8.29	-6.83	-13.9	-11.3
0.545	-3.80	-5.68	-6.78	-9.94	-6.82	-13.8	-10.4
0.618	-4.50	-6.13	-3.44	-9.83	-9.12	-14.0	-6.36
0.691	-8.50	-11.6	-4.78	-11.1	-8.51	-14.6	-5.24
0.764	-8.78	-12.4	-7.22	-11.1	-12.6	-13.6	-5.91
0.836	-6.64	-11.9	-9.07	-12.3	-14.3	-13.4	-9.16
0.909	-8.50	-12.2	-11.6	-10.0	-14.6	-11.4	-9.41
0.945	-8.91	-12.4	-9.87	-11.8	-12.6	-12.2	-8.00
0.982	-7.15	-9.30	-12.4	-13.5	-7.68	-14.0	-3.03

Table 3.2.3 Deviation of Tangential Velocity at Re,i = 13700 to Average Tangential Velocity (near Exit Section)

%	R_e/R_o	R_e/R_o	R_e/R_o	R_e/R_o	R_e/R_o	R_e/R_o
r/R_o	= 0.25	= 0.30	= 0.40	= 0.50	= 0.58	= 0.75
0.036	-3.86	8.87	5.10	-24.9	10.4	-18.2
0.109	-5.20	-5.19	-3.05	22.1	18.7	-25.1
0.182	-1.73	-7.12	-7.72	4.30	15.8	-19.4
0.255	-0.50	-1.15	-10.7	-2.89	6.50	-16.9
0.327	-2.10	-4.88	-5.58	-6.78	-2.23	-8.59
0.400	2.35	1.59	2.66	-7.26	-6.58	-4.91
0.473	3.90	3.39	1.49	-3.24	-5.86	-4.73
0.545	3.09	3.08	-0.01	-4.41	-0.03	-5.81
0.618	5.04	3.49	0.40	-5.04	1.36	-4.66
0.691	3.50	2.81	0.88	-1.73	0.69	-4.09
0.764	3.43	4.13	1.91	0.00	1.17	-0.77
0.836	3.35	4.77	3.96	-0.99	-1.97	0.27
0.909	1.48	3.54	3.56	-1.39	-5.01	-4.49
0.945	0.67	3.36	2.07	-2.85	0.30	-4.80
0.982	3.83	3.60	1.92	-0.78	-0.96	-2.41

Table 3.2.4 Computational Results of Vortex Core Radii

R_e/R_o	0.25	0.30	0.40	0.50	0.58	0.75
R_c/R_o	0.114	0.155	0.241	0.330	0.403	0.555

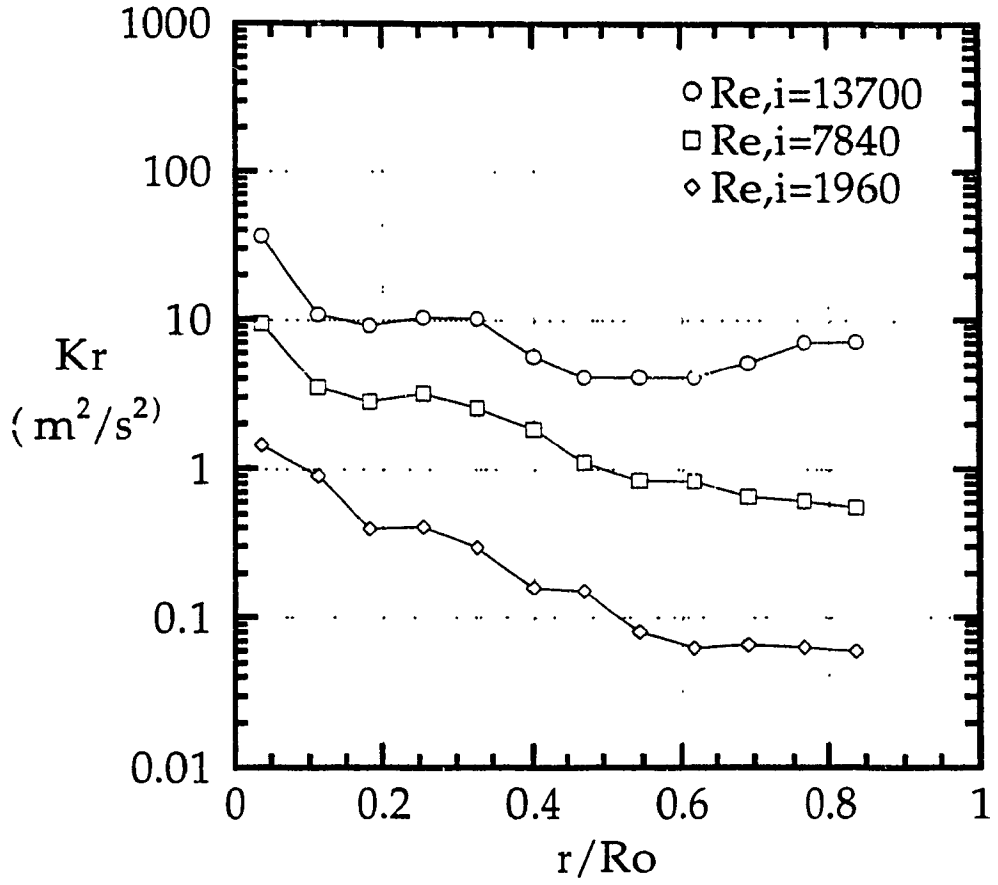

Figure 5.5.4.2 Experimental Radial Component of Turbulence Kinetic Energy near Exit Section (Re/Ro = 0.30)

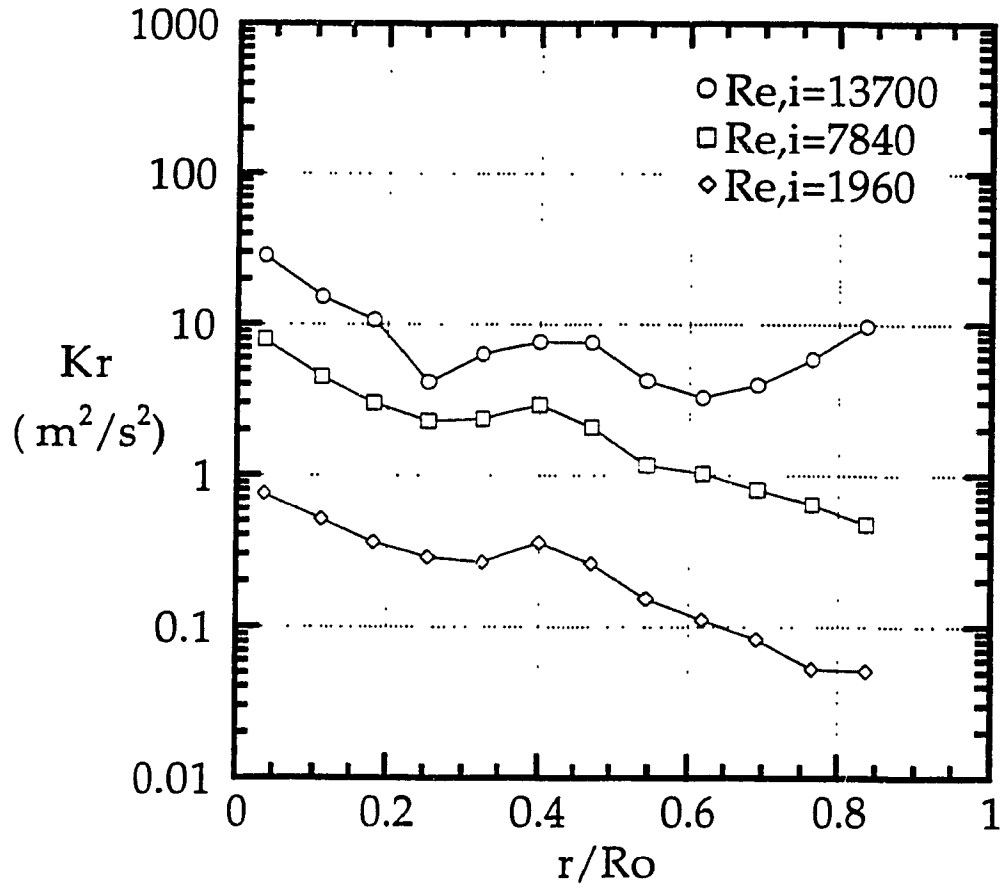

Figure 5.5.4.3 Experimental Radial Component of Turbulence Kinetic Energy near Exit Section (Re/Ro = 0.40)

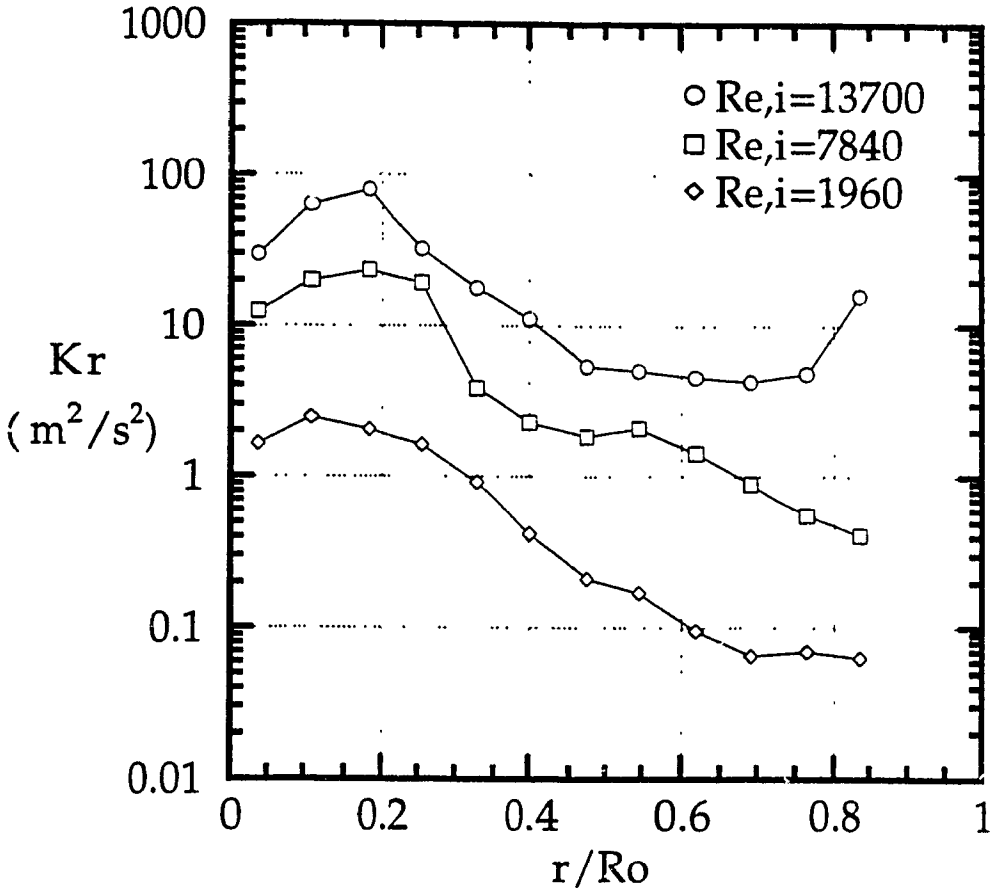

Figure 5.5.4.4 Experimental Radial Component of Turbulence Kinetic Energy near Exit Section (Re/Ro = 0.50)

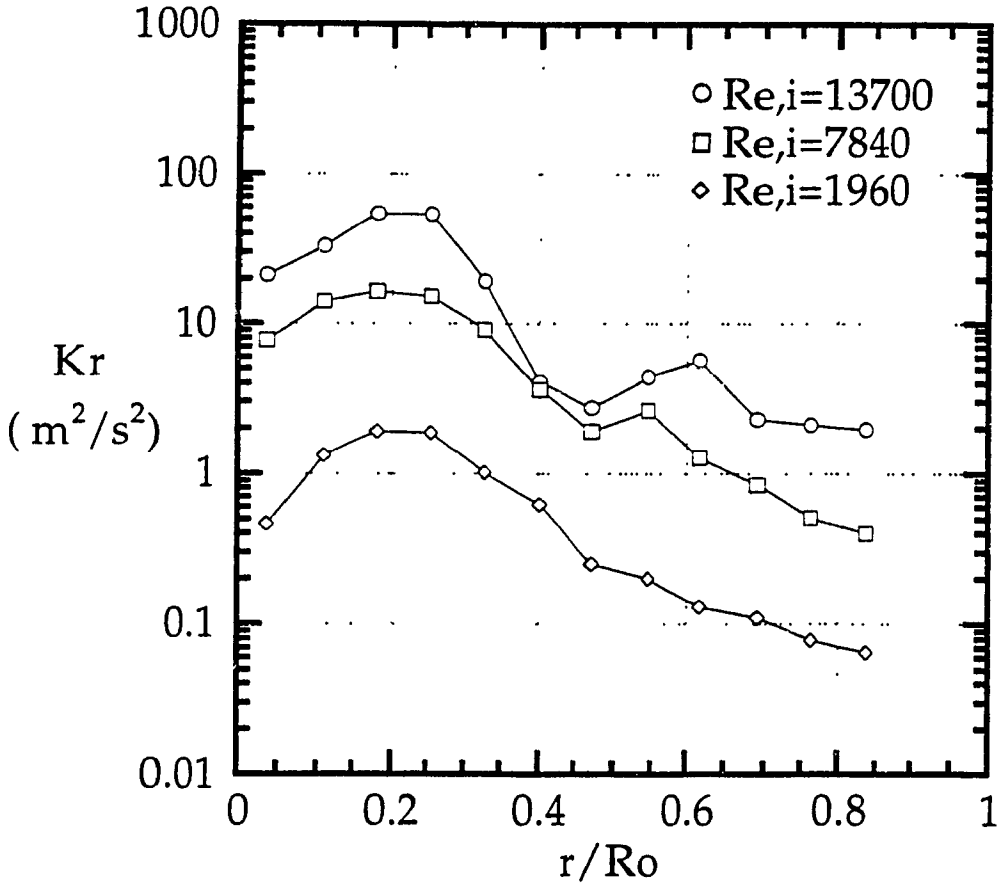

Figure 5.5.4.5 Experimental Radial Component of Turbulence Kinetic Energy near Exit Section (Re/Ro = 0.58)

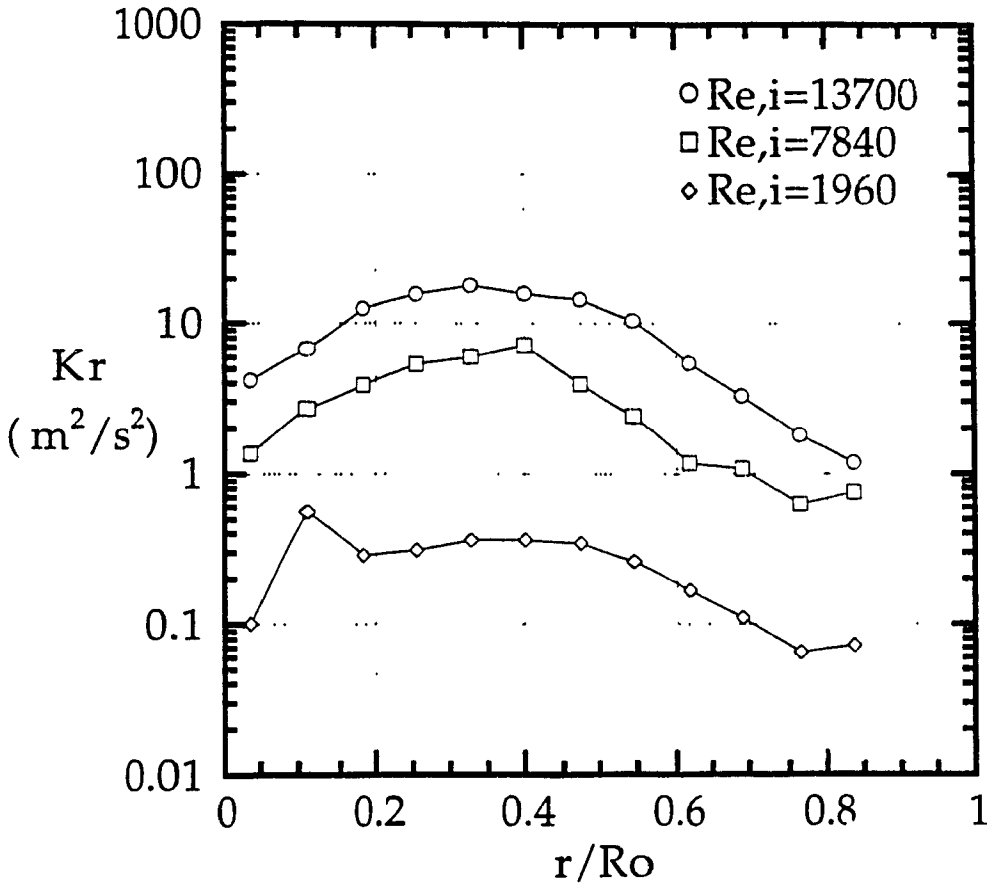

Figure 5.5.4.6 Experimental Radial Component of Turbulence Kinetic Energy near Exit Section (Re/Ro = 0.75)

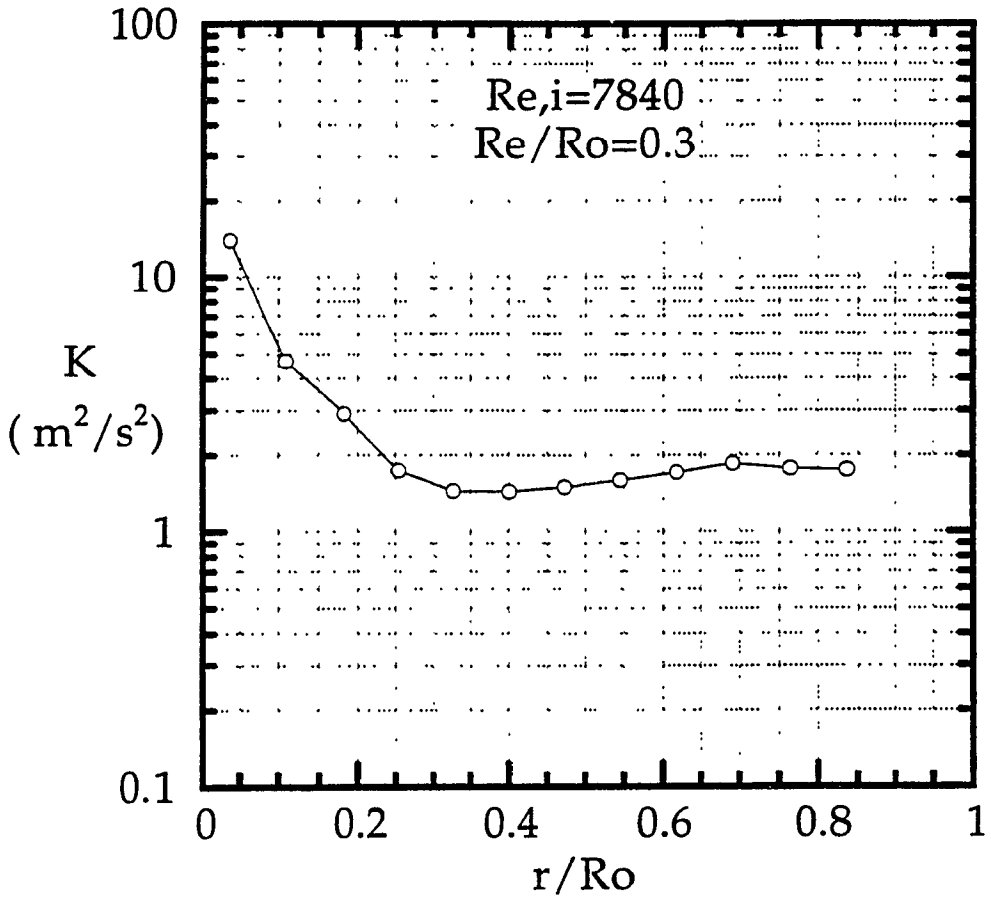

Figure 5.5.5.1 Experimental Total Turbulence Kinetic Energy at Main Section (69% Vortex Chamber Length)

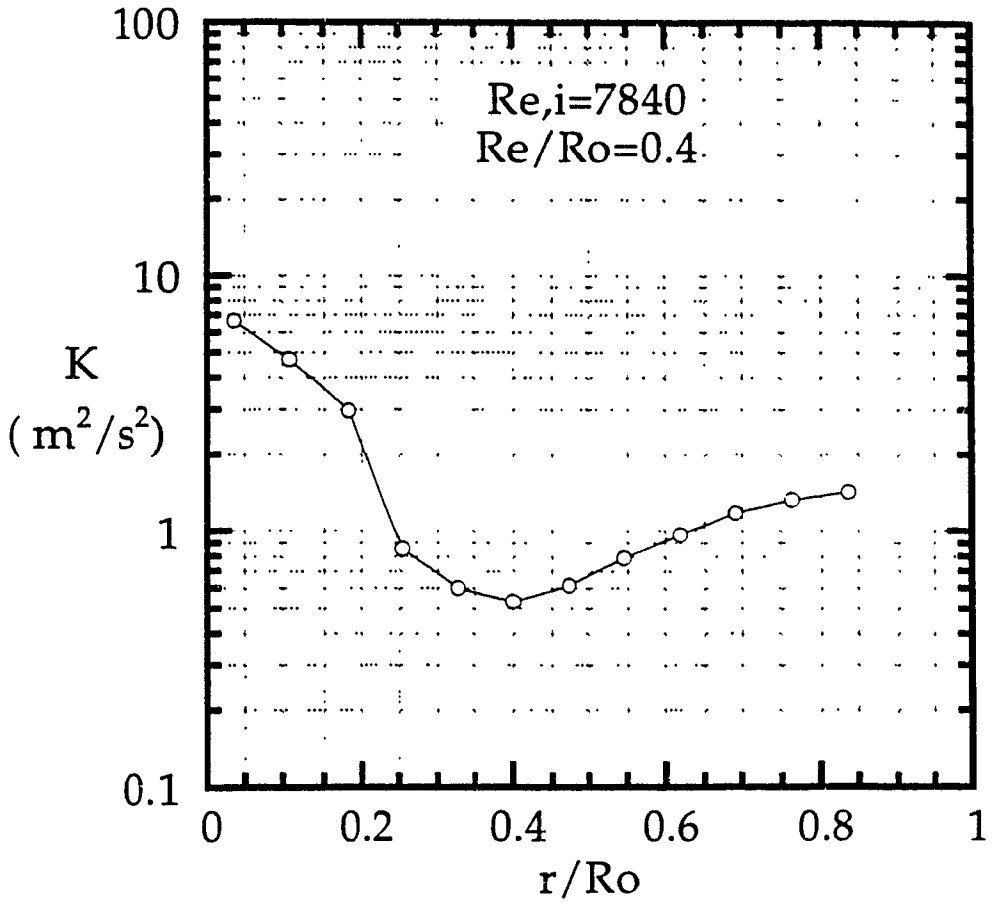

Figure 5.5.5.2 Experimental Total Turbulence Kinetic Energy at Main Section (50% Vortex Chamber Length)

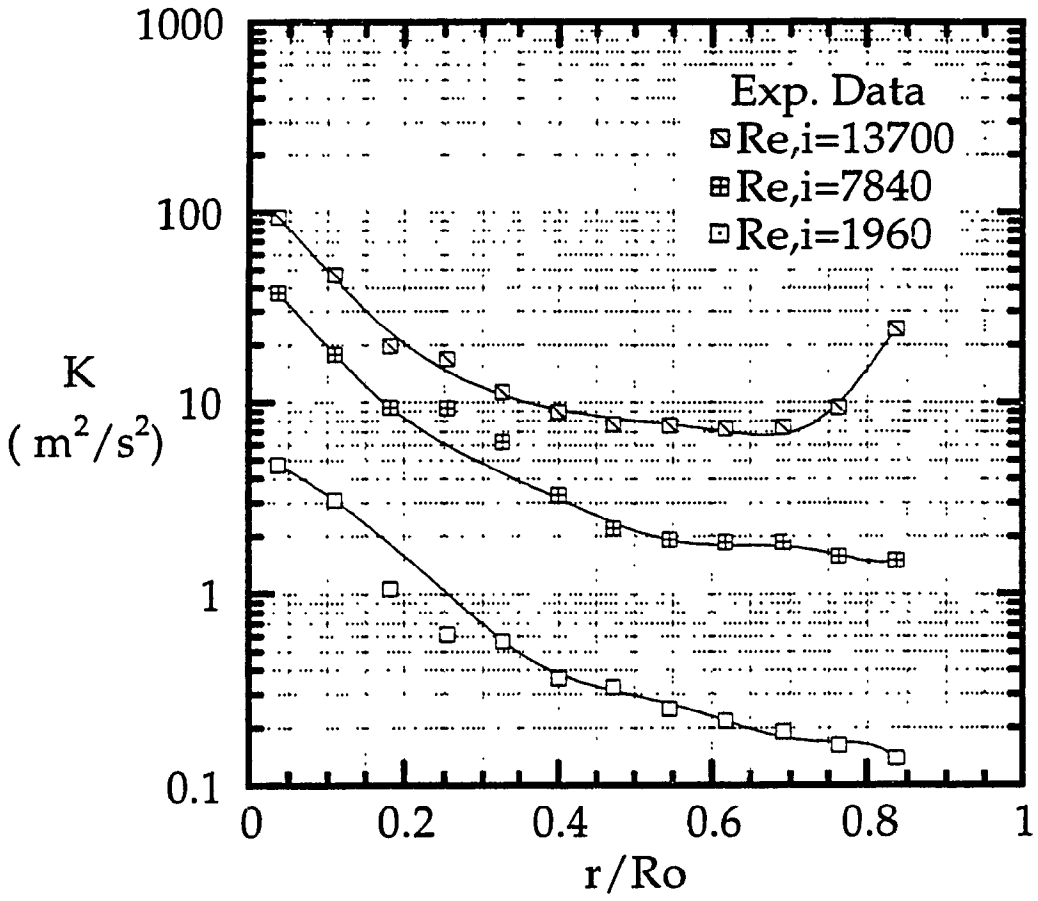

Figure 5.5.5.3 Total Turbulence Kinetic Energy near Exit Section at Re/Ro = 0.25 (lines - curve fitting)

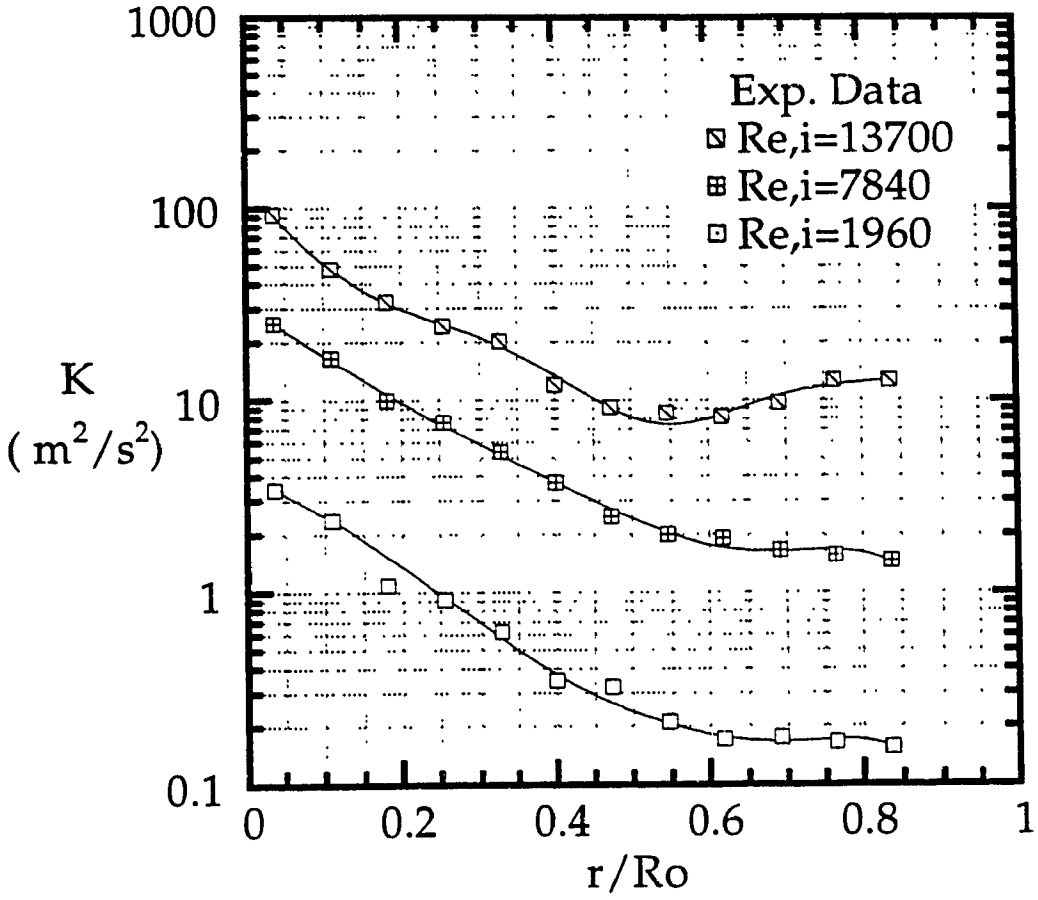

Figure 5.5.5.4 Total Turbulence Kinetic Energy near Exit Section at Re/Ro = 0.30 (lines - curve fitting)

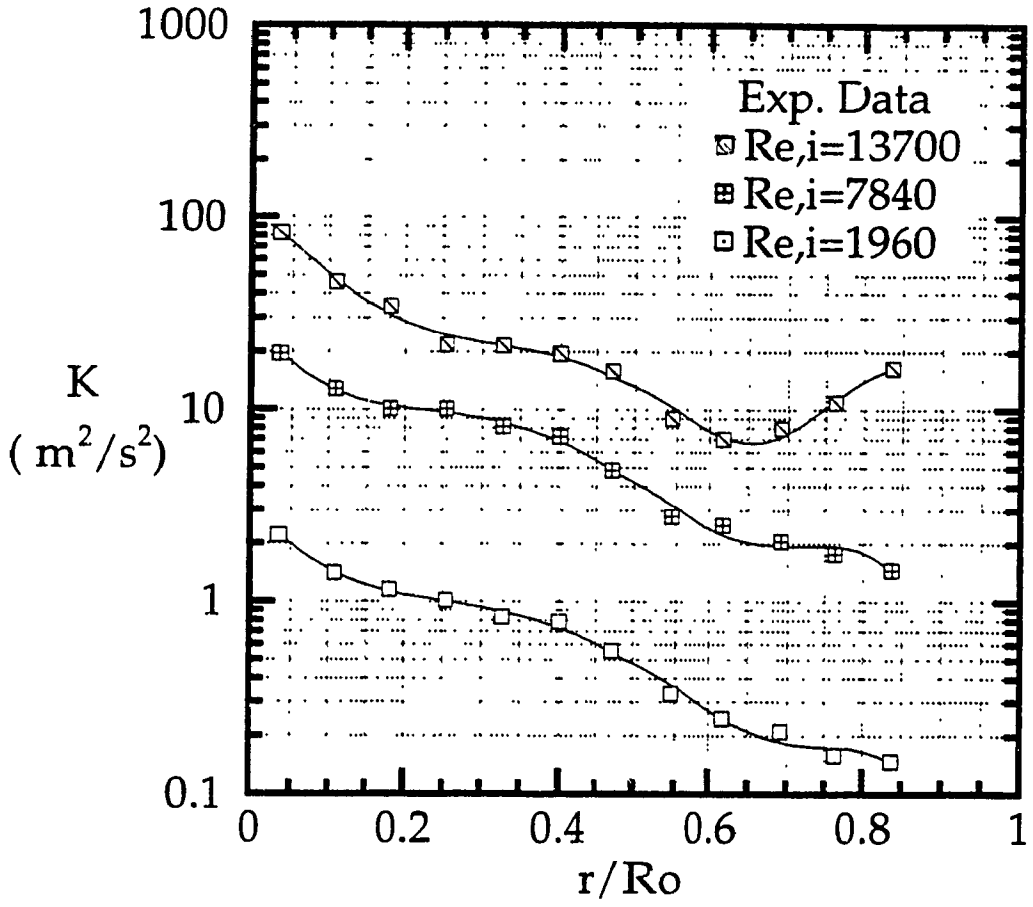

Figure 5.5.5.5 Total Turbulence Kinetic Energy near Exit Section at Re/Ro = 0.40 (lines - curve fitting)

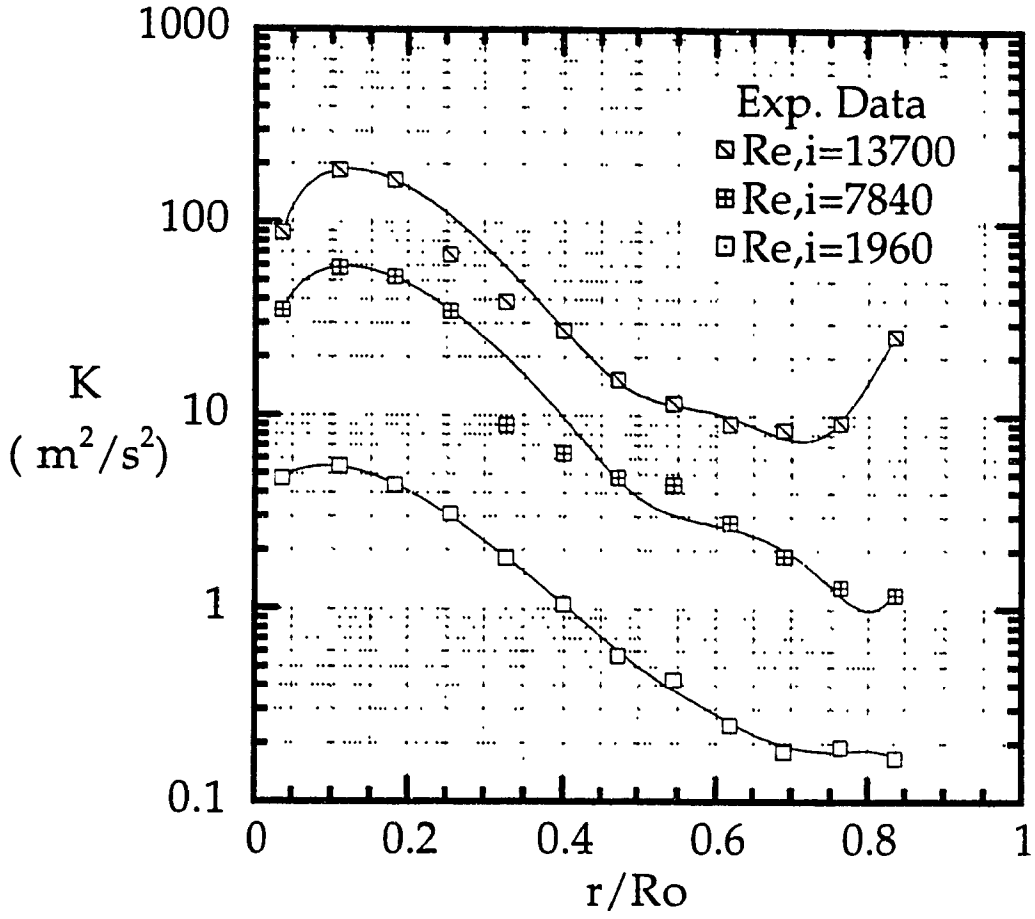

Figure 5.5.5.6 Total Turbulence Kinetic Energy near Exit Section at Re/Ro = 0.50 (lines - curve fitting)

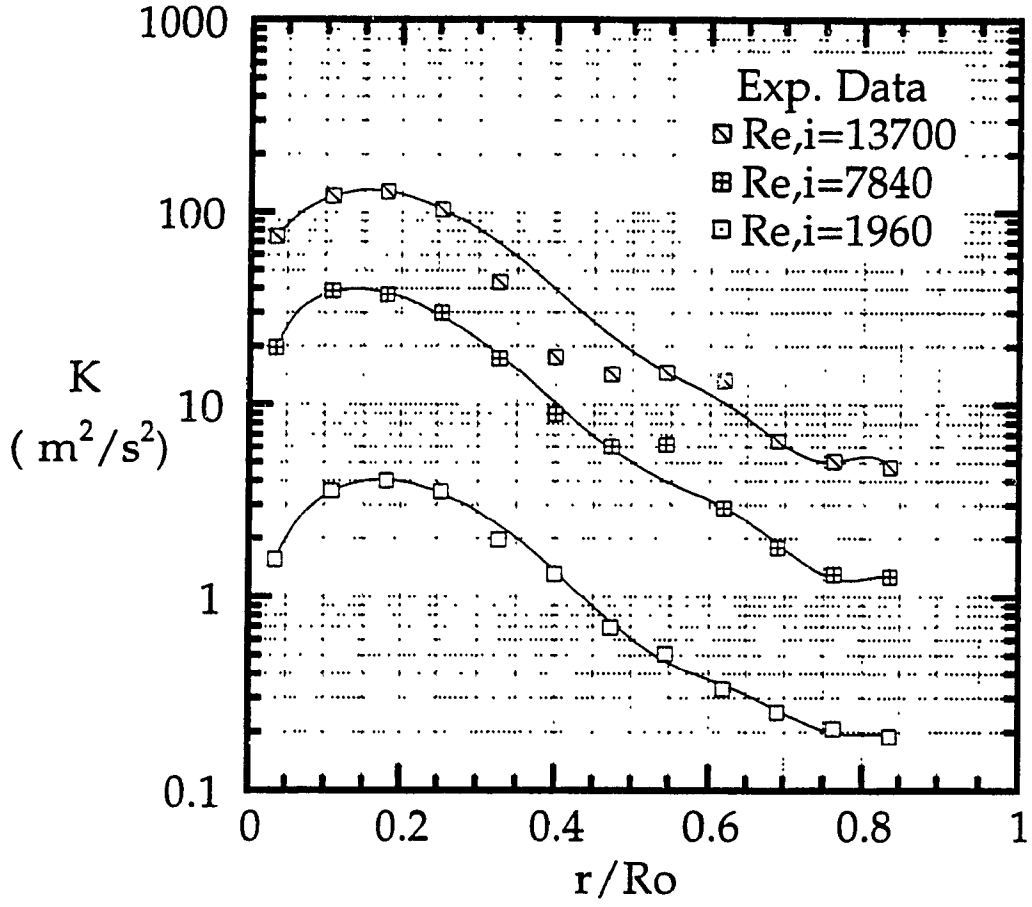

Figure 5.5.5.7 Total Turbulence Kinetic Energy near Exit Section at Re/Ro = 0.58 (lines - curve fitting)

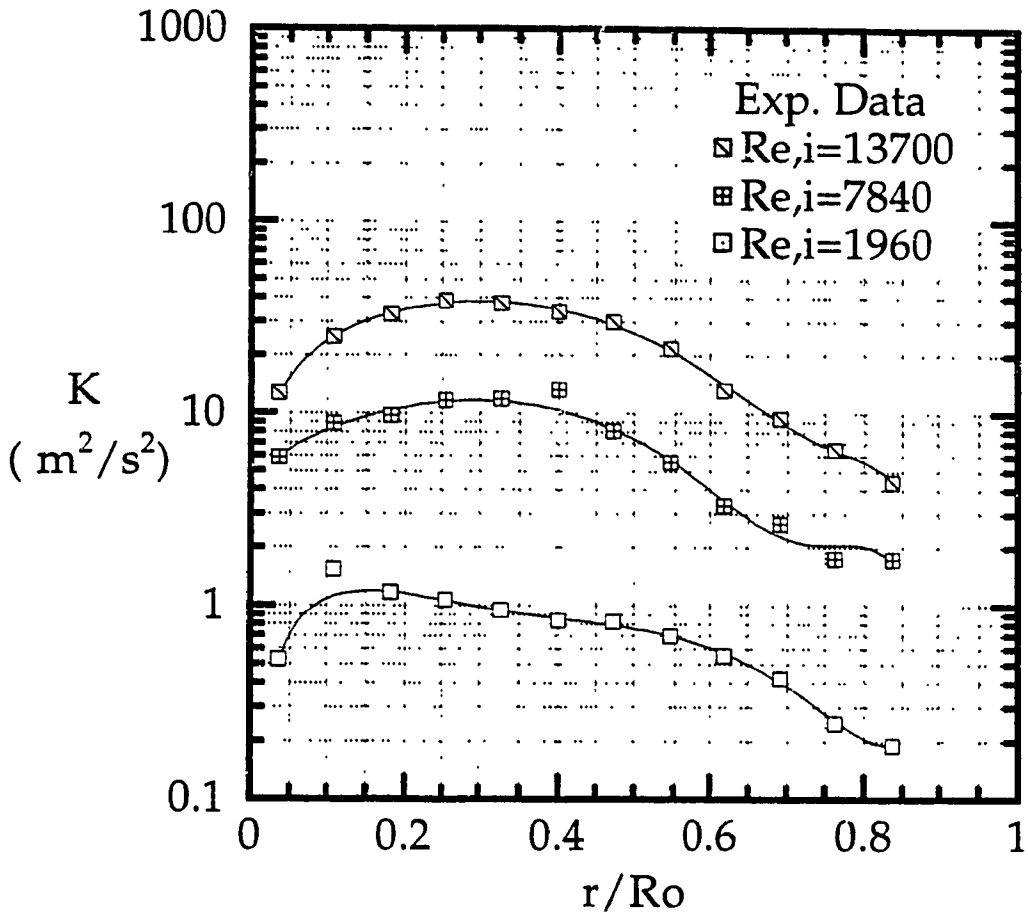

Figure 5.5.5.8 Total Turbulence Kinetic Energy near Exit Section at Re/Ro = 0.75 (lines - curve fitting)

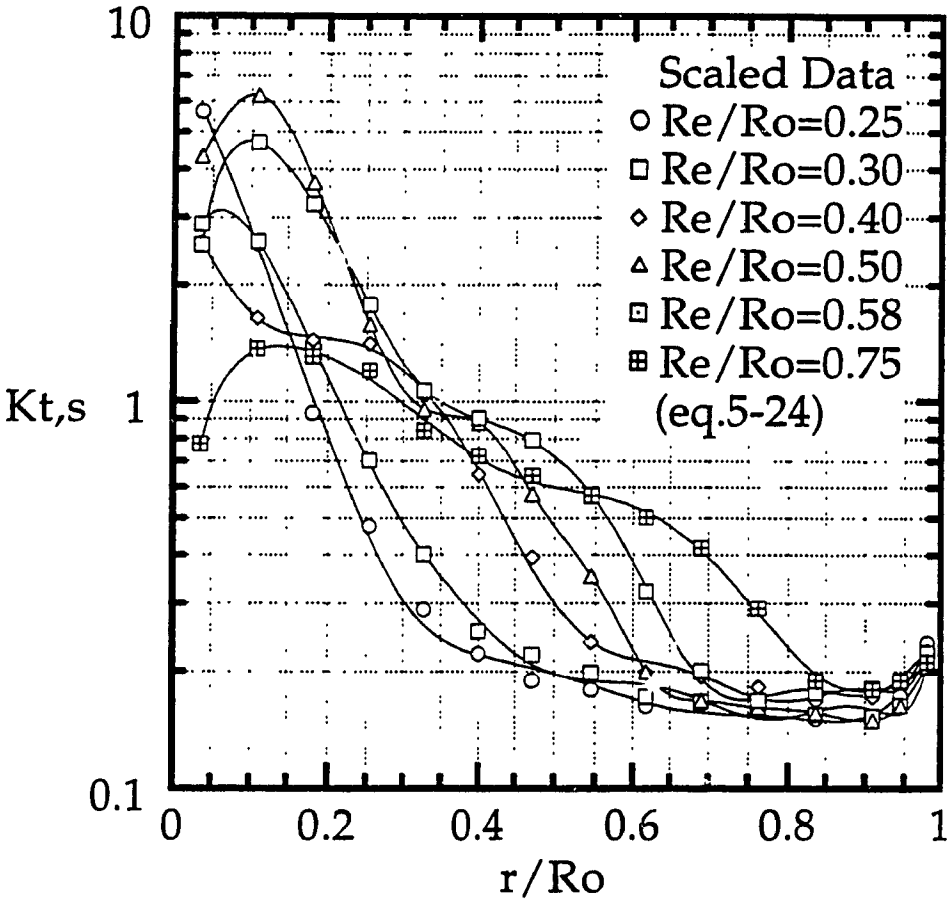

Figure 5.6.1 Scaled Tangential Component of Turbulence Kinetic Energy near Exit Section

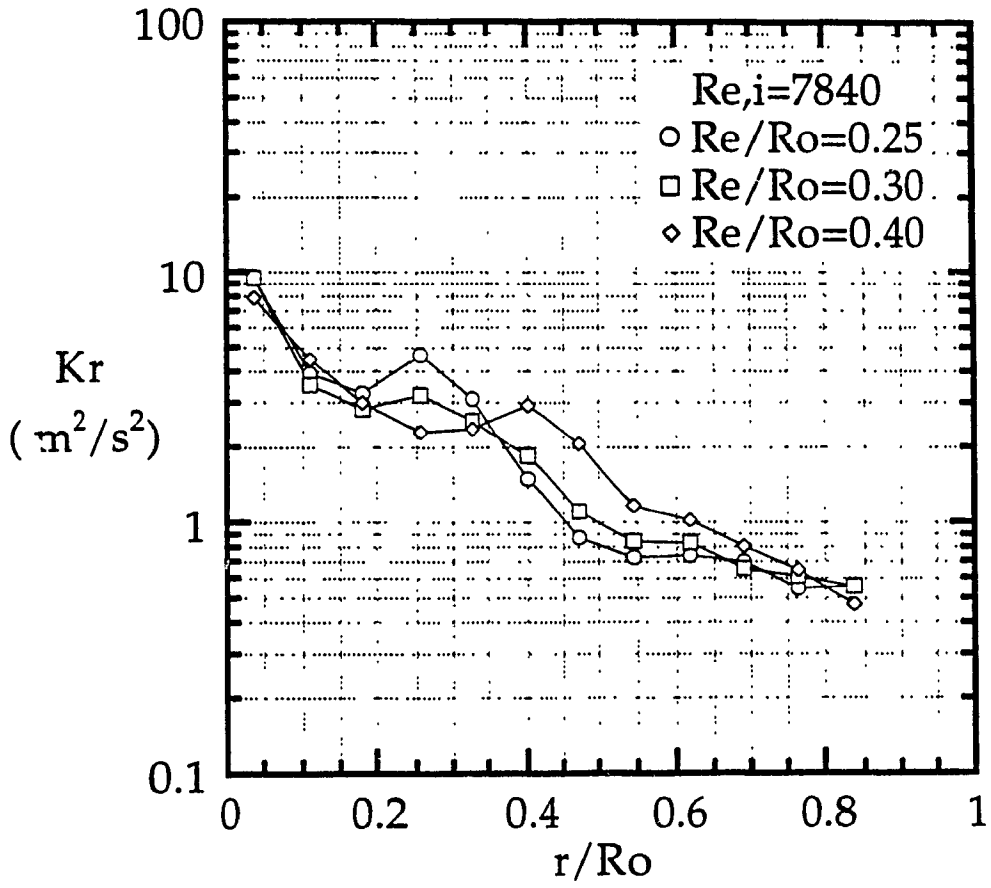

Figure 5.6.2 Experimental Radial Component of Turbulence Kinetic Energy near Exit Section (Re/Ro < 0.50)

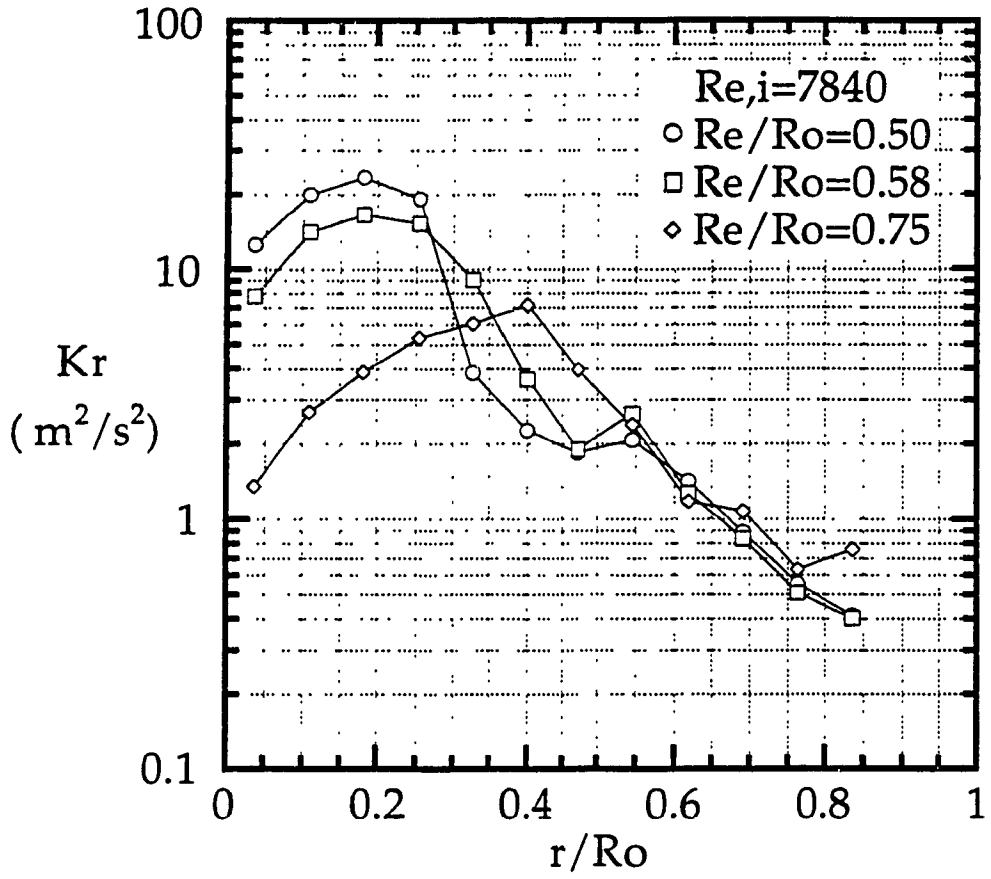

Figure 5.6.3 Experimental Radial Component of Turbulence Kinetic Energy near Exit Section (Re/Ro ≥ 0.50)

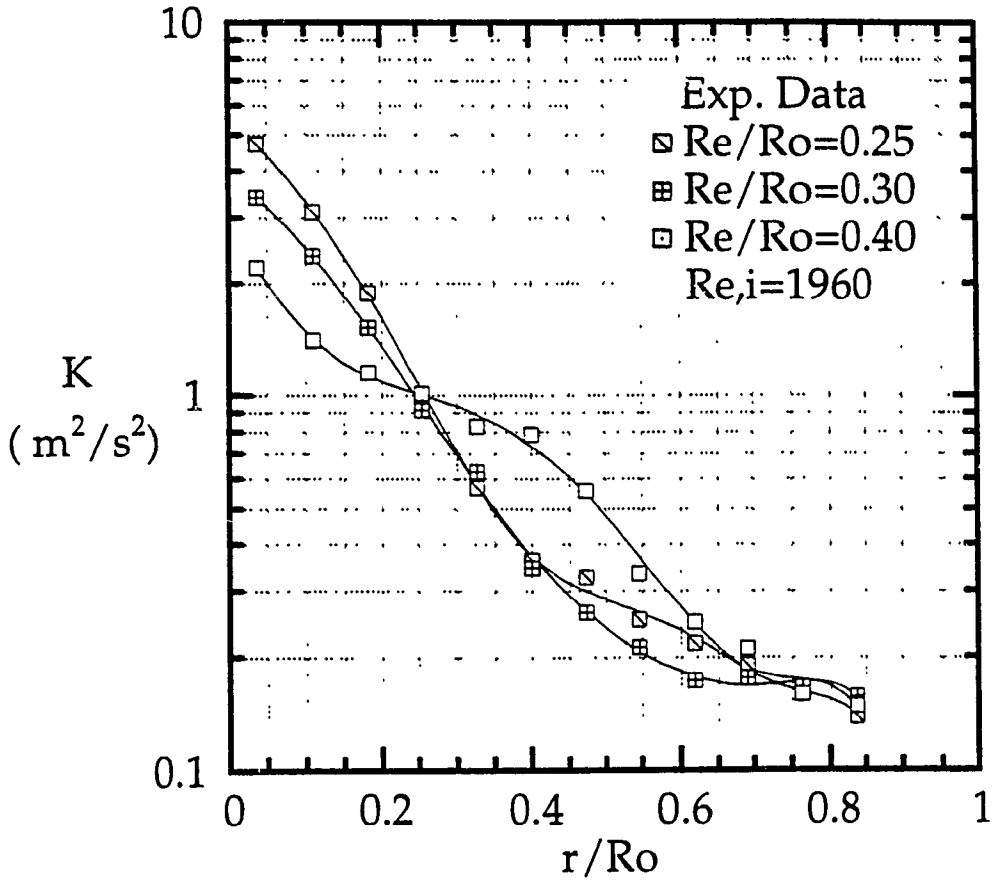

Figure 5.6.4 Total Turbulence Kinetic Energy near Exit Section at Re/Ro < 0.50 (lines - curve fitting)

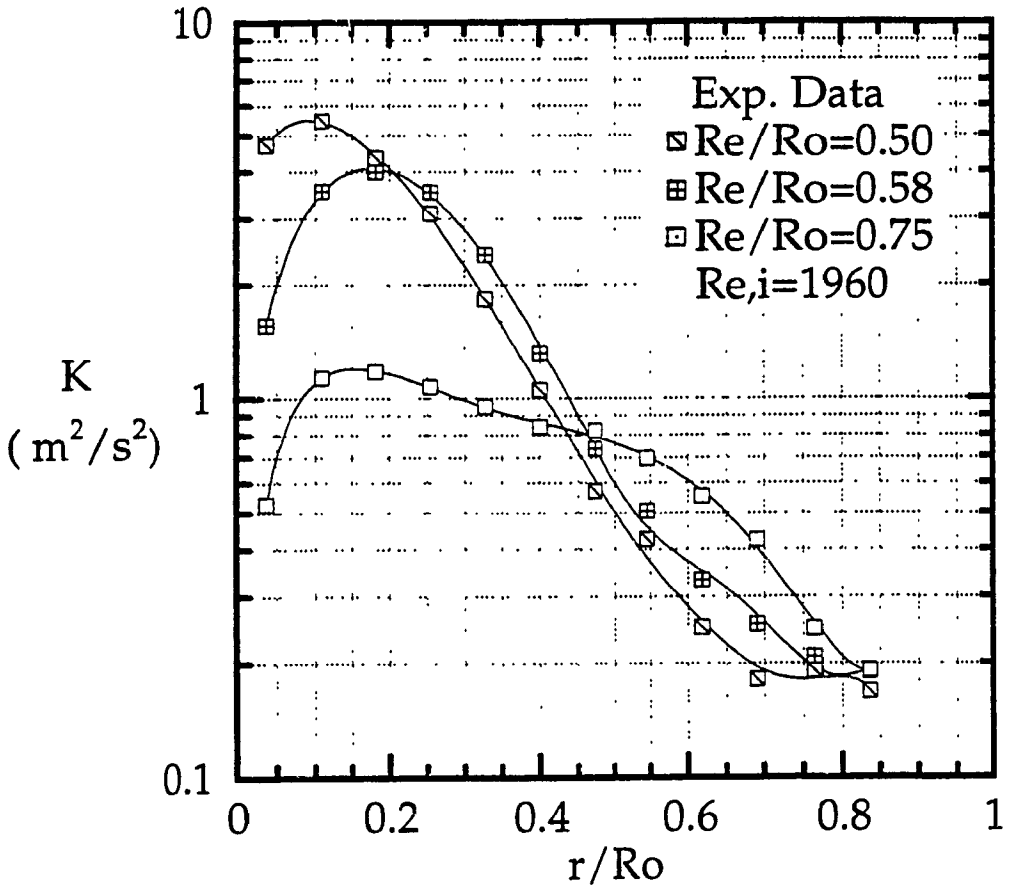

Figure 5.6.5 Total Turbulence Kinetic Energy near Exit Section at Re/Ro ≥ 0.50 (lines - curve fitting)

Table 5.6.1 Influence Factors on Magnitude of Turbulence Kinetic Energy

Tur. Kinetic Energy	Influence Parameters			Empiric.
Section	$R_{e,i}$	R_e/R_o	β	Equation
T.,Main ($R_e/R_o<0.5$)	Scaled	Yes	Yes	5-20
T.,Main ($R_e/R_o\geq0.5$)	Scaled	Yes	Yes	5-23
Tangent., near Exit	Scaled	Yes	Yes	5-24
Radial, near Exit	Yes	Yes	Yes	
Total, near Exit	Yes	Yes	Yes	5-26

Tur. = Turbulence
T. = Tangential

Table 5.6.2 Influence Factors on Locations of Maximum and Minimum Turbulence Kinetic Energy

Tur. Kinetic Energy		Influence Parameters			Location
Section	Point	$R_{e,i}$	R_e/R_o	β	
T., Main	L_{max}	No	No	No	Centre
$R_e/R_o<.5$	L_{min}	No	No	No	$r/R_o\approx0.6$
T., Main	L_{max}	No	Yes	Yes	Core R.
$R_e/R_o\geq.5$	L_{min}	No	Yes	Yes	Outer R.
T., Exit	L_{max}	No	No	No	Centre
$R_e/R_o<.5$	L_{min}	No	Yes	Yes	near B.L.
T., Exit	L_{max}	No	No	No	$r/R_o\approx0.1$
$R_e/R_o\geq.5$	L_{min}	No	Yes	Yes	near B.L.
Rad., Exit	L_{max}	No	No	No	Centre
$R_e/R_o<.5$	L_{min}	Yes	No	No	near B.L.
Rad., Exit	L_{max}	No	Yes	Yes	Core R.
$R_e/R_o\geq.5$	L_{min}	Yes	Yes	Yes	near B.L.
Tot., Exit	L_{max}	No	No	No	Centre
$R_e/R_o<.5$	L_{min}	Yes	Yes	Yes	near B.L.
Tot., Exit	L_{max}	No	Yes	Yes	Core R.
$R_e/R_o\geq.5$	L_{min}	Yes	Yes	Yes	near B.L.

R. = Region
B.L. = Boundary Layer
Rad. = Radial
Tot. = Total

Table 5.6.3 Deviation of Scaled Tangential Component of Turbulence Kinetic Energy at Re/Ro = 0.30 (Main Section)

% r/R_o	$R_{e,i}$ = 13700	$R_{e,i}$ = 7840	$R_{e,i}$ = 1960
0.036	67.0	-24.9	-42.0
0.109	54.5	-26.9	-27.6
0.182	-5.77	3.18	2.60
0.255	-2.29	-1.21	3.50
0.327	2.69	-8.35	5.66
0.400	4.51	-4.90	0.39
0.473	9.34	-3.91	-5.43
0.545	9.64	4.72	-14.4
0.618	16.0	-2.59	-13.4
0.691	0.36	6.50	-6.87
0.764	-0.84	5.70	-4.87
0.836	1.11	5.20	-6.31
0.909	23.4	-14.0	-9.43
0.945	13.8	-5.85	-7.95
0.982	7.32	-24.6	17.2

Table 5.6.4 Deviation of Scaled Tangential Component of Turbulence Kinetic Energy at Re/Ro = 0.30 (near Exit Section)

% r/R_o	$R_{e,i}$ = 13700	$R_{e,i}$ = 7840	$R_{e,i}$ = 1960
0.036	13.9	-15.8	1.94
0.109	7.09	-1.36	-5.73
0.182	18.8	-5.57	-13.2
0.255	8.71	-9.83	1.11
0.327	5.33	-12.3	6.98
0.400	18.0	-18.3	0.26
0.473	16.1	-17.1	1.02
0.545	7.11	-16.6	9.45
0.618	3.81	-12.4	8.63
0.691	-0.39	-9.54	9.93
0.764	5.52	-9.64	4.12
0.836	6.23	-9.74	3.51
0.909	5.03	3.79	-8.82
0.945	2.70	4.91	-7.62
0.982	-11.8	[illegible]14	5.70

Table 5.6.5 Deviation of Curve Fitting of Total Turbulence Kinetic Energy at Re/Ro < 0.5 (near Exit Section, Re,i = 1960)

%	R_e/R_o	R_e/R_o	R_e/R_o
r/R_o	= 0.25	= 0.30	= 0.40
0.036	-0.08	0.06	-0.13
0.109	0.56	-0.27	1.05
0.182	-1.54	-0.03	-2.04
0.255	1.41	3.19	-0.72
0.327	0.91	-7.60	7.45
0.400	2.61	7.51	-7.13
0.473	-8.45	0.57	-1.94
0.545	4.93	-2.47	11.3
0.618	3.14	2.51	-0.62
0.691	-2.95	-4.49	-11.4
0.764	0.02	3.58	9.51
0.836	0.36	-0.93	-2.01

Table 5.6.6 Deviation of Curve Fitting of Total Turbulence Kinetic Energy at Re/Ro ≥ 0.5 (near Exit Section, Re,i = 1960)

%	Re/Ro	Re/Ro	Re/Ro
r/R_o	= 0.50	= 0.58	= 0.75
0.036	0.12	0.35	0.04
0.109	-0.61	-0.90	-0.14
0.182	1.64	1.75	0.40
0.255	-2.10	-1.61	-0.56
0.327	0.65	-0.84	-0.36
0.400	0.17	4.01	2.62
0.473	6.65	0.71	-3.35
0.545	-10.9	-9.34	0.99
0.618	3.63	5.34	3.09
0.691	7.66	5.83	-4.64
0.764	-4.80	-6.12	3.55
0.836	0.93	1.47	-0.77

CHAPTER 6

REYNOLDS STRESSES

6.1 General

As presented in the previous Chapter, equations (5-1) to (5-3) are usually referred to as the Reynolds equations in cylindrical coordinates. Additional stresses, namely Reynolds stresses $\rho\overline{V_i'V_j'}$, appear in the Reynolds equations if these equations for the mean motion are compared with the Navier-Stokes equations. The term $\rho\overline{V_i'V_j'}$, which can be explained as momentum transfer per unit time through an unit area, is always equivalent to an equal and opposite force exerted on the area by the surroundings. Therefore, the Reynolds stresses represent the exchange of momentum in the turbulent mixing process. In the turbulent transfer, Reynolds stresses characterize the important nonlinear mechanism. As a result of Reynolds stresses, production or diffusion of turbulent energy takes place from the energy of the mean motion.

The Reynolds stresses are apparent stresses, different from the viscous stresses and the pressure. Only the viscous stresses and the pressure can be considered as the instantaneous stresses. The viscous stresses are the results of the mean motion, represented in terms of the mean velocity gradients and the mean velocities. For overall consideration, the Reynolds stresses must be added to the stresses caused by the mean flow.

Reynolds stresses have normal as well as tangential components. The normal components are obtained when subscript i is equal to j, such as $\rho\overline{V_r'^2}$, $\rho\overline{V_\theta'^2}$ and $\rho\overline{V_z'^2}$. The normal component may be interpreted as a normal stress because the flux of momentum causes a reaction such as pressure in the direction normal to the surface. In addition, the magnitude of momentum is

equivalent to a stress with a negative sign. The tangential components are obtained when the subscript i is not equal to j, such as $\rho\overline{V_r'V_\theta'}$, $\rho\overline{V_\theta'V_z'}$ and $\rho\overline{V_z'V_r'}$. The tangential component may be interpreted as a shear stress because the flux of momentum causes a reaction in the direction along the surface.

In general, it is very difficult to obtain a numerical value for the Reynolds stresses by directly solving the Reynolds differential equations analytically. To obtain the Reynolds stresses, experimental determination using an advanced apparatus such as a Laser Doppler Anemometer is a possible approach. In this work, some analytical results for Reynolds shear stresses, fortunately, are obtained by solving differential equations derived in the previous Chapter. Detailed steps are included in Appendix B. The numerical values of the Reynolds normal stresses are obtained from the experiments. In this work, the density ρ is considered as a constant. Therefore, it is not included in the analysis of the Reynolds stresses.

6.2 Analytical Approach for Reynolds Shear Stress

6.2.1 Radial-Tangential Component of Reynolds Shear Stress

The radial-tangential component of the Reynolds shear stress $\overline{V_r'V_\theta'}$ can be found in the equation of the tangential component of the kinetic energy for the mean motion as follows:

$$\overline{V}_r\frac{\partial}{\partial r}\left(\frac{1}{2}\overline{V}_\theta^2\right) + \overline{V}_r\left(\frac{\overline{V}_\theta^2}{r}\right)$$
$$= \nu\overline{V}_\theta\left(\frac{\partial^2\overline{V}_\theta}{\partial r^2} + \frac{1}{r}\frac{\partial\overline{V}_\theta}{\partial r} - \frac{\overline{V}_\theta}{r^2}\right) - \overline{V}_\theta\left[\frac{\partial}{\partial r}\left(\overline{V_r'V_\theta'}\right) + \frac{2}{r}\overline{V_r'V_\theta'}\right] \qquad (5\text{-}8)$$

Rewriting equation (5-8) to approach scaled units yields

$$\left(\frac{\overline{V}_r}{\overline{V}_{in}}\cdot R_{e,i}^{0.25}\right)\left(\frac{\overline{V}_{in}}{R_{e,i}^{0.25}}\right)\frac{\partial}{\partial(r/R_o)}\left[\frac{1}{2}\left(\frac{\overline{V}_\theta}{\overline{V}_{in}}\right)^2\right]\left(\frac{\overline{V}_{in}^2}{R_o}\right) +$$

$$+ \left(\frac{\overline{V}_r}{\overline{V}_{in}} R_{e,i}^{0.25}\right)\left(\frac{\overline{V}_{in}}{R_{e,i}^{0.25}}\right)\left[\frac{R_o}{r}\left(\frac{\overline{V}_\theta}{\overline{V}_{in}}\right)^2\right]\left(\frac{\overline{V}_{in}^2}{R_o}\right)$$

$$= \nu\left(\frac{\overline{V}_\theta}{\overline{V}_{in}}\right)(\overline{V}_{in})\left\{\frac{\partial}{\partial(r/R_o)}\left[\frac{\partial(\overline{V}_\theta/\overline{V}_{in})}{\partial(r/R_o)}\right]\left(\frac{\overline{V}_{in}}{R_o^2}\right) +\right.$$

$$\left. + \left(\frac{R_o}{r}\right)\frac{\partial(\overline{V}_\theta/\overline{V}_{in})}{\partial(r/R_o)}\left(\frac{\overline{V}_{in}}{R_o^2}\right) - \left(\frac{R_o}{r}\right)^2\left(\frac{\overline{V}_\theta}{\overline{V}_{in}}\right)\left(\frac{\overline{V}_{in}}{R_o^2}\right)\right\} -$$

$$- \left(\frac{\overline{V}_\theta}{\overline{V}_{in}}\right)(\overline{V}_{in})\left[\frac{\partial}{\partial(r/R_o)}\left(\frac{\overline{V_r'V_\theta'}}{\overline{V}_{in}^2}\right)\left(\frac{\overline{V}_{in}^2}{R_o}\right) + 2\left(\frac{R_o}{r}\right)\left(\frac{\overline{V_r'V_\theta'}}{\overline{V}_{in}^2}\right)\left(\frac{\overline{V}_{in}^2}{R_o}\right)\right] \qquad (6\text{-}1)$$

Let

$$\overline{R} = r/R_o$$

$$\overline{V}_R = \frac{\overline{V}_r}{\overline{V}_{in}} R_{e,i}^{0.25}$$

$$\overline{V}_T = \frac{\overline{V}_\theta}{\overline{V}_{in}}$$

$$\overline{V_R'V_T'} = \frac{\overline{V_r'V_\theta'}}{\overline{V}_{in}^2} \qquad (6\text{-}2)$$

Substituting equation (6-2) into (6-1) and rearranging the equation yield

$$\frac{1}{R_{e,i}^{0.25}}\overline{V}_R\left[\frac{\partial}{\partial\overline{R}}\left(\frac{1}{2}\overline{V}_T^2\right) + \frac{\overline{V}_T^2}{\overline{R}}\right]$$

$$= \left(\frac{\nu}{\overline{V}_{in}R_o}\right)\overline{V}_T\left(\frac{\partial^2\overline{V}_T}{\partial\overline{R}^2} + \frac{1}{\overline{R}}\frac{\partial\overline{V}_T}{\partial\overline{R}} - \frac{\overline{V}_T}{\overline{R}^2}\right) - \overline{V}_T\left[\frac{\partial}{\partial\overline{R}}(\overline{V_R'V_T'}) + \frac{2}{\overline{R}}(\overline{V_R'V_T'})\right] \qquad (6\text{-}3)$$

Let

$$R_{e,o} = \frac{\overline{V}_{in}D_o}{\nu} \qquad (6\text{-}4)$$

Substituting equation (6-4) into (6-3) and rearranging the equation yield

$$\frac{\partial}{\partial\overline{R}}(\overline{V_R'V_T'}) + \frac{2}{\overline{R}}(\overline{V_R'V_T'}) +$$

$$+ \left[\frac{1}{R_{e,i}^{0.25}}\overline{V}_R\left(\frac{\partial\overline{V}_T}{\partial\overline{R}} + \frac{\overline{V}_T}{\overline{R}}\right) - \frac{2}{R_{e,o}}\left(\frac{\partial^2\overline{V}_T}{\partial\overline{R}^2} + \frac{1}{\overline{R}}\frac{\partial\overline{V}_T}{\partial\overline{R}} - \frac{\overline{V}_T}{\overline{R}^2}\right)\right] = 0 \qquad (6\text{-}5)$$

It is found that from the experimental results the velocities $\overline{V}_R$ and $\overline{V}_T$ are functions of normalized radius $\overline{R}$, and can be expressed by polynomials. That is,

$$\overline{V}_R = f_a(\overline{R})$$

$$= \sum_0^n a_n \overline{R}^n \qquad (n = 0, 1, 2, ...) \qquad (6\text{-}6)$$

$$\overline{V}_T = f_b(\overline{R})$$

$$= \sum_0^n b_n \overline{R}^n \qquad (n = 0, 1, 2, ...) \qquad (6\text{-}7)$$

For any given flow and vortex chamber structure conditions, $R_{e,i}$ and $R_{e,o}$ are known constants. Therefore, the third part of equation (6-5) is a function of normalized radius $\overline{R}$ under the given condition. That is,

$$\frac{1}{R_{e,i}^{0.25}} \overline{V}_R \left(\frac{\partial \overline{V}_T}{\partial \overline{R}} + \frac{\overline{V}_T}{\overline{R}}\right) - \frac{2}{R_{e,o}} \left(\frac{\partial^2 \overline{V}_T}{\partial \overline{R}^2} + \frac{1}{\overline{R}} \frac{\partial \overline{V}_T}{\partial \overline{R}} - \frac{\overline{V}_T}{\overline{R}^2}\right) = F(\overline{R}) \qquad (6\text{-}8)$$

Substituting equation (6-8) into (6-5) yields

$$\frac{d}{d\overline{R}}(\overline{V_R' V_T'}) + \frac{2}{\overline{R}}(\overline{V_R' V_T'}) + F(\overline{R}) = 0 \qquad (6\text{-}9)$$

This is a linear differential equation. The solution of the equation of the scaled radial-tangential component of the Reynolds shear stress $\overline{V_R' V_T'}$ can be obtained using the following boundary layer condition: at the centre of the vortex chamber, $\overline{V_R' V_T'}$ is zero. Thus,

$$\overline{V_R' V_T'} = -\frac{1}{\overline{R}^2} \int \overline{R}^2 \cdot F(\overline{R})\, d\overline{R} \qquad (\overline{R} \neq 0) \qquad (6\text{-}10)$$

Combining equations (6-6), (6-7) with (6-8) yields

$$F(\bar{R}) = \frac{1}{R_{e,i}^{0.25}} \sum_{0}^{n} a_n \bar{R}^n \cdot \sum_{0}^{n} (n+1) b_n \bar{R}^{n-1} - \frac{2}{R_{e,o}} \sum_{0}^{n} (n-1)(n+1) b_n \bar{R}^{n-2} \tag{6-11}$$

Substituting equation (6-11) into (6-10) yields the scaled radial-tangential component of the Reynolds shear stress $\overline{V_R' V_T'}$ as

$$\overline{V_R' V_T'} = -\frac{1}{R_{e,i}^{0.25} \cdot \bar{R}^2} \int \sum_{0}^{n} a_n \bar{R}^n \cdot \sum_{0}^{n} (n+1) b_n \bar{R}^{n+1} \, d\bar{R} +$$

$$+ \frac{2}{R_{e,o} \cdot \bar{R}^2} \int \sum_{0}^{n} (n-1)(n+1) b_n \bar{R}^n \, d\bar{R} \tag{6-12}$$

Since

$$\int \sum_{0}^{n} a_n \bar{R}^n \cdot \sum_{0}^{n} (n+1) b_n \bar{R}^{n+1} \, d\bar{R} = \bar{R}^2 \sum_{0}^{n} \left[\sum_{0}^{m} a_m \bar{R}^m \cdot \frac{n+1}{(n+2)+m} \right] b_n \bar{R}^n \tag{6-13}$$

and

$$\int \sum_{0}^{n} (n-1)(n+1) b_n \bar{R}^n \, d\bar{R} = \bar{R}^2 \sum_{0}^{n} (n-1) b_n \bar{R}^{n-1} \tag{6-14}$$

Substituting equations (6-13), (6-14) into (6-12) yields

$$\overline{V_R' V_T'} = -\frac{1}{R_{e,i}^{0.25}} \sum_{0}^{n} \left[\sum_{0}^{m} a_m \bar{R}^m \cdot \frac{n+1}{(n+2)+m} \right] b_n \bar{R}^n + \frac{2}{R_{e,o}} \sum_{0}^{n} (n-1) b_n \bar{R}^{n-1}$$

$$(m = 0, 1, 2, \ldots\ldots, n = 0, 1, 2, \ldots\ldots) \tag{6-15}$$

There were no mathematical difficulties to obtain the radial-tangential component of the Reynolds shear stress because the radial and tangential mean velocity profiles were obtained from the experiments.

6.2.2 Radial-Axial Component of Reynolds Shear Stress

Similarly, the radial-axial component of the Reynolds shear stress $\overline{V_r'V_z'}$ can be determined from the equation of the axial component of the kinetic energy for the mean motion as follows:

$$\overline{V}_r\frac{\partial}{\partial r}(\frac{1}{2}\overline{V}_z^2) = \nu\overline{V}_z(\frac{\partial^2\overline{V}_z}{\partial r^2} + \frac{1}{r}\frac{\partial\overline{V}_z}{\partial r}) - \overline{V}_z[\frac{\partial}{\partial r}(\overline{V_r'V_z'}) + \frac{1}{r}\overline{V_r'V_z'}] \tag{5-11}$$

Equation (5-11) can be rearranged to approach scaled units as follows:

$$\begin{aligned}&(\frac{\overline{V}_r}{\overline{V}_{in}}\cdot R_{e,i}^{0.25})(\frac{\overline{V}_{in}}{R_{e,i}^{0.25}})\frac{\partial(\overline{V}_z/\overline{V}_{in})}{\partial(r/R_o)}(\frac{\overline{V}_{in}}{R_o})\\ &= \nu(\frac{1}{r/R_o})(\frac{1}{R_o})\frac{\partial}{\partial(r/R_o)}[\frac{r}{R_o}\cdot\frac{\partial(\overline{V}_z/\overline{V}_{in})}{\partial(r/R_o)}](\frac{\overline{V}_{in}}{R_o}) -\\ &- \frac{\partial}{\partial(r/R_o)}(\frac{\overline{V_r'V_z'}}{\overline{V}_{in}^2})(\frac{\overline{V}_{in}^2}{R_o}) - \frac{1}{r/R_o}(\frac{\overline{V_r'V_z'}}{\overline{V}_{in}^2})(\frac{\overline{V}_{in}^2}{R_o})\end{aligned} \tag{6-16}$$

Let

$$\overline{R} = r/R_o$$

$$\overline{V}_R = \frac{\overline{V}_r}{\overline{V}_{in}}R_{e,i}^{0.25}$$

$$\overline{V}_Z = \frac{\overline{V}_z}{\overline{V}_{in}}$$

$$\overline{V_R'V_Z'} = \frac{\overline{V_r'V_z'}}{\overline{V}_{in}^2} \tag{6-17}$$

Substituting equation (6-17) into (6-16) and rearranging the equation yield

$$\frac{\partial}{\partial\overline{R}}(\overline{V_R'V_Z'}) + \frac{1}{\overline{R}}(\overline{V_R'V_Z'}) + [\frac{1}{R_{e,i}^{0.25}}\overline{V}_R\frac{\partial\overline{V}_Z}{\partial\overline{R}} - \frac{2}{R_{e,o}\cdot\overline{R}}\frac{\partial}{\partial\overline{R}}(\overline{R}\frac{\partial\overline{V}_Z}{\partial\overline{R}})] = 0 \tag{6-18}$$

It is found that from the experimental results the velocities $\overline{V}_R$ and $\overline{V}_Z$ are functions of normalized radius $\overline{R}$, and can be expressed by polynomials. That is,

$$\overline{V}_R = f_a(\overline{R})$$

$$= \sum_0^n a_n \overline{R}^n \qquad (n = 0, 1, 2, ...) \qquad (6\text{-}6)$$

$$\overline{V}_Z = f_d(\overline{R})$$

$$= \sum_0^n d_n \overline{R}^n \qquad (n = 0, 1, 2, ...) \qquad (6\text{-}19)$$

For any given flow and vortex chamber structure conditions, $R_{e,i}$ and $R_{e,o}$ are known constants. Therefore, the third part of equation (6-18) is a function of normalized radius $\overline{R}$ under the given condition. That is,

$$\frac{1}{R_{e,i}^{0.25}} \overline{V}_R \frac{\partial \overline{V}_Z}{\partial \overline{R}} - \frac{2}{R_{e,o} \cdot \overline{R}} \frac{\partial}{\partial \overline{R}} (\overline{R} \frac{\partial \overline{V}_Z}{\partial \overline{R}}) = G(\overline{R}) \qquad (6\text{-}20)$$

Substituting equation (6-20) into (6-18) yields

$$\frac{d}{d\overline{R}} (\overline{V_R' V_Z'}) + \frac{1}{\overline{R}} (\overline{V_R' V_Z'}) + G(\overline{R}) = 0 \qquad (6\text{-}21)$$

This is a linear differential equation. The solution of the equation of the scaled radial-axial component of the Reynolds shear stress $\overline{V_R' V_Z'}$, can be obtained using the following boundary layer condition: at the centre of the vortex chamber, $\overline{V_R' V_Z'}$ is zero. Thus,

$$\overline{V_R' V_Z'} = -\frac{1}{\overline{R}} \int \overline{R} \cdot G(\overline{R}) \, d\overline{R} \qquad (\overline{R} \neq 0) \qquad (6\text{-}22)$$

Combining equations (6-6), (6-19)with (6-20) yields

$$G(\bar{R}) = \frac{1}{R_{e,i}^{0.25}} \sum_{0}^{n} a_n \bar{R}^n \cdot \sum_{0}^{n} n d_n \bar{R}^{n-1} - \frac{2}{R_{e,o}} \cdot \sum_{0}^{n} n^2 d_n \bar{R}^{n-2} \tag{6-23}$$

Substituting equation (6-23) into (6-22) yields the scaled radial-axial component of the Reynolds shear stress $\overline{V_R' V_Z'}$ as

$$\overline{V_R' V_Z'} = -\frac{1}{R_{e,i}^{0.25} \cdot \bar{R}} \int \sum_{0}^{n} a_n \bar{R}^n \cdot \sum_{0}^{n} n d_n \bar{R}^n \, d\bar{R} +$$

$$+ \frac{2}{R_{e,o} \cdot \bar{R}} \int \sum_{0}^{n} n^2 d_n \bar{R}^{n-1} \, d\bar{R} \tag{6-24}$$

Since

$$\int \sum_{0}^{n} a_n \bar{R}^n \cdot \sum_{0}^{n} n d_n \bar{R}^n \, d\bar{R} = \bar{R} \sum_{0}^{n} \left[\sum_{0}^{m} a_m \bar{R}^m \cdot \frac{n}{(n+1)+m} \right] d_n \bar{R}^n \tag{6-25}$$

and

$$\int \sum_{0}^{n} n^2 d_n \bar{R}^{n-1} \, d\bar{R} = \bar{R} \sum_{0}^{n} n d_n \bar{R}^{n-1} \tag{6-26}$$

Substituting equations (6-25), (6-26) into (6-24) yields

$$\overline{V_R' V_Z'} = -\frac{1}{R_{e,i}^{0.25}} \sum_{0}^{n} \left[\sum_{0}^{m} a_m \bar{R}^m \cdot \frac{n}{(n+1)+m} \right] d_n \bar{R}^n + \frac{2}{R_{e,o}} \sum_{0}^{n} n d_n \bar{R}^{n-1}$$

$$(m = 0, 1, 2, \ldots\ldots, n = 0, 1, 2, \ldots\ldots) \tag{6-27}$$

There are no mathematical difficulties to obtain the radial-axial component of the Reynolds shear stress.

6.3 Computation of Reynolds Shear Stress

6.3.1 General

A FORTRAN computer program was developed to perform the computation of Reynolds shear stress, which is based on the derived analytical solutions of the differential equations detailed in the previous section "Analytical Approach for Reynolds Shear Stress".

The inlet velocity of the air flow, V_{in}, the diameter of the air flow inlet, D_{in}, the diameter of the vortex chamber, D_o, and the kinematic viscosity of the air, ν, are input parameters; The coefficients of polynomials, a_n and b_n, which are determined from the velocity profiles are input parameters; Number of coefficient points and number of computation points which are determined by the computer program users are input parameters.

The output of the computational results includes the Reynolds shear stress in both the dimensionless form and the absolute value form. The computational results concerning the contributions from each item, such as the viscous effects, the kinetic energy and the inertia part, to the Reynolds shear stress can be presented upon request.

The detailed computer program listings and samples of typical output of computer calculation are attached as Appendix C.

6.3.2 Analysis of Computational Results

A plot of the computational results of the radial-tangential component of the Reynolds shear stress at the main section of the vortex chamber is shown in Figure 6.3.2.1. The computational results of the radial-tangential component of the Reynolds shear stress near the exit section inside the vortex chamber are plotted as shown in Figures 6.3.2.2 to 6.3.2.7.

It is observed that both the inlet Reynolds number and the contraction ratio, further referring to the swirl number, affect the Reynolds shear stress. The flow with the higher inlet Reynolds number will have higher Reynolds shear stress.

Among small contraction ratios ($R_e/R_o < 0.5$), the flow at relatively smaller contraction ratio will have larger value of the radial-tangential component of the Reynolds shear stress. Among large contraction ratios ($R_e/R_o \geq 0.5$), similarly, the flow at relatively smaller contraction ratio will still have larger value of the radial-tangential component of the Reynolds shear stress.

It is found that with the change of the contraction ratio, the acting direction of Reynolds shear stress will change, which is reflected by the changing of the numerical value from positive to negative. At small contraction ratios such as 0.25 and 0.30, the radial-tangential component of the Reynolds shear stresses shows a positive value. At large contraction ratios such as 0.58 and 0.75, it shows a negative value. At the contraction ratios of 0.40 and 0.50, it appears in the transition stage.

In general, the location of the maximum value of the radial-tangential component of the Reynolds shear stress will change corresponding to the contraction ratio. The smaller the value of the contraction ratio, the closer the location of the maximum value of the radial-tangential component of the Reynolds shear stress to the centre of the vortex chamber. Obviously, at the centre of the vortex chamber, the Reynolds shear stress is zero.

6.4 Experimental Approach for Reynolds Normal Stress

6.4.1 Tangential Component of Reynolds Normal Stress

The tangential component of the Reynolds normal stress is equivalent to the momentum transfer per unit area in the tangential direction through the plane normal to the tangential direction.

The distributions of the tangential component of the Reynolds normal stress at the main section of the vortex chamber are presented in Figures 6.4.1.1 to 6.4.1.7 based on the measurement results.

To eliminate the influence of the inlet condition such as the air flow rate, scaling formulas for the main section are found as follows:

For $R_e/R_o < 0.5$,

$$\bar{\tau}_{\theta\theta} = R_{e,i} \cdot \frac{\overline{V_\theta'^2}}{\overline{V}_{in}^2} \qquad (6\text{-}28)$$

For $0.5 \le R_e/R_o \le 0.75$

$$\bar{\tau}_{\theta\theta} = R_{e,i}^{0.6} \cdot \frac{\overline{V_\theta'^2}}{\overline{V}_{in}^2} \qquad (6\text{-}29)$$

The distributions of the scaled tangential component of the Reynolds normal stress at the main section based on the above equations are shown in Figures 6.4.1.8 to 6.4.1.13.

Near the exit section inside the vortex chamber, the distributions of the scaled tangential component of the Reynolds normal stress obtained from the experiments are presented in Figures 6.4.1.14 to 6.4.1.19.

Similarly, a scaling formula which can be applied for near the exit section and cover all contraction ratios is found as follows:

$$\bar{\tau}_{\theta\theta} = R_{e,i}^{0.3} \cdot \frac{\overline{V_\theta'^2}}{\overline{V}_{in}^2} \qquad (6\text{-}30)$$

The plots based on this equation are illustrated in Figures 6.4.1.20 to 6.4.1.25.

It is found that the inlet Reynolds number (or the inlet air flow rate) does not affect the locations of the maximum and the minimum values of the scaled tangential component of the Reynolds normal stress. For the small contraction ratios, the maximum value will appear at the centre of the vortex chamber. For the large contraction ratios, the maximum value will appear within the central core region. Only at the main section with a large contraction ratio, referring to a large swirl number, will the contraction ratio affect the maximum value location.

6.4.2 Radial Component of Reynolds Normal Stress

The radial component of the Reynolds normal stress is equivalent to the momentum transfer per unit area in the radial direction through the plane normal to the radial direction.

At the main section of the vortex chamber, as shown in Figure 6.4.2.1 and 6.4.2.2, the radial component of the Reynolds shear stress appears a higher level of the magnitude at a smaller contraction ratio and at a location closer to the exit.

Near the exit section inside the vortex chamber, the inlet Reynolds number does not affect the location of the maximum value of the radial component of the Reynolds shear stress as shown in Figures 6.4.2.3 to 6.4.2.8.. At a contraction ratio less than 0.5, the contraction ratio does not affect the maximum value location either. The maximum value appears at the centre of the vortex chamber for the contraction ratio less than 0.5 or within the central core region for the contraction ratio greater than 0.5.

6.5 Contribution of Viscosity

6.5.1 Contribution of Viscosity in Tangential Direction

The tangential component of the kinetic energy due to the fluctuating motion can be described by the following equation:

$$\frac{\partial}{\partial r}(\frac{1}{2}\overline{V_\theta'^2}) + \frac{2}{r}(\frac{1}{2}\overline{V_\theta'^2}) + \frac{2}{\overline{V}_r}\frac{\nu}{r^2}(\frac{1}{2}\overline{V_\theta'^2})$$
$$= \frac{\nu}{\overline{V}_r}(\overline{V_\theta'\frac{\partial^2 V_\theta'}{\partial r^2}} + \frac{1}{r}\overline{V_\theta'\frac{\partial V_\theta'}{\partial r}}) + \frac{\overline{V}_\theta}{\overline{V}_r}[\frac{\partial}{\partial r}(\overline{V_r'V_\theta'}) + \frac{2}{r}(\overline{V_r'V_\theta'})] -$$
$$- \frac{1}{\overline{V}_r}[\frac{1}{2}\overline{V_r'\frac{\partial}{\partial r}(V_\theta'^2)} + \frac{1}{r}\overline{V_r'V_\theta'^2}] \qquad (5\text{-}18)$$

In certain cases, the third order items in the above equation are so small when compared to other items that they could be neglected. The equation (5-18) can be simplified and rearranged as

$$\nu(\overline{V_\theta'\frac{\partial^2 V_\theta'}{\partial r^2}} + \frac{1}{r}\overline{V_\theta'\frac{\partial V_\theta'}{\partial r}})$$
$$= \overline{V}_r\frac{\partial}{\partial r}(\frac{1}{2}\overline{V_\theta'^2}) + \overline{V}_r\frac{2}{r}(\frac{1}{2}\overline{V_\theta'^2}) + \frac{2\nu}{r^2}(\frac{1}{2}\overline{V_\theta'^2}) - \overline{V}_\theta[\frac{\partial}{\partial r}(\overline{V_r'V_\theta'}) + \frac{2}{r}(\overline{V_r'V_\theta'})] \qquad (6\text{-}31)$$

The left-hand side of the equation represents the contributions of the viscous effects. The right-hand side of the equation contains the terms of the tangential component of the turbulence kinetic energy and the Reynolds shear stress to the radial-tangential component. The equation can be rearranged to approach a normalized form as follows:

$$\nu[(\frac{V_\theta'}{\overline{V}_{in}})\frac{\partial^2(V_\theta'/\overline{V}_{in})}{\partial(r/R_o)^2}(\frac{\overline{V}_{in}}{R_o})^2 + \frac{1}{r/R_o}(\frac{V_\theta'}{\overline{V}_{in}})\frac{\partial(V_\theta'/\overline{V}_{in})}{\partial(r/R_o)}(\frac{\overline{V}_{in}}{R_o})^2]$$
$$= (\frac{\overline{V}_r}{\overline{V}_{in}}R_{e,i}^{0.25})(\frac{\overline{V}_{in}}{R_{e,i}^{0.25}})\frac{\partial}{\partial(r/R_o)}(\frac{\frac{1}{2}\overline{V_\theta'^2}}{\frac{1}{2}\overline{V}_{in}^2}R_{e,i}^{0.3})(\frac{\frac{1}{2}\overline{V}_{in}^2}{R_{e,i}^{0.3}R_o}) +$$
$$+ (\frac{\overline{V}_r}{\overline{V}_{in}}R_{e,i}^{0.25})(\frac{\overline{V}_{in}}{R_{e,i}^{0.25}})\frac{2}{r/R_o}(\frac{\frac{1}{2}\overline{V_\theta'^2}}{\frac{1}{2}\overline{V}_{in}^2}R_{e,i}^{0.3})(\frac{\frac{1}{2}\overline{V}_{in}^2}{R_{e,i}^{0.3}R_o}) +$$

$$+\frac{2\nu}{(r/R_o)^2}\left(\frac{\frac{1}{2}\overline{V_\theta'^2}}{\frac{1}{2}\overline{V}_{in}^2}R_{e,i}^{0.3}\right)\left(\frac{\frac{1}{2}\overline{V}_{in}^2}{R_{e,i}^{0.3}R_o^2}\right) -$$

$$-\left(\frac{\overline{V}_\theta}{\overline{V}_{in}}\right)(\overline{V}_{in})\left[\frac{\partial}{\partial(r/R_o)}\left(\frac{\overline{V_r'V_\theta'}}{\overline{V}_{in}^2}\right)\left(\frac{\overline{V}_{in}^2}{R_o}\right) + \frac{2}{r/R_o}\left(\frac{\overline{V_r'V_\theta'}}{\overline{V}_{in}^2}\right)\left(\frac{\overline{V}_{in}^2}{R_o}\right)\right] \qquad (6\text{-}32)$$

Let

$$V_T' = V_\theta'/\overline{V}_{in}$$

$$V_R' = V_r'/\overline{V}_{in}$$

$$V_T'^2 = V_\theta'^2/\overline{V}_{in}^2$$

$$V_R'V_T'^2 = V_r'V_\theta'^2/\overline{V}_{in}^3$$

$$K_{t,s} = \frac{\frac{1}{2}\overline{V_\theta'^2}}{\frac{1}{2}\overline{V}_{in}^2}R_{e,i}^{0.3} \qquad (6\text{-}33)$$

Substituting equations (6-33) into (6-32) and rearranging the equation yield

$$\frac{2}{R_{e,o}}\left(\overline{V_T'\frac{\partial^2 V_T'}{\partial \overline{R}^2}} + \frac{1}{\overline{R}}\overline{V_T'\frac{\partial V_T'}{\partial \overline{R}}}\right)$$

$$= \frac{1}{2R_{e,i}^{0.55}}\overline{V}_R\frac{\partial K_{t,s}}{\partial \overline{R}} + \frac{1}{R_{e,i}^{0.55}}\overline{V}_R\frac{K_{t,s}}{\overline{R}} + \frac{2}{R_{e,i}^{0.3}R_{e,o}}\frac{K_{t,s}}{\overline{R}^2} -$$

$$-\overline{V}_T\left[\frac{\partial}{\partial \overline{R}}(\overline{V_R'V_T'}) + \frac{2}{\overline{R}}(\overline{V_R'V_T'})\right] \qquad (6\text{-}34)$$

It is found that from the experimental results the scaled tangential component of the turbulence kinetic energy K_t' is a function of normalized radius $\overline{R}$, and can be expressed by a polynomial. That is,

$$K_{t,s} = f_c(\overline{R})$$

$$= \sum_0^n c_n\overline{R}^n \qquad (n = 0, 1, 2, ...) \qquad (6\text{-}35)$$

Substituting equations (6-6), (6-7), (6-9), (6-11), and (6-35) into (6-34) and rearranging the equation yield

$$\Phi_t = \frac{1}{2R_{e,i}^{0.55}} \cdot \sum_0^n a_n \bar{R}^n \cdot \sum_0^n (n+2) c_n \bar{R}^{n-1} + \frac{2}{R_{e,i}^{0.3} \cdot R_{e,o}} \cdot \sum_0^n c_n \bar{R}^{n-2} +$$
$$+ \sum_0^n b_n \bar{R}^n \cdot [\frac{1}{R_{e,i}^{0.25}} \sum_0^n a_n \bar{R}^n \cdot \sum_0^n (n+1) b_n \bar{R}^{n-1} - \frac{2}{R_{e,o}} \cdot \sum_0^n (n-1)(n+1) b_n \bar{R}^{n-2}] \tag{6-36}$$

where

Φ_t = viscous effects in the tangential direction

$$\Phi_t = \frac{2}{R_{e,o}} (\overline{V_T' \frac{\partial^2 V_T'}{\partial \bar{R}^2}} + \frac{1}{\bar{R}} \cdot \overline{V_T' \frac{\partial V_T'}{\partial \bar{R}}}) \tag{6-37}$$

The contribution of the viscosity in the tangential direction can be determined as the radial and tangential mean velocity profiles and the tangential component of the turbulence kinetic energy profile are available from the experiments.

6.5.2 Contribution of Viscosity in Axial Direction

The axial component of the kinetic energy due to the fluctuating motion can be described by the following equation:

$$\frac{\partial}{\partial r}(\frac{1}{2}\overline{V_z'^2}) = \frac{\nu}{\bar{V}_r}(\overline{V_z' \frac{\partial^2 V_z'}{\partial r^2}} + \frac{1}{r}\overline{V_z' \frac{\partial V_z'}{\partial r}}) + \frac{\bar{V}_z}{\bar{V}_r}[\frac{\partial}{\partial r}(\overline{V_r' V_z'}) + \frac{1}{r}(\overline{V_r' V_z'})]$$
$$+ \frac{1}{2\bar{V}_r} \overline{V_r' \frac{\partial}{\partial r}(V_z'^2)} \tag{5-19}$$

If the third order items in the above equation are much smaller than other items and can be neglected. The equation (5-19) can be simplified and rearranged as

$$\nu\left(\overline{V_z'\frac{\partial^2 V_z'}{\partial r^2}} + \frac{1}{r}\overline{V_z'\frac{\partial V_z'}{\partial r}}\right) = \overline{V}_r\frac{\partial}{\partial r}\left(\frac{1}{2}\overline{V_z'^2}\right) - \overline{V}_z\left[\frac{\partial}{\partial r}\left(\overline{V_r'V_z'}\right) + \frac{1}{r}\left(\overline{V_r'V_z'}\right)\right] \tag{6-38}$$

The left-hand side of the equation represents the contributions of the viscous effects. The right-hand side of the equation contains the terms of the axial component of the turbulence kinetic energy and the Reynolds shear stress to the radial-axial component. The equation can be rearranged to approach a normalized form as follows:

$$\begin{aligned}
&\nu\left[\left(\frac{V_z'}{\overline{V}_{in}}\right)\frac{\partial^2(V_z'/\overline{V}_{in})}{\partial(r/R_o)^2}\left(\frac{\overline{V}_{in}}{R_o}\right)^2 + \frac{1}{r/R_o}\overline{\left(\frac{V_z'}{\overline{V}_{in}}\right)\frac{\partial(V_z'/\overline{V}_{in})}{\partial(r/R_o)}}\left(\frac{\overline{V}_{in}}{R_o}\right)^2\right] \\
&= \left(\frac{\overline{V}_r}{\overline{V}_{in}}R_{e,i}^{0.25}\right)\left(\frac{\overline{V}_{in}}{R_{e,i}^{0.25}}\right)\frac{\partial}{\partial(r/R_o)}\left(\frac{\frac{1}{2}\overline{V_z'^2}}{\frac{1}{2}\overline{V}_{in}^2}\right)\left(\frac{\frac{1}{2}\overline{V}_{in}^2}{R_o}\right) - \\
&- \left(\frac{\overline{V}_z}{\overline{V}_{in}}\right)(\overline{V}_{in})\left[\frac{\partial}{\partial(r/R_o)}\left(\frac{\overline{V_r'V_z'}}{\overline{V}_{in}^2}\right)\left(\frac{\overline{V}_{in}^2}{R_o}\right) + \frac{1}{r/R_o}\left(\frac{\overline{V_r'V_z'}}{\overline{V}_{in}^2}\right)\left(\frac{\overline{V}_{in}^2}{R_o}\right)\right]
\end{aligned} \tag{6-39}$$

Let

$$V_Z' = V_z'/\overline{V}_{in}$$

$$V_Z'^2 = V_z'^2/\overline{V}_{in}^2$$

$$K_{z,s} = \frac{\frac{1}{2}\overline{V_z'^2}}{\frac{1}{2}\overline{V}_{in}^2} \tag{6-40}$$

Substituting equations (6-40) into (6-39) and rearranging the equation yield

$$\begin{aligned}
&\frac{2}{R_{e,o}}\left(\overline{V_Z'\frac{\partial^2 V_Z'}{\partial \bar{R}^2}} + \frac{1}{\bar{R}}\overline{V_Z'\frac{\partial V_Z'}{\partial \bar{R}}}\right) \\
&= \frac{1}{2R_{e,i}^{0.25}}\overline{V}_R\frac{\partial K_{z,s}}{\partial \bar{R}} - \overline{V}_Z\left[\frac{\partial}{\partial \bar{R}}\left(\overline{V_R'V_Z'}\right) + \frac{1}{\bar{R}}\left(\overline{V_R'V_Z'}\right)\right]
\end{aligned} \tag{6-41}$$

It is found that from the experimental results the scaled axial component of the turbulence kinetic energy K_z' is a function of normalized radius $\bar{R}$, and can be expressed by a polynomial. That is,

$$K_{z,s} = f_e(\bar{R})$$

$$= \sum_0^n e_n \bar{R}^n \qquad (n = 0, 1, 2, ...) \qquad (6\text{-}42)$$

Substituting equations (6-6), (6-19), (6-21), (6-23) and (6-42) into (6-41) yields

$$\Phi_z = \frac{1}{2R_{e,i}^{0.25}} \sum_0^n a_n \bar{R}^n \cdot \sum_0^n n e_n \bar{R}^{n-1} +$$
$$+ \sum_0^n d_n \bar{R}^n \left(\frac{1}{R_{e,i}^{0.25}} \sum_0^n a_n \bar{R}^n \cdot \sum_0^n n d_n \bar{R}^{n-1} - \frac{2}{R_{e,o}} \sum_0^n n^2 d_n \bar{R}^{n-2} \right) \qquad (6\text{-}43)$$

where

Φ_z = viscous effects in the axial direction

$$\Phi_z = \frac{2}{R_{e,o}} \left(\overline{V_Z' \frac{\partial^2 V_Z'}{\partial \bar{R}^2}} + \frac{1}{\bar{R}} \overline{V_Z' \frac{\partial V_Z'}{\partial \bar{R}}} \right) \qquad (6\text{-}44)$$

The contribution of the viscosity in the axial direction can be determined as the radial and axial mean velocity profiles and the axial component of the turbulence kinetic energy profile are available from the experiments.

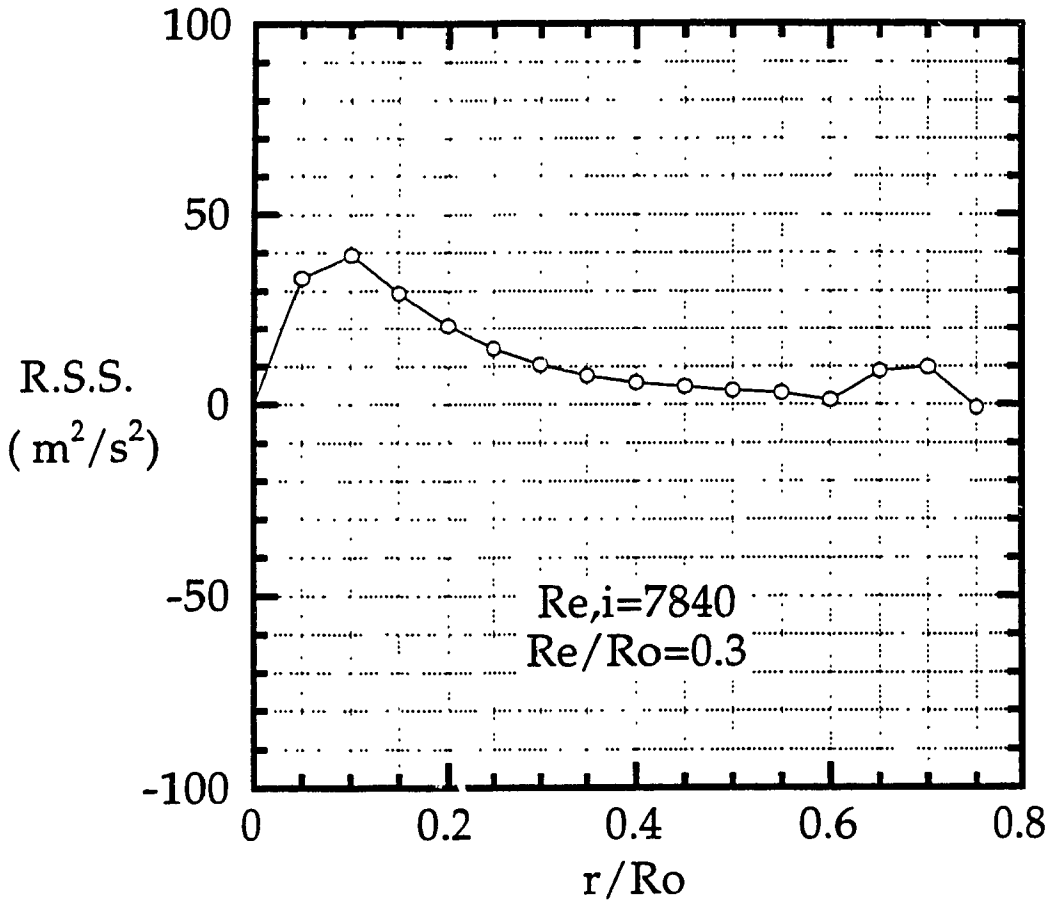

Figure 6.3.2.1 Computational Reynolds Radial-Tangential Shear Stress at Main Section

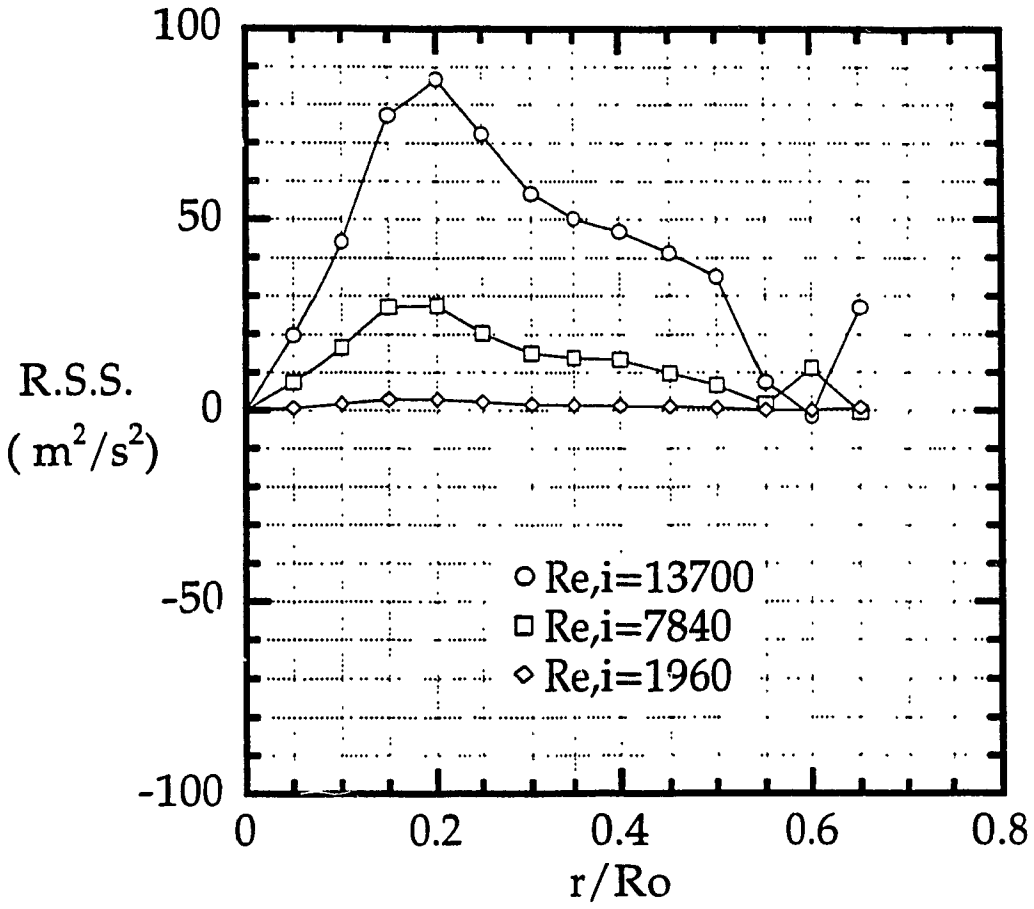

Figure 6.3.2.2 Computational Reynolds Radial-Tangential Shear Stress near Exit Section (Re/Ro = 0.25)

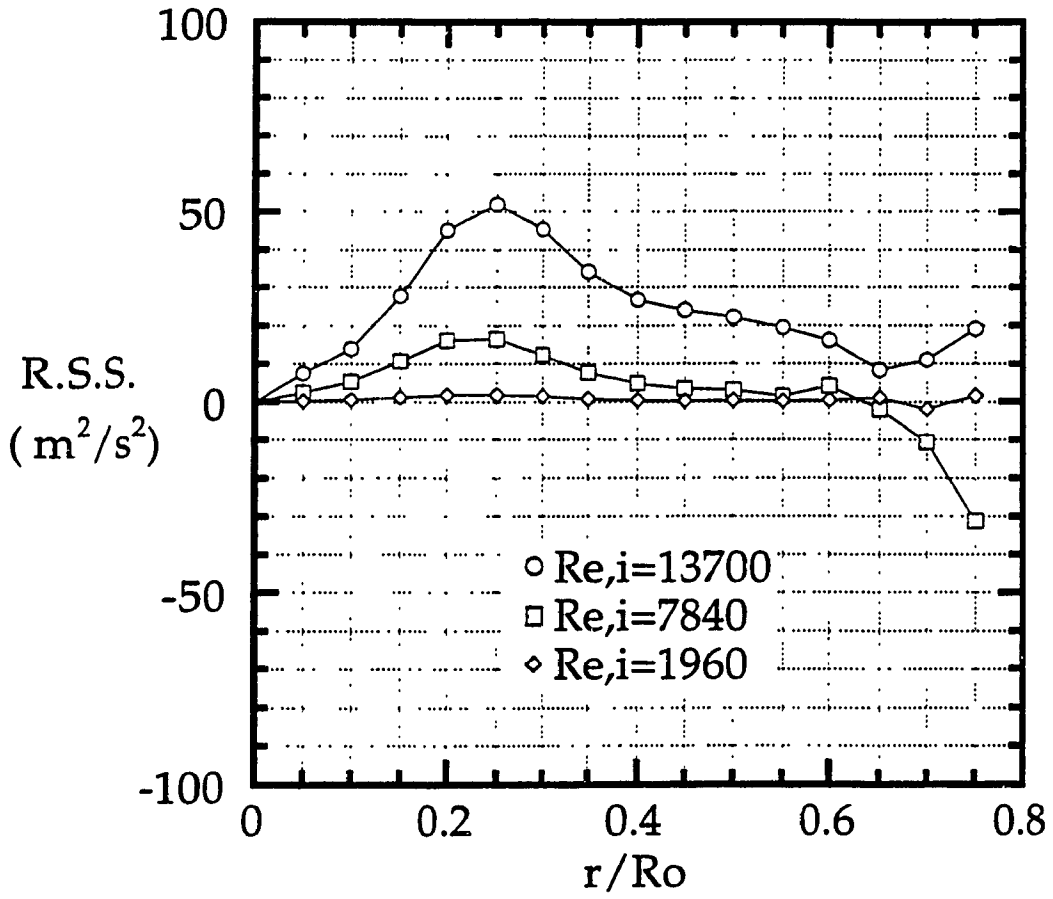

Figure 6.3.2.3 Computational Reynolds Radial-Tangential Shear Stress near Exit Section (Re/Ro = 0.30)

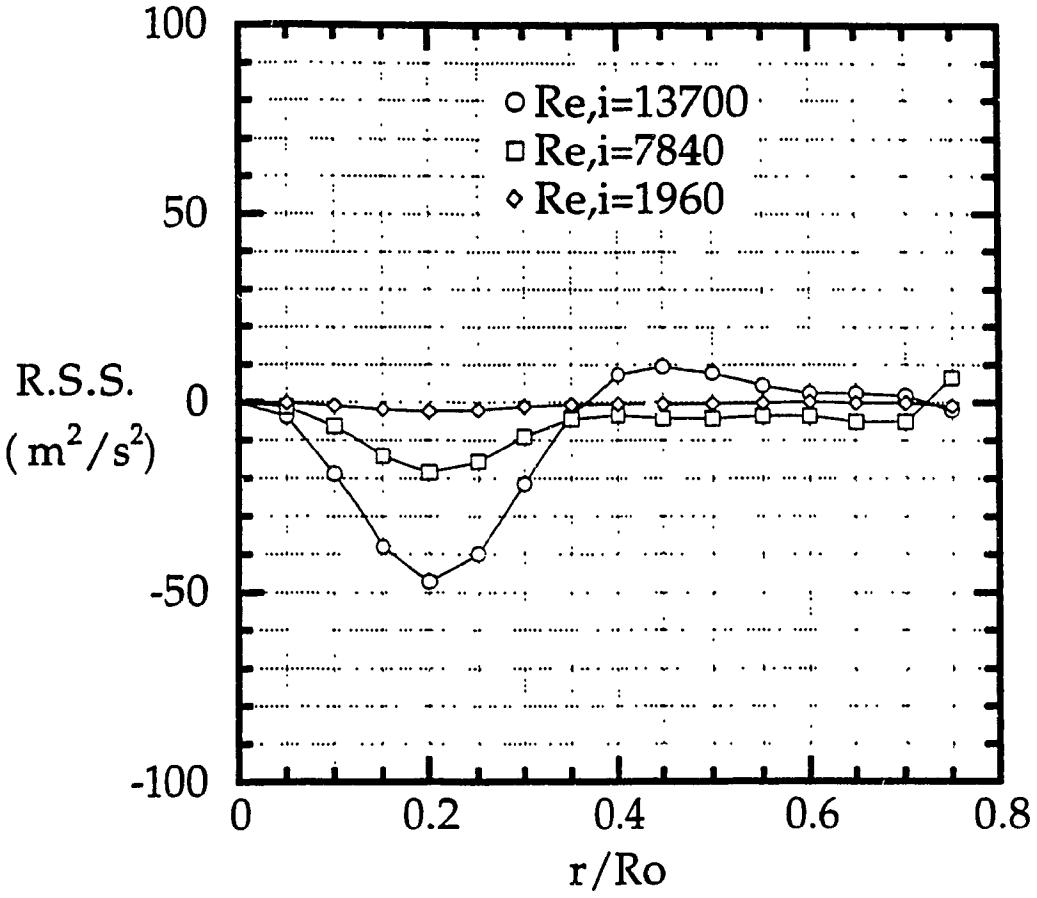

Figure 6.3.2.4 Computational Reynolds Radial-Tangential Shear Stress near Exit Section (Re/Ro = 0.40)

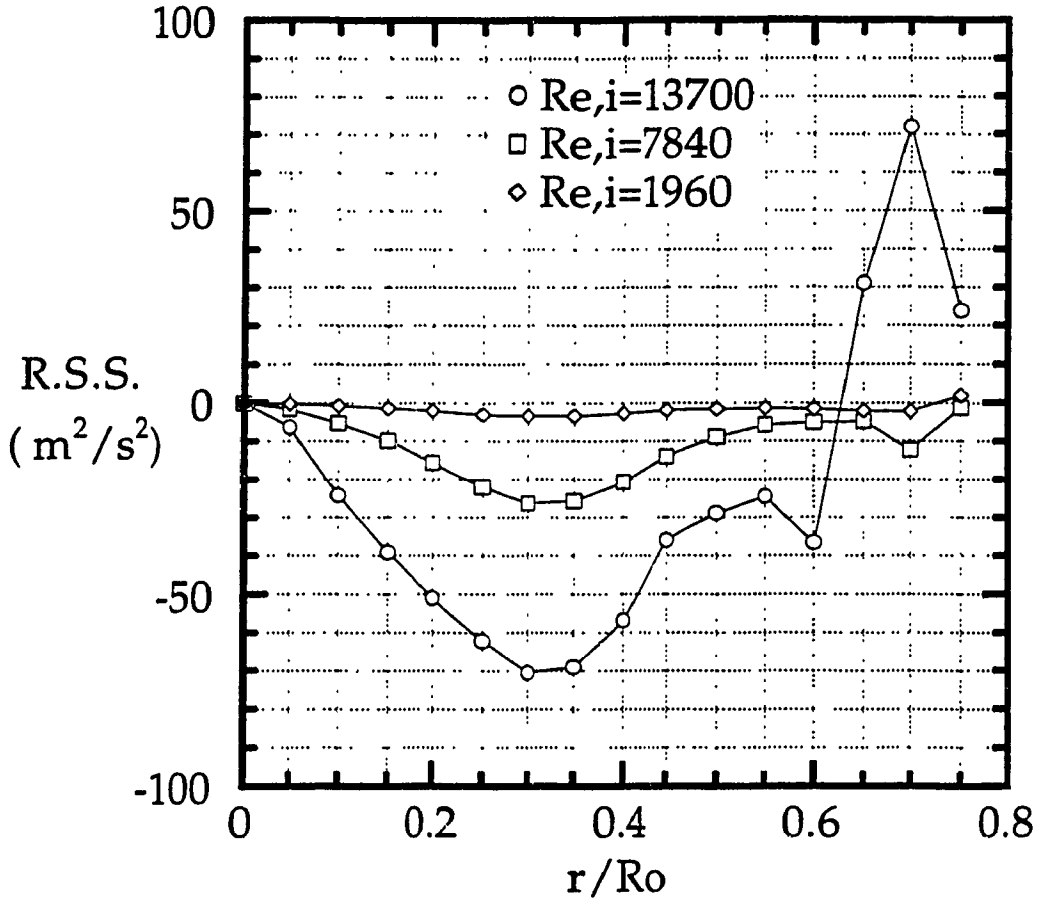

Figure 6.3.2.5 Computational Reynolds Radial-Tangential Shear Stress near Exit Section (Re/Ro = 0.50)

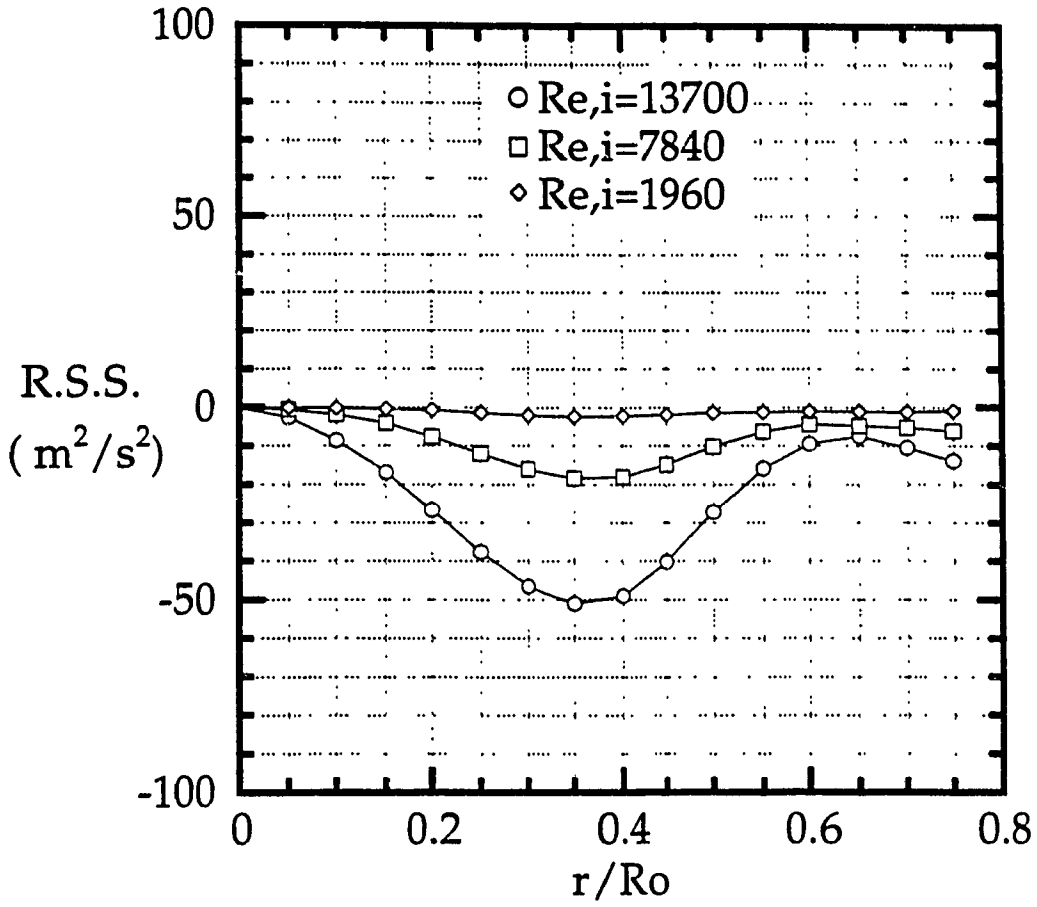

Figure 6.3.2.6 Computational Reynolds Radial-Tangential Shear Stress near Exit Section (Re/Ro = 0.58)

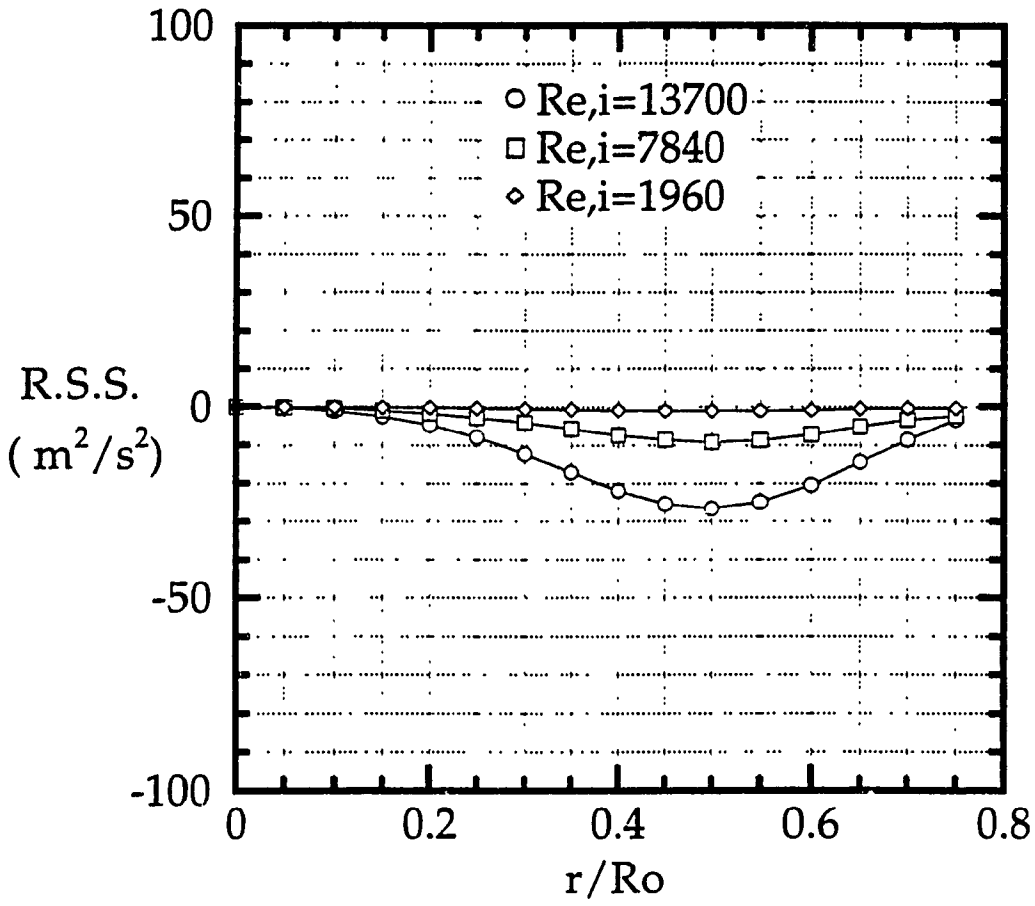

Figure 6.3.2.7 Computational Reynolds Radial-Tangential Shear Stress near Exit Section (Re/Ro = 0.75)

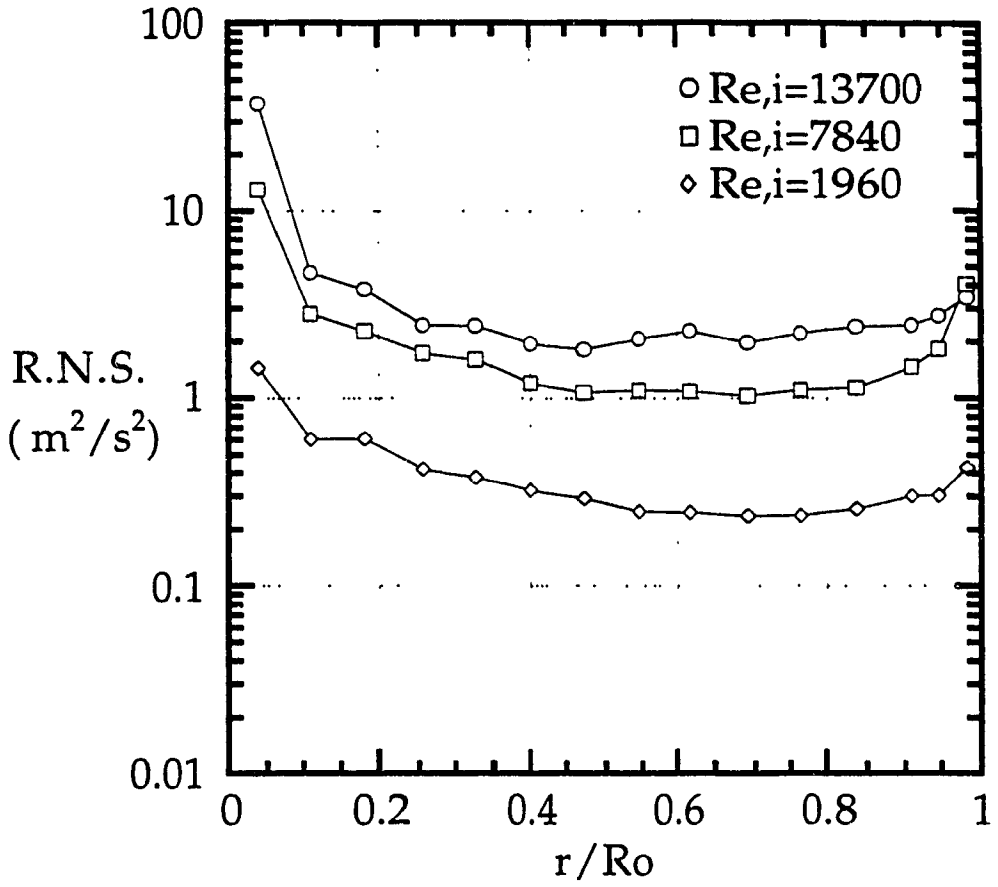

Figure 6.4.1.1 Experimental Tangential Component of Reynolds Normal Stress at Main Section (Re/Ro = 0.25)

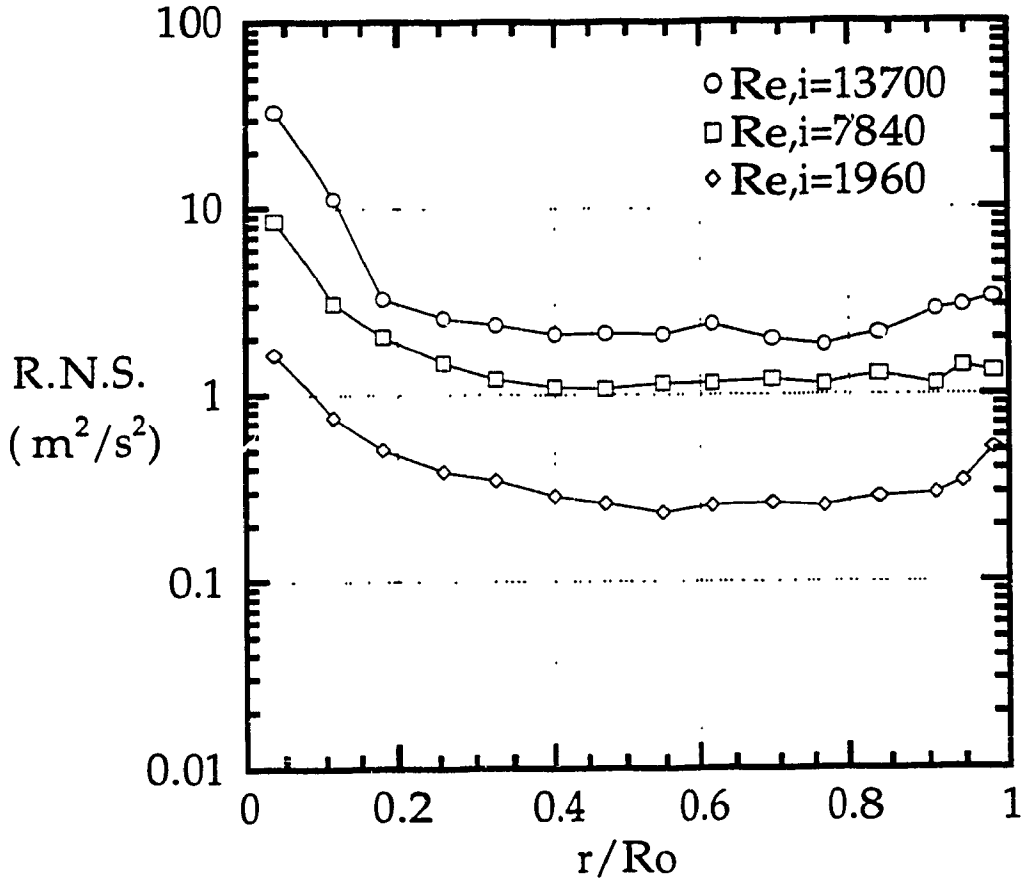

Figure 6.4.1.2 Experimental Tangential Component of Reynolds Normal Stress at Main Section (Re/Ro = 0.30)

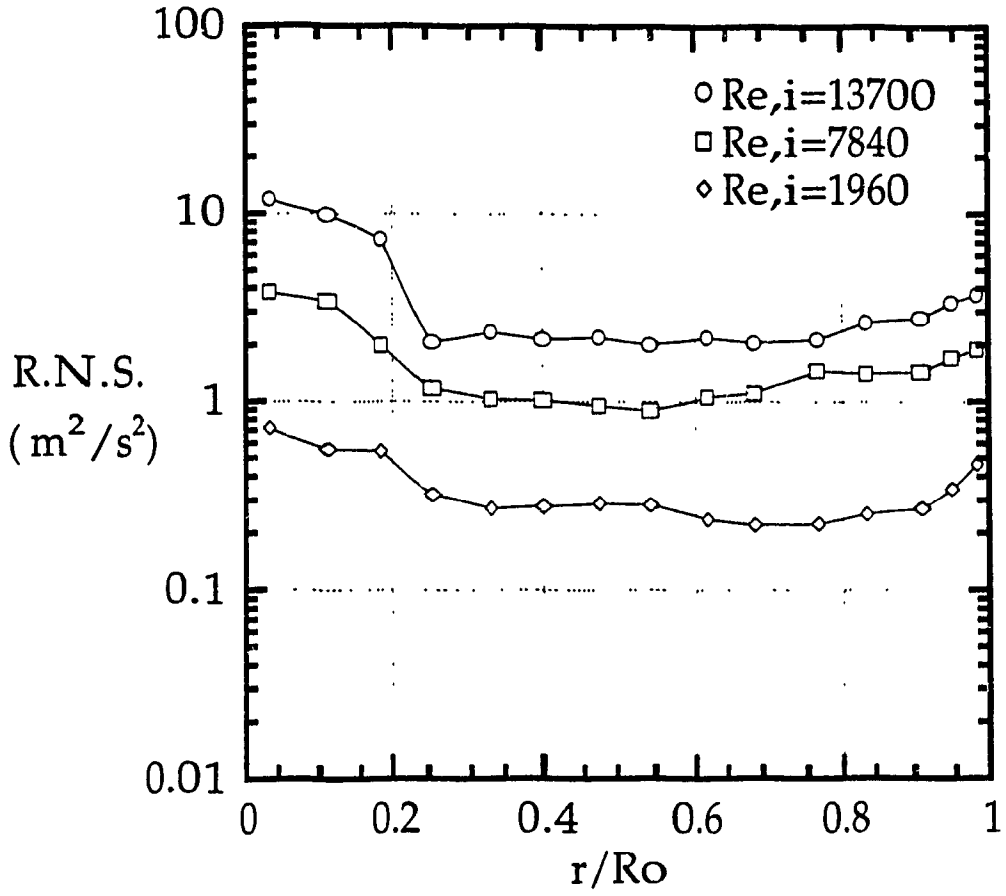

Figure 6.4.1.3 Experimental Tangential Component of Reynolds Normal Stress at Main Section (Re/Ro = 0.40)

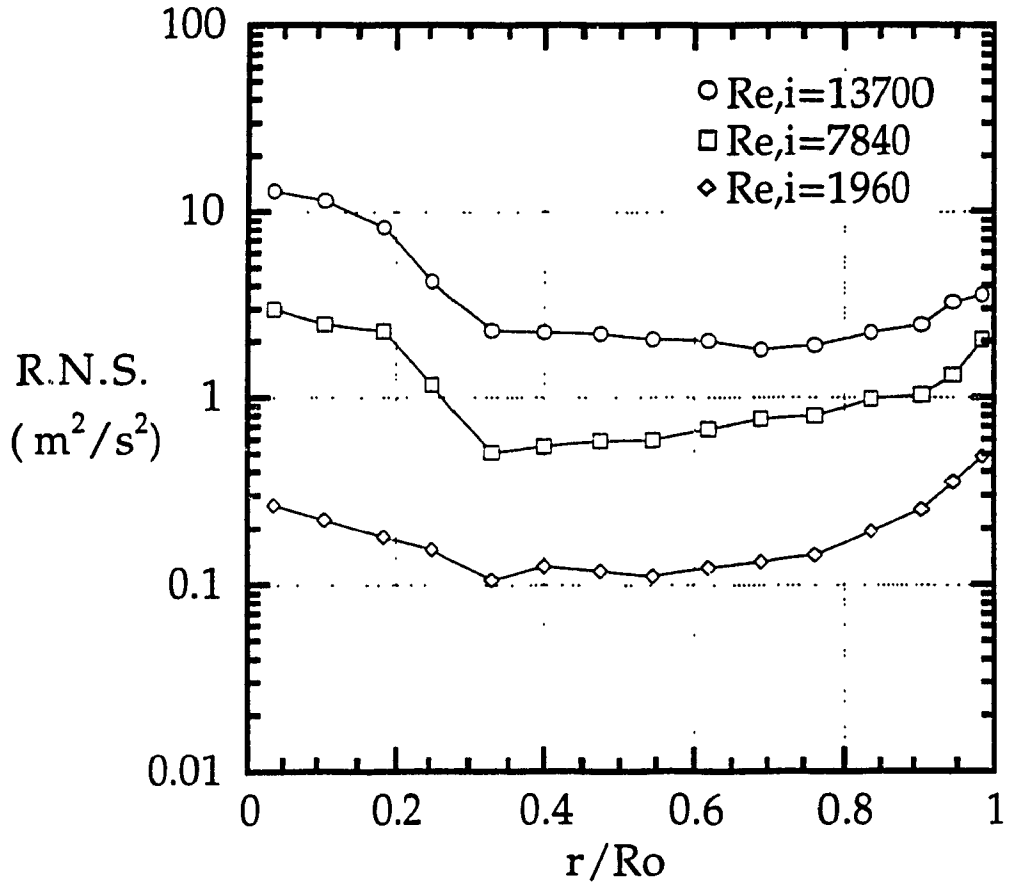

Figure 6.4.1.4 Experimental Tangential Component of Reynolds Normal Stress at Main Section (Re/Ro = 0.50)

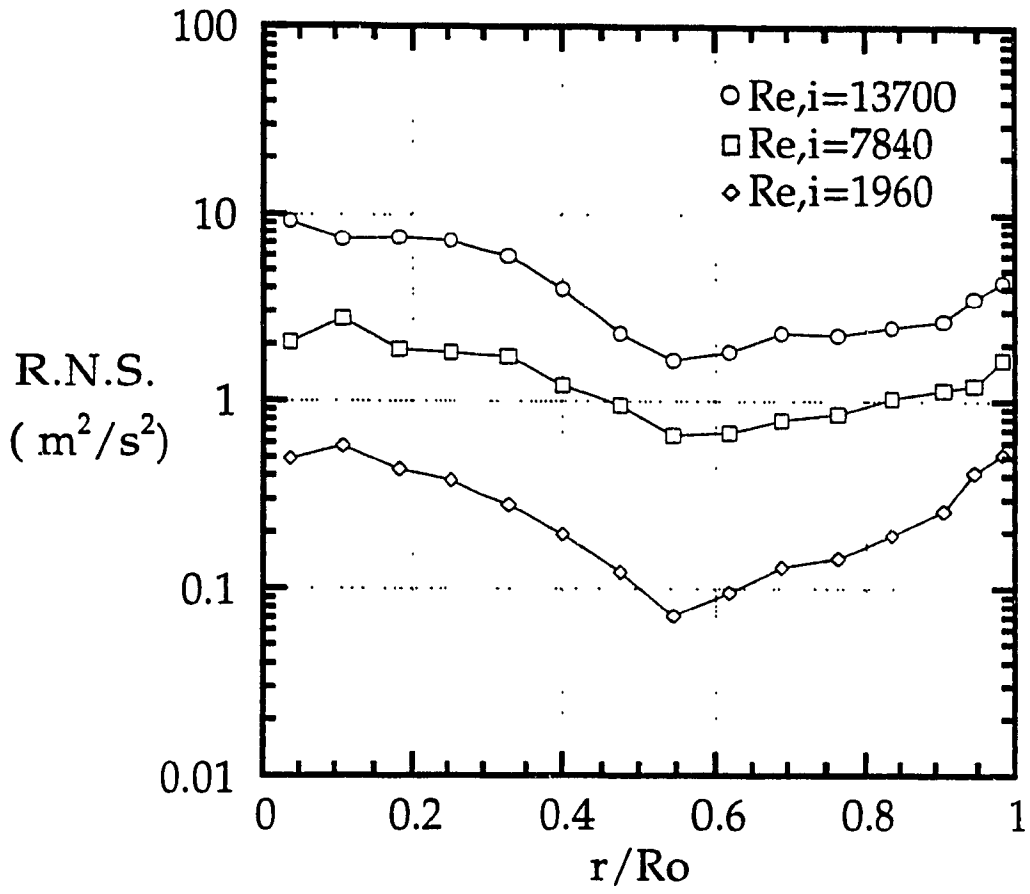

Figure 6.4.1.5 Experimental Tangential Component of Reynolds Normal Stress at Main Section (Re/Ro = 0.58)

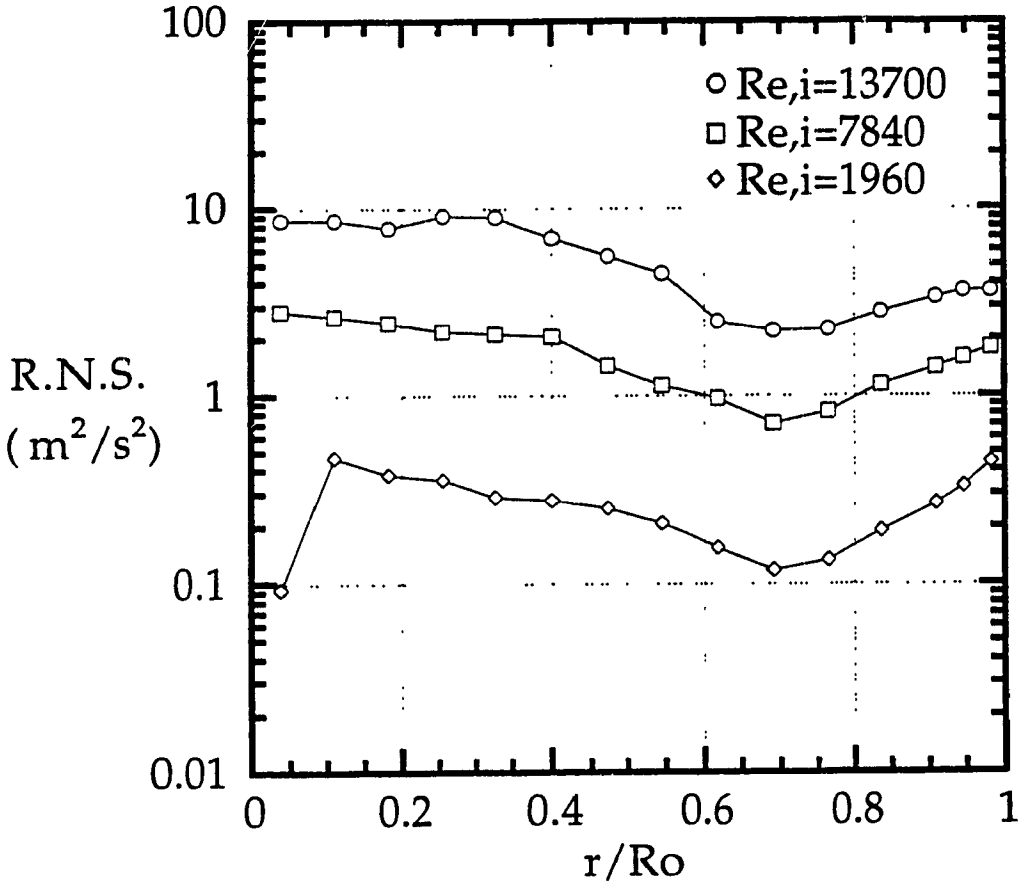

Figure 6.4.1.6 Experimental Tangential Component of Reynolds Normal Stress at Main Section (Re/Ro = 0.75)

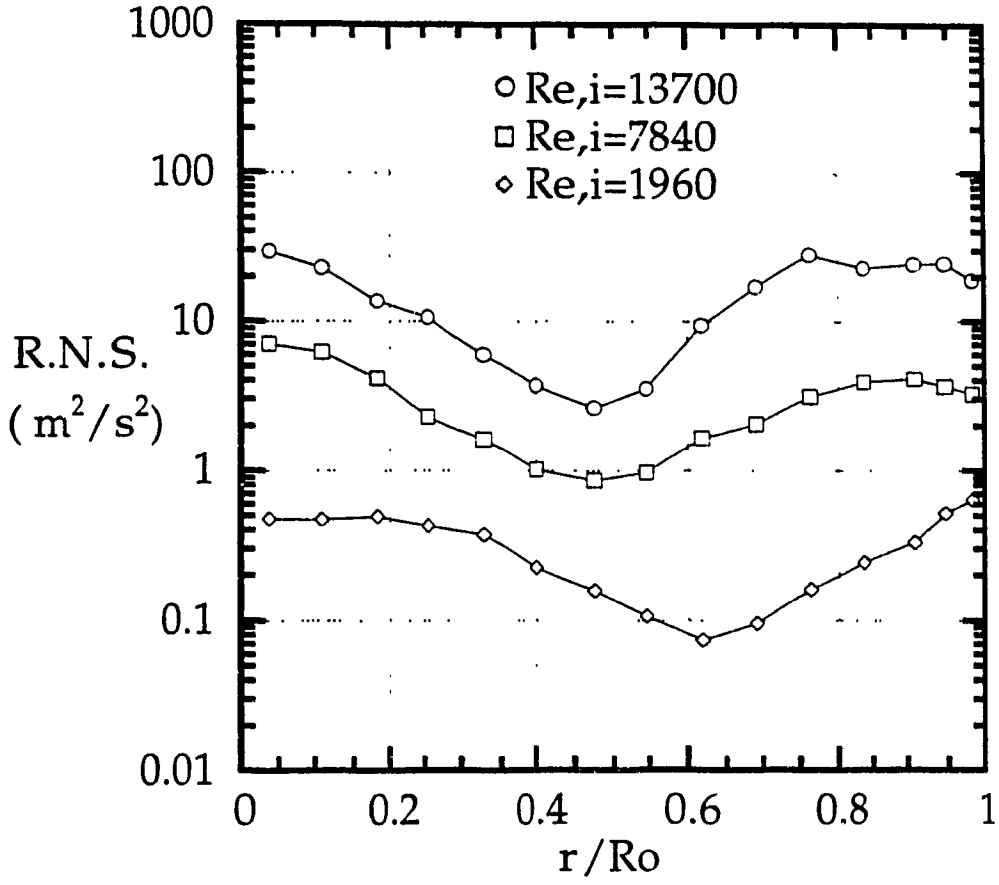

Figure 6.4.1.7 Experimental Tangential Component of Reynolds Normal Stress at Main Section (Re/Ro = 1.0)

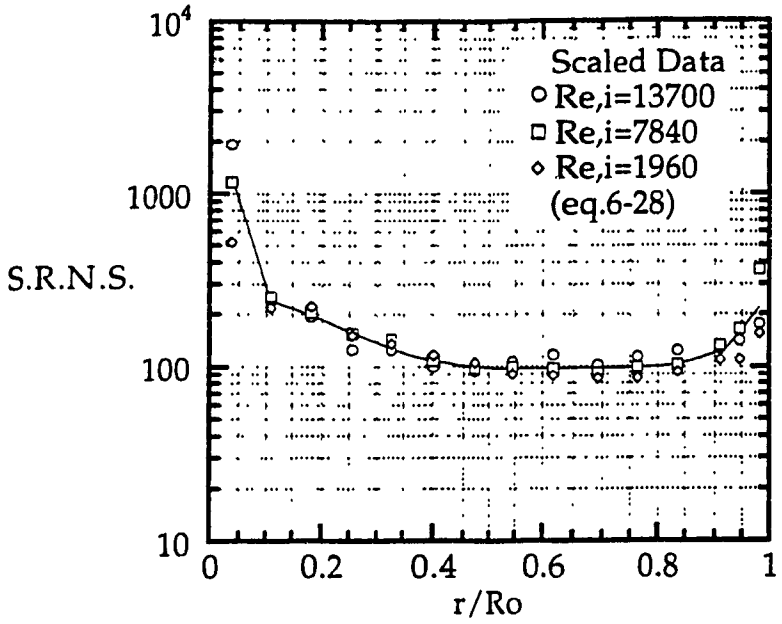

Figure 6.4 1.8 Scaled Tangential Component of Reynolds Normal Stress at Main Section at Re/Ro = 0.25 (line - average value)

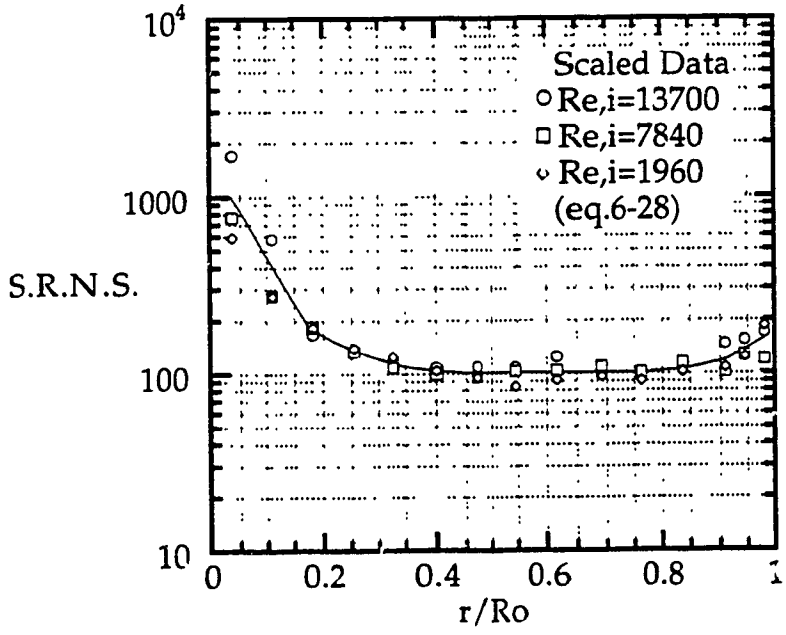

Figure 6.4.1.9 Scaled Tangential Component of Reynolds Normal Stress at Main Section at Re/Ro = 0.30 (line - average value)

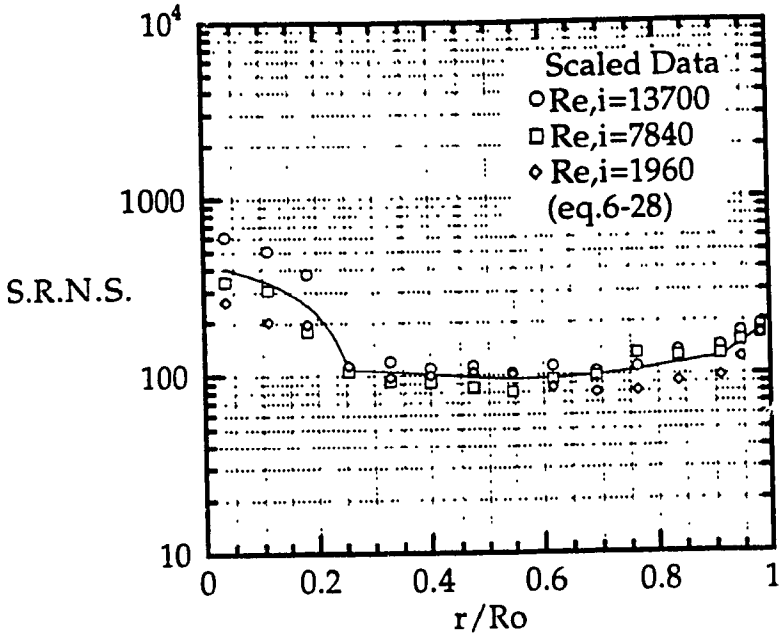

Figure 6.4.1.10 Scaled Tangential Component of Reynolds Normal Stress at Main Section at Re/Ro = 0.40 (line - average value)

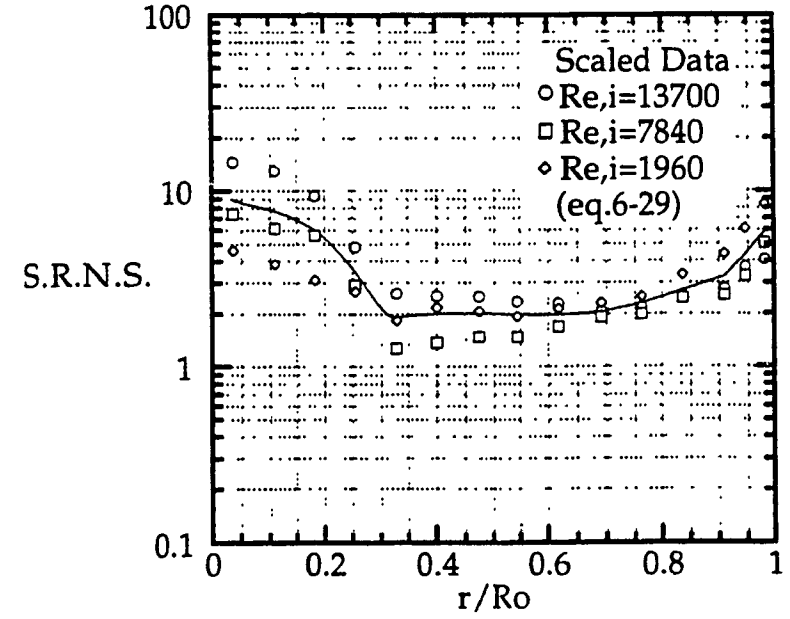

Figure 6.4.1.11 Scaled Tangential Component of Reynolds Normal Stress at Main Section at Re/Ro = 0.50 (line - average value)

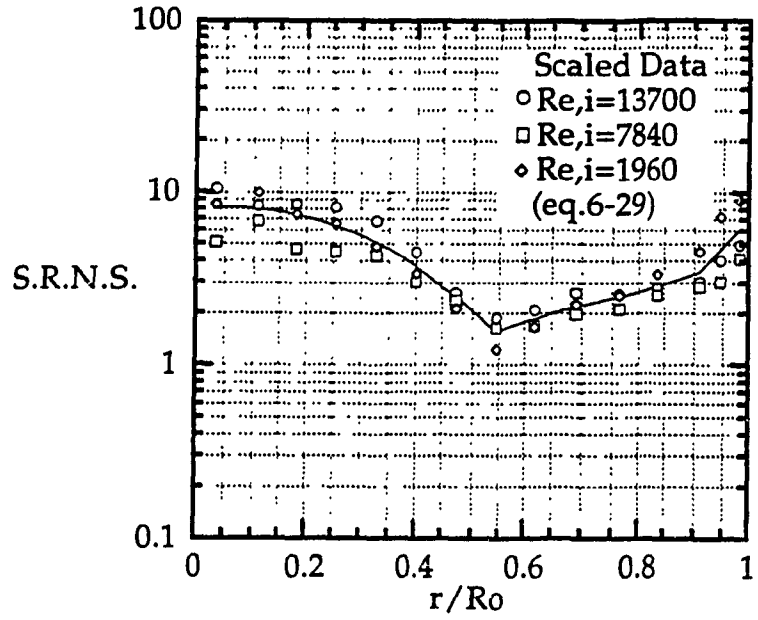

Figure 6.4.1.12 Scaled Tangential Component of Reynolds Normal Stress at Main Section at Re/Ro = 0.58 (line - average value)

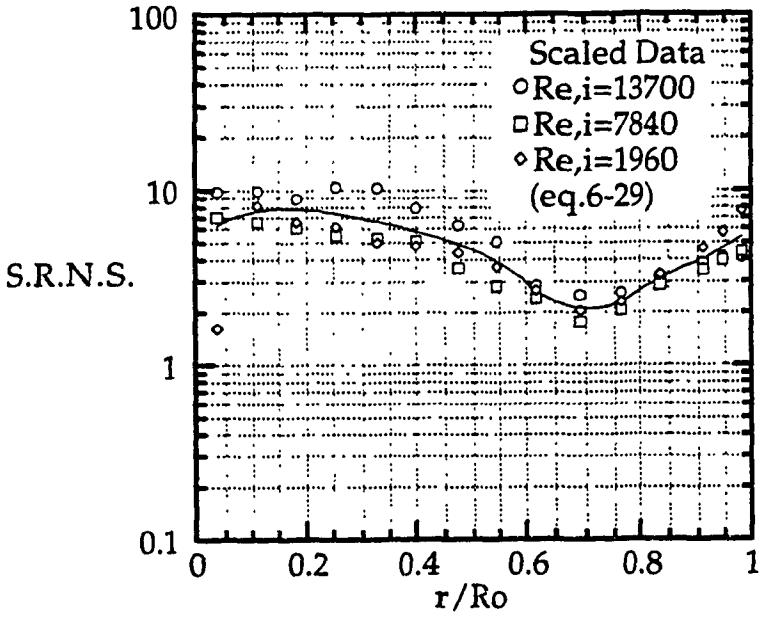

Figure 6.4.1.13 Scaled Tangential Component of Reynolds Normal Stress at Main Section at Re/Ro = 0.75 (line - average value)

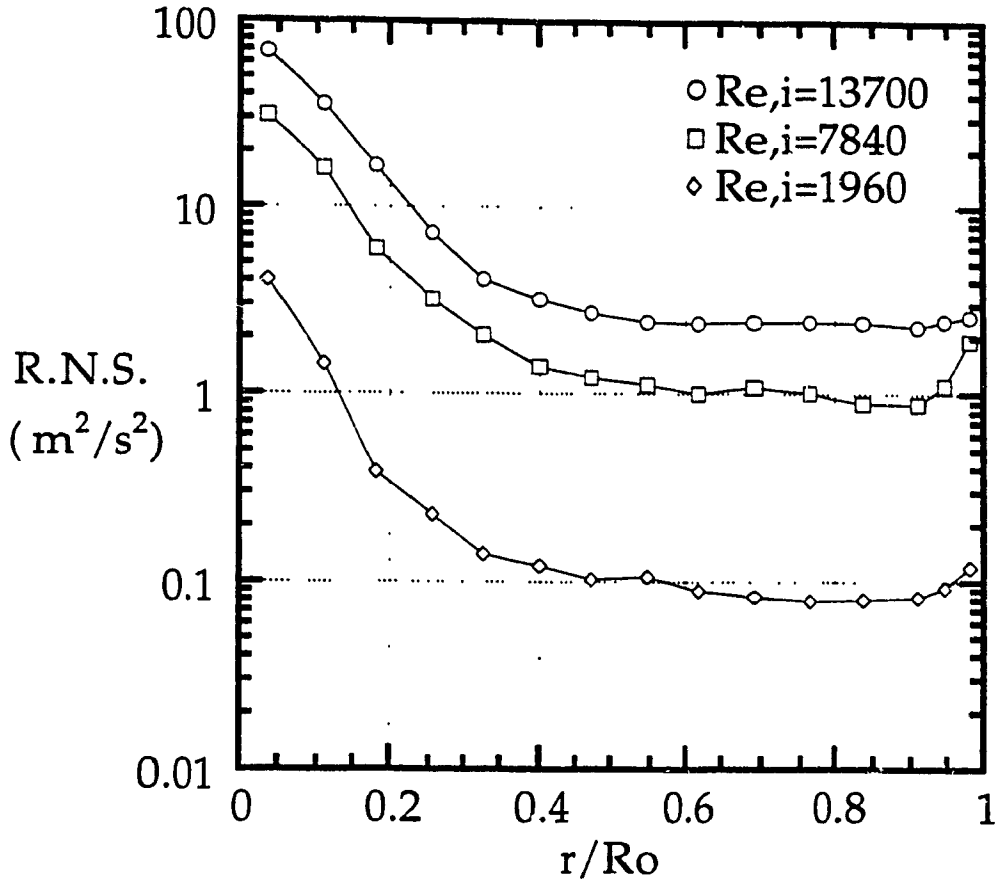

Figure 6.4.1.14 Experimental Tangential Component of Reynolds Normal Stress near Exit Section (Re/Ro = 0.25)

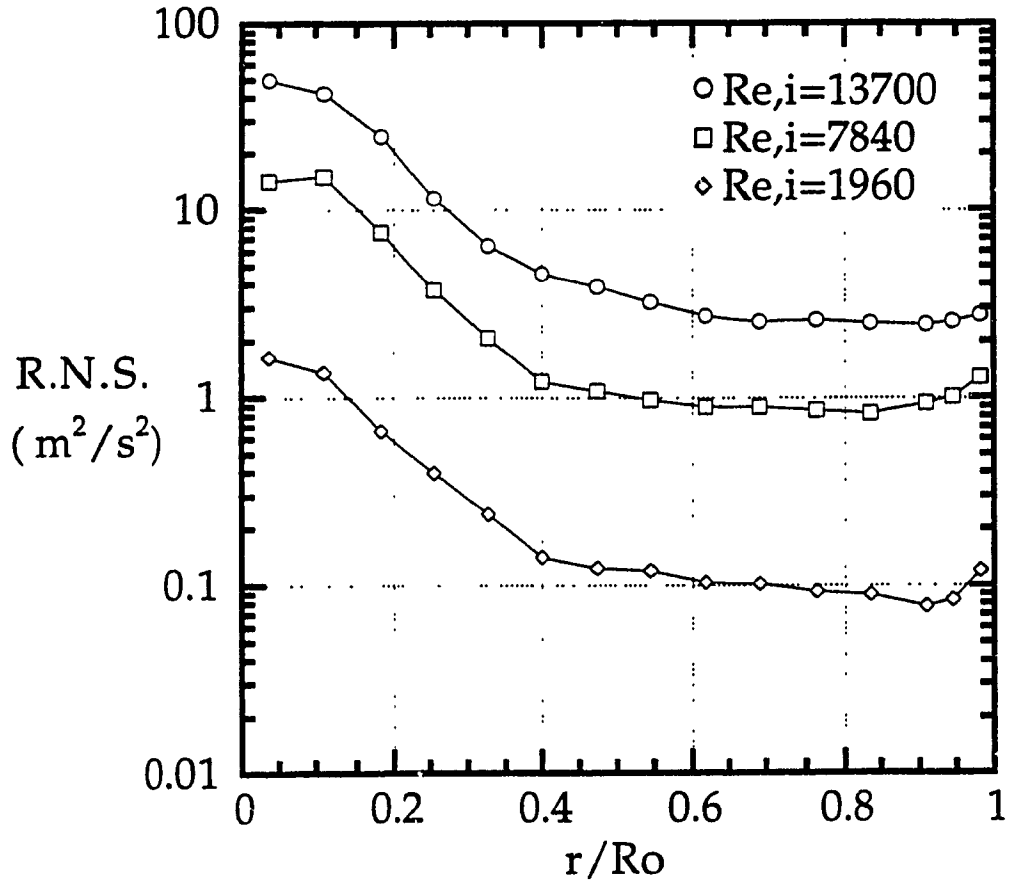

Figure 6.4.1.15 Experimental Tangential Component of Reynolds Normal Stress near Exit Section (Re/Ro = 0.30)

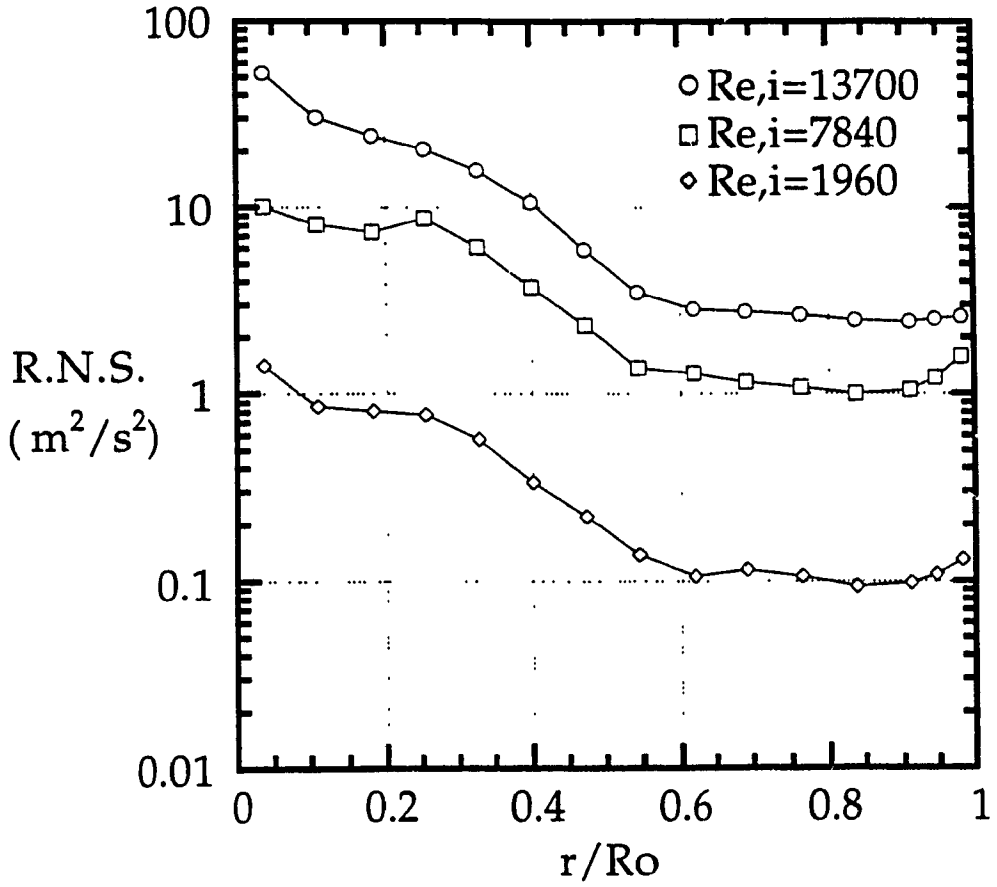

Figure 6.4.1.16 Experimental Tangential Component of Reynolds Normal Stress near Exit Section (Re/Ro = 0.40)

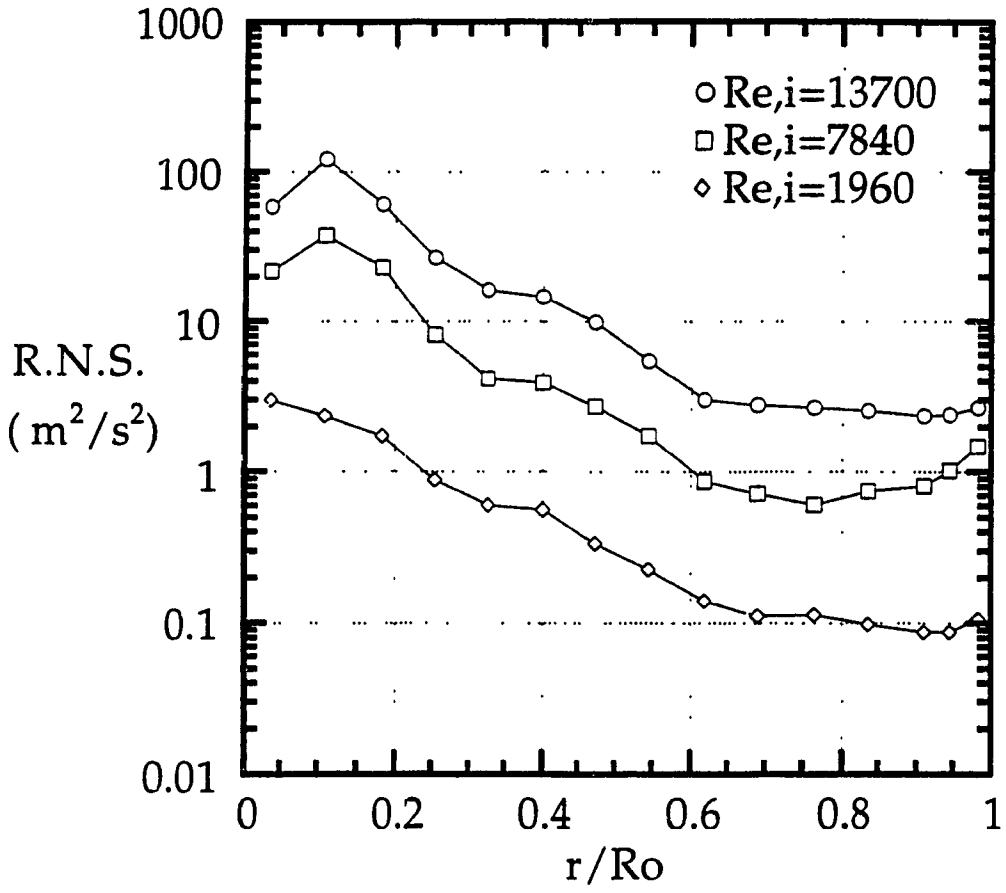

Figure 6.4.1.17 Experimental Tangential Component of Reynolds Normal Stress near Exit Section (Re/Ro = 0.50)

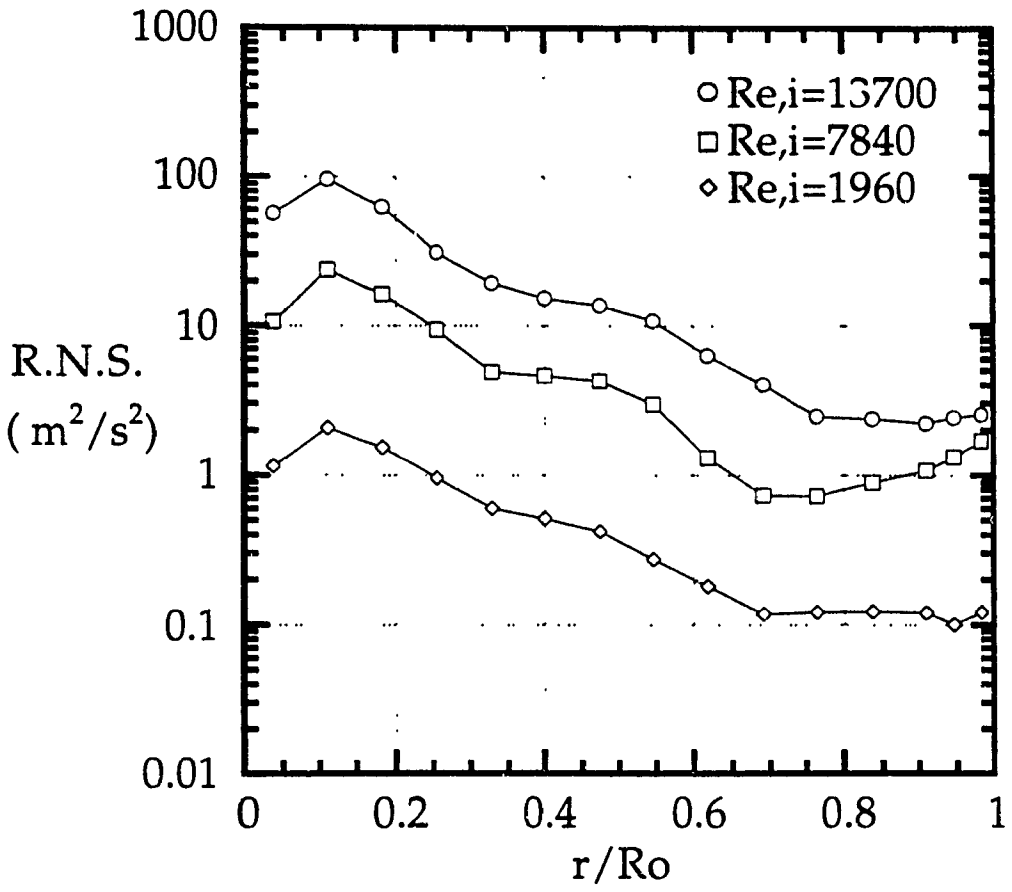

Figure 6.4.1.18 Experimental Tangential Component of Reynolds Normal Stress near Exit Section (Re/Ro = 0.58)

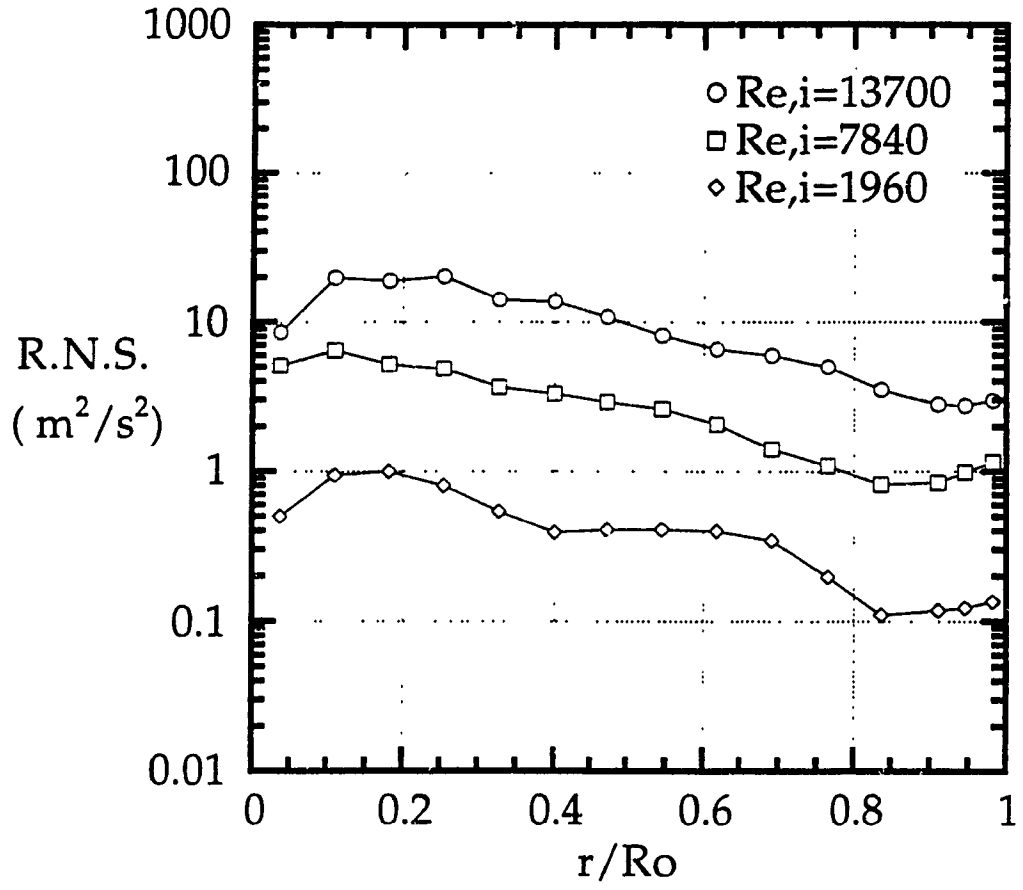

Figure 6.4.1.19 Experimental Tangential Component of Reynolds Normal Stress near Exit Section (Re/Ro = 0.75)

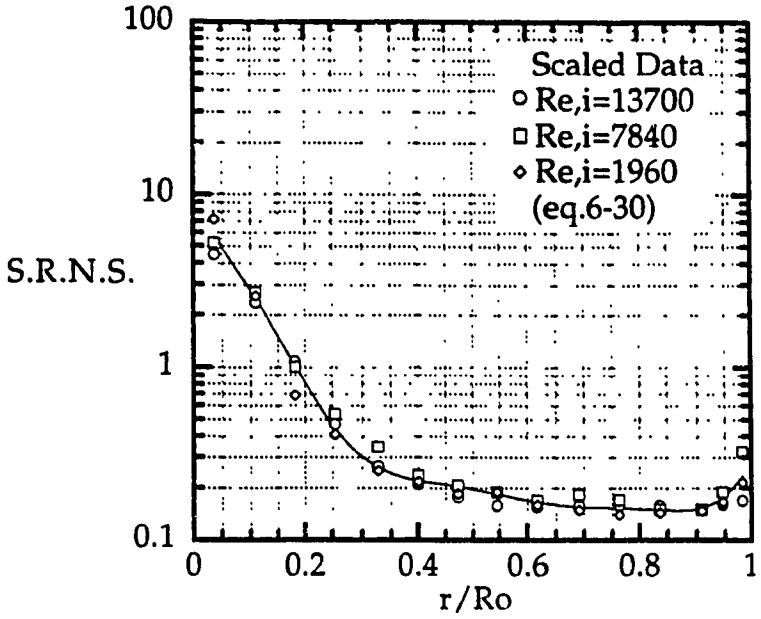

Figure 6.4.1.20 Scaled Tangential Component of Reynolds Normal Stress near Exit Section (Re/Ro = 0.25, line - average value)

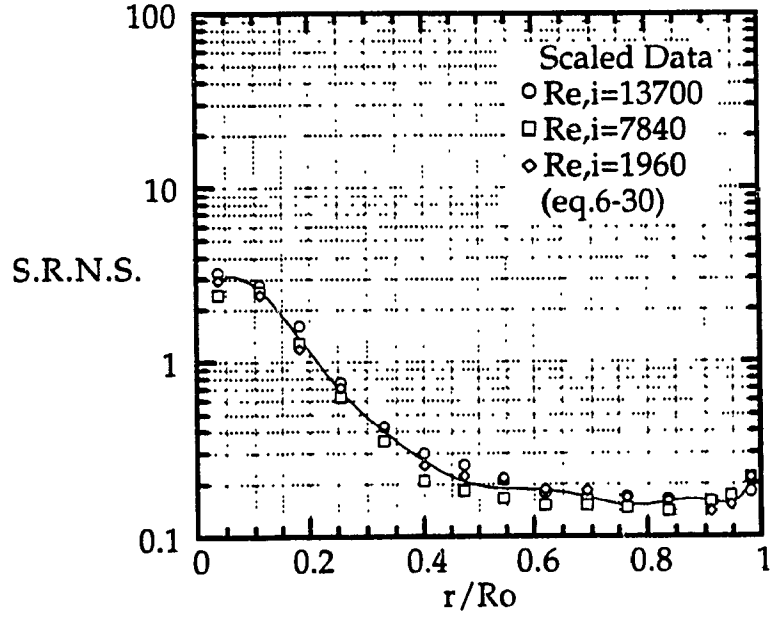

Figure 6.4.1.21 Scaled Tangential Component of Reynolds Normal Stress near Exit Section (Re/Ro = 0.30, line - average value)

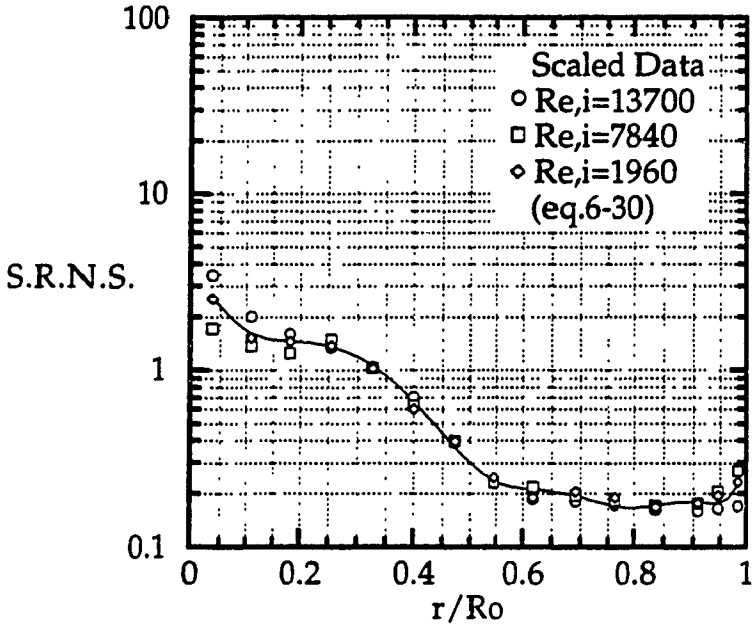

Figure 6.4.1.22 Scaled Tangential Component of Reynolds Normal Stress near Exit Section (Re/Ro = 0.40, line - average value)

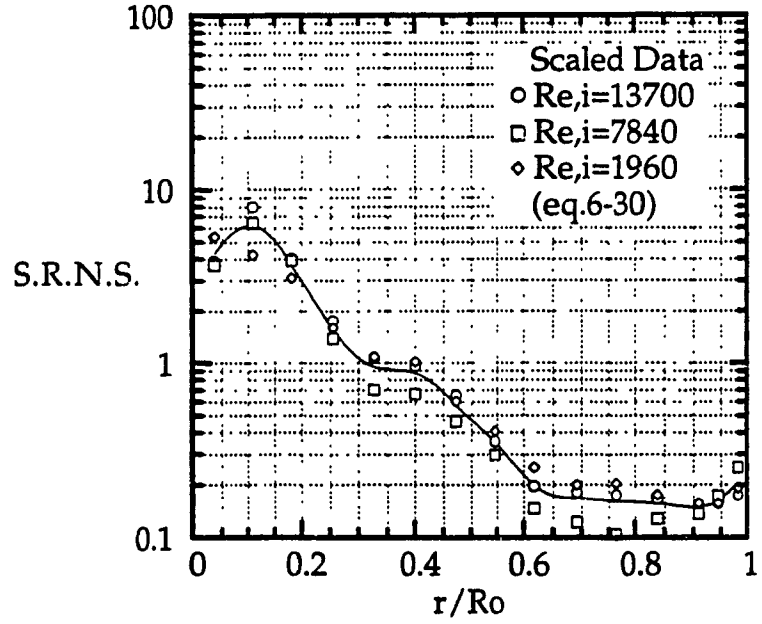

Figure 6.4.1.23 Scaled Tangential Component of Reynolds Normal Stress near Exit Section (Re/Ro = 0.50, line - average value)

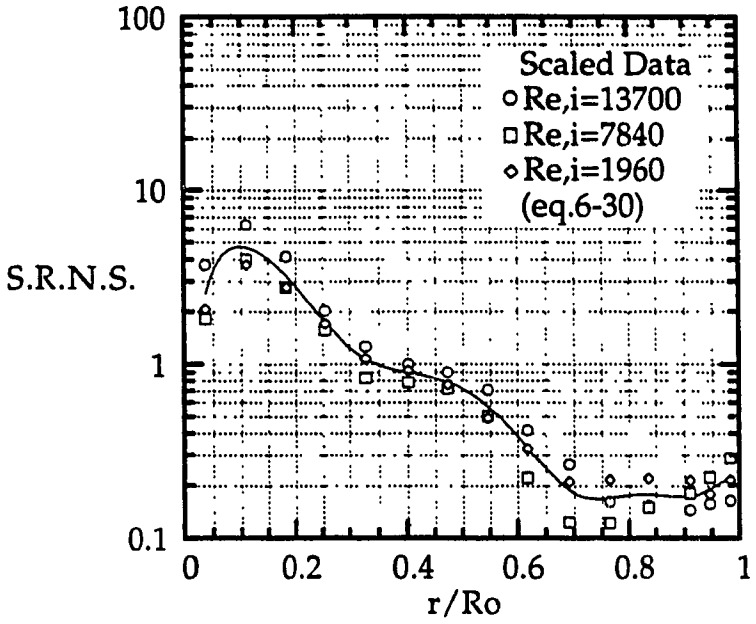

Figure 6.4.1.24 Scaled Tangential Component of Reynolds Normal Stress near Exit Section (Re/Ro = 0.58, line - average value)

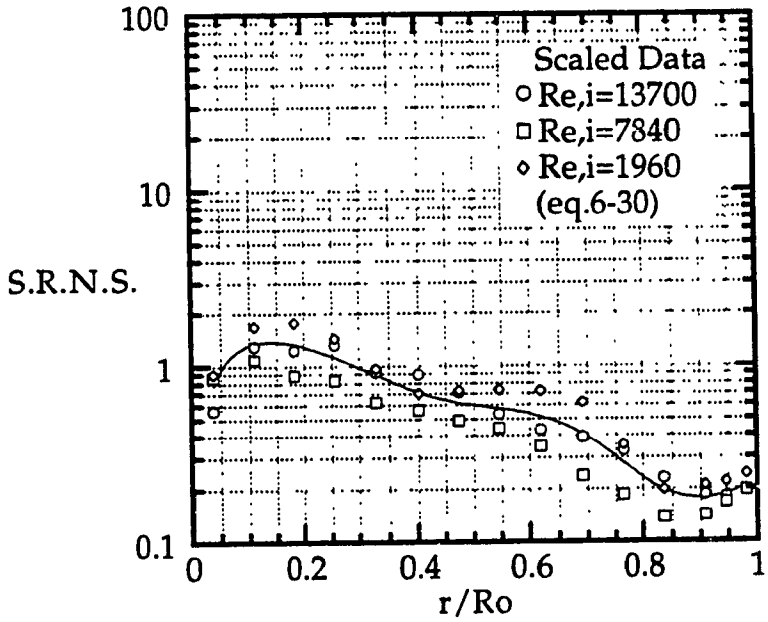

Figure 6.4.1.25 Scaled Tangential Component of Reynolds Normal Stress near Exit Section (Re/Ro = 0.75, line - average value)

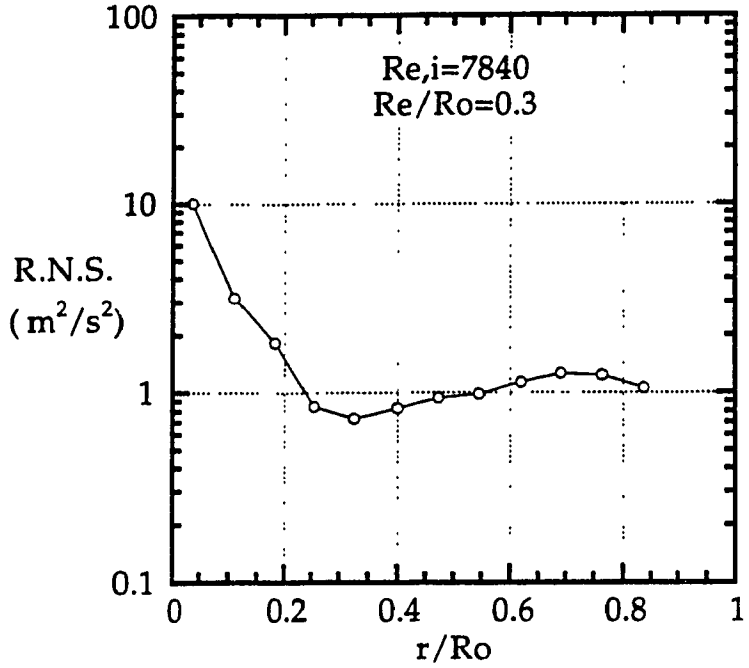

Figure 6.4.2.1 Experimental Radial Component of Reynolds Normal Stress at Main Section (69 % Vortex Chamber Length)

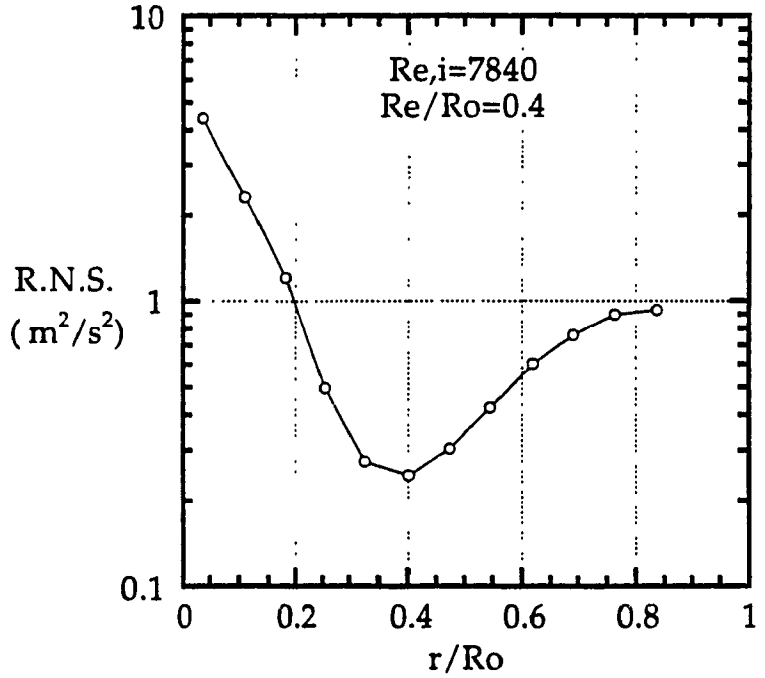

Figure 6.4.2.2 Experimental Radial Component of Reynolds Normal Stress at Main Section (50 % Vortex Chamber Length)

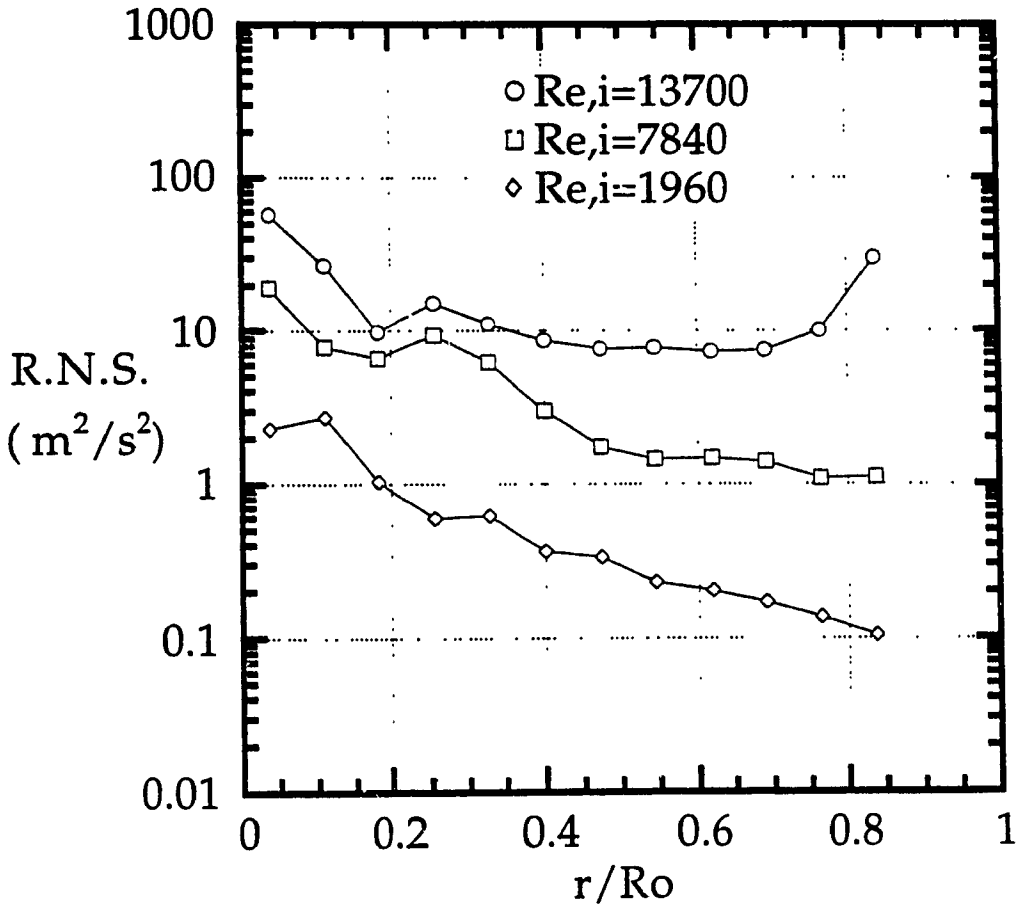

Figure 6.4.2.3 Experimental Radial Component of Reynolds Normal Stress near Exit Section (Re/Ro = 0.25)

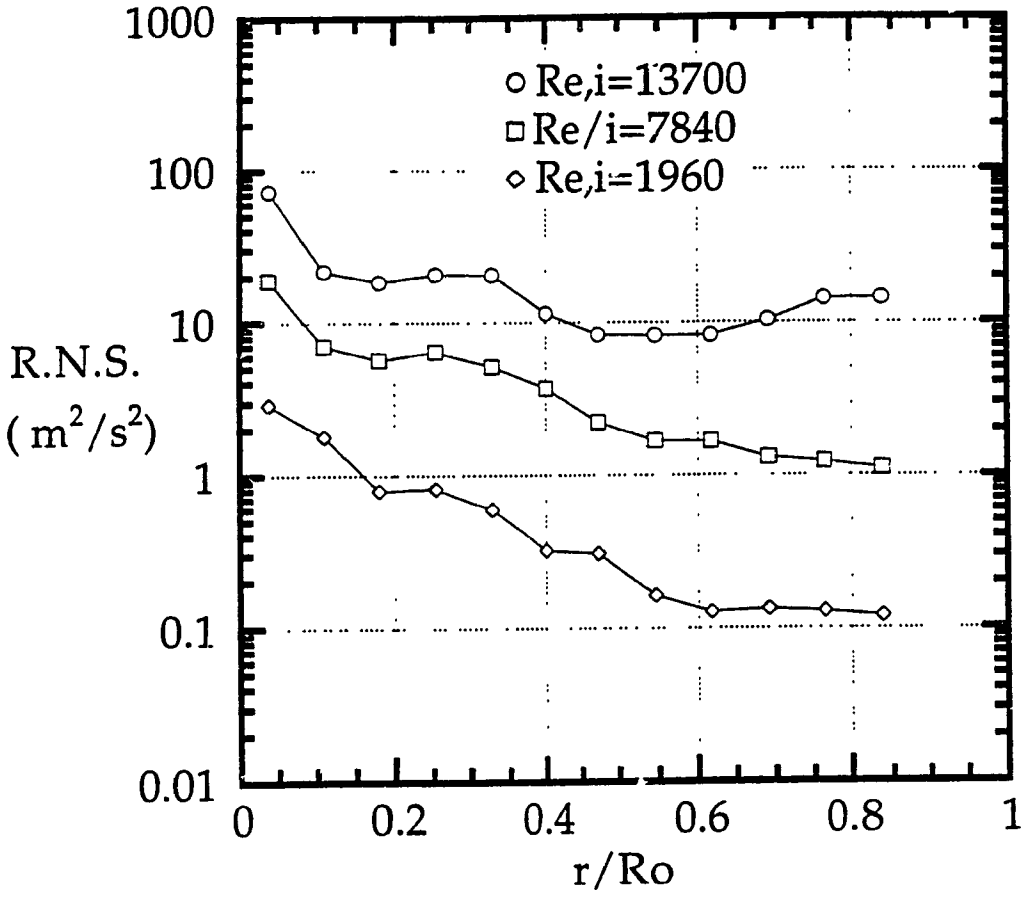

Figure 6.4.2.4 Experimental Radial Component of Reynolds Normal Stress near Exit Section (Re/Ro = 0.30)

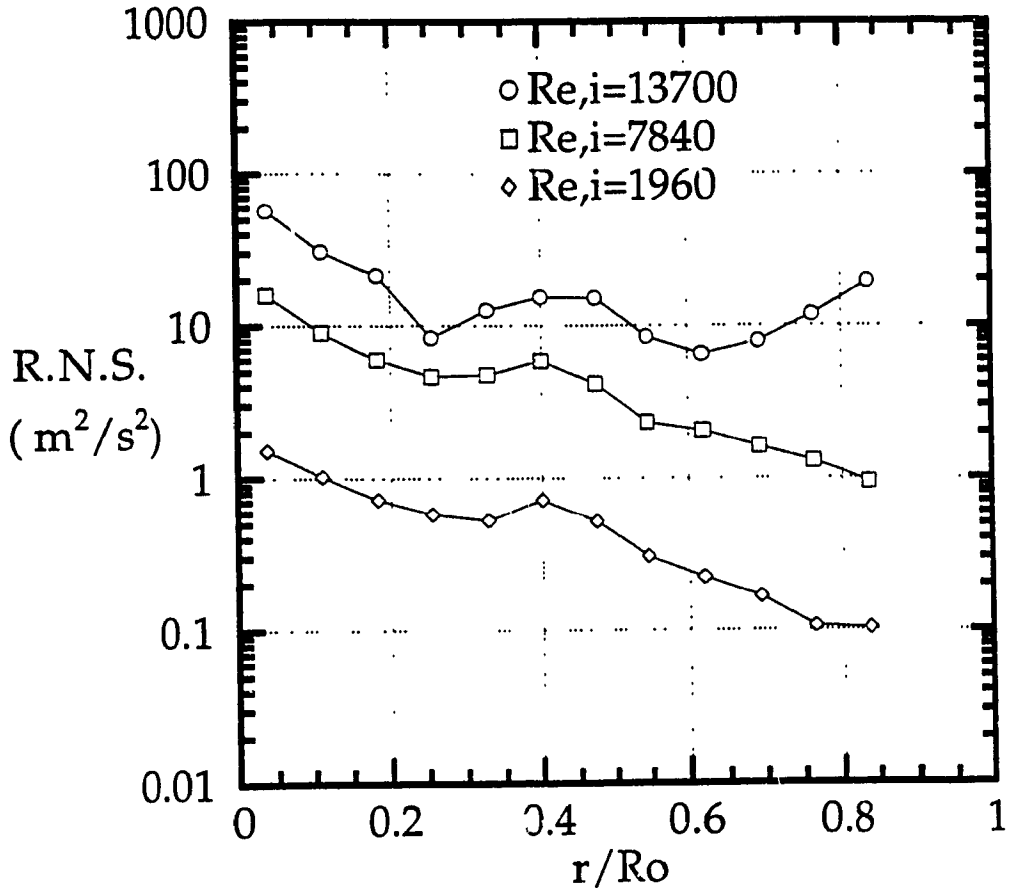

Figure 6.4.2.5 Experimental Radial Component of Reynolds Normal Stress near Exit Section (Re/Ro = 0.40)

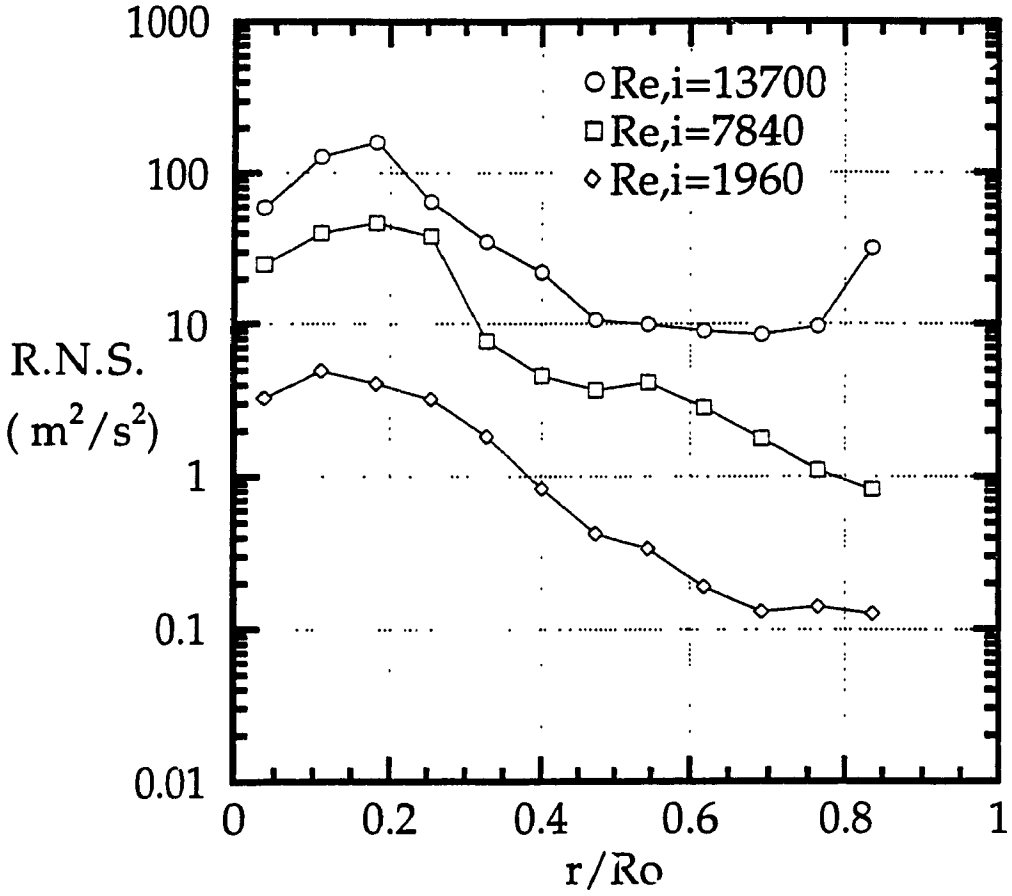

Figure 6.4.2.6 Experimental Radial Component of Reynolds Normal Stress near Exit Section (Re/Ro = 0.50)

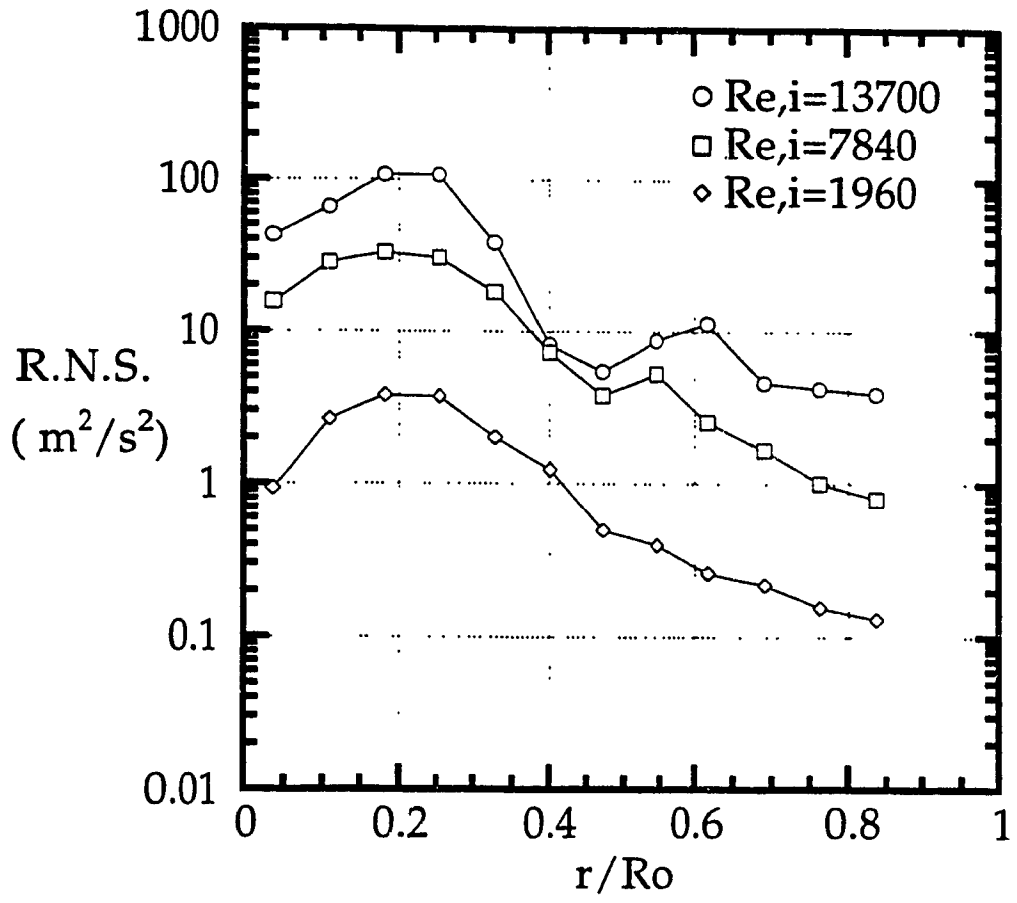

Figure 6.4.2.7 Experimental Radial Component of Reynolds Normal Stress near Exit Section (Re/Ro = 0.58)

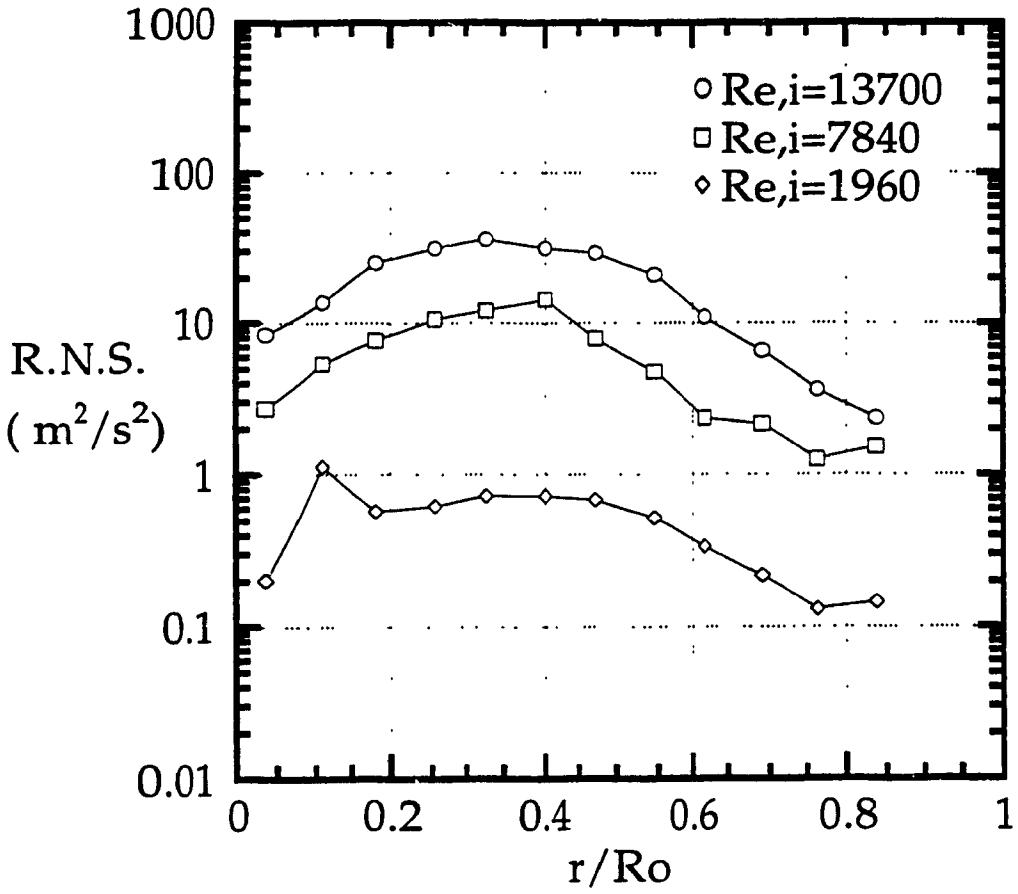

Figure 6.4.2.8 Experimental Radial Component of Reynolds Normal Stress near Exit Section (Re/Ro = 0.75)

CHAPTER 7

CONCLUSIONS

The confined air vortex flow structure has been studied extensively through experimental and analytical approaches.

The technique applying Laser Doppler Velocimetry to investigate confined air vortex flow was developed for the first time. The development not only made the LDV air vortex flow measurement possible, but also extended the investigation from the main section to very close to the exit section inside the vortex chamber, which was impossible by any conventional method. The LDV measurements indicated that the mean tangential velocity near the exit section was higher than that at the main section. Within the main section, it was found that the mean tangential velocity profiles at different locations were practically identical. The LDV measurements also indicated that, at the main section, the mean radial velocity was much smaller than the mean tangential velocity. The radial velocity profiles near the exit section had completely different shapes under different conditions. However, the radial velocity could be scaled to eliminate the effect of the inlet Reynolds number. Based on the flow measurements, the new findings on the turbulence intensity, the kinetic energy and the Reynolds stresses were obtained.

A three-region model was proposed for the tangential component of the turbulence intensity in a confined air vortex flow. The model classified the behaviour of the tangential component of the turbulence intensity along the radius of the vortex chamber. It was found that the strongest turbulence intensity in the tangential direction appeared at the centre of the vortex

chamber. The lowest one was at the border where the central core region ended and the outer region began. In the central core region, the magnitude of the tangential component of the turbulence intensity depended on both the inlet Reynolds number and the contraction ratio. However, in the outer and the boundary layer regions, its magnitude depended on the inlet Reynolds number only. Furthermore, the proposed three-region model was also suitable to describe the characteristics of the radial component of the turbulence intensity.

Mathematical expressions were found and proposed to predict the tangential component of the turbulence intensity for all three regions under a variety of conditions, not only qualitatively but also quantitatively. The verification showed that the deviation between the predicted turbulence intensity and the experimental results was satisfactory.

It was found that the locations of the minimum turbulence intensity of the tangential and radial components depended on the swirl number only. The minimum value and its location had approximate linear correlations with the contraction ratio. Empirical equations were proposed to determine the location and the magnitude quantitatively.

A theoretical work resulted in the equations for the total kinetic energy and the kinetic energies due to the mean motion and the fluctuating motion. The factors contributing to the kinetic energies were analyzed. The scaling formulas were found to eliminate the complexity of the inlet flow conditions. Based on the experimental data, the magnitude and the location of the maximum and the minimum values of the turbulence kinetic energy in the confined air vortex flow were determined. In the confined air vortex flow with viscous domination, the turbulence kinetic energy would tend to its maximum value at the centre of the vortex chamber. The characteristics of

the turbulence kinetic energy and the related influence factors were summarized.

Differential equations concerning the Reynolds shear stresses of the radial-tangential component and radial-axial component were derived in this study. These equations were solved directly as that the velocity profiles could be expressed analytically. Numerical results were obtained using a developed computer program according to the analytical solutions. The contributions of viscosity in the tangential and the axial directions were demonstrated. The Reynolds normal stresses in the tangential and radial directions were obtained from the air vortex flow experiments. Using the proposed scaling formulas, the number of influence factors on the Reynolds normal stress was reduced.

A new approximation to the tangential velocity distribution was proposed, which well matched the experimental results. Based on the energy conservation and the new velocity profile, an integration equation was derived to determine the critical radius of the vortex core. A computer program was developed to predict the vortex core radii corresponding to different vortex chamber configurations.

This study contemplates, in depth, the fundamental research of the confined air vortex flows with aim to reveal the flow structure and to better understand the flow regime. The developed models and formulated empirical equations are very useful not only for the fundamental work in the confined vortex flows but also for the industrial applications such as the energy savings in the vortex separators and the performance improving in the combustion chambers. Most of the results presented in this thesis are directly from the LDV measurements without any assumption, which will definitely give more confidence to applicators. The conclusions drawn in this

thesis and the information provided in this thesis can be applied for matters using or related to the vortex mechanism. Certainly, further investigation on the flow behaviour and characteristics in the axial direction would be most meaningful.

REFERENCES

1. Weber's Dictionary, 1991, Lexicon Publications, Inc.
2. McGraw-Hill Dictionary of Scientific and Technical Terms, 1994, McGraw-Hill Book Company.
3. Rankine, W.J.M., 1876, "Manual of Applied Mechanics", Charles Griffin and Co., London.
4. Burgers, J.M., 1948, "A Mathematical Model Illustrating the Theory of Turbulence", Advances in Applied Mechanics, Vol. 1, pp.171-199.
5. Lewellen, W.S., 1971, "A Review of Confined Vortex Flows", NASA Contractor Report (NASA CR-1772), July.
6. Wormley, D.N., 1968, "An Analytical Model for the Incompressible Flow in Short Vortex Chamber", Transactions of the ASME, Journal of Basic Engineering, Paper No. 68-WA/FE-17.
7. Kwok, C.K., N.D.Thin and S.Lin, 1972, "An Investigation of Confined Vortex Flow Phenomena", Transactions of the ASME, Journal of Basic Engineering, Sep., pp.689-696.
8. Baluev, E.D. and Y.U.Troyankin, 1967, "Study of the Aerodynamic Structure of Gas Flow in a Cyclone", Thermal Engineering, Vol. 14, pp.84-87.
9. Troyankin, Y.U. and E.D.Baleuv, 1969, "The Aerodynamic Resistance and Efficiency of a Cyclone Chamber", Thermal Engineering, Vol. 16, pp.29.
10. Ustimenko, B.P. and M.A.Buchman, 1968, "Turbulent Flow Structure in a Cyclone Chamber", Thermal Engineering, Vol. 15, pp.64.

11. Bank, N. and W.H. Ganvin, 1977, "Measurements of Flow Characteristics in a Confined Vortex Flow", The Canadian Journal of Chemical Engineering, Vol. 55, pp.397.

12. Reydon, R.F. and W.H.Gauvin, 1981, "Theoretical and Experimental Studies of Confined Vortex Flows", The Canadian Journal of Chemical Engineering, Vol. 59, Feb., pp.14-23.

13. Stephan, K., S.Lin, M.Durst, F.Huang and D.Seher, 1983, "An Investigation of Energy Separation in a Vortex Tube", International Journal of Heat and Mass Transfer, Vol. 26, No. 3, pp.341-348.

14. Georgantas, A., T.Krepec and C.K.Kwok, 1983, "Investigation of Double Vortex Structure and Its Ability to Retain Fuel Particles in a Cyclone Combustion Chamber", 1983 Fall Technical Meeting of the Combustion Institute, Eastern Section, Providence, Rhode Island.

15. Kerrebrock, J.L. and R.V.Meghreblian, 1961, "Vortex Containment for the Gaseous Fission Rocket", Journal of Aerospace Science, Vol. 28, pp.710.

16. Dietz, P.W., 1981, "Collection Efficiency of Cyclone Separators", AICHE Journal, Vol. 27, No. 6, Nov., pp.888-892.

17. Stephan, K., S.Lin, M.Durst, F.Huang and D.Seher, 1983, "An Investigation of Energy Separation in a Vortex Tube", International Journal of Heat and Mass Transfer, Vol. 26, pp.341-348.

18. Shakespeare, W.J. and E.K.Levy, 1980, "Pressure Drop in a Confined Vortex with High Flow Rate", The Winter Annual Meeting of the ASME, Chicago, Illinois, Nov.

19. Vatistas, G.H., S.Lin and C.K.Kwok, 1986, "Theoretical and Experimental Studies on Vortex Chamber Flows", AIAA Journal, Vol. 24, No.4, April, pp.635-642.

20. Vatistas, G.H., S.Lin and C.K.Kwok, 1986, "Reverse Flow Radius in Vortex Chambers", AIAA Journal, Vol. 24, No. 11, Nov., pp.1872-1873.

21. Vatistas, G.H., C.K.Kwok and S.Lin, 1985, "The Reduction of Pressure Drop Across a Vortex Chamber", AIAA Journal, Vol. 23, No. 6, June, pp.974-975.

22. Vatistas, G.H., C.Lam and S.Lin, 1989, "A Similarity Relationship for the Pressure Drop in Vortex Chambers", The Canadian Journal of Chemical Engineering, Vol. 67, Aug., pp.540-544.

23. Vatistas, G.H., S.Lin and P.M.Li, 1988, "A Similar Profile for the Tangential Velocity in Vortex Chambers", Experiments in Fluids, 6 (1988), pp.135-137.

24. Vatistas, G.H., V.Kozel and W.C.Mih, 1991, "A Simpler Model for Concentrated Vortices", Experiments in Fluids, 11(1991), pp.73-76.

25. Launder, D.E. and D.B.Spalding, 1974, "The Numerical Computation of Turbulent Flow", Computational Method in Applied Mechanics and Engineering, Vol. 3, pp.269-288.

26. Nejad, A.S., S.P.Vanka, S.C.Favaloro, M.Samimy and C.Langenfeld, 1989, "Application of Laser Velocimetry for Characterization of Confined Swirling Flow", Transactions of the ASME, Journal of Engineering for Gas Turbines and Power, Vol. 111, Jan., pp.36-45.

27. Eaton, J.K. and J.P.Johnston, 1981, "A Review of Research on Subsonic Turbulent Flow Reattachment", AIAA Journal, Vol. 19, No. 9, pp.1093-1100.

28. Escudier, M.P., J.Bornstein and N.Zehuder, 1980, "Observations and LDA Measurements of Confined Vortex Flow", Journal of Fluid Mechanics, Vol 98, Part 1, pp.49-63.

29. Granger, R.A., 1993, "Some Experimental Observations of Secondary Motions in a Confined Vortex Flow", Journal of Fluid Mechanics, Vol. 246, pp.653-674.

30. Durret, R.P., W.H.Stevenson and H.D.Thompson, 1988, "Radial and Axial Turbulent Flow Measurements with an LDV in an Axisymmetric Sudden Expansion Air Flow", Transactions of the ASME, Journal of Fluids Engineering, Vol. 110, Dec., pp.367-372.

31. Donohue, G.L., D.K.Mclaughlin and W.G.Tiederman, 1972, "Turbulence Measurements with a Laser Anemometer Measuring Individual Realizations", Rep. ER 72-F-11, School of Mechanical and Aerospace Engineering, OK State University.

32. Yanta, W.J. and R.A.Smith, 1973, "Measurements of Turbulence - Transport Properties with a Laser Doppler Velocimeter", AIAA Paper 73-169.

33. Gouldin, F.C., J.S.Depsky and S-L. Lee, 1985, "Velocity Field Characteristics of a Swirling Flow Combustor", AIAA Journal, Vol. 23, No. 1, Jan., pp.95-102.

34. Singler, T.J., 1989, "Boundary Layer Measurements at an Internal Free Surface in a Partially Filled Horizontal and Rapidly - Rotating Container", Journal of Fluids Engineering, Vol. 111, Dec., pp.457-463.

35. Goebel, S.G. and J.C.Dutton, 1991, "Experimental Study of Compressible Turbulence Mixing Layers", AIAA Journal, Vol. 29, No. 4, April, pp.538-546.

36. Yuan, S.N., 1967, "Foundations of Fluid Mechanics", Prentice - Hall, Inc., Englewood Cliffs, N.J.

37. Hinze, J.O., 1975, "Turbulence", McGraw - Hill, Inc.

38. Dryden, H.L. and A.M.Kuethe, 1930, National Advisory Committee of Aeronautics Technical Reports No. 342.

39. Stieglmeier, M., C.Tropea, N.Weiser and W.Nitsche, 1989, "Experimental Investigation of the Flow through Axisymmetric Expansions", Transactions of the ASME, Journal of Fluids Engineering, Vol. 111, Dec. 1989, pp.464-471.

40. Liou, T.-M., Y.-Y.Wu and Y.Chang, 1993, "LDV Measurements of Periodic Fully Developed Main and Secondary Flows in a Channel with Rib-Disturbed Walls", Transactions of the ASME, Journal of Fluids Engineering, Vol. 115, March 1993, pp.109-115.

BIBLIOGRAPHY

1. Anthony, D.G. and W.W.Willmarth, 1992, "Turbulence Measurements in a Round Jet beneath a Free Surface", Journal of Fluid Mechanics, Vol. 243, pp.699-720.
2. Bradshaw, P. (Editor), 1978, "Turbulence" (Second Corrected and Updated Edition), Springer-Verlag Berlin Heidelberg.
3. Dantec Elektronik, 1990, Handbooks.
4. Eckmann, D.E. and J B.Grotberg, 1991, "Experiments on Transition to Turbulence in Oscillatory Pipe Flow", Journal of Fluid Mechanics, Vol. 222, pp.329-350.
5. Gould, R.D., W.H.Stevenson and H.D.Thompson, 1990, "Investigation of Turbulent Transport in an Axisymmetric Sudden Expansion", AIAA Journal, Vol. 28, No. 2, Feb., pp.276-283.
6. Gupta, A.K., D.G.Lilley and N.Syred, 1984, "Swirl Flows", Abacus Press.
7. Lin, C.C. (Editor), 1959, "Turbulent Flows and Heat Transfer", Princeton University Press.
8. Matovic, D. and C.Tropea, 1991, "Spectral Peak Interpolation with Application to LDA Signal Processing", Measurement Science and Technology, No. 2, pp.1100-1106.
9. Nishigaki, M., M.Ippommatsu, Y.Ikeda and T.Nakajima, 1992, "New High-Performance Tracer Particles for Optical Gas Flow Diagnostics", Measurement Science and Technology, No. 3, pp.619-621.
10. Ogawa, A., 1993, "Vortex Flow", CRC Press, Inc.
11. Owen, F.K., R.B.Miles and R.Menon, 1992, "Tracking a Particle's Progress", Aerospace America, Nov., pp.34-38.

12. Samimy, M. and G.S.Elliott, 1990, "Effects of Compressibility on the Characteristics of Free Shear Layers", AIAA Journal, Vol. 28, No. 3, March, pp.439-445.

13. Schlichting, H., 1960, "Boundary Layer Theory" (Fourth Edition), McGraw-Hill Book Company, Inc.

14. Stevenson, W.H., H.D.Thompson and R.R.Craig, 1984, "Laser Velocimeter Measurements in Highly Turbulent Recirculating Flows", Transactions of the ASME, Journal of Fluids Engineering, Vol. 106, June, pp.173-180.

APPENDIX A

Derivation of Equations for Turbulent Flows in Cylindrical Coordinates

A.1 Equation of Continuity

To an incompressible flow at steady state, the equation of continuity is as follows:

$$\frac{\partial V_r}{\partial r} + \frac{1}{r}\cdot\frac{\partial V_\theta}{\partial \theta} + \frac{\partial V_z}{\partial z} + \frac{V_r}{r} = 0 \qquad \text{(A1-1)}$$

Averaging each term in the above equation yields the equation of continuity used for turbulent flows as follows:

$$\frac{\partial \overline{V}_r}{\partial r} + \frac{1}{r}\cdot\frac{\partial \overline{V}_\theta}{\partial \theta} + \frac{\partial \overline{V}_z}{\partial z} + \frac{\overline{V}_r}{r} = 0 \qquad \text{(A1-2)}$$

A.2 Equation of Motion in Radial Direction

$$\rho\left(\frac{DV_r}{Dt} - \frac{V_\theta^2}{r}\right) = F_r + \frac{1}{r}\left[\frac{\partial(r\sigma_{rr})}{\partial r} + \frac{\partial\sigma_{r\theta}}{\partial\theta} + \frac{\partial(r\sigma_{zr})}{\partial z}\right] - \frac{1}{r}\sigma_{\theta\theta}$$
$$= F_r + \frac{\partial\sigma_{rr}}{\partial r} + \frac{1}{r}\frac{\partial\sigma_{r\theta}}{\partial\theta} + \frac{\partial\sigma_{zr}}{\partial z} + \frac{1}{r}(\sigma_{rr} - \sigma_{\theta\theta}) \qquad \text{(A2-1)}$$

where

$$\frac{D}{Dt} = \frac{\partial}{\partial t} + V_r\frac{\partial}{\partial r} + \frac{1}{r}V_\theta\frac{\partial}{\partial\theta} + V_z\frac{\partial}{\partial z} \qquad \text{(A2-2)}$$

To steady state incompressible flow without body force F_r, equation (A2-1) becomes

$$\rho\left(V_r\frac{\partial V_r}{\partial r} + \frac{1}{r}V_\theta\frac{\partial V_r}{\partial\theta} + V_z\frac{\partial V_r}{\partial z} - \frac{V_\theta^2}{r}\right)$$
$$= \frac{\partial}{\partial r}(\sigma_{rr}) + \frac{1}{r}\frac{\partial}{\partial\theta}(\sigma_{r\theta}) + \frac{\partial}{\partial z}(\sigma_{zr}) + \frac{1}{r}(\sigma_{rr} - \sigma_{\theta\theta}) \qquad \text{(A2-3)}$$

To steady state incompressible flow, the Continuity Equation is as follows:

$$\vec{\nabla}\cdot\vec{q} = \frac{\partial V_r}{\partial r} + \frac{1}{r}\frac{\partial V_\theta}{\partial\theta} + \frac{\partial V_z}{\partial z} + \frac{V_r}{r} = 0 \qquad \text{(A2-4)}$$

and

$$\rho V_r\vec{\nabla}\cdot\vec{q} = \rho V_r\frac{\partial V_r}{\partial r} + \rho\frac{1}{r}V_r\frac{\partial V_\theta}{\partial\theta} + \rho V_r\frac{\partial V_z}{\partial z} + \rho\frac{V_r^2}{r} = 0 \qquad \text{(A2-5)}$$

Substituting equation (A2-5) into (A2-3) yields

$$\rho\left(V_r\frac{\partial V_r}{\partial r} + \frac{1}{r}V_\theta\frac{\partial V_r}{\partial\theta} + V_z\frac{\partial V_r}{\partial z} - \frac{V_\theta^2}{r}\right) + \rho\left(V_r\frac{\partial V_r}{\partial r} + \frac{1}{r}V_r\frac{\partial V_\theta}{\partial\theta} + V_r\frac{\partial V_z}{\partial z} + \frac{V_r^2}{r}\right)$$
$$= \rho\left[\frac{\partial}{\partial r}(V_r^2) + \frac{1}{r}\frac{\partial}{\partial\theta}(V_rV_\theta) + \frac{\partial}{\partial z}(V_rV_z) + \frac{1}{r}(V_r^2 - V_\theta^2)\right]$$
$$= \frac{\partial}{\partial r}(\sigma_{rr}) + \frac{1}{r}\frac{\partial}{\partial\theta}(\sigma_{r\theta}) + \frac{\partial}{\partial z}(\sigma_{zr}) + \frac{1}{r}(\sigma_{rr} - \sigma_{\theta\theta}) \qquad \text{(A2-6)}$$

Rearranging equation (A2-6) yields

$$\frac{\partial}{\partial r}(\sigma_{rr} - \rho V_r^2) + \frac{1}{r}\frac{\partial}{\partial \theta}(\sigma_{r\theta} - \rho V_r V_\theta) + \frac{\partial}{\partial z}(\sigma_{zr} - \rho V_r V_z) +$$
$$+ \frac{1}{r}(\sigma_{rr} - \sigma_{\theta\theta}) - \frac{\rho}{r}(V_r^2 - V_\theta^2) = 0 \qquad \text{(A2-7)}$$

Averaging each term of equation (A2-7) yields

$$\frac{\partial}{\partial r}(\bar{\sigma}_{rr} - \rho\overline{V_r^2}) + \frac{1}{r}\frac{\partial}{\partial \theta}(\bar{\sigma}_{r\theta} - \rho\overline{V_r V_\theta}) + \frac{\partial}{\partial z}(\bar{\sigma}_{zr} - \rho\overline{V_r V_z}) +$$
$$+ \frac{1}{r}(\bar{\sigma}_{rr} - \bar{\sigma}_{\theta\theta}) - \frac{\rho}{r}(\overline{V_r^2} - \overline{V_\theta^2}) = 0 \qquad \text{(A2-8)}$$

Since

$$V_r'(t) = V_r(t) - \bar{V}_r$$
$$V_\theta'(t) = V_\theta(t) - \bar{V}_\theta$$
$$V_z'(t) = V_z(t) - \bar{V}_z \qquad \text{(A2-9)}$$

Applying to equation (A2-8) yields

$$\frac{\partial}{\partial r}(\bar{\sigma}_{rr} - \rho\bar{V}_r^2 - \rho\overline{V_r'^2}) + \frac{1}{r}\frac{\partial}{\partial \theta}(\bar{\sigma}_{r\theta} - \rho\bar{V}_r\bar{V}_\theta - \rho\overline{V_r'V_\theta'}) +$$
$$+ \frac{\partial}{\partial z}(\bar{\sigma}_{zr} - \rho\bar{V}_r\bar{V}_z - \rho\overline{V_r'V_z'}) + \frac{1}{r}(\bar{\sigma}_{rr} - \bar{\sigma}_{\theta\theta}) - \frac{\rho}{r}(\bar{V}_r^2 + \overline{V_r'^2} - \bar{V}_\theta^2 - \overline{V_\theta'^2}) = 0 \qquad \text{(A2-10)}$$

$$\frac{\partial}{\partial r}(\rho\bar{V}_r^2) + \frac{1}{r}\frac{\partial}{\partial \theta}(\rho\bar{V}_r\bar{V}_\theta) + \frac{\partial}{\partial z}(\rho\bar{V}_r\bar{V}_z) + \frac{\rho}{r}(\bar{V}_r^2 - \bar{V}_\theta^2)$$
$$= \frac{\partial}{\partial r}(\bar{\sigma}_{rr} - \rho\overline{V_r'^2}) + \frac{1}{r}\frac{\partial}{\partial \theta}(\bar{\sigma}_{r\theta} - \rho\overline{V_r'V_\theta'}) + \frac{\partial}{\partial z}(\bar{\sigma}_{zr} - \rho\overline{V_r'V_z'}) + \frac{1}{r}(\bar{\sigma}_{rr} - \bar{\sigma}_{\theta\theta}) -$$
$$- \frac{\rho}{r}(\overline{V_r'^2} - \overline{V_\theta'^2}) \qquad \text{(A2-11)}$$

$$2\rho\bar{V}_r\frac{\partial\bar{V}_r}{\partial r} + \rho\frac{1}{r}\bar{V}_\theta\frac{\partial\bar{V}_r}{\partial\theta} + \rho\frac{1}{r}\bar{V}_r\frac{\partial\bar{V}_\theta}{\partial\theta} + \rho\bar{V}_z\frac{\partial\bar{V}_r}{\partial z} + \rho\bar{V}_r\frac{\partial\bar{V}_z}{\partial z} + \frac{\rho}{r}(\bar{V}_r^2 - \bar{V}_\theta^2)$$
$$= \frac{\partial}{\partial r}(\bar{\sigma}_{rr} - \rho\overline{V_r'^2}) + \frac{1}{r}\frac{\partial}{\partial \theta}(\bar{\sigma}_{r\theta} - \rho\overline{V_r'V_\theta'}) + \frac{\partial}{\partial z}(\bar{\sigma}_{zr} - \rho\overline{V_r'V_z'}) + \frac{1}{r}(\bar{\sigma}_{rr} - \bar{\sigma}_{\theta\theta}) -$$
$$- \frac{\rho}{r}(\overline{V_r'^2} - \overline{V_\theta'^2}) \qquad \text{(A2-12)}$$

$$\rho(\bar{V}_r\frac{\partial\bar{V}_r}{\partial r}+\frac{1}{r}\bar{V}_\theta\frac{\partial\bar{V}_r}{\partial\theta}+\bar{V}_z\frac{\partial\bar{V}_r}{\partial z}-\frac{\bar{V}_\theta^2}{r})+\rho\bar{V}_r(\frac{\partial\bar{V}_r}{\partial r}+\frac{1}{r}\frac{\partial\bar{V}_\theta}{\partial\theta}+\frac{\partial\bar{V}_z}{\partial z}+\frac{\bar{V}_r}{r})$$
$$=\rho(\bar{V}_r\frac{\partial\bar{V}_r}{\partial r}+\frac{1}{r}\bar{V}_\theta\frac{\partial\bar{V}_r}{\partial\theta}+\bar{V}_z\frac{\partial\bar{V}_r}{\partial z}-\frac{\bar{V}_\theta^2}{r})+\rho\bar{V}_r\overline{\vec{\nabla}\cdot\vec{q}}$$
$$=\frac{\partial}{\partial r}(\bar{\sigma}_{rr}-\rho\overline{V_r'^2})+\frac{1}{r}\frac{\partial}{\partial\theta}(\bar{\sigma}_{r\theta}-\rho\overline{V_r'V_\theta'})+\frac{\partial}{\partial z}(\bar{\sigma}_{zr}-\rho\overline{V_r'V_z'})+\frac{1}{r}(\bar{\sigma}_{rr}-\sigma_{\theta\theta})-$$
$$-\frac{\rho}{r}(\overline{V_r'^2}-\overline{V_\theta'^2}) \qquad \text{(A2-13)}$$

Since

$$\overline{\vec{\nabla}\cdot\vec{q}}=0 \qquad \text{(A2-14)}$$

Applying to equation (A2-13) yields

$$\rho(\bar{V}_r\frac{\partial\bar{V}_r}{\partial r}+\frac{1}{r}\bar{V}_\theta\frac{\partial\bar{V}_r}{\partial\theta}+\bar{V}_z\frac{\partial\bar{V}_r}{\partial z}-\frac{\bar{V}_\theta^2}{r})$$
$$=\frac{\partial}{\partial r}(\bar{\sigma}_{rr})+\frac{1}{r}\frac{\partial}{\partial\theta}(\bar{\sigma}_{r\theta})+\frac{\partial}{\partial z}(\bar{\sigma}_{zr})+\frac{1}{r}(\bar{\sigma}_{rr}-\bar{\sigma}_{\theta\theta})-$$
$$-[\frac{\partial}{\partial r}(\rho\overline{V_r'^2})+\frac{1}{r}\frac{\partial}{\partial\theta}(\rho\overline{V_r'V_\theta'})+\frac{\partial}{\partial z}(\rho\overline{V_r'V_z'})+\frac{\rho}{r}(\overline{V_r'^2}-\overline{V_\theta'^2})]$$
$$=S1+S2 \qquad \text{(A2-15)}$$

where

$$S1=\frac{\partial}{\partial r}(\bar{\sigma}_{rr})+\frac{1}{r}\frac{\partial}{\partial\theta}(\bar{\sigma}_{r\theta})+\frac{\partial}{\partial z}(\bar{\sigma}_{zr})+\frac{1}{r}(\bar{\sigma}_{rr}-\bar{\sigma}_{\theta\theta}) \qquad \text{(A2-16)}$$

$$S2=-[\frac{\partial}{\partial r}(\rho\overline{V_r'^2})+\frac{1}{r}\frac{\partial}{\partial\theta}(\rho\overline{V_r'V_\theta'})+\frac{\partial}{\partial z}(\rho\overline{V_r'V_z'})+\frac{\rho}{r}(\overline{V_r'^2}-\overline{V_\theta'^2})] \qquad \text{(A2-17)}$$

Since

$$\bar{\sigma}_{rr}=-\bar{p}+2\mu\bar{\varepsilon}_{rr}-\frac{2}{3}\mu\overline{\vec{\nabla}\cdot\vec{q}}=-\bar{p}+2\mu\frac{\partial\bar{V}_r}{\partial r}-\frac{2}{3}\mu\overline{\vec{\nabla}\cdot\vec{q}}$$

$$\bar{\sigma}_{\theta\theta}=-\bar{p}+2\mu\bar{\varepsilon}_{\theta\theta}-\frac{2}{3}\mu\overline{\vec{\nabla}\cdot\vec{q}}=-\bar{p}+2\mu(\frac{1}{r}\frac{\partial\bar{V}_\theta}{\partial\theta}+\frac{\bar{V}_r}{r})-\frac{2}{3}\mu\overline{\vec{\nabla}\cdot\vec{q}}$$

$$\bar{\sigma}_{r\theta}=\mu\bar{\gamma}_{r\theta}=\mu(\frac{\partial\bar{V}_\theta}{\partial r}-\frac{\bar{V}_\theta}{r}+\frac{1}{r}\frac{\partial\bar{V}_r}{\partial\theta})$$

$$\bar{\sigma}_{zr} = \mu\bar{\gamma}_{zr} = \mu\left(\frac{\partial \overline{V}_r}{\partial z} + \frac{\partial \overline{V}_z}{\partial r}\right) \tag{A2-18}$$

Substituting into equation (A2-16) yields

$$\begin{aligned} S1 &= \frac{\partial}{\partial r}\left(-\overline{p} + 2\mu\frac{\partial \overline{V}_r}{\partial r} - \frac{2}{3}\mu\overline{\vec{\nabla}\cdot\vec{q}}\right) + \frac{1}{r}\frac{\partial}{\partial\theta}\left[\mu\left(\frac{\partial \overline{V}_\theta}{\partial r} - \frac{\overline{V}_\theta}{r} + \frac{1}{r}\frac{\partial \overline{V}_r}{\partial\theta}\right)\right] + \\ &+ \frac{\partial}{\partial z}\left[\mu\left(\frac{\partial \overline{V}_r}{\partial z} + \frac{\partial \overline{V}_z}{\partial r}\right)\right] + \frac{1}{r}\left\{\left[-\overline{p} + 2\mu\frac{\partial \overline{V}_r}{\partial r} - \frac{2}{3}\mu\overline{\vec{\nabla}\cdot\vec{q}}\right] - \right. \\ &\left. - \left[-\overline{p} + 2\mu\left(\frac{1}{r}\frac{\partial \overline{V}_\theta}{\partial\theta} + \frac{\overline{V}_r}{r}\right) - \frac{2}{3}\mu\overline{\vec{\nabla}\cdot\vec{q}}\right]\right\} \\ &= -\frac{\partial \overline{p}}{\partial r} + 2\mu\frac{\partial^2 \overline{V}_r}{\partial r^2} + \mu\frac{1}{r}\frac{\partial^2 \overline{V}_\theta}{\partial r\partial\theta} - \mu\frac{1}{r^2}\frac{\partial \overline{V}_\theta}{\partial\theta} + \mu\frac{1}{r^2}\frac{\partial^2 \overline{V}_r}{\partial\theta^2} + \\ &+ \mu\frac{\partial^2 \overline{V}_r}{\partial z^2} + \mu\frac{\partial^2 \overline{V}_z}{\partial r\partial z} + 2\mu\left(\frac{1}{r}\frac{\partial \overline{V}_r}{\partial r} - \frac{1}{r^2}\frac{\partial \overline{V}_\theta}{\partial\theta} - \frac{\overline{V}_r}{r^2}\right) \end{aligned} \tag{A2-19}$$

$$\begin{aligned} S1 &= -\frac{\partial \overline{p}}{\partial r} + \mu\left(\frac{\partial^2 \overline{V}_r}{\partial r^2} + \frac{1}{r}\frac{\partial^2 \overline{V}_\theta}{\partial r\partial\theta} + \frac{\partial^2 \overline{V}_z}{\partial r\partial z} + \frac{1}{r}\frac{\partial \overline{V}_r}{\partial r}\right) + \\ &+ \mu\left(\frac{\partial^2 \overline{V}_r}{\partial r^2} - \frac{1}{r^2}\frac{\partial \overline{V}_\theta}{\partial\theta} + \frac{1}{r^2}\frac{\partial^2 \overline{V}_r}{\partial\theta^2} + \frac{\partial^2 \overline{V}_r}{\partial z^2} + \frac{1}{r}\frac{\partial \overline{V}_r}{\partial r} - \frac{2}{r^2}\frac{\partial \overline{V}_\theta}{\partial\theta} - 2\frac{\overline{V}_r}{r^2}\right) \\ &= -\frac{\partial \overline{p}}{\partial r} + \mu\left\{\frac{\partial}{\partial r}\left(\frac{\partial \overline{V}_r}{\partial r}\right) + \left[\frac{\partial}{\partial r}\left(\frac{1}{r}\frac{\partial \overline{V}_\theta}{\partial\theta}\right) + \frac{1}{r^2}\frac{\partial \overline{V}_\theta}{\partial\theta}\right] + \frac{\partial}{\partial r}\left(\frac{\partial \overline{V}_z}{\partial z}\right) + \left[\frac{\partial}{\partial r}\left(\frac{\overline{V}_r}{r}\right) + \frac{\overline{V}_r}{r^2}\right]\right\} + \\ &+ \mu\left(\frac{\partial^2 \overline{V}_r}{\partial r^2} + \frac{1}{r^2}\frac{\partial^2 \overline{V}_r}{\partial\theta^2} + \frac{\partial^2 \overline{V}_r}{\partial z^2} + \frac{1}{r}\frac{\partial \overline{V}_r}{\partial r} - 2\frac{\overline{V}_r}{r^2} - \frac{3}{r^2}\frac{\partial \overline{V}_\theta}{\partial\theta}\right) \\ &= -\frac{\partial \overline{p}}{\partial r} + \mu\frac{\partial}{\partial r}\left(\overline{\vec{\nabla}\cdot\vec{q}}\right) + \mu\left[\left(\frac{\partial^2 \overline{V}_r}{\partial r^2} + \frac{1}{r^2}\frac{\partial^2 \overline{V}_r}{\partial\theta^2} + \frac{\partial^2 \overline{V}_r}{\partial z^2} + \frac{1}{r}\frac{\partial \overline{V}_r}{\partial r}\right) - \frac{\overline{V}_r}{r^2} - \frac{2}{r^2}\frac{\partial \overline{V}_\theta}{\partial\theta}\right] \end{aligned} \tag{A2-20}$$

Since

$$\overline{\vec{\nabla}\cdot\vec{q}} = 0 \tag{A2-14}$$

Applying to equation (A2-20) yields

$$S1 = -\frac{\partial \overline{p}}{\partial r} + \mu\left(\nabla^2 \overline{V}_r - \frac{\overline{V}_r}{r^2} - \frac{2}{r^2}\frac{\partial \overline{V}_\theta}{\partial\theta}\right) \tag{A2-21}$$

where

$$\nabla^2 = \frac{\partial^2}{\partial r^2} + \frac{1}{r}\frac{\partial}{\partial r} + \frac{1}{r^2}\frac{\partial^2}{\partial \theta^2} + \frac{\partial^2}{\partial z^2} \tag{A2-22}$$

Substituting equations (A2-21) and (A2-17) into (A2-15) yields

$$\begin{aligned}
&\rho(\overline{V}_r\frac{\partial \overline{V}_r}{\partial r} + \frac{1}{r}\overline{V}_\theta\frac{\partial \overline{V}_r}{\partial \theta} + \overline{V}_z\frac{\partial \overline{V}_r}{\partial z} - \frac{\overline{V}_\theta^{\,2}}{r}) \\
&= -\frac{\partial \overline{p}}{\partial r} + \mu(\nabla^2 \overline{V}_r - \frac{\overline{V}_r}{r^2} - \frac{2}{r^2}\frac{\partial \overline{V}_\theta}{\partial \theta}) - \\
&- \rho[\frac{\partial}{\partial r}(\overline{V_r'^2}) + \frac{1}{r}\frac{\partial}{\partial \theta}(\overline{V_r'V_\theta'}) + \frac{\partial}{\partial z}(\overline{V_r'V_z'}) + \frac{1}{r}(\overline{V_r'^2} - \overline{V_\theta'^2})]
\end{aligned} \tag{A2-23}$$

or substituting equation (A2-18) into (A2-11) and rearranging equation (A2-11) yields

$$\begin{aligned}
&\frac{\partial}{\partial r}(\rho\overline{V}_r^{\,2}) + \frac{1}{r}\frac{\partial}{\partial \theta}(\rho\overline{V}_r\overline{V}_\theta) + \frac{\partial}{\partial z}(\rho\overline{V}_r\overline{V}_z) + \frac{\rho}{r}(\overline{V}_r^{\,2} - \overline{V}_\theta^{\,2}) \\
&= -\frac{\partial \overline{p}}{\partial r} + \mu(\nabla^2 \overline{V}_r - \frac{\overline{V}_r}{r^2} - \frac{2}{r^2}\frac{\partial \overline{V}_\theta}{\partial \theta}) - \\
&- \rho[\frac{\partial}{\partial r}(\overline{V_r'^2}) + \frac{1}{r}\frac{\partial}{\partial \theta}(\overline{V_r'V_\theta'}) + \frac{\partial}{\partial z}(\overline{V_r'V_z'}) + \frac{1}{r}(\overline{V_r'^2} - \overline{V_\theta'^2})]
\end{aligned} \tag{A2-24}$$

A.3 Equation of Motion in Tangential Direction

$$\rho\left(\frac{DV_\theta}{Dt} + \frac{V_r V_\theta}{r}\right) = F_\theta + \frac{1}{r}\left[\frac{\partial(r\sigma_{r\theta})}{\partial r} + \frac{\partial \sigma_{\theta\theta}}{\partial \theta} + \frac{\partial(r\sigma_{\theta z})}{\partial z}\right] + \frac{1}{r}\sigma_{r\theta}$$

$$= F_\theta + \frac{\partial \sigma_{r\theta}}{\partial r} + \frac{1}{r}\frac{\partial \sigma_{\theta\theta}}{\partial \theta} + \frac{\partial \sigma_{\theta z}}{\partial z} + \frac{2}{r}\sigma_{r\theta} \qquad \text{(A3-1)}$$

To steady state incompressible flow without body force F_θ, equation (A3-1) becomes

$$\rho\left(V_r\frac{\partial V_\theta}{\partial r} + \frac{1}{r}V_\theta\frac{\partial V_\theta}{\partial \theta} + V_z\frac{\partial V_\theta}{\partial z} + \frac{V_r V_\theta}{r}\right)$$

$$= \frac{\partial}{\partial r}(\sigma_{r\theta}) + \frac{1}{r}\cdot\frac{\partial}{\partial \theta}(\sigma_{\theta\theta}) + \frac{\partial}{\partial z}(\sigma_{\theta z}) + \frac{2}{r}(\sigma_{r\theta}) \qquad \text{(A3-2)}$$

From the Continuity Equation (A2-4), there is

$$\rho V_\theta \vec{\nabla}\cdot\vec{q} = \rho\left(V_\theta\frac{\partial V_r}{\partial r} + \frac{1}{r}V_\theta\frac{\partial V_\theta}{\partial \theta} + V_\theta\frac{\partial V_z}{\partial z} + \frac{V_\theta V_r}{r}\right) = 0 \qquad \text{(A3-3)}$$

Substituting equation (A3-3) into (A3-2) yields

$$\rho\left(V_r\frac{\partial V_\theta}{\partial r} + \frac{1}{r}V_\theta\frac{\partial V_\theta}{\partial \theta} + V_z\frac{\partial V_\theta}{\partial z} + \frac{V_r V_\theta}{r}\right) +$$

$$+ \rho\left(V_\theta\frac{\partial V_r}{\partial r} + \frac{1}{r}V_\theta\frac{\partial V_\theta}{\partial \theta} + V_\theta\frac{\partial V_z}{\partial z} + \frac{V_\theta V_r}{r}\right)$$

$$= \rho\left[\frac{\partial}{\partial r}(V_r V_\theta) + \frac{1}{r}\cdot\frac{\partial}{\partial \theta}(V_\theta^2) + \frac{\partial}{\partial z}(V_\theta V_z) + \frac{2}{r}(V_r V_\theta)\right]$$

$$= \frac{\partial}{\partial r}(\sigma_{r\theta}) + \frac{1}{r}\cdot\frac{\partial}{\partial \theta}(\sigma_{\theta\theta}) + \frac{\partial}{\partial z}(\sigma_{\theta z}) + \frac{2}{r}(\sigma_{r\theta}) \qquad \text{(A3-4)}$$

Rearranging equation (A3-4) yields

$$\frac{\partial}{\partial r}(\sigma_{r\theta} - \rho V_r V_\theta) + \frac{1}{r}\cdot\frac{\partial}{\partial \theta}(\sigma_{\theta\theta} - \rho V_\theta^2) + \frac{\partial}{\partial z}(\sigma_{\theta z} - \rho V_\theta V_z) + \frac{2}{r}(\sigma_{r\theta} - \rho V_r V_\theta) = 0 \qquad \text{(A3-5)}$$

Averaging each term of equation (A3-5) yields

$$\frac{\partial}{\partial r}(\bar{\sigma}_{r\theta} - \rho\overline{V_r V_\theta}) + \frac{1}{r}\cdot\frac{\partial}{\partial \theta}(\bar{\sigma}_{\theta\theta} - \rho\overline{V_\theta^2}) + \frac{\partial}{\partial z}(\bar{\sigma}_{\theta z} - \rho\overline{V_\theta V_z}) + \frac{2}{r}(\bar{\sigma}_{r\theta} - \rho\overline{V_r V_\theta}) = 0 \qquad \text{(A3-6)}$$

Since

$$V_r'(t) = V_r(t) - \overline{V}_r$$
$$V_\theta'(t) = V_\theta(t) - \overline{V}_\theta$$
$$V_z'(t) = V_z(t) - \overline{V}_z \qquad \text{(A2-}$$

Applying to equation (A3-6) yields

$$\frac{\partial}{\partial r}(\overline{\sigma}_{r\theta} - \rho\overline{V}_r\overline{V}_\theta - \rho\overline{V_r'V_\theta'}) + \frac{1}{r}\frac{\partial}{\partial\theta}(\overline{\sigma}_{\theta\theta} - \rho\overline{V}_\theta^2 - \rho\overline{V_\theta'^2}) +$$
$$+ \frac{\partial}{\partial z}(\overline{\sigma}_{\theta z} - \rho\overline{V}_\theta\overline{V}_z - \rho\overline{V_\theta'V_z'}) + \frac{2}{r}(\overline{\sigma}_{r\theta} - \rho\overline{V}_r\overline{V}_\theta - \rho\overline{V_r'V_\theta'}) = 0 \qquad \text{(A3-7)}$$

$$\frac{\partial}{\partial r}(\rho\overline{V}_r\overline{V}_\theta) + \frac{1}{r}\frac{\partial}{\partial\theta}(\rho\overline{V}_\theta^2) + \frac{\partial}{\partial z}(\rho\overline{V}_\theta\overline{V}_z) + \frac{2}{r}(\rho\overline{V}_r\overline{V}_\theta)$$
$$= \frac{\partial}{\partial r}(\overline{\sigma}_{r\theta} - \rho\overline{V_r'V_\theta'}) + \frac{1}{r}\frac{\partial}{\partial\theta}(\overline{\sigma}_{\theta\theta} - \rho\overline{V_\theta'^2}) + \frac{\partial}{\partial z}(\overline{\sigma}_{\theta z} - \rho\overline{V_\theta'V_z'}) + \frac{2}{r}(\overline{\sigma}_{r\theta} - \rho\overline{V_r'V_\theta'}) \qquad \text{(A3-8)}$$

$$\rho\overline{V}_r\frac{\partial\overline{V}_\theta}{\partial r} + \rho\overline{V}_\theta\frac{\partial\overline{V}_r}{\partial r} + \frac{2\rho}{r}\overline{V}_\theta\frac{\partial\overline{V}_\theta}{\partial\theta} + \rho\overline{V}_z\frac{\partial\overline{V}_\theta}{\partial z} + \rho\overline{V}_\theta\frac{\partial\overline{V}_z}{\partial z} + \frac{2\rho}{r}\overline{V}_r\overline{V}_\theta$$
$$= \frac{\partial}{\partial r}(\overline{\sigma}_{r\theta} - \rho\overline{V_r'V_\theta'}) + \frac{1}{r}\frac{\partial}{\partial\theta}(\overline{\sigma}_{\theta\theta} - \rho\overline{V_\theta'^2}) + \frac{\partial}{\partial z}(\overline{\sigma}_{\theta z} - \rho\overline{V_\theta'V_z'}) + \frac{2}{r}(\overline{\sigma}_{r\theta} - \rho\overline{V_r'V_\theta'}) \qquad \text{(A3-9)}$$

$$\rho(\overline{V}_r\frac{\partial\overline{V}_\theta}{\partial r} + \frac{1}{r}\overline{V}_\theta\frac{\partial\overline{V}_\theta}{\partial\theta} + \overline{V}_z\frac{\partial\overline{V}_\theta}{\partial z} + \frac{\overline{V}_r\overline{V}_\theta}{r}) + \rho\overline{V}_\theta(\frac{\partial\overline{V}_r}{\partial r} + \frac{1}{r}\frac{\partial\overline{V}_\theta}{\partial\theta} + \frac{\partial\overline{V}_z}{\partial z} + \frac{\overline{V}_r}{r})$$
$$= \rho(\overline{V}_r\frac{\partial\overline{V}_\theta}{\partial r} + \frac{1}{r}\overline{V}_\theta\frac{\partial\overline{V}_\theta}{\partial\theta} + \overline{V}_z\frac{\partial\overline{V}_\theta}{\partial z} + \frac{\overline{V}_r\overline{V}_\theta}{r}) + \rho\overline{V}_\theta\overline{\vec{\nabla}\cdot\vec{q}}$$
$$= \frac{\partial}{\partial r}(\overline{\sigma}_{r\theta} - \rho\overline{V_r'V_\theta'}) + \frac{1}{r}\frac{\partial}{\partial\theta}(\overline{\sigma}_{\theta\theta} - \rho\overline{V_\theta'^2}) + \frac{\partial}{\partial z}(\overline{\sigma}_{\theta z} - \rho\overline{V_\theta'V_z'}) + \frac{2}{r}(\overline{\sigma}_{r\theta} - \rho\overline{V_r'V_\theta'}) \qquad \text{(A3-10)}$$

Since

$$\overline{\vec{\nabla}\cdot\vec{q}} = 0 \qquad \text{(A2-14)}$$

Applying to equation (A3-10) yields

$$\rho(\bar{V}_r\frac{\partial\bar{V}_\theta}{\partial r} + \frac{1}{r}\bar{V}_\theta\frac{\partial\bar{V}_\theta}{\partial\theta} + \bar{V}_z\frac{\partial\bar{V}_\theta}{\partial z} + \frac{\bar{V}_r\bar{V}_\theta}{r})$$
$$= \frac{\partial}{\partial r}(\bar{\sigma}_{r\theta}) + \frac{1}{r}\frac{\partial}{\partial\theta}(\bar{\sigma}_{\theta\theta}) + \frac{\partial}{\partial z}(\bar{\sigma}_{\theta z}) + \frac{2}{r}(\bar{\sigma}_{r\theta}) -$$
$$-[\frac{\partial}{\partial r}(\rho\overline{V_r'V_\theta'}) + \frac{1}{r}\frac{\partial}{\partial\theta}(\rho\overline{V_\theta'^2}) + \frac{\partial}{\partial z}(\rho\overline{V_\theta'V_z'}) + \frac{2}{r}(\rho\overline{V_r'V_\theta'})]$$
$$= S3 + S4 \qquad \text{(A3-11)}$$

where

$$S3 = \frac{\partial}{\partial r}(\bar{\sigma}_{r\theta}) + \frac{1}{r}\frac{\partial}{\partial\theta}(\bar{\sigma}_{\theta\theta}) + \frac{\partial}{\partial z}(\bar{\sigma}_{\theta z}) + \frac{2}{r}(\bar{\sigma}_{r\theta}) \qquad \text{(A3-12)}$$

$$S4 = -[\frac{\partial}{\partial r}(\rho\overline{V_r'V_\theta'}) + \frac{1}{r}\frac{\partial}{\partial\theta}(\rho\overline{V_\theta'^2}) + \frac{\partial}{\partial z}(\rho\overline{V_\theta'V_z'}) + \frac{2}{r}(\rho\overline{V_r'V_\theta'})] \qquad \text{(A3-13)}$$

Since

$$\bar{\sigma}_{\theta z} = \bar{\sigma}_{z\theta} = \mu\bar{\gamma}_{\theta z} = \mu\bar{\gamma}_{z\theta} = \mu(\frac{1}{r}\frac{\partial\bar{V}_z}{\partial\theta} + \frac{\partial\bar{V}_\theta}{\partial z}) \qquad \text{(A3-14)}$$

Substituting equations (A2-18) and (A3-14) into (A3-12) yields

$$S3 = \frac{\partial}{\partial r}[\mu(\frac{\partial\bar{V}_\theta}{\partial r} - \frac{\bar{V}_\theta}{r} + \frac{1}{r}\frac{\partial\bar{V}_r}{\partial\theta})] + \frac{1}{r}\frac{\partial}{\partial\theta}[-\bar{p} + 2\mu(\frac{1}{r}\frac{\partial\bar{V}_\theta}{\partial\theta} + \frac{\bar{V}_r}{r}) - \frac{2}{3}\mu\overrightarrow{\nabla\cdot q}] +$$
$$+ \frac{\partial}{\partial z}[\mu(\frac{1}{r}\frac{\partial\bar{V}_z}{\partial\theta} + \frac{\partial\bar{V}_\theta}{\partial z})] + \mu\frac{2}{r}(\frac{\partial\bar{V}_\theta}{\partial r} - \frac{\bar{V}_\theta}{r} + \frac{1}{r}\frac{\partial\bar{V}_r}{\partial\theta})$$
$$= -\frac{1}{r}\frac{\partial\bar{p}}{\partial\theta} + \mu\frac{\partial^2\bar{V}_\theta}{\partial r^2} + \mu\frac{1}{r}\frac{\partial\bar{V}_\theta}{\partial r} - \mu\frac{\bar{V}_\theta}{r^2} + \mu\frac{1}{r}\frac{\partial^2\bar{V}_r}{\partial\theta\partial r} +$$
$$+ \mu\frac{3}{r^2}\frac{\partial\bar{V}_r}{\partial\theta} + \mu\frac{2}{r^2}\frac{\partial^2\bar{V}_\theta}{\partial\theta^2} + \mu\frac{1}{r}\frac{\partial^2\bar{V}_z}{\partial\theta\partial z} + \mu\frac{\partial^2\bar{V}_\theta}{\partial z^2} \qquad \text{(A3-15)}$$

$$S3 = -\frac{1}{r}\frac{\partial\bar{p}}{\partial\theta} + \frac{\mu}{r}(\frac{\partial^2\bar{V}_r}{\partial\theta\partial r} + \frac{1}{r}\frac{\partial^2\bar{V}_\theta}{\partial\theta^2} + \frac{\partial^2\bar{V}_z}{\partial\theta\partial z} + \frac{1}{r}\frac{\partial\bar{V}_r}{\partial\theta}) +$$
$$+ \mu(\frac{\partial^2\bar{V}_\theta}{\partial r^2} + \frac{1}{r^2}\frac{\partial^2\bar{V}_\theta}{\partial\theta^2} + \frac{\partial^2\bar{V}_\theta}{\partial z^2} + \frac{1}{r}\frac{\partial\bar{V}_\theta}{\partial r} - \frac{\bar{V}_\theta}{r^2} + \frac{2}{r^2}\frac{\partial\bar{V}_r}{\partial\theta})$$
$$= -\frac{1}{r}\frac{\partial\bar{p}}{\partial\theta} + \frac{\mu}{r}\frac{\partial}{\partial\theta}(\overrightarrow{\nabla\cdot q}) + \mu(\frac{\partial^2\bar{V}_\theta}{\partial r^2} + \frac{1}{r^2}\frac{\partial^2\bar{V}_\theta}{\partial\theta^2} + \frac{\partial^2\bar{V}_\theta}{\partial z^2} + \frac{1}{r}\frac{\partial\bar{V}_\theta}{\partial r} - \frac{\bar{V}_\theta}{r^2} + \frac{2}{r^2}\frac{\partial\bar{V}_r}{\partial\theta})$$
(A3-16)

Since

$$\overline{\vec{\nabla}\cdot\vec{q}} = 0 \tag{A2-14}$$

Applying to equation (A3-16) yields

$$S3 = -\frac{1}{r}\frac{\partial \overline{P}}{\partial \theta} + \mu\left(\nabla^2 \overline{V}_\theta - \frac{\overline{V}_\theta}{r^2} + \frac{2}{r^2}\frac{\partial \overline{V}_r}{\partial \theta}\right) \tag{A3-17}$$

Substituting equations (A3-17) and (A3-13) into (A3-11) yields

$$\begin{aligned}
&\rho\left(\overline{V}_r\frac{\partial \overline{V}_\theta}{\partial r} + \frac{1}{r}\overline{V}_\theta\frac{\partial \overline{V}_\theta}{\partial \theta} + \overline{V}_z\frac{\partial \overline{V}_\theta}{\partial z} + \frac{\overline{V}_r\overline{V}_\theta}{r}\right) \\
&= -\frac{1}{r}\frac{\partial \overline{p}}{\partial \theta} + \mu\left(\nabla^2 \overline{V}_\theta - \frac{\overline{V}_\theta}{r^2} + \frac{2}{r^2}\frac{\partial \overline{V}_r}{\partial \theta}\right) - \\
&- \rho\left[\frac{\partial}{\partial r}\left(\overline{V_r' V_\theta'}\right) + \frac{1}{r}\frac{\partial}{\partial \theta}\left(\overline{V_\theta'^2}\right) + \frac{\partial}{\partial z}\left(\overline{V_\theta' V_z'}\right) + \frac{2}{r}\left(\overline{V_r' V_\theta'}\right)\right]
\end{aligned} \tag{A3-18}$$

or Substituting equations (A2-18), (A3-14) into (A3-8) and rearranging equation (A3-8) yields

$$\begin{aligned}
&\frac{\partial}{\partial r}\left(\rho\overline{V}_r\overline{V}_\theta\right) + \frac{1}{r}\frac{\partial}{\partial \theta}\left(\rho\overline{V}_\theta^2\right) + \frac{\partial}{\partial z}\left(\rho\overline{V}_\theta\overline{V}_z\right) + \frac{2}{r}\left(\rho\overline{V}_r\overline{V}_\theta\right) \\
&= -\frac{1}{r}\frac{\partial \overline{p}}{\partial \theta} + \mu\left(\nabla^2 \overline{V}_\theta - \frac{\overline{V}_\theta}{r^2} + \frac{2}{r^2}\frac{\partial \overline{V}_r}{\partial \theta}\right) - \\
&- \rho\left[\frac{\partial}{\partial r}\left(\overline{V_r' V_\theta'}\right) + \frac{1}{r}\frac{\partial}{\partial \theta}\left(\overline{V_\theta'^2}\right) + \frac{\partial}{\partial z}\left(\overline{V_\theta' V_z'}\right) + \frac{2}{r}\left(\overline{V_r' V_\theta'}\right)\right]
\end{aligned} \tag{A3-19}$$

A.4 Equation of Motion in Axial Direction

$$\rho\left(\frac{DV_z}{Dt}\right) = F_z + \frac{1}{r}\left[\frac{\partial(r\sigma_{zr})}{\partial r} + \frac{\partial\sigma_{\theta z}}{\partial\theta} + \frac{\partial(r\sigma_{zz})}{\partial z}\right]$$
$$= F_z + \frac{\partial\sigma_{zr}}{\partial r} + \frac{1}{r}\frac{\partial\sigma_{\theta z}}{\partial\theta} + \frac{\partial\sigma_{zz}}{\partial z} + \frac{1}{r}\sigma_{zr} \qquad \text{(A4-1)}$$

To steady state incompressible flow without body force F_z, equation (A4-1) becomes

$$\rho\left(V_r\frac{\partial V_z}{\partial r} + \frac{1}{r}V_\theta\frac{\partial V_z}{\partial\theta} + V_z\frac{\partial V_z}{\partial z}\right) = \frac{\partial}{\partial r}(\sigma_{zr}) + \frac{1}{r}\frac{\partial}{\partial\theta}(\sigma_{\theta z}) + \frac{\partial}{\partial z}(\sigma_{zz}) + \frac{1}{r}(\sigma_{zr}) \qquad \text{(A4-2)}$$

From the Continuity Equation (A2-4), there is

$$\rho V_z\vec{\nabla}\cdot\vec{q} = \rho\left(V_z\frac{\partial V_r}{\partial r} + \frac{1}{r}V_z\frac{\partial V_\theta}{\partial\theta} + V_z\frac{\partial V_z}{\partial z} + \frac{V_zV_r}{r}\right) = 0 \qquad \text{(A4-3)}$$

Substituting equation (A4-3) into (A4-2) yields

$$\rho\left(V_r\frac{\partial V_z}{\partial r} + \frac{1}{r}V_\theta\frac{\partial V_z}{\partial\theta} + V_z\frac{\partial V_z}{\partial z}\right) + \rho\left(V_z\frac{\partial V_r}{\partial r} + \frac{1}{r}V_z\frac{\partial V_\theta}{\partial\theta} + V_z\frac{\partial V_z}{\partial z} + \frac{V_zV_r}{r}\right)$$
$$= \rho\left[\frac{\partial}{\partial r}(V_rV_z) + \frac{1}{r}\frac{\partial}{\partial\theta}(V_\theta V_z) + \frac{\partial}{\partial z}(V_z^2) + \frac{1}{r}(V_zV_r)\right]$$
$$= \frac{\partial}{\partial r}(\sigma_{zr}) + \frac{1}{r}\frac{\partial}{\partial\theta}(\sigma_{\theta z}) + \frac{\partial}{\partial z}(\sigma_{zz}) + \frac{1}{r}(\sigma_{zr}) \qquad \text{(A4-4)}$$

Rearranging equation (A4-4) yields

$$\frac{\partial}{\partial r}(\sigma_{rr} - \rho V_rV_z) + \frac{1}{r}\frac{\partial}{\partial\theta}(\sigma_{\theta z} - \rho V_\theta V_z) + \frac{\partial}{\partial z}(\sigma_{zz} - \rho V_z^2) + \frac{1}{r}(\sigma_{zr} - \rho V_rV_z) = 0 \qquad \text{(A4-5)}$$

Averaging each term of equation (A4-5) yields

$$\frac{\partial}{\partial r}(\bar{\sigma}_{rr} - \rho\overline{V_rV_z}) + \frac{1}{r}\frac{\partial}{\partial\theta}(\bar{\sigma}_{\theta z} - \rho\overline{V_\theta V_z}) + \frac{\partial}{\partial z}(\bar{\sigma}_{zz} - \rho\overline{V_z^2}) + \frac{1}{r}(\bar{\sigma}_{zr} - \rho\overline{V_rV_z}) = 0 \qquad \text{(A4-6)}$$

Since

$$V_r'(t) = V_r(t) - \overline{V}_r$$
$$V_\theta'(t) = V_\theta(t) - \overline{V}_\theta$$
$$V_z'(t) = V_z(t) - \overline{V}_z \qquad \text{(A2-9)}$$

Applying to equation (A4-6) yields

$$\frac{\partial}{\partial r}(\overline{\sigma}_{zr} - \rho\overline{V}_r\overline{V}_z - \rho\overline{V_r'V_z'}) + \frac{1}{r}\frac{\partial}{\partial\theta}(\overline{\sigma}_{\theta z} - \rho\overline{V}_\theta\overline{V}_z - \rho\overline{V_\theta'V_z'}) +$$
$$+ \frac{\partial}{\partial z}(\overline{\sigma}_{zz} - \rho\overline{V}_z^2 - \rho\overline{V_z'^2}) + \frac{1}{r}(\overline{\sigma}_{zr} - \rho\overline{V}_r\overline{V}_z - \rho\overline{V_r'V_z'}) = 0 \qquad \text{(A4-7)}$$

$$\frac{\partial}{\partial r}(\rho\overline{V}_r\overline{V}_z) + \frac{1}{r}\frac{\partial}{\partial\theta}(\rho\overline{V}_\theta\overline{V}_z) + \frac{\partial}{\partial z}(\rho\overline{V}_z^2) + \frac{1}{r}(\rho\overline{V}_r\overline{V}_z)$$
$$= \frac{\partial}{\partial r}(\overline{\sigma}_{zr} - \rho\overline{V_r'V_z'}) + \frac{1}{r}\frac{\partial}{\partial\theta}(\overline{\sigma}_{\theta z} - \rho\overline{V_\theta'V_z'}) + \frac{\partial}{\partial z}(\overline{\sigma}_{zz} - \rho\overline{V_z'^2}) + \frac{1}{r}(\sigma_{zr} - \rho V_r'V_z') \qquad \text{(A4-8)}$$

$$\rho\overline{V}_r\frac{\partial\overline{V}_z}{\partial r} + \rho\overline{V}_z\frac{\partial\overline{V}_r}{\partial r} + \rho\frac{1}{r}\overline{V}_\theta\frac{\partial\overline{V}_z}{\partial\theta} + \rho\frac{1}{r}\overline{V}_z\frac{\partial\overline{V}_\theta}{\partial\theta} + 2\rho\overline{V}_z\frac{\partial\overline{V}_z}{\partial z} + \frac{\rho}{r}V_rV_z$$
$$= \frac{\partial}{\partial r}(\overline{\sigma}_{zr} - \rho\overline{V_r'V_z'}) + \frac{1}{r}\frac{\partial}{\partial\theta}(\overline{\sigma}_{\theta z} - \rho\overline{V_\theta'V_z'}) + \frac{\partial}{\partial z}(\overline{\sigma}_{zz} - \rho\overline{V_z'^2}) + \frac{1}{r}(\sigma_{zr} - \rho V_r'V_z') \qquad \text{(A4-9)}$$

$$\rho(\overline{V}_r\frac{\partial\overline{V}_z}{\partial r} + \frac{1}{r}\overline{V}_\theta\frac{\partial\overline{V}_z}{\partial\theta} + \overline{V}_z\frac{\partial\overline{V}_z}{\partial z}) + \rho\overline{V}_z(\frac{\partial\overline{V}_r}{\partial r} + \frac{1}{r}\frac{\partial\overline{V}_\theta}{\partial\theta} + \frac{\partial V_z}{\partial z} + \frac{V_r}{r})$$
$$= \rho(\overline{V}_r\frac{\partial\overline{V}_z}{\partial r} + \frac{1}{r}\overline{V}_\theta\frac{\partial\overline{V}_z}{\partial\theta} + \overline{V}_z\frac{\partial\overline{V}_z}{\partial z}) + \rho\overline{V}_z\overline{\vec{\nabla}\cdot\vec{q}}$$
$$= \frac{\partial}{\partial r}(\overline{\sigma}_{zr} - \rho\overline{V_r'V_z'}) + \frac{1}{r}\frac{\partial}{\partial\theta}(\overline{\sigma}_{\theta z} - \rho\overline{V_\theta'V_z'}) + \frac{\partial}{\partial z}(\overline{\sigma}_{zz} - \rho\overline{V_z'^2}) + \frac{1}{r}(\sigma_{zr} - \rho\overline{V_r'V_z'}) \qquad \text{(A4-10)}$$

Since

$$\overline{\vec{\nabla}\cdot\vec{q}} = 0 \qquad \text{(A2-14)}$$

Applying to equation (A4-10) yields

$$\rho(\overline{V}_r\frac{\partial\overline{V}_z}{\partial r} + \frac{1}{r}\overline{V}_\theta\frac{\partial\overline{V}_z}{\partial\theta} + \overline{V}_z\frac{\partial\overline{V}_z}{\partial z})$$

$$= \frac{\partial}{\partial r}(\bar{\sigma}_{zr}) + \frac{1}{r}\frac{\partial}{\partial \theta}(\bar{\sigma}_{\theta z}) + \frac{\partial}{\partial z}(\bar{\sigma}_{zz}) + \frac{1}{r}(\bar{\sigma}_{zr}) -$$
$$- [\frac{\partial}{\partial r}(\rho\overline{V_r'V_z'}) + \frac{1}{r}\frac{\partial}{\partial \theta}(\rho\overline{V_\theta'V_z'}) + \frac{\partial}{\partial z}(\rho\overline{V_z'^2}) + \frac{1}{r}(\rho\overline{V_r'V_z'})]$$
$$= S5 + S6 \qquad \text{(A4-11)}$$

where

$$S5 = \frac{\partial}{\partial r}(\bar{\sigma}_{zr}) + \frac{1}{r}\frac{\partial}{\partial \theta}(\bar{\sigma}_{\theta z}) + \frac{\partial}{\partial z}(\bar{\sigma}_{zz}) + \frac{1}{r}(\bar{\sigma}_{zr}) \qquad \text{(A4-12)}$$

$$S6 = - [\frac{\partial}{\partial r}(\rho\overline{V_r'V_z'}) + \frac{1}{r}\frac{\partial}{\partial \theta}(\rho\overline{V_\theta'V_z'}) + \frac{\partial}{\partial z}(\rho\overline{V_z'^2}) + \frac{1}{r}(\rho\overline{V_r'V_z'})] \qquad \text{(A4-13)}$$

Since

$$\bar{\sigma}_{zz} = - \bar{p} + 2\mu\bar{\varepsilon}_{zz} - \frac{2}{3}\mu\overline{\vec{\nabla}\cdot\vec{q}} = - \bar{p} + 2\mu\frac{\partial \bar{V}_z}{\partial z} - \frac{2}{3}\mu\overline{\vec{\nabla}\cdot\vec{q}} \qquad \text{(A4-14)}$$

Substituting equations (A2-18), (A3-14) and (A4-14) into (A4-12) yields

$$S5 = \frac{\partial}{\partial r}[\mu(\frac{\partial \bar{V}_r}{\partial z} + \frac{\partial \bar{V}_z}{\partial r})] + \frac{1}{r}\frac{\partial}{\partial \theta}[\mu(\frac{1}{r}\frac{\partial \bar{V}_z}{\partial \theta} + \frac{\partial \bar{V}_\theta}{\partial z})] +$$
$$+ \frac{\partial}{\partial z}(- \bar{p} + 2\mu\frac{\partial \bar{V}_z}{\partial z} - \frac{2}{3}\mu\overline{\vec{\nabla}\cdot\vec{q}}) + \mu\frac{1}{r}(\frac{\partial \bar{V}_r}{\partial z} + \frac{\partial \bar{V}_z}{\partial r})$$
$$= - \frac{\partial \bar{p}}{\partial z} + \mu\frac{\partial^2 \bar{V}_r}{\partial r \partial z} + \mu\frac{\partial^2 \bar{V}_z}{\partial r^2} + \mu\frac{1}{r^2}\frac{\partial^2 \bar{V}_z}{\partial \theta^2} + \mu\frac{1}{r}\frac{\partial^2 \bar{V}_\theta}{\partial \theta \partial z} + 2\mu\frac{\partial^2 \bar{V}_z}{\partial z^2} +$$
$$+ \mu\frac{1}{r}\frac{\partial \bar{V}_r}{\partial z} + \mu\frac{1}{r}\frac{\partial \bar{V}_z}{\partial r} \qquad \text{(A4-15)}$$

$$S5 = - \frac{\partial \bar{p}}{\partial z} + \mu(\frac{\partial^2 \bar{V}_r}{\partial z \partial r} + \frac{1}{r}\frac{\partial^2 \bar{V}_\theta}{\partial z \partial \theta} + \frac{\partial^2 \bar{V}_z}{\partial z^2} + \frac{1}{r}\frac{\partial \bar{V}_r}{\partial z}) +$$
$$+ \mu(\frac{\partial^2 \bar{V}_z}{\partial r^2} + \frac{1}{r^2}\frac{\partial^2 \bar{V}_z}{\partial \theta^2} + \frac{\partial^2 \bar{V}_z}{\partial z^2} + \frac{1}{r}\frac{\partial \bar{V}_z}{\partial r})$$
$$= - \frac{\partial \bar{p}}{\partial z} + \mu\frac{\partial}{\partial z}(\overline{\vec{\nabla}\cdot\vec{q}}) + \mu(\frac{\partial^2 \bar{V}_z}{\partial r^2} + \frac{1}{r^2}\frac{\partial^2 \bar{V}_z}{\partial \theta^2} + \frac{\partial^2 \bar{V}_z}{\partial z^2} + \frac{1}{r}\frac{\partial \bar{V}_z}{\partial r}) \qquad \text{(A4-16)}$$

Since

$$\overline{\vec{\nabla}\cdot\vec{q}^{\,\cdot}} = 0 \tag{A2-14}$$

Applying to equation (A-59) yields

$$S5 = -\frac{\partial \overline{p}}{\partial z} + \mu \nabla^2 \overline{V}_z \tag{A4-17}$$

Substituting equations (A4-17) and (A4-13) into (A4-11) yields

$$\rho(\overline{V}_r\frac{\partial \overline{V}_z}{\partial r} + \frac{1}{r}\overline{V}_\theta\frac{\partial \overline{V}_z}{\partial \theta} + \overline{V}_z\frac{\partial \overline{V}_z}{\partial z})$$
$$= -\frac{\partial \overline{p}}{\partial z} + \mu \nabla^2 \overline{V}_z - \rho[\frac{\partial}{\partial r}(\overline{V_r'V_z'}) + \frac{1}{r}\cdot\frac{\partial}{\partial \theta}(\overline{V_\theta'V_z'}) + \frac{\partial}{\partial z}(\overline{V_z'^2}) + \frac{1}{r}(\overline{V_r'V_z'})] \tag{A4-18}$$

or Substituting equations (A2-18), (A3-14), (A4-14) into (A4-8) and rearranging equation (A4-8) yields

$$\frac{\partial}{\partial r}(\rho\overline{V}_r\overline{V}_z) + \frac{1}{r}\cdot\frac{\partial}{\partial \theta}(\rho\overline{V}_\theta\overline{V}_z) + \frac{\partial}{\partial z}(\rho\overline{V}_z^2) + \frac{1}{r}(\rho\overline{V}_r\overline{V}_z)$$
$$= -\frac{\partial \overline{p}}{\partial z} + \mu \nabla^2 \overline{V}_z - \rho[\frac{\partial}{\partial r}(\overline{V_r'V_z'}) + \frac{1}{r}\cdot\frac{\partial}{\partial \theta}(\overline{V_\theta'V_z'}) + \frac{\partial}{\partial z}(\overline{V_z'^2}) + \frac{1}{r}(\overline{V_r'V_z'})] \tag{A4-19}$$

A.5 Equations of Kinetic Energy for Mean Motion

A.5.1 Equation for Radial Direction

Multiplying mean radial velocity, $\overline{V}_r$, on the equation of motion in the radial direction, equation (A2-23), yields the equation of kinetic energy for the mean motion in the radial direction as follows:

$$\overline{V}_r\frac{\partial}{\partial r}(\frac{1}{2}\overline{V}_r^2) + \frac{1}{r}\overline{V}_\theta\frac{\partial}{\partial\theta}(\frac{1}{2}\overline{V}_r^2) + \overline{V}_z\frac{\partial}{\partial z}(\frac{1}{2}\overline{V}_r^2) - \overline{V}_r\frac{\overline{V}_\theta^2}{r}$$
$$= -\frac{\overline{V}_r}{\rho}\frac{\partial\overline{p}}{\partial r} + \nu\overline{V}_r(\nabla^2\overline{V}_r - \frac{\overline{V}_r}{r^2} - \frac{2}{r^2}\frac{\partial\overline{V}_\theta}{\partial\theta}) -$$
$$-\overline{V}_r[\frac{\partial}{\partial r}(\overline{V_r'^2}) + \frac{1}{r}\frac{\partial}{\partial\theta}(\overline{V_r'V_\theta'}) + \frac{\partial}{\partial z}(\overline{V_r'V_z'}) + \frac{1}{r}(\overline{V_r'^2} - \overline{V_\theta'^2})] \qquad (A5\text{-}1)$$

Combining above equation with the equation of continuity yields the expression of the rate of change of kinetic energy in the radial direction for the mean motion as follows:

$$\frac{\partial}{\partial r}(\frac{1}{2}\overline{V}_r^2\cdot\overline{V}_r) + \frac{1}{r}\frac{\partial}{\partial\theta}(\frac{1}{2}\overline{V}_r^2\cdot\overline{V}_\theta) + \frac{\partial}{\partial z}(\frac{1}{2}\overline{V}_r^2\cdot\overline{V}_z)$$
$$= -\frac{\overline{V}_r}{\rho}\frac{\partial\overline{p}}{\partial r} + \nu\overline{V}_r(\nabla^2\overline{V}_r - \frac{\overline{V}_r}{r^2} - \frac{2}{r^2}\frac{\partial\overline{V}_\theta}{\partial\theta}) -$$
$$-\overline{V}_r[\frac{\partial}{\partial r}(\overline{V_r'^2}) + \frac{1}{r}\frac{\partial}{\partial\theta}(\overline{V_r'V_\theta'}) + \frac{\partial}{\partial z}(\overline{V_r'V_z'}) + \frac{1}{r}(\overline{V_r'^2} - \overline{V_\theta'^2})] - \frac{\overline{V}_r}{r}(\frac{1}{2}V_r^2 - V_\theta^2) \qquad (A5\text{-}2)$$

To an axisymmetric flow with negligible axial gradient, the equation of kinetic energy, equation (A5-1), can be simplified as follows:

$$\overline{V}_r\frac{\partial}{\partial r}(\frac{1}{2}\overline{V}_r^2) - \overline{V}_r(\frac{\overline{V}_\theta^2}{r})$$
$$= -\frac{\overline{V}_r}{\rho}\frac{\partial\overline{p}}{\partial r} + \nu\overline{V}_r[(\frac{\partial^2\overline{V}_r}{\partial r^2} + \frac{1}{r}\frac{\partial\overline{V}_r}{\partial r}) - \frac{\overline{V}_r}{r^2}] - \overline{V}_r[\frac{\partial}{\partial r}(\overline{V_r'^2}) + \frac{1}{r}(\overline{V_r'^2} - \overline{V_\theta'^2})] \qquad (A5\text{-}3)$$

Dividing $\overline{V}_r$ on equation (A5-3) and integrating that equation yield the expression of kinetic energy for the mean motion of vortex flows in the radial direction as follows:

$$\frac{1}{2}\overline{V}_r^2 = \int \{-\frac{1}{\rho}\frac{\partial \overline{p}}{\partial r} + \nu(\frac{\partial^2 \overline{V}_r}{\partial r^2} + \frac{1}{r}\frac{\partial \overline{V}_r}{\partial r} - \frac{\overline{V}_r}{r^2}) -$$
$$- [\frac{\partial}{\partial r}(\overline{V_r'^2}) + \frac{1}{r}(\overline{V_r'^2} - \overline{V_\theta'^2})] + \frac{\overline{V}_\theta^2}{r}\} dr \qquad \text{(A5-4)}$$

A.5.2 Equation for Tangential Direction

Multiplying mean tangential velocity, $\overline{V}_\theta$, on the equation of motion in the tangential direction, equation (A3-18), yields the equation of kinetic energy for the mean motion in the tangential direction as follows:

$$\overline{V}_r\frac{\partial}{\partial r}(\frac{1}{2}\overline{V}_\theta^2) + \frac{1}{r}\overline{V}_\theta\frac{\partial}{\partial \theta}(\frac{1}{2}\overline{V}_\theta^2) + \overline{V}_z\frac{\partial}{\partial z}(\frac{1}{2}\overline{V}_\theta^2) + \frac{2\overline{V}_r}{r}(\frac{1}{2}\overline{V}_\theta^2)$$
$$= -\frac{\overline{V}_\theta}{\rho r}\frac{\partial \overline{p}}{\partial \theta} + \nu\overline{V}_\theta(\nabla^2\overline{V}_\theta - \frac{\overline{V}_\theta}{r^2} + \frac{2}{r^2}\frac{\partial \overline{V}_r}{\partial \theta}) -$$
$$- \overline{V}_\theta[\frac{\partial}{\partial r}(\overline{V_r'V_\theta'}) + \frac{1}{r}\frac{\partial}{\partial \theta}(\overline{V_\theta'^2}) + \frac{\partial}{\partial z}(\overline{V_\theta'V_z'}) + \frac{2}{r}\overline{V_r'V_\theta'}] \qquad \text{(A5-5)}$$

Combining above equation with the equation of continuity yields the expression of the rate of change of kinetic energy in the tangential direction for the mean motion as follows:

$$\frac{\partial}{\partial r}(\frac{1}{2}\overline{V}_\theta^2\cdot\overline{V}_r) + \frac{1}{r}\frac{\partial}{\partial \theta}(\frac{1}{2}\overline{V}_\theta^2\cdot\overline{V}_\theta) + \frac{\partial}{\partial z}(\frac{1}{2}\overline{V}_\theta^2\cdot\overline{V}_z)$$
$$= -\frac{\overline{V}_\theta}{\rho r}\frac{\partial \overline{p}}{\partial \theta} + \nu\overline{V}_\theta(\nabla^2\overline{V}_\theta - \frac{\overline{V}_\theta}{r^2} + \frac{2}{r^2}\frac{\partial \overline{V}_r}{\partial \theta}) -$$
$$- \overline{V}_\theta[\frac{\partial}{\partial r}(\overline{V_r'V_\theta'}) + \frac{1}{r}\frac{\partial}{\partial \theta}(\overline{V_\theta'^2}) + \frac{\partial}{\partial z}(\overline{V_\theta'V_z'}) + \frac{2}{r}\overline{V_r'V_\theta'}] - \frac{3}{2r}\overline{V}_r\overline{V}_\theta^2 \qquad \text{(A5-6)}$$

To an axisymmetric flow with neglible axial gradient, the equation of kinetic energy, equation (A5-5), can be simplified as follows:

$$\overline{V}_r\frac{\partial}{\partial r}(\frac{1}{2}\overline{V}_\theta^2) + \overline{V}_r(\frac{\overline{V}_\theta^2}{r})$$
$$= \nu\overline{V}_\theta(\frac{\partial^2\overline{V}_\theta}{\partial r^2} + \frac{1}{r}\frac{\partial \overline{V}_\theta}{\partial r} - \frac{\overline{V}_\theta}{r^2}) - \overline{V}_\theta[\frac{\partial}{\partial r}(\overline{V_r'V_\theta'}) + \frac{2}{r}\overline{V_r'V_\theta'}] \qquad \text{(A5-7)}$$

Dividing $\overline{V}_r$ on equation (A5-7) and integrating that equation yield the expression of kinetic energy for the mean motion of vortex flows in the tangential direction as follows:

$$\frac{1}{2}\overline{V}_\theta^2 = \int \{\nu\frac{\overline{V}_\theta}{\overline{V}_r}(\frac{\partial^2\overline{V}_\theta}{\partial r^2} + \frac{1}{r}\frac{\partial\overline{V}_\theta}{\partial r} - \frac{\overline{V}_\theta}{r^2}) - \\ - \frac{\overline{V}_\theta}{\overline{V}_r}[\frac{\partial}{\partial r}(\overline{V_r'V_\theta'}) + \frac{2}{r}\overline{V_r'V_\theta'}] - \frac{\overline{V}_\theta^2}{r}\} dr \qquad (A5\text{-}8)$$

A.5.3 Equation for Axial Direction

Multiplying mean axial velocity, $\overline{V}_z$, on the equation of motion in the axial direction, equation (A4-18), yields the equation of kinetic energy for the mean motion in the axial direction as follows:

$$\overline{V}_r\frac{\partial}{\partial r}(\frac{1}{2}\overline{V}_z^2) + \frac{1}{r}\overline{V}_\theta\frac{\partial}{\partial\theta}(\frac{1}{2}\overline{V}_z^2) + \overline{V}_z\frac{\partial}{\partial z}(\frac{1}{2}\overline{V}_z^2) \\ = -\frac{\overline{V}_z}{\rho}\frac{\partial\overline{p}}{\partial z} + \nu\overline{V}_z\nabla^2\overline{V}_z - \overline{V}_z[\frac{\partial}{\partial r}(\overline{V_r'V_z'}) + \frac{1}{r}\frac{\partial}{\partial\theta}(\overline{V_\theta'V_z'}) + \frac{\partial}{\partial z}(\overline{V_z'^2}) + \frac{1}{r}V_r'V_z'] \qquad (A5\text{-}9)$$

Combining above equation with the equation of continuity yields the expression of the rate of change of kinetic energy in the axial direction for the mean motion as follows:

$$\frac{\partial}{\partial r}(\frac{1}{2}\overline{V}_z^2\cdot\overline{V}_r) + \frac{1}{r}\frac{\partial}{\partial\theta}(\frac{1}{2}\overline{V}_z^2\cdot\overline{V}_\theta) + \frac{\partial}{\partial z}(\frac{1}{2}\overline{V}_z^2\cdot\overline{V}_z) \\ = -\frac{\overline{V}_z}{\rho}\frac{\partial\overline{p}}{\partial z} + \nu\overline{V}_z\nabla^2\overline{V}_z - \overline{V}_z[\frac{\partial}{\partial r}(\overline{V_r'V_z'}) + \frac{1}{r}\frac{\partial}{\partial\theta}(\overline{V_\theta'V_z'}) + \frac{\partial}{\partial z}(\overline{V_z'^2}) + \frac{1}{r}V_r'V_z'] - \\ - \frac{\overline{V}_r}{r}(\frac{1}{2}\overline{V}_z^2) \qquad (A5\text{-}10)$$

To an axisymmetric flow with negligible axial gradient, the equation of kinetic energy, equation (A5-9), can be simplified as follows:

$$\overline{V}_r\frac{\partial}{\partial r}(\frac{1}{2}\overline{V}_z^2) = \nu\overline{V}_z(\frac{\partial^2\overline{V}_z}{\partial r^2} + \frac{1}{r}\frac{\partial\overline{V}_z}{\partial r}) - \overline{V}_z[\frac{\partial}{\partial r}(\overline{V_r'V_z'}) + \frac{1}{r}\overline{V_r'V_z'}] \qquad (A5\text{-}11)$$

Dividing $\overline{V}_r$ on equation (A5-11) and integrating that equation yield the expression of kinetic energy for the mean motion of vortex flows in the axial direction as follows:

$$\frac{1}{2}\overline{V}_z^2 = \int \{\nu\frac{\overline{V}_z}{\overline{V}_r}(\frac{\partial^2\overline{V}_z}{\partial r^2} + \frac{1}{r}\cdot\frac{\partial\overline{V}_z}{\partial r}) - \frac{\overline{V}_z}{\overline{V}_r}[\frac{\partial}{\partial r}(\overline{V_r'V_z'}) + \frac{1}{r}\overline{V_r'V_z'}]\}\, dr \qquad \text{(A5-12)}$$

A.6 Equations of Total Kinetic Energy

A.6.1 Equation for Radial Direction

To a steady state incompressible flow without body forces, the equation of motion in the radial direction is as follows:

$$\rho(V_r\frac{\partial V_r}{\partial r} + \frac{1}{r}V_\theta\frac{\partial V_r}{\partial \theta} + V_z\frac{\partial V_r}{\partial z} - \frac{V_\theta^2}{r})$$
$$= -\frac{\partial p}{\partial r} + \mu\nabla^2 V_r - \mu(\frac{V_r}{r^2} + \frac{2}{r^2}\frac{\partial V_\theta}{\partial \theta}) \qquad (A6\text{-}1)$$

Multiplying radial velocity, V_r, on the equation of motion in the radial direction, equation (A6-1), yields the equation of total kinetic energy in the radial direction for a steady state incompressible flow without body forces as follows:

$$V_r\frac{\partial}{\partial r}(\frac{1}{2}V_r^2) + \frac{1}{r}V_\theta\frac{\partial}{\partial \theta}(\frac{1}{2}V_r^2) + V_z\frac{\partial}{\partial z}(\frac{1}{2}V_r^2) - V_r\frac{V_\theta^2}{r}$$
$$= -\frac{V_r}{\rho}\frac{\partial p}{\partial r} + \nu V_r\nabla^2 V_r - \frac{\nu}{r^2}V_r^2 - \frac{2\nu}{r^2}V_r\frac{\partial V_\theta}{\partial \theta} \qquad (A6\text{-}2)$$

Applying the statistical principle of turbulent flow to above equation yields the equation of total kinetic energy in radial direction for turbulent flows as follows:

$$[\overline{V}_r\frac{\partial}{\partial r}(\frac{1}{2}\overline{V}_r^2) + \frac{1}{r}\overline{V}_\theta\frac{\partial}{\partial \theta}(\frac{1}{2}\overline{V}_r^2) + \overline{V}_z\frac{\partial}{\partial z}(\frac{1}{2}\overline{V}_r^2)] +$$
$$+ [\overline{V}_r\frac{\partial}{\partial r}(\frac{1}{2}\overline{V_r'^2}) + \frac{1}{r}\overline{V}_\theta\frac{\partial}{\partial \theta}(\frac{1}{2}\overline{V_r'^2}) + \overline{V}_z\frac{\partial}{\partial z}(\frac{1}{2}\overline{V_r'^2})]$$
$$= -\frac{\overline{V}_r}{\rho}\frac{\partial p}{\partial r} + \nu(\overline{V}_r\overline{\nabla^2 V_r} + \overline{V_r'\nabla^2 V_r'} - \frac{\overline{V}_r^2}{r^2} - \frac{\overline{V_r'^2}}{r^2} -$$
$$- \frac{2}{r^2}\overline{V}_r\frac{\partial \overline{V}_\theta}{\partial \theta} - \frac{2}{r^2}\overline{V_r'\frac{\partial V_\theta'}{\partial \theta}}) - \frac{1}{2}[\overline{V_r\frac{\partial}{\partial r}(V_r^2)} + \frac{1}{r}\overline{V_\theta'\frac{\partial}{\partial \theta}(V_r^2)} + \overline{V_z'\frac{\partial}{\partial z}(V_r^2)}] +$$
$$+ \frac{1}{r}(\overline{V}_r\overline{V}_\theta^2 + \overline{V}_r\overline{V_\theta'^2} + \overline{V_r'V_\theta^2}) \qquad (A6\text{-}3)$$

Combining equation (A6-2) with the equation of continuity yields the expression of the rate of change of total kinetic energy in the radial direction for the turbulent flows as follows:

$$
\begin{aligned}
&[\frac{\partial}{\partial r}(\frac{1}{2}\overline{V}_r^2 \cdot \overline{V}_r) + \frac{1}{r}\frac{\partial}{\partial \theta}(\frac{1}{2}\overline{V}_r^2 \cdot \overline{V}_\theta) + \frac{\partial}{\partial z}(\frac{1}{2}\overline{V}_r^2 \cdot \overline{V}_z)] + \\
&+ [\frac{\partial}{\partial r}(\frac{1}{2}\overline{V_r'^2} \cdot \overline{V}_r) + \frac{1}{r}\frac{\partial}{\partial \theta}(\frac{1}{2}\overline{V_r'^2} \cdot \overline{V}_\theta) + \frac{\partial}{\partial z}(\frac{1}{2}\overline{V_r'^2} \cdot \overline{V}_z)] \\
&= -\frac{\overline{V}_r}{\rho}\frac{\partial p}{\partial r} + \nu(\overline{V}_r\overline{\nabla^2 V_r} + \overline{V_r'\nabla^2 V_r'} - \frac{\overline{V}_r^2}{r^2} - \frac{\overline{V_r'^2}}{r^2} - \\
&- \frac{2}{r^2}\overline{V}_r\frac{\partial \overline{V}_\theta}{\partial \theta} - \frac{2}{r^2}\overline{V_r'\frac{\partial V_\theta'}{\partial \theta}}) - \frac{1}{2}[\overline{\frac{\partial}{\partial r}(V_r'^2 \cdot V_r')} + \frac{1}{r}\overline{\frac{\partial}{\partial \theta}(V_r'^2 \cdot V_\theta')} + \overline{\frac{\partial}{\partial z}(V_r'^2 \cdot V_z')}] + \\
&+ \frac{1}{r}(\overline{V}_r\overline{V}_\theta^2 + \overline{V}_r\overline{V_\theta'^2} + \overline{V_r'V_\theta'^2}) - \frac{1}{2r}(\overline{V}_r\overline{V}_r^2 + \overline{V}_r\overline{V_r'^2} + \overline{V_r'V_r'^2})
\end{aligned}
\qquad \text{(A6-4)}
$$

To an axisymmetric flow with negligible axial gradient, the equation of total kinetic energy, equation (A6-3), can be simplified as follows:

$$
\begin{aligned}
&\frac{\partial}{\partial r}(\frac{1}{2}\overline{V}_r^2) + \frac{\partial}{\partial r}(\frac{1}{2}\overline{V_r'^2}) \\
&= -\frac{1}{\rho}\frac{\partial p}{\partial r} + \frac{\nu}{\overline{V}_r}(\overline{V}_r\overline{\nabla^2 V_r} + \overline{V_r'\nabla^2 V_r'} - \frac{2}{r^2}\overline{V}_r^2 - \frac{2}{r^2}\overline{V_r'^2}) - \\
&- \frac{1}{\overline{V}_r}[\frac{1}{2}\overline{V_r'\frac{\partial}{\partial r}(V_r'^2)} - \frac{1}{r}\overline{V_r'V_\theta'^2}] + \frac{1}{r}(\overline{V}_\theta^2 + \overline{V_\theta'^2})
\end{aligned}
\qquad \text{(A6-5)}
$$

or

$$
\begin{aligned}
&\frac{1}{2}\overline{V}_r^2 + \frac{1}{2}\overline{V_r'^2} \\
&= \int \{-\frac{1}{\rho}\frac{\partial p}{\partial r} + \frac{\nu}{\overline{V}_r}(\overline{V}_r\overline{\nabla^2 V_r} + \overline{V_r'\nabla^2 V_r'} - \frac{2}{r^2}\overline{V}_r^2 - \frac{2}{r^2}\overline{V_r'^2}) - \\
&- \frac{1}{\overline{V}_r}[\frac{1}{2}\overline{V_r'\frac{\partial}{\partial r}(V_r'^2)} - \frac{1}{r}\overline{V_r'V_\theta'^2}] + \frac{1}{r}(\overline{V}_\theta^2 + \overline{V_\theta'^2})\}\, dr
\end{aligned}
\qquad \text{(A6-6)}
$$

where

$$\nabla^2 = \frac{\partial^2}{\partial r^2} + \frac{1}{r}\frac{\partial}{\partial r}$$

A.6.2 Equation for Tangential Direction

To a steady state incompressible flow without body forces, the equation of motion in the tangential direction is as follows:

$$\rho(V_r\frac{\partial V_\theta}{\partial r} + \frac{1}{r}V_\theta\frac{\partial V_\theta}{\partial \theta} + V_z\frac{\partial V_\theta}{\partial z} + \frac{V_rV_\theta}{r})$$
$$= -\frac{1}{r}\frac{\partial p}{\partial \theta} + \mu\nabla^2 V_\theta - \mu(\frac{V_\theta}{r^2} - \frac{2}{r^2}\frac{\partial V_r}{\partial \theta}) \qquad \text{(A6-7)}$$

Multiplying tangential velocity, V_θ, on the equation of motion in the tangential direction, equation (A6-7), yields the equation of total kinetic energy in the tangential direction for a steady state incompressible flow without body forces as follows:

$$V_r\frac{\partial}{\partial r}(\frac{1}{2}V_\theta^2) + \frac{1}{r}V_\theta\frac{\partial}{\partial \theta}(\frac{1}{2}V_\theta^2) + V_z\frac{\partial}{\partial z}(\frac{1}{2}V_\theta^2) + \frac{V_rV_\theta^2}{r}$$
$$= -\frac{V_\theta}{\rho r}\frac{\partial p}{\partial \theta} + \nu V_\theta\nabla^2 V_\theta - \frac{\nu}{r^2}V_\theta^2 + \frac{2\nu}{r^2}V_\theta\frac{\partial V_r}{\partial \theta} \qquad \text{(A6-8)}$$

Applying the statistical principle of turbulent flow to above equation yields the equation of total kinetic energy in tangential direction for turbulent flows as follows:

$$[\overline{V}_r\frac{\partial}{\partial r}(\frac{1}{2}\overline{V}_\theta^2) + \frac{1}{r}\overline{V}_\theta\frac{\partial}{\partial \theta}(\frac{1}{2}\overline{V}_\theta^2) + \overline{V}_z\frac{\partial}{\partial z}(\frac{1}{2}\overline{V}_\theta^2)] +$$
$$+ [\overline{V}_r\frac{\partial}{\partial r}(\frac{1}{2}\overline{V_\theta'^2}) + \frac{1}{r}\overline{V}_\theta\frac{\partial}{\partial \theta}(\frac{1}{2}\overline{V_\theta'^2}) + \overline{V}_z\frac{\partial}{\partial z}(\frac{1}{2}\overline{V_\theta'^2})]$$
$$= -\frac{\overline{V}_\theta}{\rho r}\frac{\partial \overline{p}}{\partial \theta} + \nu(\overline{V}_\theta\overline{\nabla^2 V_\theta} + \overline{V_\theta'\nabla^2 V_\theta'} - \frac{\overline{V}_\theta^2}{r^2} - \frac{\overline{V_\theta'^2}}{r^2} +$$
$$+ \frac{2}{r^2}\overline{V}_\theta\frac{\partial \overline{V}_r}{\partial \theta} + \frac{2}{r^2}\overline{V_\theta'\frac{\partial V_r'}{\partial \theta}}) - \frac{1}{2}[\overline{V_r'\frac{\partial}{\partial r}(V_\theta'^2)} + \frac{1}{r}\overline{V_\theta'\frac{\partial}{\partial \theta}(V_\theta'^2)} + \overline{V_z'\frac{\partial}{\partial z}(V_\theta'^2)}] -$$
$$- \frac{1}{r}(\overline{V}_r\overline{V}_\theta^2 + \overline{V}_r\overline{V_\theta'^2} + \overline{V_r'V_\theta'^2}) \qquad \text{(A6-9)}$$

Combining equation (A6-8) with the equation of continuity yields the expression of the rate of change of total kinetic energy in the tangential direction for the turbulent flows as follows:

$$[\frac{\partial}{\partial r}(\frac{1}{2}\overline{V}_\theta^2 \cdot \overline{V}_r) + \frac{1}{r}\frac{\partial}{\partial \theta}(\frac{1}{2}\overline{V}_\theta^2 \cdot \overline{V}_\theta) + \frac{\partial}{\partial z}(\frac{1}{2}\overline{V}_\theta^2 \cdot \overline{V}_z)] +$$
$$+ [\frac{\partial}{\partial r}(\frac{1}{2}\overline{V_\theta'^2} \cdot \overline{V}_r) + \frac{1}{r}\frac{\partial}{\partial \theta}(\frac{1}{2}\overline{V_\theta'^2} \cdot \overline{V}_\theta) + \frac{\partial}{\partial z}(\frac{1}{2}\overline{V_\theta'^2} \cdot \overline{V}_z)]$$
$$= -\frac{\overline{V}_\theta}{\rho r}\frac{\partial p}{\partial \theta} + \nu(\overline{V}_\theta \overline{\nabla^2 V_\theta} + \overline{V_\theta' \nabla^2 V_\theta'} - \frac{\overline{V}_\theta^2}{r^2} - \frac{\overline{V_\theta'^2}}{r^2} +$$
$$+ \frac{2}{r^2}\overline{V}_\theta \frac{\partial \overline{V}_r}{\partial \theta} + \frac{2}{r^2}\overline{V_\theta' \frac{\partial V_r'}{\partial \theta}}) - \frac{1}{2}[\overline{\frac{\partial}{\partial r}(V_\theta'^2 V_r')} + \frac{1}{r}\overline{\frac{\partial}{\partial \theta}(V_\theta'^2 V_\theta')} + \overline{\frac{\partial}{\partial z}(V_\theta'^2 V_z')}] -$$
$$- \frac{3}{2r}(\overline{V}_r \overline{V}_\theta^2 + \overline{V}_r \overline{V_\theta'^2} + \overline{V_r' V_\theta'^2}) \qquad \text{(A6-10)}$$

To an axisymmetric flow with negligible axial gradient, the equation of total kinetic energy, equation (A6-9), can be simplified as follows:

$$\frac{\partial}{\partial r}(\frac{1}{2}\overline{V}_\theta^2) + \frac{\partial}{\partial r}(\frac{1}{2}\overline{V_\theta'^2})$$
$$= \frac{\nu}{\overline{V}_r}(\overline{V}_\theta \overline{\nabla^2 V_\theta} + \overline{V_\theta' \nabla^2 V_\theta'} - \frac{\overline{V}_\theta^2}{r^2} - \frac{\overline{V_\theta'^2}}{r^2}) -$$
$$- \frac{1}{\overline{V}_r}[\frac{1}{2}\overline{V_r' \frac{\partial}{\partial r}(V_\theta'^2)} + \frac{1}{r}\overline{V_r' V_\theta'^2}] - \frac{1}{r}(\overline{V}_\theta^2 + \overline{V_\theta'^2}) \qquad \text{(A6-11)}$$

or

$$\frac{1}{2}\overline{V}_\theta^2 + \frac{1}{2}\overline{V_\theta'^2}$$
$$= \int \{\frac{\nu}{\overline{V}_r}(\overline{V}_\theta \overline{\nabla^2 V_\theta} + \overline{V_\theta' \nabla^2 V_\theta'} - \frac{\overline{V}_\theta^2}{r^2} - \frac{\overline{V_\theta'^2}}{r^2}) -$$
$$- \frac{1}{\overline{V}_r}[\frac{1}{2}\overline{V_r' \frac{\partial}{\partial r}(V_\theta'^2)} + \frac{1}{r}\overline{V_r' V_\theta'^2}] - \frac{1}{r}(\overline{V}_\theta^2 + \overline{V_\theta'^2})\} \, dr \qquad \text{(A6-12)}$$

A.6.3 Equation for Axial Direction

For a steady state incompressible flow without body forces, the equation of motion in the axial direction is as follows:

$$\rho(V_r \frac{\partial V_z}{\partial r} + \frac{1}{r}V_\theta \frac{\partial V_z}{\partial \theta} + V_z \frac{\partial V_z}{\partial z}) = -\frac{\partial p}{\partial z} + \mu \nabla^2 V_z \qquad \text{(A6-13)}$$

Multiplying axial velocity, V_z, on the equation of motion in the axial direction, equation (A6-13), yields the equation of total kinetic energy in the axial direction for a steady state incompressible flow without body forces as follows:

$$V_r\frac{\partial}{\partial r}(\frac{1}{2}V_z^2) + \frac{1}{r}V_\theta\frac{\partial}{\partial\theta}(\frac{1}{2}V_z^2) + V_z\frac{\partial}{\partial z}(\frac{1}{2}V_z^2) = -\frac{V_z}{\rho}\frac{\partial p}{\partial z} + \nu V_z\nabla^2 V_z \qquad \text{(A6-14)}$$

Applying the statistical principle of turbulent flow to above equation yields the equation of total kinetic energy in axial direction for turbulent flows as follows:

$$\begin{aligned}
&[\overline{V}_r\frac{\partial}{\partial r}(\frac{1}{2}\overline{V}_z^2) + \frac{1}{r}\overline{V}_\theta\frac{\partial}{\partial\theta}(\frac{1}{2}\overline{V}_z^2) + \overline{V}_z\frac{\partial}{\partial z}(\frac{1}{2}\overline{V}_z^2)] + \\
&+ [\overline{V}_r\frac{\partial}{\partial r}(\frac{1}{2}\overline{V_z'^2}) + \frac{1}{r}\overline{V}_\theta\frac{\partial}{\partial\theta}(\frac{1}{2}\overline{V_z'^2}) + \overline{V}_z\frac{\partial}{\partial z}(\frac{1}{2}\overline{V_z'^2})] \\
&= -\frac{\overline{V}_z}{\rho}\frac{\partial p}{\partial z} + \nu(\overline{V}_z\overline{\nabla^2 V_z} + \overline{V_z'\nabla^2 V_z'}) - \frac{1}{2}[\overline{V_r'\frac{\partial}{\partial r}(V_z'^2)} + \frac{1}{r}\overline{V_\theta'\frac{\partial}{\partial\theta}(V_z'^2)} + \overline{V_z'\frac{\partial}{\partial z}(V_z'^2)}]
\end{aligned} \qquad \text{(A6-15)}$$

Combining equation (A6-14) with the equation of continuity yields the expression of the rate of change of total kinetic energy in the axial direction for the turbulent flows as follows:

$$\begin{aligned}
&[\frac{\partial}{\partial r}(\frac{1}{2}\overline{V}_z^2\cdot\overline{V}_r) + \frac{1}{r}\frac{\partial}{\partial\theta}(\frac{1}{2}\overline{V}_z^2\cdot\overline{V}_\theta) + \frac{\partial}{\partial z}(\frac{1}{2}\overline{V}_z^2\cdot\overline{V}_z)] + \\
&+ [\frac{\partial}{\partial r}(\frac{1}{2}\overline{V_z'^2}\cdot\overline{V}_r) + \frac{1}{r}\frac{\partial}{\partial\theta}(\frac{1}{2}\overline{V_z'^2}\cdot\overline{V}_\theta) + \frac{\partial}{\partial z}(\frac{1}{2}\overline{V_z'^2}\cdot\overline{V}_z)] \\
&= -\frac{\overline{V}_z}{\rho}\frac{\partial p}{\partial z} + \nu(\overline{V}_z\overline{\nabla^2 V_z} + \overline{V_z'\nabla^2 V_z'}) - \frac{1}{2r}(\overline{V}_r\overline{V}_z^2 + \overline{V}_r\overline{V_z'^2} + \overline{V_r'V_z'^2})
\end{aligned} \qquad \text{(A6-16)}$$

To an axisymmetric flow with negligible axial gradient, the equation of total kinetic energy, equation (A6-15), can be simplified as follows:

$$\frac{\partial}{\partial r}(\frac{1}{2}\overline{V}_z^2) + \frac{\partial}{\partial r}(\frac{1}{2}\overline{V_z'^2}) = \frac{\nu}{\overline{V}_r}(\overline{V}_z\overline{\nabla^2 V_z} + \overline{V_z'\nabla^2 V_z'}) - \frac{1}{2\overline{V}_r}\overline{V_r'\frac{\partial}{\partial r}(V_z'^2)} \qquad \text{(A6-17)}$$

or

$$\frac{1}{2}\bar{V}_z^2 + \frac{1}{2}\overline{V_z'^2} = \int \left[\frac{\nu}{\bar{V}_r}\left(\bar{V}_z\overline{\nabla^2 V_z} + \overline{V_z'\nabla^2 V_z'}\right) - \frac{1}{2\bar{V}_r}\overline{V_r'\frac{\partial}{\partial r}(V_z'^2)}\right] dr \qquad \text{(A6-18)}$$

A.7 Equations of Kinetic Energy for Fluctuating Motion

A.7.1 Equation for Radial Direction

To an axisymmetric flow with negligible axial gradient, the rate of change of kinetic energy for the fluctuating motion in the radial direction can be expressed as follows:

$$\frac{\partial}{\partial r}(\frac{1}{2}\overline{V_r'^2}) = -\frac{1}{\rho}\frac{\partial p}{\partial r} + \frac{\nu}{\overline{V}_r}(\overline{V}_r\overline{\nabla^2 V_r} + \overline{V_r'\nabla^2 V_r'} - \frac{\overline{V}_r^2}{r^2} - \frac{\overline{V_r'^2}}{r^2}) -$$
$$-\frac{1}{\overline{V}_r}[\frac{1}{2}\overline{V_r'\frac{\partial}{\partial r}(V_r'^2)} - \frac{1}{r}\overline{V_r'V_\theta'^2}] + \frac{1}{r}(\overline{V}_\theta^2 + \overline{V_\theta'^2}) - \frac{\partial}{\partial r}(\frac{1}{2}\overline{V}_r^2) \qquad (A7\text{-}1)$$

Substituting equation (A5-4) into above equation and rearranging that equation yield the equation of kinetic energy for the fluctuating motion in the radial direction as follows:

$$\frac{\partial}{\partial r}(\frac{1}{2}\overline{V_r'^2}) - \frac{2}{r}(\frac{1}{2}\overline{V_r'^2}) - \frac{2}{\overline{V}_r}\frac{\nu}{r^2}(\frac{1}{2}\overline{V_r'^2})$$
$$= -\frac{\nu}{\overline{V}_r}(\overline{V_r'\frac{\partial^2 V_r'}{\partial r^2}} + \frac{1}{r}\overline{V_r'\frac{\partial V_r'}{\partial r}}) + \frac{1}{\overline{V}_r}[\frac{1}{2}\overline{V_r'\frac{\partial}{\partial r}(V_r'^2)} - \frac{1}{r}\overline{V_r'V_\theta'^2}] \qquad (A7\text{-}2)$$

A.7.2 Equation for Tangential Direction

To an axisymmetric flow with negligible axial gradient, the rate of change of kinetic energy for the fluctuating motion in the tangential direction can be expressed as follows:

$$\frac{\partial}{\partial r}(\frac{1}{2}\overline{V_\theta'^2}) = \frac{\nu}{\overline{V}_r}(\overline{V}_\theta\overline{\nabla^2 V_\theta} + \overline{V_\theta'\nabla^2 V_\theta'} - \frac{\overline{V}_\theta^2}{r^2} - \frac{\overline{V_\theta'^2}}{r^2}) -$$
$$-\frac{1}{\overline{V}_r}[\frac{1}{2}\overline{V_r'\frac{\partial}{\partial r}(V_\theta'^2)} + \frac{1}{r}\overline{V_r'V_\theta'^2}] - \frac{1}{r}(\overline{V}_\theta^2 + \overline{V_\theta'^2}) - \frac{\partial}{\partial r}(\frac{1}{2}\overline{V}_\theta^2) \qquad (A7\text{-}3)$$

Substituting equation (A5-8) into above equation and rearranging that equation yield the equation of kinetic energy for the fluctuating motion in the tangential direction as follows:

$$\frac{\partial}{\partial r}(\frac{1}{2}\overline{V_\theta'^2}) + \frac{2}{r}(\frac{1}{2}\overline{V_\theta'^2}) + \frac{2}{\overline{V}_r}\frac{\nu}{r^2}(\frac{1}{2}\overline{V_\theta'^2})$$
$$= \frac{\nu}{\overline{V}_r}(\overline{V_\theta'\frac{\partial^2 V_\theta'}{\partial r^2}} + \frac{1}{r}\overline{V_\theta'\frac{\partial V_\theta'}{\partial r}}) + \frac{\overline{V}_\theta}{\overline{V}_r}[\frac{\partial}{\partial r}(\overline{V_r'V_\theta'}) + \frac{2}{r}(\overline{V_r'V_\theta'})] -$$
$$- \frac{1}{\overline{V}_r}[\frac{1}{2}\overline{V_r'\frac{\partial}{\partial r}(V_\theta'^2)} + \frac{1}{r}\overline{V_r'V_\theta'^2}] \qquad \text{(A7-4)}$$

A.7.3 Equation for Axial Direction

To an axisymmetric flow with negligible axial gradient, the rate of change of kinetic energy for the fluctuating motion in the axial direction can be expressed as follows:

$$\frac{\partial}{\partial r}(\frac{1}{2}\overline{V_z'^2}) = \frac{\nu}{\overline{V}_r}(\overline{V}_z\overline{\nabla^2 V_z} + \overline{V_z'\nabla^2 V_z'}) - \frac{1}{2\overline{V}_r}\overline{V_r'\frac{\partial}{\partial r}(V_z'^2)} - \frac{\partial}{\partial r}(\frac{1}{2}\overline{V}_z^2) \qquad \text{(A7-5)}$$

Substituting equation (A5-12) into above equation and rearranging that equation yield the equation of kinetic energy for the fluctuating motion in the axial direction as follows:

$$\frac{\partial}{\partial r}(\frac{1}{2}\overline{V_z'^2}) = \frac{\nu}{\overline{V}_r}(\overline{V_z'\frac{\partial^2 V_z'}{\partial r^2}} + \frac{1}{r}\overline{V_z'\frac{\partial V_z'}{\partial r}}) + \frac{\overline{V}_z}{\overline{V}_r}[\frac{\partial}{\partial r}(\overline{V_r'V_z'}) + \frac{1}{r}(\overline{V_r'V_z'})]$$
$$+ \frac{1}{2\overline{V}_r}\overline{V_r'\frac{\partial}{\partial r}(V_z'^2)} \qquad \text{(A7-6)}$$

or

$$\frac{1}{2}\overline{V_z'^2} = \int \{\frac{\nu}{\overline{V}_r}(\overline{V_z'\frac{\partial^2 V_z'}{\partial r^2}} + \frac{1}{r}\overline{V_z'\frac{\partial V_z'}{\partial r}}) + \frac{\overline{V}_z}{\overline{V}_r}[\frac{\partial}{\partial r}(\overline{V_r'V_z'}) + \frac{1}{r}(\overline{V_r'V_z'})] +$$
$$+ \frac{1}{2\overline{V}_r}\overline{V_r'\frac{\partial}{\partial r}(V_z'^2)}\} \, dr \qquad \text{(A7-7)}$$

APPENDIX B

Derivation of Reynolds Shear Stresses

B.1 Reynolds Shear Stress to Radial-Tangential Component

The Reynolds shear stress referring to the radial-tangential component, $\overline{V_r'V_\theta'}$, can be found in the equation of the tangential component of the kinetic energy for the mean motion as follows

$$\overline{V}_r\frac{\partial}{\partial r}(\frac{1}{2}\overline{V}_\theta^2) + \overline{V}_r(\frac{\overline{V}_\theta^2}{r})$$
$$= \nu\overline{V}_\theta(\frac{\partial^2\overline{V}_\theta}{\partial r^2} + \frac{1}{r}\frac{\partial\overline{V}_\theta}{\partial r} - \frac{\overline{V}_\theta}{r^2}) - \overline{V}_\theta[\frac{\partial}{\partial r}(\overline{V_r'V_\theta'}) + \frac{2}{r}\overline{V_r'V_\theta'}] \qquad \text{(B1-1)}$$

Rewriting equation (B1-1) to approach scaled units yields

$$(\frac{\overline{V}_r}{\overline{V}_{in}}R_{e,i}^{0.25})(\frac{\overline{V}_{in}}{R_{e,i}^{0.25}})\frac{\partial}{\partial(r/R_o)}[\frac{1}{2}(\frac{\overline{V}_\theta}{\overline{V}_{in}})^2](\frac{\overline{V}_{in}^2}{R_o}) +$$
$$+ (\frac{\overline{V}_r}{\overline{V}_{in}}R_{e,i}^{0.25})(\frac{\overline{V}_{in}}{R_{e,i}^{0.25}})[\frac{R_o}{r}(\frac{\overline{V}_\theta}{\overline{V}_{in}})^2](\frac{\overline{V}_{in}^2}{R_o})$$
$$= \nu(\frac{\overline{V}_\theta}{\overline{V}_{in}})(\overline{V}_{in})\{\frac{\partial}{\partial(r/R_o)}[\frac{\partial(\overline{V}_\theta/\overline{V}_{in})}{\partial(r/R_o)}](\frac{\overline{V}_{in}}{R_o^2}) +$$
$$+ (\frac{R_o}{r})\frac{\partial(\overline{V}_\theta/\overline{V}_{in})}{\partial(r/R_o)}(\frac{\overline{V}_{in}}{R_o^2}) - (\frac{R_o}{r})^2(\frac{\overline{V}_\theta}{\overline{V}_{in}})(\frac{\overline{V}_{in}}{R_o^2})\} -$$
$$- (\frac{\overline{V}_\theta}{\overline{V}_{in}})(\overline{V}_{in})[\frac{\partial}{\partial(r/R_o)}(\frac{\overline{V_r'V_\theta'}}{\overline{V}_{in}^2})(\frac{\overline{V}_{in}^2}{R_o}) + 2(\frac{R_o}{r})(\frac{\overline{V_r'V_\theta'}}{\overline{V}_{in}^2})(\frac{\overline{V}_{in}^2}{R_o})] \qquad \text{(B1-2)}$$

Let

$$\overline{R} = r/R_o$$

$$\overline{V}_R = \frac{\overline{V}_r}{\overline{V}_{in}}R_{e,i}^{0.25}$$

$$\overline{V}_T = \frac{\overline{V}_\theta}{\overline{V}_{in}}$$

$$\overline{V_R'V_T'} = \frac{\overline{V_r'V_\theta'}}{\overline{V}_{in}^2} \tag{B1-3}$$

Substituting equation (B1-3) into (B1-2) yields

$$\begin{aligned}
&\overline{V}_R\left(\frac{\overline{V}_{in}}{R_{e,i}^{0.25}}\right)\frac{\partial}{\partial\overline{R}}\left(\frac{1}{2}\overline{V}_T^2\right)\left(\frac{\overline{V}_{in}^2}{R_o}\right) + \overline{V}_R\left(\frac{\overline{V}_{in}}{R_{e,i}^{0.25}}\right)\left(\frac{\overline{V}_T^2}{\overline{R}}\right)\left(\frac{\overline{V}_{in}^2}{R_o}\right) \\
&= \nu\overline{V}_T(\overline{V}_{in})\left[\frac{\partial}{\partial\overline{R}}\left(\frac{\partial\overline{V}_T}{\partial\overline{R}}\right)\left(\frac{\overline{V}_{in}}{R_o^2}\right) + \frac{1}{\overline{R}}\frac{\partial\overline{V}_T}{\partial\overline{R}}\left(\frac{\overline{V}_{in}}{R_o^2}\right) - \frac{\overline{V}_T}{\overline{R}^2}\left(\frac{\overline{V}_{in}}{R_o^2}\right)\right] - \\
&- \overline{V}_T(\overline{V}_{in})\left[\frac{\partial}{\partial\overline{R}}\left(\overline{V_R'V_T'}\right)\left(\frac{\overline{V}_{in}^2}{R_o}\right) + \frac{2}{\overline{R}}\left(\overline{V_R'V_T'}\right)\left(\frac{\overline{V}_{in}^2}{R_o}\right)\right]
\end{aligned} \tag{B1-4}$$

Rearranging equation (B1-4) yields

$$\begin{aligned}
&\left(\frac{\overline{V}_{in}^3}{R_o}\right)\cdot\frac{1}{R_{e,i}^{0.25}}\overline{V}_R\left[\frac{\partial}{\partial\overline{R}}\left(\frac{1}{2}\overline{V}_T^2\right) + \frac{\overline{V}_T^2}{\overline{R}}\right] \\
&= \left(\frac{\overline{V}_{in}^2}{R_o^2}\right)\nu\overline{V}_T\left(\frac{\partial^2\overline{V}_T}{\partial\overline{R}^2} + \frac{1}{\overline{R}}\frac{\partial\overline{V}_T}{\partial\overline{R}} - \frac{\overline{V}_T}{\overline{R}^2}\right) - \left(\frac{\overline{V}_{in}^3}{R_o}\right)\overline{V}_T\left[\frac{\partial}{\partial\overline{R}}\left(\overline{V_R'V_T'}\right) + \frac{2}{\overline{R}}\left(\overline{V_R'V_T'}\right)\right]
\end{aligned} \tag{B1-5}$$

Multiplying $R_o/\overline{V}_{in}^3$ on the both sides of equation (B1-5) yields

$$\begin{aligned}
&\frac{1}{R_{e,i}^{0.25}}\overline{V}_R\left[\frac{\partial}{\partial\overline{R}}\left(\frac{1}{2}\overline{V}_T^2\right) + \frac{\overline{V}_T^2}{\overline{R}}\right] \\
&= \left(\frac{\nu}{\overline{V}_{in}R_o}\right)\overline{V}_T\left(\frac{\partial^2\overline{V}_T}{\partial\overline{R}^2} + \frac{1}{\overline{R}}\frac{\partial\overline{V}_T}{\partial\overline{R}} - \frac{\overline{V}_T}{\overline{R}^2}\right) - \overline{V}_T\left[\frac{\partial}{\partial\overline{R}}\left(\overline{V_R'V_T'}\right) + \frac{2}{\overline{R}}\left(\overline{V_R'V_T'}\right)\right]
\end{aligned} \tag{B1-6}$$

Let

$$R_{e,o} = \frac{\overline{V}_{in}D_o}{\nu} \tag{B1-7}$$

and

$$\frac{\partial}{\partial\overline{R}}\left(\frac{1}{2}\overline{V}_T^2\right) = \overline{V}_T\frac{\partial\overline{V}_T}{\partial\overline{R}} \tag{B1-8}$$

Substituting equations (B1-7), (B1-8) into (B1-6) and rearranging the equation yield

$$\frac{\partial}{\partial \overline{R}}(\overline{V_R' V_T'}) + \frac{2}{\overline{R}}(\overline{V_R' V_T'}) +$$

$$+ [\frac{1}{R_{e,i}^{0.25}} \overline{V}_R (\frac{\partial \overline{V}_T}{\partial \overline{R}} + \frac{\overline{V}_T}{\overline{R}}) - \frac{2}{R_{e,o}} (\frac{\partial^2 \overline{V}_T}{\partial \overline{R}^2} + \frac{1}{\overline{R}} \frac{\partial \overline{V}_T}{\partial \overline{R}} - \frac{\overline{V}_T}{\overline{R}^2})] = 0 \qquad \text{(B1-9)}$$

It is found that from the experimental results the velocities V_R and V_T are functions of normalized radius $\overline{R}$, and can be expressed by polynomials, that is,

$$\overline{V}_R = f_a(\overline{R})$$

$$= \sum_0^n a_n \overline{R}^n \qquad (n = 0, 1, 2, ...) \qquad \text{(B1-10)}$$

$$\overline{V}_T = f_b(\overline{R})$$

$$= \sum_0^n b_n \overline{R}^n \qquad (n = 0, 1, 2, ...) \qquad \text{(B1-11)}$$

$$\frac{\partial \overline{V}_T}{\partial \overline{R}} = f_b'(\overline{R})$$

$$= \sum_0^n n b_n \overline{R}^{n-1} \qquad (n = 0, 1, 2, ...) \qquad \text{(B1-12)}$$

$$\frac{\partial^2 \overline{V}_T}{\partial \overline{R}^2} = f_b''(\overline{R})$$

$$= \sum_0^n (n-1) n b_n \overline{R}^{n-2} \qquad (n = 0, 1, 2, ...) \qquad \text{(B1-13)}$$

For any given flow and vortex chamber structure conditions, $R_{e,i}$ and $R_{e,o}$ are known constants. Therefore, the third part of equation (B1-9) is a function of normalized radius $\overline{R}$ under the given condition, that is,

$$\frac{1}{R_{e,i}^{0.25}}\cdot\overline{V}_R\left(\frac{\partial\overline{V}_T}{\partial\overline{R}}+\frac{\overline{V}_T}{\overline{R}}\right)-\frac{2}{R_{e,o}}\cdot\left(\frac{\partial^2\overline{V}_T}{\partial\overline{R}^2}+\frac{1}{\overline{R}}\cdot\frac{\partial\overline{V}_T}{\partial\overline{R}}-\frac{\overline{V}_T}{\overline{R}^2}\right)=F(\overline{R}) \tag{B1-14}$$

Substituting equation (B1-14) into (B1-9) yields

$$\frac{d}{d\overline{R}}(\overline{V_R'V_T'})+\frac{2}{\overline{R}}(\overline{V_R'V_T'})+F(\overline{R})=0 \tag{B1-15}$$

This is a linear differential equation. The solution of the equation, scaled Reynolds shear stress $\overline{V_R'V_T'}$, can be obtained as follows:

Let

$$\vartheta=\exp\left(\int\frac{2}{\overline{R}}\,d\overline{R}\right)=\overline{R}^2 \tag{B1-16}$$

Equation (B1-15) can be rewritten as

$$\frac{d}{d\overline{R}}(\vartheta\cdot\overline{V_R'V_T'})=-\vartheta\cdot F(\overline{R}) \tag{B1-17}$$

$$\vartheta\cdot\overline{V_R'V_T'}=-\int\vartheta\cdot F(\overline{R})\,d\overline{R}+C \tag{B1-18}$$

or

$$\overline{R}^2\cdot\overline{V_R'V_T'}=-\int\overline{R}^2\cdot F(\overline{R})\,d\overline{R}+C \tag{B1-19}$$

At the centre of the vortex chamber, the Reynolds shear stress $\overline{V_R'V_T'}$ is zero, that is,

At $r=0$

$\overline{R}=0$

$$\overline{V_R'V_T'}=0 \tag{B1-20}$$

Substituting equation (B1-20) into (B1-19) yields

$$C=0 \tag{B1-21}$$

Equation (B1-19) becomes

$$\overline{R}^2 \cdot \overline{V_R' V_T'} = -\int \overline{R}^2 \cdot F(\overline{R})\, d\overline{R} \tag{B1-22}$$

or

$$\overline{V_R' V_T'} = -\frac{1}{\overline{R}^2}\int \overline{R}^2 \cdot F(\overline{R})\, d\overline{R} \qquad (\overline{R} \neq 0) \tag{B1-23}$$

Since

$$\overline{V}_R\left(\frac{\partial \overline{V}_T}{\partial \overline{R}} + \frac{\overline{V}_T}{\overline{R}}\right)$$

$$= \overline{V}_R\{[b_1 + 2b_2\overline{R} + \cdots\cdots + (n-1)b_{n-1}\overline{R}^{n-2} + nb_n\overline{R}^{n-1}] +$$

$$+ [\frac{b_0}{\overline{R}} + b_1 + b_2\overline{R} + \cdots\cdots + b_{n-1}\overline{R}^{n-2} + b_n\overline{R}^{n-1}]\}$$

$$= \overline{V}_R[\frac{b_0}{\overline{R}} + 2b_1 + 3b_2\overline{R} + \cdots\cdots + nb_{n-1}\overline{R}^{n-2} + (n+1)b_n\overline{R}^{n-1}]$$

$$= \sum_0^n a_n\overline{R}^n \cdot \sum_0^n (n+1)b_n\overline{R}^{n-1} \tag{B1-24}$$

and

$$\frac{\partial^2 \overline{V}_T}{\partial \overline{R}^2} + \frac{1}{\overline{R}}\cdot\frac{\partial \overline{V}_T}{\partial \overline{R}} - \frac{\overline{V}_T}{\overline{R}^2}$$

$$= [2b_2 + \cdots\cdots + (n-2)(n-1)b_{n-1}\overline{R}^{n-3} + (n-1)nb_n\overline{R}^{n-2}] +$$

$$+ [\frac{b_1}{\overline{R}} + 2b_2 + \cdots\cdots + (n-1)b_{n-1}\overline{R}^{n-3} + nb_n\overline{R}^{n-2}] -$$

$$- [\frac{b_0}{\overline{R}^2} + \frac{b_1}{\overline{R}} + b_2 + \cdots\cdots + b_{n-1}\overline{R}^{n-3} + b_n\overline{R}^{n-2}]$$

$$= -\frac{b_0}{\overline{R}^2} + 3b_2 + \cdots\cdots + (n-2)nb_{n-1}\overline{R}^{n-3} + (n-1)(n+1)b_n\overline{R}^{n-2}$$

$$= \sum_{0}^{n} (n-1)(n+1)b_n\bar{R}^{n-2} \tag{B1-25}$$

Substituting equations (B1-24) and (B1-25) into (B1-14) yields

$$F(\bar{R}) = \frac{1}{R_{e,i}^{0.25}} \sum_{0}^{n} a_n\bar{R}^n \cdot \sum_{0}^{n} (n+1)b_n\bar{R}^{n-1} - \frac{2}{R_{e,o}} \sum_{0}^{n} (n-1)(n+1)b_n\bar{R}^{n-2} \tag{B1-26}$$

Substituting equation (B1-26) into (B1-23) yields the scaled Reynolds shear stress $\overline{V_R'V_T'}$ as

$$\overline{V_R'V_T'} = -\frac{1}{R_{e,i}^{0.25}\cdot\bar{R}^2} \int \sum_{0}^{n} a_n\bar{R}^n \cdot \sum_{0}^{n} (n+1)b_n\bar{R}^{n+1}\, d\bar{R} +$$

$$+ \frac{2}{R_{e,o}\cdot\bar{R}^2} \int \sum_{0}^{n} (n-1)(n+1)b_n\bar{R}^n\, d\bar{R} \tag{B1-27}$$

or

$$\overline{V_R'V_T'} = -\frac{1}{R_{e,i}^{0.25}\cdot\bar{R}^2} I_1 + \frac{2}{R_{e,o}\cdot\bar{R}^2} I_2 \tag{B1-28}$$

where

$$I_1 = \int \sum_{0}^{n} a_n\bar{R}^n \cdot \sum_{0}^{n} (n+1)b_n\bar{R}^{n+1}\, d\bar{R} \tag{B1-29}$$

$$I_2 = \int \sum_{0}^{n} (n-1)(n+1)b_n\bar{R}^n\, d\bar{R} \tag{B1-30}$$

Since

$$\sum_{0}^{n} a_n\bar{R}^n \cdot \sum_{0}^{n} (n+1)b_n\bar{R}^{n+1}$$

$$= (a_0 + a_1\bar{R} + \cdots\cdots + a_{n-1}\bar{R}^{n-1} + a_n\bar{R}^n)\sum_{0}^{n} (n+1)b_n\bar{R}^{n+1}$$

$$= a_0 \sum_0^n (n+1) b_n \bar{R}^{n+1} + a_1 \bar{R} \sum_0^n (n+1) b_n \bar{R}^{n+1} + \cdots\cdots +$$

$$+ a_{n-1} \bar{R}^{n-1} \sum_0^n (n+1) b_n \bar{R}^{n+1} + a_n \bar{R}^n \sum_0^n (n+1) b_n \bar{R}^{n+1}$$

$$= a_0 [b_0 \bar{R} + 2b_1 \bar{R}^2 + 3b_2 \bar{R}^3 + \cdots\cdots + nb_{n-1} \bar{R}^n + (n+1) b_n \bar{R}^{n+1}] +$$

$$+ a_1 [b_0 \bar{R}^2 + 2b_1 \bar{R}^3 + 3b_2 \bar{R}^4 + \cdots\cdots + nb_{n-1} \bar{R}^{n+1} + (n+1) b_n \bar{R}^{n+2}] + \cdots\cdots +$$

$$+ a_{n-1} [b_0 \bar{R}^n + 2b_1 \bar{R}^{n+1} + 3b_2 \bar{R}^{n+2} + \cdots\cdots + nb_{n-1} \bar{R}^{2n-1} + (n+1) b_n \bar{R}^{2n}] +$$

$$+ a_n [b_0 \bar{R}^{n+1} + 2b_1 \bar{R}^{n+2} + 3b_2 \bar{R}^{n+3} + \cdots\cdots + nb_{n-1} \bar{R}^{2n} + (n+1) b_n \bar{R}^{2n+1}] \quad \text{(B1-31)}$$

$$I_1 = \int \sum_0^n a_n \bar{R}^n \cdot \sum_0^n (n+1) b_n \bar{R}^{n+1} \, d\bar{R}$$

$$= a_0 (\frac{1}{2} b_0 \bar{R}^2 + \frac{2}{3} b_1 \bar{R}^3 + \frac{3}{4} b_2 \bar{R}^4 + \cdots\cdots + \frac{n}{n+1} b_{n-1} \bar{R}^{n+1} + \frac{n+1}{n+2} b_n R^{n+2}) +$$

$$+ a_1 (\frac{1}{3} b_0 \bar{R}^3 + \frac{2}{4} b_1 \bar{R}^4 + \frac{3}{5} b_2 \bar{R}^5 + \cdots\cdots + \frac{n}{n+2} b_{n-1} \bar{R}^{n+2} + \frac{n+1}{n+3} b_n \bar{R}^{n+3}) + \cdots\cdots +$$

$$+ a_{n-1} (\frac{1}{n+1} b_0 \bar{R}^{n+1} + \frac{2}{n+2} b_1 \bar{R}^{n+2} + \cdots\cdots + \frac{n}{2n} b_{n-1} \bar{R}^{2n} + \frac{n+1}{2n+1} b_n \bar{R}^{2n+1}) +$$

$$+ a_n (\frac{1}{n+2} b_0 \bar{R}^{n+2} + \frac{2}{n+3} b_1 \bar{R}^{n+3} + \cdots\cdots + \frac{n}{2n+1} b_{n-1} \bar{R}^{2n+1} + \frac{n+1}{2n+2} b_n \bar{R}^{2n+2})$$

$$= \bar{R}^2 (a_0 \sum_0^n \frac{n+1}{n+2} b_n \bar{R}^n + a_1 \sum_0^n \frac{n+1}{n+3} b_n \bar{R}^{n+1} + \cdots\cdots +$$

$$+ a_{n-1} \sum_0^n \frac{n+1}{2n+1} b_n \bar{R}^{2n-1} + a_n \sum_0^n \frac{n+1}{2n+2} b_n \bar{R}^{2n}) \quad \text{(B1-32)}$$

Let m = 0, 1, 2, ..., n = 0, 1, 2, ...

Equation (B1-32) can be simplified as

$$I_1 = \bar{R}^2 \sum_0^n \left[\sum_0^m a_m \bar{R}^m \cdot \frac{n+1}{(n+2)+m}\right] b_n \bar{R}^n \qquad \text{(B1-33)}$$

$$I_2 = \int \sum_0^n (n-1)(n+1) b_n \bar{R}^n \, d\bar{R}$$

$$= \int \left[- b_0 + 3b_2 \bar{R}^2 + \cdots\cdots + (n-2)n b_{n-1} \bar{R}^{n-1} + (n-1)(n+1) b_n \bar{R}^n\right] d\bar{R}$$

$$= - b_0 \bar{R} + b_2 \bar{R}^3 + \cdots\cdots + (n-2) b_{n-1} \bar{R}^n + (n-1) b_n \bar{R}^{n+1}$$

$$= \bar{R}^2 \sum_0^n (n-1) b_n \bar{R}^{n-1} \qquad \text{(B1-34)}$$

Substituting equations (B1-33), (B1-34) into (B1-28) yields

$$\overline{V_R' V_T'} = - \frac{1}{R_{e,i}^{0.25}} \sum_0^n \left[\sum_0^m a_m \bar{R}^m \cdot \frac{n+1}{(n+2)+m}\right] b_n \bar{R}^n + \frac{2}{R_{e,o}} \sum_0^n (n-1) b_n \bar{R}^{n-1} \qquad \text{(B1-35)}$$

B.2 Reynolds Shear Stress to Radial-Axial Component

The Reynolds shear stress referring to the radial-axial component, $\overline{V_r'V_z'}$, can be found in the equation of the axial component of the kinetic energy for the mean motion as follows:

$$\overline{V}_r\frac{\partial}{\partial r}(\frac{1}{2}\overline{V}_z^2) = \nu\overline{V}_z(\frac{\partial^2\overline{V}_z}{\partial r^2} + \frac{1}{r}\cdot\frac{\partial\overline{V}_z}{\partial r}) - \overline{V}_z[\frac{\partial}{\partial r}(\overline{V_r'V_z'}) + \frac{1}{r}\overline{V_r'V_z'}] \tag{B2-1}$$

Since

$$\frac{\partial}{\partial r}(\frac{1}{2}\overline{V}_z^2) = \overline{V}_z\frac{\partial\overline{V}_z}{\partial r} \tag{B2-2}$$

and

$$\frac{1}{r}\cdot\frac{\partial}{\partial r}(r\cdot\frac{\partial\overline{V}_z}{\partial r}) = \frac{\partial^2\overline{V}_z}{\partial r^2} + \frac{1}{r}\cdot\frac{\partial\overline{V}_z}{\partial r} \tag{B2-3}$$

Substituting equations (B2-2), (B2-3) into (B2-1) and simplifying that equation yield

$$\overline{V}_r\frac{\partial\overline{V}_z}{\partial r} = \nu\cdot\frac{1}{r}\cdot\frac{\partial}{\partial r}(r\cdot\frac{\partial\overline{V}_z}{\partial r}) - [\frac{\partial}{\partial r}(\overline{V_r'V_z'}) + \frac{1}{r}\overline{V_r'V_z'}] \tag{B2-4}$$

Rewriting equation (B2-4) to approach scaled units yields

$$\begin{aligned}&(\frac{\overline{V}_r}{\overline{V}_{in}}R_{e,i}^{0.25})(\frac{\overline{V}_{in}}{R_{e,i}^{0.25}})\frac{\partial(\overline{V}_z/\overline{V}_{in})}{\partial(r/R_o)}(\frac{\overline{V}_{in}}{R_o})\\ &= \nu(\frac{1}{r/R_o})(\frac{1}{R_o})\frac{\partial}{\partial(r/R_o)}[\frac{r}{R_o}\cdot\frac{\partial(\overline{V}_z/\overline{V}_{in})}{\partial(r/R_o)}](\frac{\overline{V}_{in}}{R_o}) -\\ &- \frac{\partial}{\partial(r/R_o)}(\frac{\overline{V_r'V_z'}}{\overline{V}_{in}^2})(\frac{\overline{V}_{in}^2}{R_o}) - \frac{1}{r/R_o}(\frac{\overline{V_r'V_z'}}{\overline{V}_{in}^2})(\frac{\overline{V}_{in}^2}{R_o})\end{aligned} \tag{B2-5}$$

Let

$$\overline{R} = r/R_o$$

$$\overline{V}_R = \frac{\overline{V}_r}{\overline{V}_{in}}R_{e,i}^{0.25}$$

$$\overline{V}_Z = \frac{\overline{V}_z}{\overline{V}_{in}}$$

$$\overline{V_R' V_Z'} = \frac{\overline{V_r' V_z'}}{\overline{V}_{in}^2} \tag{B2-6}$$

Substituting equation (B2-6) into (B2-5) yields

$$\overline{V}_R \left(\frac{1}{R_{e,i}^{0.25}}\right) \frac{\partial \overline{V}_Z}{\partial \overline{R}} \left(\frac{\overline{V}_{in}^2}{R_o}\right)$$
$$= \frac{1}{\overline{R}} \left(\frac{\nu}{\overline{V}_{in} \cdot R_o}\right) \frac{\partial}{\partial \overline{R}} \left(\overline{R} \frac{\partial \overline{V}_Z}{\partial \overline{R}}\right) \left(\frac{\overline{V}_{in}^2}{R_o}\right) - \frac{\partial}{\partial \overline{R}} \left(\overline{V_R' V_Z'}\right) \left(\frac{\overline{V}_{in}^2}{R_o}\right) - \frac{1}{\overline{R}} \left(\overline{V_R' V_Z'}\right) \left(\frac{\overline{V}_{in}^2}{R_o}\right) \tag{B2-7}$$

Multiplying $R_o/\overline{V}_{in}^2$ on the both sides of equation (B2-7) yields

$$\frac{1}{R_{e,i}^{0.25}} \overline{V}_R \frac{\partial \overline{V}_Z}{\partial \overline{R}} = \left(\frac{\nu}{\overline{V}_{in} \cdot R_o}\right) \frac{1}{\overline{R}} \cdot \frac{\partial}{\partial \overline{R}} \left(\overline{R} \frac{\partial \overline{V}_Z}{\partial \overline{R}}\right) - \frac{\partial}{\partial \overline{R}} \left(\overline{V_R' V_Z'}\right) - \frac{1}{\overline{R}} \left(\overline{V_R' V_Z'}\right) \tag{B2-8}$$

Since

$$R_{e,o} = \frac{\overline{V}_{in} D_o}{\nu} \tag{B2-9}$$

Substituting equation (B2-9) into (B2-8) and rearranging equation (B2-8) yield

$$\frac{\partial}{\partial \overline{R}} \left(\overline{V_R' V_Z'}\right) + \frac{1}{\overline{R}} \left(\overline{V_R' V_Z'}\right) + \left[\frac{1}{R_{e,i}^{0.25}} \overline{V}_R \frac{\partial \overline{V}_Z}{\partial \overline{R}} - \frac{2}{R_{e,o} \cdot \overline{R}} \cdot \frac{\partial}{\partial \overline{R}} \left(\overline{R} \frac{\partial \overline{V}_Z}{\partial \overline{R}}\right)\right] = 0 \tag{B2-10}$$

It is found that from the experimental results the velocities $\overline{V}_R$ and $\overline{V}_Z$ are functions of normalized radius $\overline{R}$, and can be expressed by polynomials, that is,

$$\overline{V}_R = f_a(\overline{R})$$
$$= \sum_0^n a_n \overline{R}^n \qquad (n = 0, 1, 2, ...) \tag{B2-11}$$

$$\overline{V}_Z = f_d(\overline{R})$$

$$= \sum_0^n d_n \overline{R}^n \qquad (n = 0, 1, 2, ...) \qquad \text{(B2-12)}$$

$$\frac{\partial \overline{V}_Z}{\partial \overline{R}} = \sum_0^n n d_n \overline{R}^{n-1} \qquad (n = 0, 1, 2, ...) \qquad \text{(B2-13)}$$

$$\frac{\partial}{\partial \overline{R}}(\overline{R}\frac{\partial \overline{V}_Z}{\partial \overline{R}})$$

$$= \frac{\partial}{\partial \overline{R}}(\sum_0^n n d_n \overline{R}^n)$$

$$= \sum_0^n n^2 d_n \overline{R}^{n-1} \qquad (n = 0, 1, 2, ...) \qquad \text{(B2-14)}$$

To any given flow and vortex chamber structure conditions, $R_{e,i}$ and $R_{e,o}$ are known constants. Therefore, the third part of equation (B2-10) is a function of normalized radius $\overline{R}$ under the given condition, that is,

$$\frac{1}{R_{e,i}^{0.25}} \overline{V}_R \frac{\partial \overline{V}_Z}{\partial \overline{R}} - \frac{2}{R_{e,o} \cdot \overline{R}} \cdot \frac{\partial}{\partial \overline{R}}(\overline{R}\frac{\partial \overline{V}_Z}{\partial \overline{R}}) = G(\overline{R}) \qquad \text{(B2-15)}$$

Substituting equation (B2-15) into (B2-10) yields

$$\frac{d}{d\overline{R}}(\overline{V_R' V_Z'}) + \frac{1}{\overline{R}}(\overline{V_R' V_Z'}) + G(\overline{R}) = 0 \qquad \text{(B2-16)}$$

This is a linear differential equation. The solution of the equation, scaled Reynolds shear stress $\overline{V_R' V_Z'}$, can be obtained as follows:

Let

$$\eta = \exp(\int \frac{1}{\overline{R}} d\overline{R}) = \overline{R} \qquad \text{(B2-17)}$$

Equation (B2-16) can be rewritten as

$$\frac{d}{d\bar{R}}(\eta\cdot\overline{V_R'V_Z'}) = -\eta\cdot G(\bar{R}) \tag{B2-18}$$

$$\eta\cdot\overline{V_R'V_Z'} = -\int \eta\cdot G(\bar{R})\, d\bar{R} + C \tag{B2-19}$$

or

$$\bar{R}\cdot\overline{V_R'V_Z'} = -\int \bar{R}\cdot G(\bar{R})\, d\bar{R} + C \tag{B2-20}$$

At the centre of the vortex chamber, the Reynolds shear stress $\overline{V_R'V_Z'}$ is zero, that is,

At $r = 0$

$\bar{R} = 0$

$$\overline{V_R'V_Z'} = 0 \tag{B2-21}$$

Substituting equation (B2-21) into (B2-20) yields

$$C = 0 \tag{B2-22}$$

Equation (B2-20) becomes

$$\bar{R}\cdot\overline{V_R'V_Z'} = -\int \bar{R}\cdot G(\bar{R})\, d\bar{R} \tag{B2-23}$$

or

$$\overline{V_R'V_Z'} = -\frac{1}{\bar{R}}\int \bar{R}\cdot G(\bar{R})\, d\bar{R} \qquad (\bar{R} \neq 0) \tag{B2-24}$$

Combining equations (B2-15), (B2-11), (B2-13) and (B2-14) yields

$$G(\bar{R}) = \frac{1}{R_{e,i}^{0.25}}\cdot\sum_0^n a_n\bar{R}^n\cdot\sum_0^n n d_n\bar{R}^{n-1} - \frac{2}{R_{e,o}}\cdot\sum_0^n n^2 d_n\bar{R}^{n-2} \tag{B2-25}$$

Substituting equation (B2-25) into (B2-24) yields the scaled Reynolds shear stress $\overline{V_R'V_Z'}$ as

$$\overline{V_R' V_Z'} = -\frac{1}{R_{e,1}^{0.25}\cdot\bar{R}}\int \sum_0^n a_n\bar{R}^n\cdot\sum_0^n nd_n\bar{R}^n\, d\bar{R} +$$

$$+\frac{2}{R_{e,0}\cdot\bar{R}}\int \sum_0^n n^2 d_n\bar{R}^{n-1}\, d\bar{R} \qquad \text{(B2-26)}$$

or

$$\overline{V_R' V_Z'} = -\frac{1}{R_{e,1}^{0.25}\cdot\bar{R}} I_3 + \frac{2}{R_{e,0}\cdot\bar{R}} I_4 \qquad \text{(B2-27)}$$

where

$$I_3 = \int \sum_0^n a_n\bar{R}^n\cdot\sum_0^n nd_n\bar{R}^n\, d\bar{R} \qquad \text{(B2-28)}$$

$$I_4 = \int \sum_0^n n^2 d_n\bar{R}^{n-1}\, d\bar{R} \qquad \text{(B2-29)}$$

Since

$$\sum_0^n a_n\bar{R}^n\cdot\sum_0^n nd_n\bar{R}^n$$

$$= (a_0 + a_1\bar{R} + \cdots\cdots + a_{n-1}\bar{R}^{n-1} + a_n\bar{R}^n)\sum_0^n nd_n\bar{R}^n$$

$$= a_0\sum_0^n nd_n\bar{R}^n + a_1\bar{R}\sum_0^n nd_n\bar{R}^n + \cdots\cdots +$$

$$+ a_{n-1}\bar{R}^{n-1}\sum_0^n nd_n\bar{R}^n + a_n\bar{R}^n\sum_0^n nd_n\bar{R}^n$$

$$= a_0[d_1\bar{R} + 2d_2\bar{R}^2 + 3d_3\bar{R}^3 + \cdots\cdots + (n-1)d_{n-1}\bar{R}^{n-1} + nd_n\bar{R}^n] +$$

$$+ a_1[d_1\bar{R}^2 + 2d_2\bar{R}^3 + 3d_3\bar{R}^4 + \cdots\cdots + (n-1)d_{n-1}\bar{R}^n + nd_n\bar{R}^{n+1}] + \cdots\cdots +$$

$$+ a_{n-1}\,[d_1\overline{R}^{n} + 2d_2\overline{R}^{n+1} + 3d_3\overline{R}^{n+2} + \cdots\cdots + (n-1)d_{n-1}\overline{R}^{2n-2} + nd_n\overline{R}^{2n-1}] +$$

$$+ a_n\,[d_1\overline{R}^{n+1} + 2d_2\overline{R}^{n+2} + 3d_3\overline{R}^{n+3} + \cdots\cdots + (n-1)d_{n-1}\overline{R}^{2n-1} + nd_n\overline{R}^{2n}] \quad \text{(B2-30)}$$

Substituting equation (B2-30) into (B2-28) yields

$$I_3 = \int \sum_0^n a_n\overline{R}^n \cdot \sum_0^n nd_n\overline{R}^n \, d\overline{R}$$

$$= a_0\left(\frac{1}{2}d_1\overline{R}^2 + \frac{2}{3}d_2\overline{R}^3 + \frac{3}{4}d_3\overline{R}^4 + \cdots\cdots + \frac{n-1}{n}d_{n-1}\overline{R}^n + \frac{n}{n+1}d_n\overline{R}^{n+1}\right) +$$

$$+ a_1\left(\frac{1}{3}d_1\overline{R}^3 + \frac{2}{4}d_2\overline{R}^4 + \frac{3}{5}d_3\overline{R}^5 + \cdots\cdots + \frac{n-1}{n+1}d_{n-1}\overline{R}^{n+1} + \frac{n}{n+2}d_n\overline{R}^{n+2}\right) + \cdots\cdots +$$

$$+ a_{n-1}\left(\frac{1}{n+1}d_1\overline{R}^{n+1} + \frac{2}{n+2}d_2\overline{R}^{n+2} + \cdots\cdots + \frac{n-1}{2n-1}d_{n-1}\overline{R}^{2n-1} + \frac{n}{2n}d_n\overline{R}^{2n}\right) +$$

$$+ a_n\left(\frac{1}{n+2}d_1\overline{R}^{n+2} + \frac{2}{n+3}d_2\overline{R}^{n+3} + \cdots\cdots + \frac{n-1}{2n}d_{n-1}\overline{R}^{2n} + \frac{n}{2n+1}d_n\overline{R}^{2n+1}\right)$$

$$= \overline{R}\left(a_0\sum_0^n \frac{n}{n+1}d_n\overline{R}^n + a_1\sum_0^n \frac{n}{n+2}d_n\overline{R}^{n+1} + \cdots\cdots +\right.$$

$$\left. + a_{n-1}\sum_0^n \frac{n}{2n}d_n\overline{R}^{2n-1} + a_n\sum_0^n \frac{n}{2n+1}d_n\overline{R}^{2n}\right) \quad \text{(B2-31)}$$

Let m = 0, 1, 2, ..., n = 0, 1, 2, ...

Equation (B2-31) can be simplified as follows:

$$I_3 = \overline{R}\sum_0^n \left[\sum_0^m a_m\overline{R}^m \cdot \frac{n}{(n+1)+m}\right] d_n\overline{R}^n \quad \text{(B2-32)}$$

$$I_4 = \int \sum_0^n n^2 d_n\overline{R}^{n-1} \, d\overline{R}$$

$$= \int [d_1 + 4d_2\overline{R} + 9d_3\overline{R}^2 + \cdots\cdots + (n-1)^2 d_{n-1}\overline{R}^{n-2} + n^2 d_n\overline{R}^{n-1}]\, d\overline{R}$$

$$= d_1\overline{R} + \frac{2^2}{2}d_2\overline{R}^2 + \frac{3^2}{3}d_3\overline{R}^3 + \cdots\cdots + \frac{(n-1)^2}{n-1}d_{n-1}\overline{R}^{n-1} + \frac{n^2}{n}d_n\overline{R}^n$$

$$= \overline{R}\sum_0^n n d_n \overline{R}^{n-1} \qquad \text{(B2-33)}$$

Substituting equations (B2-32), (B2-33) into (B2-27) yields

$$\overline{V_R'V_Z'} = -\frac{1}{R_{e,i}^{0.25}}\sum_0^n \left[\sum_0^m a_m \overline{R}^m \cdot \frac{n}{(n+1)+m}\right] d_n\overline{R}^n + \frac{2}{R_{e,o}}\sum_0^n n d_n \overline{R}^{n-1} \qquad \text{(B2-34)}$$

B.3 Contribution of Viscosity in Tangential Direction

The equation of tangential component of the kinetic energy for the fluctuating motion is

$$\frac{\partial}{\partial r}(\frac{1}{2}\overline{V_\theta'^2}) + \frac{2}{r}(\frac{1}{2}\overline{V_\theta'^2}) + \frac{2}{\overline{V}_r}\frac{\nu}{r^2}(\frac{1}{2}\overline{V_\theta'^2})$$
$$= \frac{\nu}{\overline{V}_r}(\overline{V_\theta'\frac{\partial^2 V_\theta'}{\partial r^2}} + \frac{1}{r}\overline{V_\theta'\frac{\partial V_\theta'}{\partial r}}) + \frac{\overline{V}_\theta}{\overline{V}_r}[\frac{\partial}{\partial r}(\overline{V_r'V_\theta'}) + \frac{2}{r}(\overline{V_r'V_\theta'})] -$$
$$- \frac{1}{\overline{V}_r}[\frac{1}{2}\overline{V_r'\frac{\partial}{\partial r}(V_\theta'^2)} + \frac{1}{r}\overline{V_r'V_\theta'^2}] \qquad \text{(A7-4)}$$

If the third order terms in the above equation can be neglected, the equation (A7-4) can be simplified and rearranged as

$$\nu(\overline{V_\theta'\frac{\partial^2 V_\theta'}{\partial r^2}} + \frac{1}{r}\overline{V_\theta'\frac{\partial V_\theta'}{\partial r}})$$
$$= \overline{V}_r\frac{\partial}{\partial r}(\frac{1}{2}\overline{V_\theta'^2}) + \overline{V}_r\frac{2}{r}(\frac{1}{2}\overline{V_\theta'^2}) + \frac{2\nu}{r^2}(\frac{1}{2}\overline{V_\theta'^2}) - \overline{V}_\theta[\frac{\partial}{\partial r}(\overline{V_r'V_\theta'}) + \frac{2}{r}(\overline{V_r'V_\theta'})] \qquad \text{(B3-1)}$$

Rewriting equation (B3-1) yields

$$\nu[(\frac{\overline{V_\theta'}}{\overline{V}_{in}})\frac{\partial^2(\overline{V_\theta'}/\overline{V}_{in})}{\partial(r/R_o)^2}\cdot(\frac{\overline{V}_{in}}{R_o})^2 + \frac{1}{r/R_o}\cdot(\frac{\overline{V_\theta'}}{\overline{V}_{in}})\frac{\partial(\overline{V_\theta'}/\overline{V}_{in})}{\partial(r/R_o)}\cdot(\frac{\overline{V}_{in}}{R_o})^2]$$
$$= (\frac{\overline{V}_r}{\overline{V}_{in}}R_{e,i}^{0.25})(\frac{\overline{V}_{in}}{R_{e,i}^{0.25}})\frac{\partial}{\partial(r/R_o)}(\frac{\frac{1}{2}\overline{V_\theta'^2}}{\frac{1}{2}\overline{V}_{in}^2}R_{e,i}^{0.3})(\frac{\frac{1}{2}\overline{V}_{in}^2}{R_{e,i}^{0.3}\cdot R_o}) +$$
$$+ (\frac{\overline{V}_r}{\overline{V}_{in}}R_{e,i}^{0.25})(\frac{\overline{V}_{in}}{R_{e,i}^{0.25}})\frac{2}{r/R_o}(\frac{\frac{1}{2}\overline{V_\theta'^2}}{\frac{1}{2}\overline{V}_{in}^2}R_{e,i}^{0.3})(\frac{\frac{1}{2}\overline{V}_{in}^2}{R_{e,i}^{0.3}\cdot R_o}) +$$
$$+ \frac{2\nu}{(r/R_o)^2}(\frac{\frac{1}{2}\overline{V_\theta'^2}}{\frac{1}{2}\overline{V}_{in}^2}R_{e,i}^{0.3})(\frac{\frac{1}{2}\overline{V}_{in}^2}{R_{e,i}^{0.3}\cdot R_o^2}) -$$
$$- (\frac{\overline{V}_\theta}{\overline{V}_{in}})(\overline{V}_{in})[\frac{\partial}{\partial(r/R_o)}(\frac{\overline{V_r'V_\theta'}}{\overline{V}_{in}^2})(\frac{\overline{V}_{in}^2}{R_o}) + \frac{2}{r/R_o}(\frac{\overline{V_r'V_\theta'}}{\overline{V}_{in}^2})(\frac{\overline{V}_{in}^2}{R_o})] \qquad \text{(B3-2)}$$

Let

$$V_T' = V_\theta'/\overline{V}_{in}$$

$$V_R' = V_r'/\overline{V}_{in}$$

$$V_T^{2'} = V_\theta^{2'}/\overline{V}_{in}^{\,2}$$

$$V_R' V_T^{2'} = V_r' V_\theta^{2'}/\overline{V}_{in}^{\,3}$$

$$K_{t,s} = \frac{\frac{1}{2}\overline{V_\theta'^{\,2}}}{\frac{1}{2}\overline{V}_{in}^{\,2}} R_{e,i}^{0.3} \qquad \text{(B3-3)}$$

Substituting equations (B1-3) and (B3-3) into (B2-2) yields

$$\nu\left(\frac{\overline{V}_{in}}{R_o}\right)^2 \left(\overline{V_T' \frac{\partial^2 V_T'}{\partial \overline{R}^2}} + \frac{1}{\overline{R}}\overline{V_T' \frac{\partial V_T'}{\partial \overline{R}}}\right)$$
$$= \frac{1}{2R_{e,i}^{0.55}}\left(\frac{\overline{V}_{in}^{\,3}}{R_o}\right)\overline{V}_R \frac{\partial K_{t,s}}{\partial \overline{R}} + \frac{1}{R_{e,i}^{0.55}}\left(\frac{\overline{V}_{in}^{\,3}}{R_o}\right)\overline{V}_R \frac{K_{t,s}}{\overline{R}} + \frac{\nu}{R_{e,i}^{0.3}}\left(\frac{\overline{V}_{in}}{R_o}\right)^2 \frac{K_{t,s}}{\overline{R}^2} -$$
$$- \left(\frac{\overline{V}_{in}^{\,3}}{R_o}\right)\overline{V}_T\left[\frac{\partial}{\partial \overline{R}}\left(\overline{V_R' V_T'}\right) + \frac{2}{\overline{R}}\left(\overline{V_R' V_T'}\right)\right] \qquad \text{(B3-4)}$$

Multiplying $R_o/\overline{V}_{in}^{\,3}$ on the both sides of equation (B3-4) yields

$$\left(\frac{\nu}{\overline{V}_{in} \cdot R_o}\right)\left(\overline{V_T' \frac{\partial^2 V_T'}{\partial \overline{R}^2}} + \frac{1}{\overline{R}}\overline{V_T' \frac{\partial V_T'}{\partial \overline{R}}}\right)$$
$$= \frac{1}{2R_{e,i}^{0.55}}\overline{V}_R \frac{K_{t,s}}{\partial \overline{R}} + \frac{1}{R_{e,i}^{0.55}}\overline{V}_R \frac{K_{t,s}}{\overline{R}} + \frac{1}{R_{e,i}^{0.3}}\left(\frac{\nu}{\overline{V}_{in} \cdot R_o}\right)\frac{K_{t,s}}{\overline{R}^2} -$$
$$- \overline{V}_T\left[\frac{\partial}{\partial \overline{R}}\left(\overline{V_R' V_T'}\right) + \frac{2}{\overline{R}}\left(\overline{V_R' V_T'}\right)\right] \qquad \text{(B3-5)}$$

Substituting equation (B1-7) into (B3-5) yields

$$\frac{2}{R_{e,o}}\left(\overline{V_T' \frac{\partial^2 V_T'}{\partial \overline{R}^2}} + \frac{1}{\overline{R}}\overline{V_T' \frac{\partial V_T'}{\partial \overline{R}}}\right)$$
$$= \frac{1}{2R_{e,i}^{0.55}}\overline{V}_R \frac{\partial K_{t,s}}{\partial \overline{R}} + \frac{1}{R_{e,i}^{0.55}}\overline{V}_R \frac{K_{t,s}}{\overline{R}} + \frac{2}{R_{e,i}^{0.3} \cdot R_{e,o}} \frac{K_{t,s}}{\overline{R}^2} -$$
$$- \overline{V}_T\left[\frac{\partial}{\partial \overline{R}}\left(\overline{V_R' V_T'}\right) + \frac{2}{\overline{R}}\left(\overline{V_R' V_T'}\right)\right] \qquad \text{(B3-6)}$$

It is found that from the experimental results the scaled tangential turbulence kinetic energy K_t' is a function of normalized radius $\overline{R}$, and can be expressed by a polynomial, that is,

$$K_{t,s} = f_c(\overline{R})$$

$$= \sum_0^n c_n \overline{R}^n \qquad (n = 0, 1, 2, ...) \qquad \text{(B3-7)}$$

$$\frac{\partial K_{t,s}}{\partial \overline{R}} = f_c'(\overline{R})$$

$$= \sum_0^n n c_n \overline{R}^{n-1} \qquad (n = 0, 1, 2, ...) \qquad \text{(B3-8)}$$

Since

$$2\frac{K_{t,s}}{\overline{R}} = \sum_0^n 2c_n \overline{R}^{n-1} \qquad (n = 0, 1, 2, ...) \qquad \text{(B3-9)}$$

and

$$\frac{\partial K_{t,s}}{\partial \overline{R}} + 2\frac{K_{t,s}}{\overline{R}} = \sum_0^n (n+2)c_n \overline{R}^{n-1} \qquad (n = 0, 1, 2, ...) \qquad \text{(B3-10)}$$

Substituting equations (B1-10), (B1-11), (B1-15), (B1-26), (B3-7), (B3-10) into (B3-6) yields

$$\frac{2}{R_{e,o}}\left(\overline{V_T' \frac{\partial^2 V_T'}{\partial \overline{R}^2}} + \frac{1}{\overline{R}} \overline{V_T' \frac{\partial V_T'}{\partial \overline{R}}}\right)$$

$$= \frac{1}{2R_{e,i}^{0.55}} \sum_0^n a_n \overline{R}^n \cdot \sum_0^n (n+2)c_n \overline{R}^{n-1} + \frac{2}{R_{e,i}^{0.3} \cdot R_{e,o}} \sum_0^n c_n \overline{R}^{n-2} +$$

$$+ \sum_0^n b_n \overline{R}^n \cdot \left[\frac{1}{R_{e,i}^{0.25}} \sum_0^n a_n \overline{R}^n \cdot \sum_0^n (n+1)b_n \overline{R}^{n-1} - \frac{2}{R_{e,o}} \cdot \sum_0^n (n-1)(n+1)b_n \overline{R}^{n-2}\right] \qquad \text{(B3-11)}$$

B.4 Contribution of Viscosity in Axial Direction

The equation of the axial component of the kinetic energy for the fluctuating motion is

$$\frac{\partial}{\partial r}(\frac{1}{2}\overline{V_z'^2}) = \frac{\nu}{\overline{V}_r}(\overline{V_z'\frac{\partial^2 V_z'}{\partial r^2}} + \frac{1}{r}\overline{V_z'\frac{\partial V_z'}{\partial r}}) + \frac{\overline{V}_z}{\overline{V}_r}[\frac{\partial}{\partial r}(\overline{V_r'V_z'}) + \frac{1}{r}(\overline{V_r'V_z'})]$$
$$+ \frac{1}{2\overline{V}_r}\overline{V_r'\frac{\partial}{\partial r}(V_z'^2)} \qquad \text{(A7-6)}$$

If the third order terms in the above equation can be neglected, the equation (A7-6) can be simplified and rearranged as

$$\overline{\nu(V_z'\frac{\partial^2 V_z'}{\partial r^2} + \frac{1}{r}V_z'\frac{\partial V_z'}{\partial r})} = \overline{V}_r\frac{\partial}{\partial r}(\frac{1}{2}\overline{V_z'^2}) - \overline{V}_z[\frac{\partial}{\partial r}(\overline{V_r'V_z'}) + \frac{1}{r}(\overline{V_r'V_z'})] \qquad \text{(B4-1)}$$

Rewriting equation (B4-1) yields

$$\overline{\nu[(\frac{V_z'}{\overline{V}_{in}})\frac{\partial^2(V_z'/\overline{V}_{in})}{\partial(r/R_o)^2}(\frac{\overline{V}_{in}}{R_o})^2 + \frac{1}{r/R_o}\cdot(\frac{V_z'}{\overline{V}_{in}})\frac{\partial(V_z'/\overline{V}_{in})}{\partial(r/R_o)}\cdot(\frac{\overline{V}_{in}}{R_o})^2]}$$
$$= (\frac{\overline{V}_r}{\overline{V}_{in}}R_{e,i}^{0.25})(\frac{\overline{V}_{in}}{R_{e,i}^{0.25}})\frac{\partial}{\partial(r/R_o)}(\frac{\frac{1}{2}\overline{V_z'^2}}{\frac{1}{2}\overline{V}_{in}^2})(\frac{\frac{1}{2}\overline{V}_{in}^2}{R_o}) -$$
$$-(\frac{\overline{V}_z}{\overline{V}_{in}})(\overline{V}_{in})[\frac{\partial}{\partial(r/R_o)}(\frac{\overline{V_r'V_z'}}{\overline{V}_{in}^2})(\frac{\overline{V}_{in}^2}{R_o}) + \frac{1}{r/R_o}(\frac{\overline{V_r'V_z'}}{\overline{V}_{in}^2})(\frac{\overline{V}_{in}^2}{R_o})] \qquad \text{(B4-2)}$$

Let

$$V_Z' = V_z'/\overline{V}_{in}$$

$$V_Z'^2 = V_z'^2/\overline{V}_{in}^2$$

$$K_{z,s} = \frac{\frac{1}{2}\overline{V_z'^2}}{\frac{1}{2}\overline{V}_{in}^2} \qquad \text{(B4-3)}$$

Substituting equations (B2-6) and (B4-3) into (B4-2) yields

$$\nu\left(\frac{\overline{V}_{in}}{R_o}\right)^2\left(\overline{V_Z'\frac{\partial^2 V_Z'}{\partial \overline{R}^2}}+\frac{1}{\overline{R}}\overline{V_Z'\frac{\partial V_Z'}{\partial \overline{R}}}\right)$$
$$=\frac{1}{2R_{e,i}^{0.25}}\left(\frac{\overline{V}_{in}^3}{R_o}\right)\overline{V}_R\frac{\partial K_{z,s}}{\partial \overline{R}}-\left(\frac{\overline{V}_{in}^3}{R_o}\right)\overline{V}_Z\left[\frac{\partial}{\partial \overline{R}}\left(\overline{V_R'V_Z'}\right)+\frac{1}{\overline{R}}\left(\overline{V_R'V_Z'}\right)\right] \qquad \text{(B4-4)}$$

Multiplying $R_o/\overline{V}_{in}^3$ on the both sides of equation (B4-4) yields

$$\left(\frac{\nu}{\overline{V}_{in}\cdot R_o}\right)\left(\overline{V_Z'\frac{\partial^2 V_Z'}{\partial \overline{R}^2}}+\frac{1}{\overline{R}}\overline{V_Z'\frac{\partial V_Z'}{\partial \overline{R}}}\right)$$
$$=\frac{1}{2R_{e,i}^{0.25}}\overline{V}_R\frac{\partial K_{z,s}}{\partial \overline{R}}-\overline{V}_Z\left[\frac{\partial}{\partial \overline{R}}\left(\overline{V_R'V_Z'}\right)+\frac{1}{\overline{R}}\left(\overline{V_R'V_Z'}\right)\right] \qquad \text{(B4-5)}$$

Substituting equation (B1-7) into (B4-5) yields

$$\frac{2}{R_{e,o}}\left(\overline{V_Z'\frac{\partial^2 V_Z'}{\partial \overline{R}^2}}+\frac{1}{\overline{R}}\overline{V_Z'\frac{\partial V_Z'}{\partial \overline{R}}}\right)$$
$$=\frac{1}{2R_{e,i}^{0.25}}\overline{V}_R\frac{\partial K_{z,s}}{\partial \overline{R}}-\overline{V}_Z\left[\frac{\partial}{\partial \overline{R}}\left(\overline{V_R'V_Z'}\right)+\frac{1}{\overline{R}}\left(\overline{V_R'V_Z'}\right)\right] \qquad \text{(B4-6)}$$

It is found that from the experimental results the scaled axial turbulence kinetic energy K_z' is a function of normalized radius $\overline{R}$, and can be expressed by a polynomial, that is,

$$K_{z,s}=f_e(\overline{R})$$
$$=\sum_0^n e_n\overline{R}^n \qquad (n=0,1,2,.....) \qquad \text{(B4-7)}$$

$$\frac{\partial K_{z,s}}{\partial \overline{R}}=f_e'(\overline{R})$$
$$=\sum_0^n n e_n\overline{R}^{n-1} \qquad (n=0,1,2,.....) \qquad \text{(B4-8)}$$

Substituting equations (B1-10), (B2-12), (B2-16), (B2-25) and (B4-8) into (B4-6) yields

$$\frac{2}{R_{e,o}}\left(\overline{V_Z'\frac{\partial^2 V_Z'}{\partial \overline{R}^2}} + \frac{1}{\overline{R}}\overline{V_Z'\frac{\partial V_Z'}{\partial \overline{R}}}\right)$$

$$= \frac{1}{2R_{e,i}^{0.25}}\sum_0^n a_n\overline{R}^n \cdot \sum_0^n n e_n \overline{R}^{n-1} +$$

$$+ \sum_0^n d_n\overline{R}^n \left(\frac{1}{R_{e,i}^{0.25}}\sum_0^n a_n\overline{R}^n \cdot \sum_0^n n d_n \overline{R}^{n-1} - \frac{2}{R_{e,o}}\sum_0^n n^2 d_n \overline{R}^{n-2}\right) \qquad \text{(B4-9)}$$

APPENDIX C

Computer Program Listings

Reynolds Shear Stress

```
      PROGRAM SHSTR

      DIMENSION A(20),B(20),R(40),TXA(40),TXB(40),TY(40),
     #TERMX(40),TERMY(40),VRV(40),VRVT(40)
      REAL EK,EL,EN,ENM
      CHARACTER*20 FNAME1,FNAME2
C*************************************************************
C     INPUT
C     VIN = INLET VELOCITY
C     DIN = INLET DIAMETER
C     DO = VORTEX CHAMBER DIAMETER
C     VK = VISCOSITY
C     IA = NUMBER OF COEFFICIENT A
C     IB = NUMBER OF COEFFICIENT B
C     IR = NUMBER OF CALCULATION POINT (RADIAL DIRECTION)
C     IRM = MAXIMUM POINT (RADIAL DIRECTION)
C     A(N) = COEFFICIENT A
C     B(N) = COEFFICIENT B
C*************************************************************
      OPEN(UNIT=5,FILE='CON')
      WRITE(5,5)
    5 FORMAT(4X,'INPUT FILE NAME?        ')
      READ(5,10) FNAME1
   10 FORMAT(A10)
      OPEN(UNIT=1,FILE=FNAME1)
      WRITE(5,15)
   15 FORMAT(4X,'OUTPUT FILE NAME?       ')
      READ(5,10) FNAME2
      OPEN(UNIT=2,FILE=FNAME2)
      WRITE(2,25) FNAME1,FNAME2
   25 FORMAT(/,10X,2A20)
      WRITE(2,30)
   30 FORMAT(/,10X,'PROGRAM SHEAR-STRESS JAN 1995')
      READ(1,*) VIN,DIN,DO,VK,IA,IB,IR,IRM
      WRITE(2,35) VIN,DIN,DO,VK,IA,IB,IR,IRM
   35 FORMAT(/,11X,'VIN          DIN          DO',
     #'          VK',  IA  IB  IR IRM',/,4F14.6,4I4)
      READ(1,*) A(1),A(2),A(3),A(4),A(5)
      WRITE(2,40) A(1),A(2),A(3),A(4),A(5)
   40 FORMAT(/,10X,'A(1)          A(2)          A(3)',
     #'          A(4)          A(5)',/,F14.11,4F14.6)
      READ(1,*) A(6),A(7),A(8),A(9),A(10)
      WRITE(2,45) A(6),A(7),A(8),A(9),A(10)
```

```
   45 FORMAT(/,10X,'A(6)          A(7)          A(8)',
     #'          A(9)         A(10)',/,5F14.6)
      READ(1,*) B(1),B(2),B(3),B(4),B(5)
      WRITE(2,50) B(1),B(2),B(3),B(4),B(5)
   50 FORMAT(/,10X,'B(1)          B(2)          B(3)',
     #'          B(4)          B(5)',/,F14.11,4F14.6)
      READ(1,*) B(6),B(7),B(8),B(9),B(10)
      WRITE(2,55) B(6),B(7),B(8),B(9),B(10)
   55 FORMAT(/,10X,'B(6)          B(7)          B(8)',
     #'                B(9)               B(10)',/,5F14.6,/)
C*************************************************************
C     CALCULATION
C*************************************************************
      REI=VIN*DIN/VK
      REO=VIN*DO/VK
      WRITE(5,*) 'REI,REO',REI,REO
      DO 160 K=1,IR
      EK=K
      EL=IRM
      R(K)=EK/EL
      DO 110 M=1,IA
      DO 100 N=1,IB
      EN=N
      ENM=N+M
      C=EN/ENM
      TXB(N)=C*B(N)*R(K)**(N+M)
C      WRITE(5,*) 'TXB(N)',TXB(N)
  100 CONTINUE
      TXBT=0.0
      DO 105 N=1,IB
      TXBT=TXBT+TXB(N)
  105 CONTINUE
C      WRITE(5,*) 'TXBT',TXBT
      TXA(M)=A(M)*TXBT
C      WRITE(5,*) 'TXA(M)',TXA(M)
  110 CONTINUE
      TXAT=0.0
      DO 115 M=1,IA
      TXAT=TXAT+TXA(M)
  115 CONTINUE
C      WRITE(5,*) 'TXAT',TXAT
      TERMX(K)=TXAT/R(K)**2.0
      WRITE(5,*) 'TERMX(K)',TERMX(K)
      DO 140 N=1,IB
      TY(N)=(N-2)*B(N)*R(K)**(N-2)
  140 CONTINUE
      TYT=0.0
      DO 145 N=1,IB
      TYT=TYT+TY(N)
  145 CONTINUE
      TERMY(K)=TYT
      WRITE(5,*) 'TERMY(K)',TERMY(K)
      VRV(K)=TERMX(K)/(-REI**0.25)+2.0*TERMY(K)/REO
      VRVT(K)=VRV(K)*VIN**2.0
```

```
  160 CONTINUE
C*************************************************************
C     OUTPUT
C     NO = NUMBER OF POINT
C     R = NORMALIZED RADIUS
C     VRV = NORMALIZED SHEAR STRESS
C     VRVT = ABSOLUTE SHEAR STRESS
C*************************************************************
      WRITE(2,165)
  165 FORMAT(/,12X,'NO              R           VRV',
     #'           VRVT',/)
      DO 170 K=1,IR
  170 WRITE(2,175) K,R(K),VRV(K),VRVT(K)
  175 FORMAT(10X,I4,F14.5,2F14.6)
      END
```

Computer Calculation Output

Reynolds Shear Stress

D6BM D6BMO

PROGRAM SHEAR-STRESS JAN 1995

VIN	DIN	DO	VK	IA IB IR IRM
9.324900	0.012700	0.139600	0.000015	10 10 15 20

A(1)	A(2)	A(3)	A(4)	A(5)
-0.009590	-154.1218	3208.159	-29112.20	145230.2

A(6)	A(7)	A(8)	A(9)	A(10)
-432067.3	785660.8	-855698.0	512439.1	-129688.4

B(1)	B(2)	B(3)	B(4)	B(5)
0.020515	61.97313	-352.9656	710.7131	-169.2022

B(6)	B(7)	B(8)	B(9)	B(10)
-1377.510	1815.317	-405.4144	-560.8911	278.6851

NO	R	VRV	VRVT
1	0.05000	0.383322	33.331295
2	0.10000	0.453378	39.422882
3	0.15000	0.336917	29.296156
4	0.20000	0.237682	20.667332
5	0.25000	0.168837	14.680976
6	0.30000	0.120022	10.436395
7	0.35000	0.087935	7.646281
8	0.40000	0.066841	5.812085
9	0.45000	0.055501	4.826011
10	0.50000	0.042440	3.690297
11	0.55000	0.036689	3.190232
12	0.60000	0.014701	1.278345
13	0.65000	0.101658	8.839526
14	0.70000	0.113772	9.892880
15	0.75000	-0.008170	-0.710447

DA75 DA750

PROGRAM SHEAR-STRESS JAN 1995

VIN	DIN	DO	VK	IA	IB	IR	IRM
16.282000	0.012700	0.139600	0.000015	10	10	15	20

A(1)	A(2)	A(3)	A(4)	A(5)
0.008598	7.347185	20.41215	-498.8565	2743.946

A(6)	A(7)	A(8)	A(9)	A(10)
-6479.670	6775.429	-2588.702	0.000000	0.000000

B(1)	B(2)	B(3)	B(4)	B(5)
0.002328	0.684583	13.64789	-152.8794	1021.251

B(6)	B(7)	B(8)	B(9)	B(10)
-3502.006	6615.504	-7038.126	3957.152	-914.4376

NO	R	VRV	VRVT
1	0.05000	-0.001050	-0.278328
2	0.10000	-0.004303	-1.140725
3	0.15000	-0.009663	-2.561574
4	0.20000	-0.017824	-4.725163
5	0.25000	-0.029723	-7.879675
6	0.30000	-0.045665	-12.105861
7	0.35000	-0.064342	-17.057159
8	0.40000	-0.082454	-21.858765
9	0.45000	-0.095637	-25.353758
10	0.50000	-0.100212	-26.566521
11	0.55000	-0.093732	-24.848598
12	0.60000	-0.077022	-20.418709
13	0.65000	-0.054302	-14.395552
14	0.70000	-0.032303	-8.563738
15	0.75000	-0.012580	-3.334874

DB75 DB750

PROGRAM SHEAR-STRESS JAN 1995

VIN	DIN	DO	VK	IA	IB	IR	IRM
9.324900	0.012700	0.139600	0.000015	10	10	5	20

A(1)	A(2)	A(3)	A(4)	A(5)
0.008598	7.347185	20.41215	-498.8565	2743.946

A(6)	A(7)	A(8)	A(9)	A(10)
-6479.670	6775.429	-2588.702	0.000000	0.000000

B(1)	B(2)	B(3)	B(4)	B(5)
0.001631	1.734159	-11.25556	102.8776	-333.4543

B(6)	B(7)	B(8)	B(9)	B(10)
417.6187	175.5054	-1065.285	1060.719	-347.7346

NO	R	VRV	VRVT
1	0.05000	-0.001411	-0.122723
2	0.10000	-0.005059	-0.439935
3	0.15000	-0.011272	-0.980100
4	0.20000	-0.020320	-1.766914
5	0.25000	-0.032418	-2.818858
6	0.30000	-0.047714	-4.148933
7	0.35000	-0.065601	-5.704284
8	0.40000	-0.083977	-7.302140
9	0.45000	-0.099035	-8.611431
10	0.50000	-0.105833	-9.202572
11	0.55000	-0.100340	-8.724899
12	0.60000	-0.082744	-7.194859
13	0.65000	-0.058890	-5.120697
14	0.70000	-0.039347	-3.421337
15	0.75000	-0.028089	-2.442474

DC75 DC750

PROGRAM SHEAR-STRESS JAN 1995

VIN	DIN	DO	VK	IA	IB	IR	IRM
2.328800	0.012700	0.139600	0.000015	10	10	15	20

A(1)	A(2)	A(3)	A(4)	A(5)
0.008598	7.347185	20.41215	-498.8565	2743.946

A(6)	A(7)	A(8)	A(9)	A(10)
-6479.670	6775.429	-2588.702	0.000000	0.000000

B(1)	B(2)	B(3)	B(4)	B(5)
0.001700	1.352799	3.982587	107.0343	-820.9883

B(6)	B(7)	B(8)	B(9)	B(10)
2493.149	-3844.990	3057.430	-1113.220	117.0318

NO	R	VRV	VRVT
1	0.05000	-0.002640	-0.014319
2	0.10000	-0.012650	-0.068605
3	0.15000	-0.029594	-0.160495
4	0.20000	-0.050415	-0.273416
5	0.25000	-0.073403	-0.398085
6	0.30000	-0.098484	-0.534111
7	0.35000	-0.125717	-0.681805
8	0.40000	-0.153648	-0.833279
9	0.45000	-0.177520	-0.962743
10	0.50000	-0.188984	-1.024919
11	0.55000	-0.179526	-0.973624
12	0.60000	-0.147703	-0.801041
13	0.65000	-0.104202	-0.565118
14	0.70000	-0.071224	-0.386268
15	0.75000	-0.066532	-0.360824

APPENDIX D

Computer Program Listings

Vortex Core Radius

```
      PROGRAM CORE10

      REAL KA1,KA2,KASI,KASM,KAS1,KAS2,LAM
      DIMENSION KASI(10),LAM(10),RE(10),RC(10)
      CHARACTER*20 FNAME1,FNAME2
C*************************************************************
C     INPUT
C     RE = EXIT RADIUS
C     KAS1, KAS2 = INITIAL RC/RE
C     CO = COEFFICIENT
C     NEL = NUMBER OF ELEMENT
C     RO = CHAMBER RADIUS
C     AIN = INLET SECTION AREA
C     FE = INLET ANGLE
C     XN = COEFFICIENT
C*************************************************************
      OPEN(UNIT=5,FILE='CON')
      WRITE(5,5)
    5 FORMAT(4X,'INPUT FILE NAME?        ')
      READ(5,10) FNAME1
   10 FORMAT(A10)
      OPEN(UNIT=1,FILE=FNAME1)
      WRITE(5,15)
   15 FORMAT(4X,'OUTPUT FILE1 NAME?      ')
      READ(5,10) FNAME2
      OPEN(UNIT=2,FILE=FNAME2)
      WRITE(2,25) FNAME1,FNAME2
   25 FORMAT(/,10X,2A20)
      WRITE(2,30)
   30 FORMAT(/,10X,'PROGRAM CORE-SIZE JUNE 1995')
      READ(1,*) RE(1),RE(2),RE(3),RE(4),RE(5),RE(6)
      WRITE(2,35) RE(1),RE(2),RE(3),RE(4),RE(5),RE(6)
   35 FORMAT(/,2X,'RE(25)  RE(30)  RE(40)  RE(50)  RE(58)',
     #'  RE(75)',/,6F8.4)
      READ(1,*) KAS1,KAS2,CO,NEL
      WRITE(2,40) KAS1,KAS2,CO,NEL
   40 FORMAT(/,4X,'KAS1    KAS2      CO     NEL',/,3F8.4,I8)
      READ(1,*) RO,AIN,FE,XN
      WRITE(2,45) RO,AIN,FE,XN
   45 FORMAT(/,6X,'RO     AIN      FE      XN',/,4F8.4)
```

```
C*************************************************************
C     CALCULATION
C*************************************************************
      FE=FE*3.14159265/180.0
      AO=3.14159265*RO**2.0
      DO 80 I=1,6
      LAM(I)=RE(I)/RO
      C=LAM(I)**(4.0-2.0*CO)*COS(FE)**2.0
      BAT=(AIN/AO)**2.0/C
      KA1=KAS1
      KA2=KAS2
C      WRITE(5,*) 'XN,FE,LAM(I),AO,C,BAT',
     #XN,FE,LAM(I),AO,C,BAT
      CALL FKAS(BAT,KA1,LAM(I),CO,NEL,XN,FK1)
      WRITE(5,*) 'FK1',FK1
      CALL FKAS(BAT,KA2,LAM(I),CO,NEL,XN,FK2)
      WRITE(5,*) 'FK2',FK2
      IF(FK1.GT.1E-5.AND.FK2.GT.1E-5) THEN
        WRITE(5,*) 'FK1,FK2',FK1,FK2
        STOP
      END IF
      IF(FK1.LT.1E-5.AND.FK2.LT.1E-5) THEN
        WRITE(5,*) 'FK1,FK2',FK1,FK2
        STOP
      END IF
   60 KASM=KA1-(KA1-KA2)*FK1/(FK1-FK2)
C      WRITE(5,*) 'KA1,KA2,FK1,FK2',KA1,KA2,FK1,FK2
      CALL FKAS(BAT,KASM,LAM(I),CO,NEL,XN,FKM)
      WRITE(5,*) 'KASM,FKM',KASM,FKM
      IF(ABS(FKM).LT.1E-5) THEN
        KASI(I)=KASM
        GOTO 80
      END IF
      IF((FK1.LT.1E-5.AND.FKM.GT.1E-5).OR.
     #(FK1.GT.1E-5.AND.FKM.LT.1E-5)) THEN
        KA2=KASM
        FK2=FKM
        GOTO 60
      ELSE
        KA1=KASM
        FK1=FKM
        GOTO 60
      END IF
C      WRITE(5,*) 'KASI(I)',KASI(I)
   80 RC(I)=KASI(I)*LAM(I)
      CONTINUE
C*************************************************************
C     OUTPUT
C     KASI = FINAL RC/RE
C     RC = CORE RADIUS
C*************************************************************
      WRITE(2,100) KASI(1),KASI(2),KASI(3),KASI(4),KASI(5),
     #KASI(6)
```

```
  100 FORMAT(/,2X,'KASI25  KASI30  KASI40  KASI50  KASI58',
     #'  KASI75',/,6F8.4)
      WRITE(5,*)  'KASI(1-6)',KASI(1),KASI(2),KASI(3),
     #KASI(4),KASI(5),KASI(6)
      WRITE(2,120) RC(1),RC(2),RC(3),RC(4),RC(5),RC(6)
  120 FORMAT(/,4X,'RC25    RC30    RC40    RC50    RC58',
     #'    RC75',/,6F8.4)
      WRITE(5,*)  'RC(1-6)',
     #RC(1),RC(2),RC(3),RC(4),RC(5),RC(6)
      END

      SUBROUTINE FKAS(BAT,KAS,LAN,CO,NEL,XN,FK)
C     INTEGRATION EQUATION
      REAL KAS,LAN
      TT1=1.0-KAS**2.0
      TT3=EXP(-XN/LAN**2.0/KAS**2.0)
      TT4=1.0-TT3
      TM3=KAS**(1.0-2.0*CO)*((1.0-EXP(-XN))/TT4)**2.0
      TM4=2.0*BAT*KAS
      CALL T1(NEL,KAS,LAN,CO,XN,S1)
      CALL T2(NEL,KAS,LAN,CO,XN,S2)
      FK=2.0*TT1*KAS*S1+TT1**2.0*(S2-TM3)+TM4
C      WRITE(5,*)  'TT1,TT3,TT4,TM3,TM4',TT1,TT3,TT4,TM3,TM4
      WRITE(5,*)  'BAT,KAS,LAN,CO,NEL,XN,FK'
     #,BAT,KAS,LAN,CO,NEL,XN,FK
      RETURN
      END

      SUBROUTINE T1(NEL,KAS,LAN,CO,XN,S1)
C     INTEGRATION OF TERM 1
      REAL KK,KAS,LAN
      H=(1.0-KAS)/NEL
      RRE=KAS
      CALL TM1(RRE,KAS,LAN,CO,XN,FA1)
      RRE=1.0
      CALL TM1(RRE,KAS,LAN,CO,XN,FB1)
      SO1=(FA1+FB1)/2.0
      SN1=0.0
      DO 180 K=1,NEL
        KK=K
        RRE=KAS+(KK-0.5)*H
        CALL TM1(RRE,KAS,LAN,CO,XN,A11)
        RRE=KAS+KK*H
        CALL TM1(RRE,KAS,LAN,CO,XN,A12)
        SN1=SN1+2*A11+A12
  180 CONTINUE
      S1=(SO1+SN1)*H/3.0
C      WRITE(5,*)  'NEL,KAS,LAN,CO,XN,S1'
C     #,NEL,KAS,LAN,CO,XN,S1
      RETURN
      END
```

```
      SUBROUTINE T2(NEL,KAS,LAN,CO,XN,S2)
C     INTEGRATION OF TERM 2
      REAL KK,KAS,LAN
      H=(1.0-KAS)/NEL
      RRE=KAS
      CALL TM2(RRE,KAS,LAN,CO,XN,FA2)
      RRE=1.0
      CALL TM2(RRE,KAS,LAN,CO,XN,FB2)
      SO2=(FA2+FB2)/2.0
      SN2=0.0
      DO 200 K=1,NEL
        KK=K
        RRE=KAS+(KK-0.5)*H
        CALL TM2(RRE,KAS,LAN,CO,XN,A21)
        RRE=KAS+KK*H
        CALL TM2(RRE,KAS,LAN,CO,XN,A22)
        SN2=SN2+2*A21+A22
  200 CONTINUE
      S2=(SO2+SN2)*H/3.0
C      WRITE(5,*) 'NEL,KAS,LAN,CO,XN,S2'
C     #,NEL,KAS,LAN,CO,XN,S2
      RETURN
      END

      SUBROUTINE TM1(RRE,KAS,LAN,CO,XN,A1)
C     TERM 1
      REAL KAS,LAN
      TT2=EXP(-XN*RRE**2.0/KAS**2.0)
      TT3=EXP(-XN/LAN**2.0/KAS**2.0)
      TT4=1.0-TT3
      TT5=(1.0-TT2)/TT4
      A1=RRE**(1.0-2.0*CO)*TT5**2.0
      RETURN
      END

      SUBROUTINE TM2(RRE,KAS,LAN,CO,XN,A2)
C     TERM 2
      REAL KAS,LAN
      TT2=EXP(-XN*RRE**2.0/KAS**2.0)
      TT3=EXP(-XN/LAN**2.0/KAS**2.0)
      TT4=1.0-TT3
      TT5=(1.0-TT2)/TT4
      A=-RRE**2.0*TT2+TT3/LAN**2.0*TT5
      B=2.0*XN*A/KAS**3.0/TT4
      A2=2.0*RRE**(1.0-2.0*CO)*TT5*B
      RETURN
      END
```

Computer Calculation Output

Vortex Core Radii

C10 C11

PROGRAM CORE-SIZE JUNE 1995

RE(25)	RE(30)	RE(40)	RE(50)	RE(58)	RE(75)
1.7463	2.0955	2.7940	3.4925	4.0513	5.2388

KAS1	KAS2	CO	NEL
.0500	1.0000	.8000	100

RO	AIN	FE	XN
6.9850	20.2683	30.0000	1.6188

KASI25	KASI30	KASI40	KASI50	KASI58	KASI75
.4565	.5154	.6015	.6597	.6940	.7395

RC25	RC30	RC40	RC50	RC58	RC75
.1141	.1546	.2406	.3299	.4025	.5546

APPENDIX E

Raw Experimental Data

Tangential Component at Main Section

Re/Ro = 0.25

Re,i = 1960

PT.	U Mean (m/s)	U RMS (m/s)	Turb
1	5.232	1.534	0.180
2	11.965	0.778	0.065
3	10.257	0.783	0.076
4	7.803	0.649	0.083
5	6.437	0.615	0.095
6	5.611	0.570	0.102
7	4.849	0.541	0.112
8	4.218	0.500	0.119
9	3.896	0.496	0.127
10	3.681	0.487	0.132
11	3.504	0.487	0.139
12	3.318	0.508	0.153
13	3.155	0.550	0.174
14	3.013	0.553	0.184
15	2.794	0.655	0.234

Radial Component at Main Section

Re/Ro = 0.30

Re,i = 7840

PT.	U Mean (m/s)	U RMS (m/s)	Turb
1	2.399	2.679	1.117
2	1.201	1.454	1.211
3	0.834	1.143	1.371
4	0.519	0.847	1.632
5	0.298	0.850	2.855
6	0.159	0.887	5.563
7	0.025	0.932	37.580
8	-0.112	0.998	8.917
9	-0.256	1.057	4.123
10	-0.393	1.105	2.813
11	-0.539	1.027	1.904
12	-0.681	1.051	1.544

Tangential Component near Exit Section

Re/Ro = 0.40

Re,i = 7840

PT.	U Mean (m/s)	U RMS (m/s)	Turb
1	5.766	3.186	0.553
2	12.685	2.855	0.225
3	18.497	2.719	0.147
4	22.326	2.974	0.133
5	19.977	2.470	0.124
6	16.925	1.937	0.114
7	14.268	1.529	0.107
8	12.103	1.175	0.097
9	10.410	1.134	0.109
10	9.151	1.075	0.117
11	8.173	1.041	0.127
12	7.300	1.004	0.138
13	6.490	1.025	0.158
14	6.249	1.104	0.177
15	6.139	1.265	0.206

Radial Component near Exit Section

Re/Ro = 0.50

Re,i = 13700

PT.	U Mean (m/s)	U RMS (m/s)	Turb
1	1.091	7.707	6.773
2	2.690	11.287	4.196
3	4.508	12.647	2.805
4	3.929	8.025	2.043
5	3.587	5.937	1.655
6	-4.428	4.693	1.060
7	-5.181	3.259	0.629
8	-7.267	3.156	0.434
9	-5.885	3.003	0.510
10	-4.807	2.908	0.605
11	-3.572	3.100	0.868
12	-2.761	5.652	2.047